WATER DIFFUSION IN CALC-ALKALINE SILICATE MELTS

by

Huaiwei Ni

A dissertation submitted in partial fulfillment
of the requirements for the degree of
Doctor of Philosophy
(Geology)
in The University of Michigan
2009

Doctoral Committee:

Professor Youxue Zhang, Chair
Professor Eric J. Essene
Professor John Kieffer
Professor Rebecca A. Lange
Professor Samuel B. Mukasa

To

Ya, Feimeng and our beloved

ACKNOWLEDGEMENTS

TABLE OF CONTENTS

<center>**LIST OF FIGURES**</center>

<u>Figure</u>

<center>vii</center>

LIST OF TABLES

LIST OF APPENDICES

CHAPTER I

INTRODUCTION

As an extremely dynamic or even violent natural process, explosive volcanic eruption is breathtaking macroscopically and causes significant geological (Self and Blake, 2008), climatical (Robock, 2000), and ecological (Tanguy et al., 1998) consequences. From microscopic point of view, explosive eruption is driven by exsolution of oversaturated volatiles, largely water, from host magma (Wilson et al., 1980; Zhang et al., 2007). Originally dissolved water in magma is continuously transported to bubbles through diffusion to sustain bubble growth (Navon et al., 1998; Proussevitch and Sahagian, 1998). At a certain temperature and pressure, the rate of bubble growth depends upon water solubility, water diffusivity, and melt viscosity (Liu and Zhang, 2000). A bubbly magma may eventually evolve into an explosive gas flow after magma fragmentation (Zhang, 1999; Gonnermann and Manga, 2003), only after which can a volcanic eruption be technically defined "explosive".

Water diffusion plays a critical role in explosive volcanic eruption, and significant progresses have been made in both experimental methods and theoretical developments. However, even for the most extensively studied rhyolitic melt, the effect of pressure on water diffusion is still not determined. This study is a systematic investigation on water diffusion in three silicate melts in calc-alkaline series: rhyolite (Chapter II), dacite

(Chapter III), and andesite (Chapter IV). In addition, a geospeedometry method based on oxygen isotope fractionation and diffusion is discussed (Chapter V).

Chapter II is an experimental study on H_2O diffusion in rhyolitic melts at 0.95-1.9 GPa. Previous studies (Zhang et al., 1991; Nowak and Behrens, 1997; Zhang and Behrens, 2000; Okumura and Nakashima, 2004; Behrens et al., 2007) explored temperature dependence and water content dependence of H_2O diffusivity, but could not constrain pressure effect accurately due to their limited pressure range. I carried out diffusion-couple experiments at 680-1902 K and 0.2-5.2 wt.% total water content (H_2O_t) in a piston-cylinder apparatus. Diffusion profiles were measured on quenched glasses with FTIR microscopy. Levenberg-Marquart algorithm (Press et al., 1998) was used to resolve water content dependence for a given diffusion profile. Comparison with previous experiments indicates a negative pressure effect on H_2O diffusion, increasingly so towards a lower temperature. Therefore decompression during magma upwelling facilitates bubble growth through promoting H_2O diffusion. Assuming molecular H_2O (H_2O_m) dominates water diffusion, both H_2O_m and H_2O_t diffusivity are modeled as a function of temperature (676-1902 K), pressure (0-2 GPa), and water concentration (0-7.7 wt.%). The new expressions, which are consistent with all literature data, can be applied to model the dynamics of H_2O-driven rhyolitic eruptions (such as bubble growth), as well as H_2O transport in granitic magma chambers. This manuscript has been published in *Chemical Geology* (Ni and Zhang, 2008).

Chapter III examines pressure effect on H_2O diffusion in dacite. Many volcanic eruptions have a dacitic overall composition, such as the 1991 Unzen eruption (Holtz et al., 2005). There are also andesitic eruptions with dacitic liquid composition, such as the

1968 eruption of Arenal Volcano (Szramek et al., 2006). Previous studies only covered either intermediate temperature and low pressure (Liu et al., 2004; Okumura and Nakashima, 2006), or high temperature and high pressure (Behrens et al., 2004). In order to elucidate the pressure influence on H_2O diffusivity in dacite and to further constrain how H_2O diffusivity depends on a wide range of H_2O content, temperature, and pressure, I have performed diffusion-couple experiments at 786-893 K, 0.48-0.95 GPa, and 0-8 wt.% H_2O_t in a piston-cylinder apparatus. My acquired diffusivity data together with previous data allow the construction of a general model of H_2O diffusivity in dacitic melt. Compared to rhyolite, H_2O diffusion in dacite shows a stronger dependence on temperature and water concentration, and its higher activation energy results in slower diffusion in dacite at T<1173 K but more rapid diffusion at T>1323 K than in rhyolite when H_2O_t <5 wt.%. The new diffusivity expression can be applied to both deep-seated magmatic processes and sub-surface volcanic eruptions. This manuscript has been submitted to *Geochimica et Cosmochima Acta*.

Chapter IV is a study on H_2O speciation and diffusion in haploandesite. Fe-free glass is used to represent andesitic composition while avoiding complexities in redox state change and FTIR measurements. Dehydration experiments were carried out at 743-873 K and 100 MPa in cold-seal pressure vessels. The low temperatures and the rapid quench design of the pressure vessel ensure the preservation of equilibrium water speciation. There is more OH in andesite than in rhyolite and in dacite at a given water content. Measured dehydration profiles demonstrate strong positive correlation between H_2O diffusivity and water concentration, which can be rationalized by H_2O_m-dominated diffusive process. H_2O_m and H_2O_t diffusivity models are constructed for haploandesite.

At below 2.5 wt.% H_2O, water diffusivity increases from andesite to dacite to rhyolite at <873 K, and this sequence is reversed at >1608 K. This manuscript has been submitted to *Geochimica et Cosmochimica Acta.*

Chapter V is a theoretical modeling on oxygen isotope fractionation and diffusion between coexisting minerals upon cooling. Based on Fast Grain Boundary model (Eiler et al., 1992), I find that the apparent equilibrium temperature (T_{ae}) defined by the mineral pair with the largest fractionation (PLIF) always lies between their Dodson (1973) closure temperatures. T_{ae} of PLIF may be used to compare thermal history of rocks, estimate cooling rate, or infer oxygen diffusivity.

Appendix A is a compilation of FTIR spectra of starting glasses used in Chapter II, III, IV. Appendices B, C, D, and E contain the data of the diffusion profiles reported in Chapter II, Chapter III, Chapter IV, and four additional diffusion profiles in haploandesite, respectively. Appendix F is a QUICKBASIC subroutine for extracting the best a and D_0 for a diffusion profile using Levenberg-Marquardt algorithm. Appendix G is a QUICKBASIC routine for convoluting a diffusion profile.

REFERENCES

Behrens, H., Zhang, Y., Xu, Z., 2004. H_2O diffusion in dacitic and andesitic melts. Geochim. Cosmochim. Acta 68, 5139-5150.

Behrens, H., Zhang, Y., Leschik, M., Wiedenbeck, M., Heide, G., Frischat, G.H., 2007. Molecular H_2O as carrier for oxygen diffusion in hydrous silicate melts. Earth Planet. Sci. Lett. 254, 69-76.

Dodson, M.H., 1973. Closure temperature in cooling geochronological and petrological systems. Contrib. Mineral. Petrol. 40, 259-274.

Eiler, J.M., Baumgartner, L.P., Valley, J.W., 1992. Intercrystalline stable isotope diffusion: a fast grain boundary model. Contrib. Mineral. Petrol. 112, 543-557.

Gonnermann, H.M., Manga, M., 2003. Explosive volcanism may not be an inevitable consequence of magma fragmentation. Nature 426, 432-435.

Holtz, F., Sato, H., Lewis, J., Behrens, H., Nakada, S., 2005. Experimental petrology of the 1991-1995 Unzen dacite, Japan. Part I: Phase relations, phase chemistry and pre-eruptive conditions. J. Petrol. 46, 319-337.

Liu, Y., Zhang, Y., 2000. Bubble growth in rhyolitic melt. Earth Planet. Sci. Lett. 181, 251-264.

Liu, Y., Zhang Y., Behrens, H., 2004. H_2O diffusion in dacitic melts. Chem. Geol. 209, 327-340.

Navon, O., Chekhmir, A., Lyakhovsky, V., 1998. Bubble growth in highly viscous melts: theory, experiments and autoexplosivity of dome lavas. Earth Planet. Sci. Lett. 160, 763-776.

Ni, H., Zhang, Y., 2008. H_2O diffusion models in rhyolitic melt with new high pressure data. Chem. Geol. 250, 68-78.

Nowak, M., Behrens, H., 1997. An experimental investigation on diffusion of water in haplogranitic melts. Contrib. Mineral. Petrol. 126, 365-376.

Okumura, S., Nakashima, S., 2004. Water diffusivity in rhyolitic glasses as determined by in situ IR spectrometry. Phys. Chem. Minerals 31, 183-189.

Okumura, S., Nakashima, S., 2006. Water diffusion in basaltic to dacitic glasses. Chem. Geol. 227, 70-82.

Press, W.H., Teukolsky, S.A., Vetterling, W.T., Flannery, B.P., 1992. Numerical recipes in Fortran 77: the art of scientific computing, 2nd edition. Cambridge University Press. New York.

Proussevitch, A.A., Sahagian, D.L., 1998. Dynamics and energetics of bubble growth in magmas: analytical formulation and numerical modeling. J. Geophys. Res. 103, 18223-18251.

Robock, A., 2000. Volcanic eruptions and climate. Rev. Geophys. 38, 191-219.

Self, S., Blake, S., 2008. Consequences of explosive supereruptions. Elements 4, 41-46.

Szramek, L., Gardner, J.E., Larsen, J., 2006. Degassing and microlite crystallization of basaltic andesite magma erupting at Arenal Volcano, Costa Rica. J. Volcanol. Geotherm. Res. 157, 182-201.

Tanguy, J.-C., Ribiere, C., Scarth, A., Tjetjep, W.S., 1998. Victims from volcanic eruptions: a revised database. Bull. Volcano. 60, 137-144.

Wilson, L., Sparks, R.S.J., Walker, G.P.L., 1980. Explosive volcanic eruptions-IV. The control of magma properties and conduit geometry on eruption column behaviour. Geophys. J. R. Astron. Soc. 63, 117-148.

Zhang, Y., 1999. A criterion for the fragmentation of bubbly magma based on brittle failure theory. Nature 402, 648-650.

Zhang, Y., Behrens, H., 2000. H_2O diffusion in rhyolitic melts and glasses. Chem. Geol. 169, 243-262.

Zhang, Y., Stolper, E.M., Wasserburg, G.J., 1991. Diffusion of water in rhyolitic glasses. Geochim. Cosmochim. Acta 55, 441-456.

Zhang, Y., Xu, Z., Zhu, M., Wang, H., 2007. Silicate melt properties and volcanic eruptions. Rev. Geophys. 45, RG4004, doi:10.1029/2006RG000216.

CHAPTER II

H$_2$O DIFFUSION MODELS IN RHYOLITIC MELT WITH NEW HIGH PRESSURE DATA

ABSTRACT

Water diffusion in silicate melts is important for understanding bubble growth in magma, magma degassing and eruption dynamics of volcanos. Previous studies have made significant progress on water diffusion in silicate melts, especially rhyolitic melt. However, the pressure dependence of H$_2$O diffusion is not constrained satisfactorily. H$_2$O diffusion in rhyolitic melt is investigated at 0.95-1.9 GPa and 407-1629°C, and 0.2-5.2 wt.% total water (H$_2$O$_t$) content with the diffusion-couple method in a piston-cylinder apparatus. Compared to previous data at 0.1-500 MPa, H$_2$O diffusivity is smaller at higher pressures, indicating a negative pressure effect. This pressure effect is more pronounced at low temperatures. Assuming H$_2$O diffusion in rhyolitic melt is controlled by the mobility of molecular H$_2$O (H$_2$O$_m$), the diffusivity of H$_2$O$_m$ ($D_{H_2O_m}$) at H$_2$O$_t$ $\leq$7.7 wt.%, 403-1629°C, and $\leq$1.9 GPa is given by

$$D_{H_2O_m} = D_0 \exp(aX),$$

with

$$D_0 = \exp\left(13.375 + 1.8875P - \frac{12939 + 3625.6P}{T}\right),$$

and
$$a=-37.256+\frac{75884}{T},$$

where D_0 is in $\mu m^2/s$, X is mole fraction of H_2O_t on a single oxygen basis, T is temperature in K, and P is pressure in GPa.

The H_2O_t diffusivity ($D_{H_2O_t}$, in $\mu m^2/s$) can be calculated from H_2O_m diffusivity, or directly from the following expression:

$$\ln\left(D_{H_2O_t}/X\right)=13.47-49.996X+7.0827\sqrt{X}+1.8875P$$
$$-\frac{9532.3-91933X+13403\sqrt{X}+3625.6P}{T}.$$

At low H_2O_t content (up to 2 wt.% if an error of a factor of 2 is allowed), H_2O_t diffusivity is approximately proportional to H_2O_t content:

$$D_{H_2O_t}=\frac{C}{C_0}\exp\left(9.5279+1.8875P-\frac{9698.5+3625.6P}{T}\right),$$

where C is H_2O_t content in wt.% and C_0 is 1 wt.%. The new expressions for H_2O diffusion not only reproduce the data produced in this laboratory, but also match data in literature from different laboratories and using different methods, indicating good inter-laboratory and multi-method consistency. The new expressions cover a wide range of geological conditions, and can be applied to H_2O diffusion in rhyolitic melts in various volcanic and magmatic processes.

INTRODUCTION

Water is a major volatile component in natural silicate melts. The diffusion of water is necessary to the understanding of a series of volcanic processes, such as bubble

growth (e.g., Liu and Zhang, 2000), magma degassing, and magma fragmentation (Zhang, 1999a). Within natural melts, rhyolite has been the most thoroughly investigated with respect to H_2O diffusion due to common occurrences of explosive rhyolitic eruptions. Early workers used measurements involving bulk hydration/dehydration (Shaw, 1974; Friedman and Long, 1976; Jambon, 1979) or the ion microprobe (Delaney and Karsten, 1981; Karsten et al., 1982; Lapham et al., 1984). They demonstrated H_2O diffusivity in rhyolitic melt increases with its concentration. Infrared and NMR studies (e.g., Orlova, 1962; Bartholomew and Schreurs, 1980; Stolper, 1982) showed that water is present in silicate melts as at least two species: molecular H_2O (H_2O_m) and hydroxyl group (OH). Therefore, in order to understand the fundamental mechanism of H_2O diffusion in melts, it is instructive to understand the role of water speciation in diffusion (Wasserburg, 1988).

Zhang et al. (1991) investigated the dehydration of rhyolite samples with total H_2O content (H_2O_t) <2 wt.% at low temperatures (403-530°C), which allows the concentrations of the two H_2O species preserved through quenching for infrared determination (Zhang et al., 1995, 1997a; Withers et al., 1999). They concluded that H_2O_m is the dominant diffusing species, whereas OH is almost immobile and its concentration profile is due to species conversion to maintain equilibrium. Furthermore, they assumed concentration-independent H_2O_m diffusivity and modeled the concentration profiles well. Later, it was found that the concentration-independent H_2O_m diffusivity assumption of Zhang et al. (1991) cannot be extended to high H_2O content (up to 9.1 wt.%) (Behrens and Nowak, 1997; Nowak and Behrens, 1997). Zhang and Behrens (2000) proposed that H_2O_m diffusivity increases exponentially with H_2O_t and successfully

reconciled all the experimental data covering a fairly wide range of temperature (403-1215°C), pressure (0.1-810 MPa) and water content (0.1-7.7 wt.%). [The exponential dependence of the diffusivity of a neutral molecular or atomic species has also been observed for CO_2 (Watson, 1991) and Ar (Behrens and Zhang, 2001).] Okumura and Nakashima (2004) reported new H_2O diffusion data using *in situ* measurements of dehydration experiments. Behrens et al. (2007) investigated both H_2O and ^{18}O diffusion at 100 MPa from hydration experiments, demonstrating H_2O_m is the carrier of ^{18}O diffusion. Other natural melts that have been investigated for H_2O diffusion include basalt (Zhang and Stolper, 1991; Okumura and Nakashima, 2006), andesite (Behrens et al., 2004, Okumura and Nakashima, 2006), dacite (Behrens et al., 2004, Liu et al., 2004, Okumura and Nakashima, 2006), and trachyte (Freda et al., 2003).

This study focuses on H_2O diffusion in rhyolitic melt. Although H_2O diffusion in rhyolite has been investigated extensively, the pressure dependence of H_2O diffusivity has not been well resolved, compared to temperature and water concentration dependence, as pointed out by Zhang and Behrens (2000) and Zhang et al. (2007). The majority of the experiments that constrained the dependence of diffusivity on H_2O content in Zhang and Behrens (2000) were obtained at 500 MPa. Therefore, application of their model to pressures other than 500 MPa may not be accurate. Behrens et al. (2007) noted that the dependence of H_2O diffusivity on H_2O content at 100 MPa differs from that predicted by Zhang and Behrens (2000). Because volcanic eruption is a decompressional process as the magma is upwelling, the pressure effect on H_2O diffusivity is crucial and needs to be evaluated more accurately. To fulfill such a need, I carried out an experimental investigation on H_2O diffusion at 0.95-1.9 GPa and 407-

1629°C, so that the pressure range (0-1.9 GPa) is large enough to constrain the pressure effect and to infer H_2O diffusivity at <0.5 GPa for modeling bubble growth and volcanic degassing. (Diffusion experiments at low pressure such as 0.1 MPa and high H_2O_t content cannot be accomplished because of bubble formation.) This study makes the rhyolitic system the first for which H_2O diffusivity is known as a function of temperature (400-1630°C), pressure (0-2 GPa) and H_2O content (0-8 wt.%).

EXPERIMENTAL AND ANALYTICAL METHODS

Starting materials

One of the starting materials, the anhydrous rhyolitic glass CIT, is a natural sample from Coso Range, California (Newman et al., 1986), containing small amounts of microlites and bubbles. These imperfections are not expected to have much effect on H_2O diffusion. The water content is 0.20-0.22 wt.%. Hydrous rhyolitic glasses with H_2O_t content of 4 to 5 wt.% are synthesized by loading dry glass powder and water into $Au_{80}Pd_{20}$ capsules in alternating portions and heated at 1000°C and 500 MPa for 3 days in an internally heated pressure vessel (IHPV) at University of Hannover, Germany. Sample GMR+2 is synthesized at 1400°C overnight from dry rhyolitic glass from Glass Mountain, California (Hui et al., 2008a). These rapidly quenched (initially 200°C/min under isobaric conditions) hydrated samples are transparent and free of crystals and bubbles, and contain 2.3 wt.%, 4.0 wt.%, and 5.2 wt.% H_2O_t homogeneously distributed (<3% relative variability). All anhydrous and hydrous rhyolite glasses are light brown in color, and are analyzed with a Cameca SX100 electron microprobe at the University of

Michigan. The dry compositions of all rhyolite samples used in this study are similar, as reported in Table 2.1, except for a slightly lower silica content for GMR-2. No significant difference in H_2O diffusivity between GMR-2 and other samples was noticed. Anhydrous rhyolite cylinders of 1.2-1.5 mm thickness, and hydrous cylinders of 2.5-2.9 mm thickness were prepared and doubly polished for infrared analysis and subsequent diffusion-couple experiments.

Diffusion-couple experiments

Diffusion-couple experiments were carried out in a 0.5″ end-loaded piston-cylinder apparatus at the University of Michigan. Anhydrous and hydrous rhyolitic glass cylinders of the same diameter (~2.4 mm) were placed into a platinum tube that was welded shut. The less dense hydrous half was always on top of the anhydrous half to mitigate convection. Crushable MgO rod and a $BaCO_3$ cell were used as pressure medium inside and outside the graphite furnace, respectively.

The experimental temperature was monitored by a type D thermocouple (Re_3W_{97}-$Re_{25}W_{75}$) and simultaneously recorded by a computer program. In high temperature runs (1118-1629°C), water diffusion is rapid and only a short duration (2-10 min) is necessary. Therefore, a stepwise heating procedure was programmed with a Eurotherm controller so that it took only ~24 s from the relaxation temperature (200°C) to the target temperature with only small overheating of 1-4°C. Because the experimental durations of low temperature runs (407-609°C) were relatively long (>24 hours), manual heating was applied and it took ~1 minute to reach the target temperature from the relaxation temperature of 100°C. The temperature fluctuation during the experiments was generally

Table 2.1 Composition of rhyolitic glasses (wt.% on anhydrous basis)

	CIT	GMR+2	Rhy4	Rhy5
SiO_2	76.93	73.12	76.87	76.05
TiO_2	0.05	0.28	0.04	0.10
Al_2O_3	13.18	14.49	13.38	13.93
FeO_T	0.94	1.35	0.97	0.75
MnO	0.04	0.06	0.04	0.04
MgO	0.02	0.29	0.03	0.12
CaO	0.44	1.30	0.55	0.87
Na_2O	4.29	4.27	4.14	4.01
K_2O	4.62	4.36	4.65	4.22
P_2O_5	0.04	0.09	0.01	0.07
Total	100.55	99.61	100.68	100.16
H_2O (IR)	0.20	2.27	3.96	5.17

Five analyses averaged for each sample. Analyses are made on a Cameca SX100 electron microprobe using a scanning beam of 5 mm raster length, 15 kV voltage, and 4 nA current. Raw oxide contents are divided by $(1-c/100)$ so as to normalize to dry composition, where c is the water content from infrared analysis in wt.%.

within ±1°C, but spikes of ±5°C were observed for several brief periods (~5 s) in long experiments. Experimental assemblages were rapidly quenched (with a mean cooling time scale of 8 s based on Zhang et al., 2000) by chilled water after turning off the power. A typical thermal history of high temperature runs, including relaxation, dwelling, and quenching, is plotted in Fig. 2.1. Effective duration accounting for diffusion during heating and cooling was estimated to be 12-16 s by assuming an activation energy of 100 kJ/mol for water diffusion, based on the method described in Zhang and Behrens (2000). Adjustment of about 20 s (including the effect of temperature spikes) for long duration experiments (>24 h) is negligible and not applied. Temperature at the center of the experimental charge is the thermocouple temperature plus a correction based on the calibrated temperature gradient inside the charge (Hui et al., 2008a). The overall uncertainty in temperature is estimated to be 10 K.

The pressure is manually kept at either 1 or 2 GPa using a piston-out procedure. Based on my pressure calibration on this piston-cylinder apparatus, the real pressure is roughly 5% lower than nominal pressure based on quartz-coesite transition (3.09 GPa at 798°C) against the phase boundary determined by Bose and Ganguly (1995). A similar calibration was carried out on another piston-cylinder apparatus in our lab by Hui et al. (2008a), and the correction is 6%. More details about the pressure calibration can be found in Hui et al. (2008a). Uncertainty associated with pressure is ~50 MPa.

At about 2 GPa, the hydrous rhyolite, especially those having high water content, readily crystallizes when the temperature is above 480°C, and the liquidus of dry rhyolite increases with pressure. These considerations significantly limit the experimental temperature range. Details of the eight successful experiments can be found in Table 2.2.
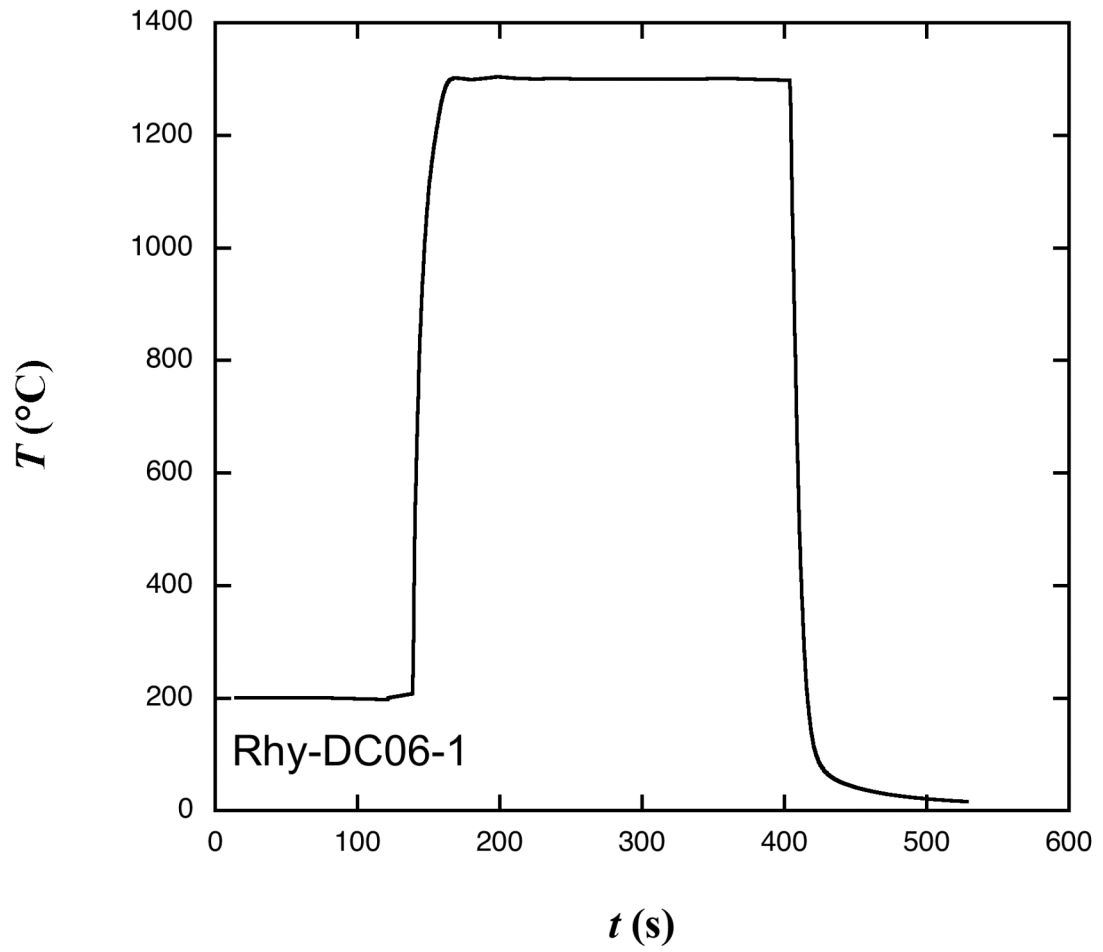
Fig. 2.1. Thermal history of experiment Rhy-DC06-1, starting from stress relaxation at 200°C and ending with quenching. The effect of heating up and quenching down on diffusion is equivalent to an extra 13 seconds at the experimental temperature.

Six other runs are deemed unsuccessful and not reported because of partial to complete crystallization of the hydrous half, or poor contact between the two halves.

Infrared analysis

Water contents of starting samples were measured with Fourier transform infrared (FTIR) spectrometry, in the dry and N_2-purged main chamber of the FTIR (Perkin-Elmer Spectrum GX) at the University of Michigan. Doubly polished rhyolite cylinders were attached to a sample holder with pinhole of 531 μm diameter. A NIR source, CaF_2 beamsplitter, and liquid nitrogen cooled InSb detector were used for 64 scans from 9000 to 2000 cm^{-1}.

After a diffusion-couple experiment the quenched sample in Pt capsule was mounted into epoxy resin and a doubly polished section of 200-250 μm thickness was prepared along the cylindrical axis for FTIR microscopy. The thinness reduces the refractive divergence of the infrared beam inside the sample, while still affording reasonable absorbance at the same time. After high temperature runs the glasses usually become lighter colored than their pre-annealing counterparts. Cracks roughly parallel to the interface in the experimental charge, presumably due to shrinkage during quenching, are always present and are a major source of difficulty and error for the FTIR measurements. For some wide cracks, distances must be subtracted to smooth the concentration profile across the cracks.

The Autoimage microscope system, with an MCT (mercury cadmium telluride) detector cooled by liquid nitrogen, is attached to the Spectrum GX spectrometer for the analysis of H_2O concentrations along the diffusion profile. The aperture is 20 μm wide

and 200 μm long, but an edge response analysis shows that the spatial distribution of the infrared signal is roughly Gaussian with a full width at half maximum (FWHM) under analysis conditions being about 30 μm. That is, the spatial resolution is much worse than 20 μm. This convolution effect is important for short profiles (<200 μm long) but negligible for longer profiles (>500 μm long), and will be treated further in Discussion.

A complete diffusion profile, typically 40-80 points, was acquired with background updated after every 5-10 points. Spectra were hand-fitted with two straight tangential baselines (TT method of Withers and Behrens, 1999) at 5230 cm^{-1} and 4500 cm^{-1}. Peak heights were measured to calculate molecular H_2O (H_2O_m) and hydroxyl group (OH) concentrations, respectively, using the calibration of Withers and Behrens (1999). The sum of H_2O_m and OH is H_2O_t concentration. Although the calibration of Withers and Behrens (1999) may not be able to retrieve accurate species concentration as that of Zhang et al. (1997b) at relatively low H_2O_t (≤ 2.7 wt.%), it can be applied to H_2O_t up to 9.2 wt.% and is less time-consuming for processing a large amount of spectra.

EXPERIMENTAL RESULTS

Details of the eight successful experiments are listed in Table 2.2. All H_2O_t diffusion profiles are illustrated in Fig. 2.2. Owing to reactions during quench, H_2O_m and OH concentrations from experiments at >700°C (depending on H_2O_t content) do not represent their concentrations under experimental conditions. Therefore, directly measured species concentrations are not used for modeling H_2O diffusion.

Table 2.2 Conditions of diffusion-couple experiments

Run #	T (°C)[a]	P (GPa)[b]	Duration (s)[c]	H_2O_t (wt.%) in the two halves	
				Initial	Final
Rhy-DC06-1	1319/1300	1.9/2.0	252/239	4.0/0.2	4.0/0.2
Rhy-DC06-6	1323/1300	1.9/2.0	587/575	2.3/0.2	2.3/0.2
Rhy-DC06-7	1629/1600	1.9/2.0	128/112	5.2/0.2	5.2/0.2
Rhy-DC06-8	609/600	1.9/2.0	86 400	2.3/0.2	2.5/0.2
Rhy-DC06-9	407/400	1.9/2.0	720 000	5.2/0.2	5.3/0.2
Rhy-DC06-11	1118/1100	1.9/2.0	624/611	5.1/0.2	5.1/0.2
Rhy-DC07-12	1321/1300	0.95/1.0	248/236	5.1/0.2	5.1/0.2
Rhy-DC07-14	1120/1100	1.9/2.0	613/601	5.1/0.2	5.1/0.2

[a] 1319/1300 means that the nominal temperature of the thermocouple is 1300°C. 1319°C is the corrected temperature based on the calibrated temperature profile.
[b] 1.9/2.0 means that the nominal pressure is 2.0 GPa, 1.9 GPa is the corrected pressure based on quartz-coesite transition against the phase boundary determined by Bose and Ganguly (1995). Pressure is manually controlled at ±20 MPa during diffusion runs.
[c] 252/239 means that the nominal duration is 239 s, and the effective duration after considering diffusion during heating up and cooling down is 252 s.
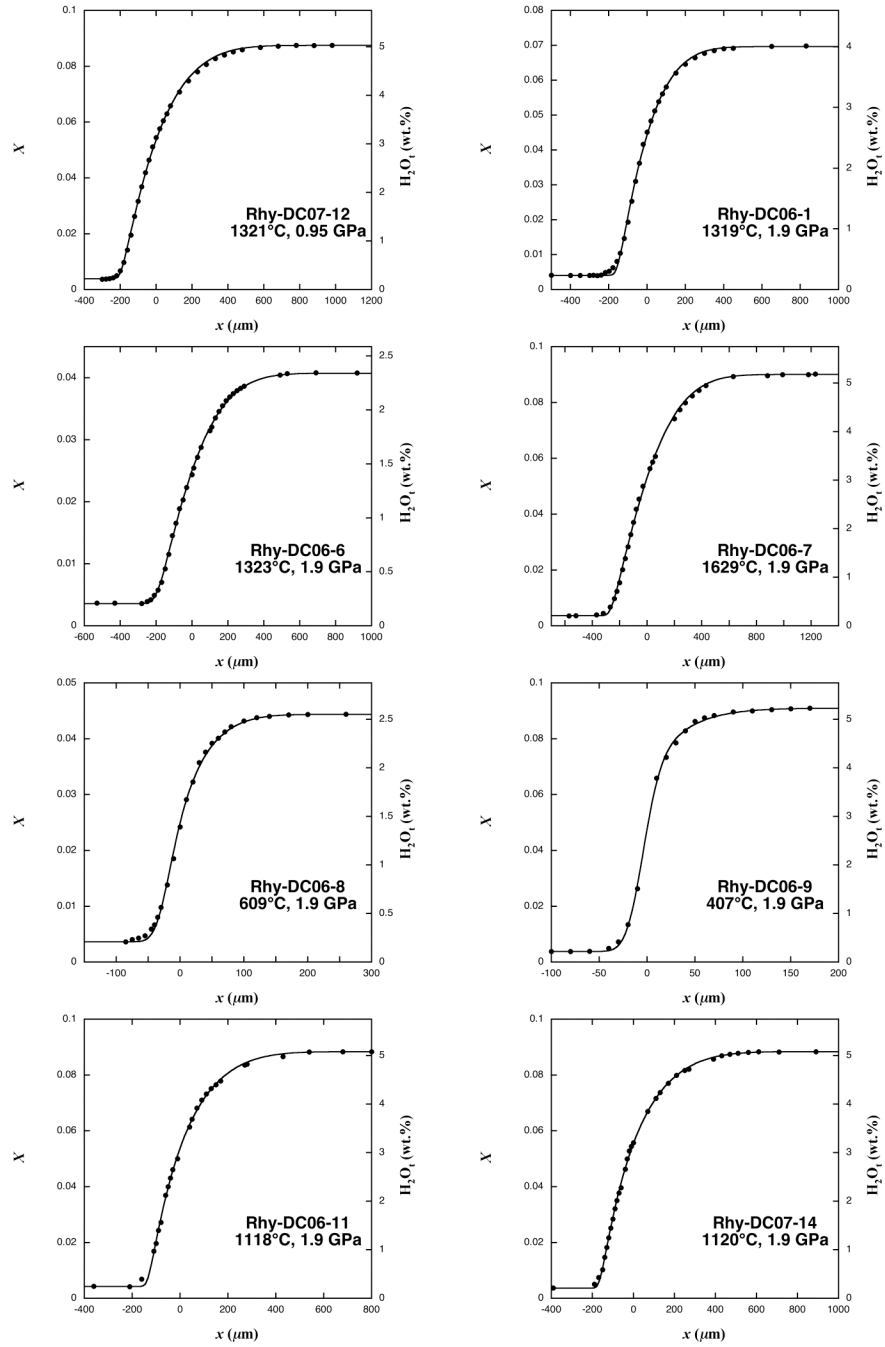
Fig. 2.2. Diffusion profiles of eight experiments. A crack of 30 μm near the interface is subtracted for Rhy-DC06-9 to smooth the diffusion profile. Solid curves are best fit by Eqs. (2-5) and (2-6), with $\ln D_0$ reported in Table 2.4. Convolution effect is applied for Rhy-DC06-8 and Rhy-DC06-9 (see text). There are data points outside the distance range, which are not shown in order to display the data more clearly.

Far away from the contact between the two halves in a diffusion couple, flat regions of H_2O_t concentration are achieved for all runs, and the averages agree well with the starting glasses (Table 2.2). Hence, the diffusive transport of H_2O from the hydrous half to the anhydrous half can be treated as diffusion in an infinite medium. Outside the flat region of the anhydrous and hydrous ends and near the capsule, water concentrations may differ from the initial concentrations, attributed to transport along cylinder walls (Zhang and Behrens, 2000). These measured points are excluded from the final data; they are not shown in Fig. 2.2 and not used for extracting H_2O diffusivity. Diffusion profiles at high temperatures are usually longer and better resolved than those at lower temperatures. Because H_2O diffusivity depends on water content, the diffusion profiles do not resemble error function curves, and it is necessary to consider the dependence of diffusivity on H_2O concentration when modeling these profiles.

This study significantly expands the experimental *P-T* conditions of H_2O diffusion in rhyolitic melts. Fig. 2.3 summarizes the coverage of *P-T*-H_2O_t conditions including data in this and previous studies. The extensive investigations on a wide range of temperature (400-1630°C), pressure (0-2 GPa), and H_2O_t (0-8 wt.%) allow the construction of a comprehensive model on H_2O diffusivity in rhyolitic melt, which can be applied to almost all relevant geologic conditions.

DISCUSSION

Modeling diffusion profiles

The equation describing the diffusion of total H_2O (H_2O_t) is as follows:
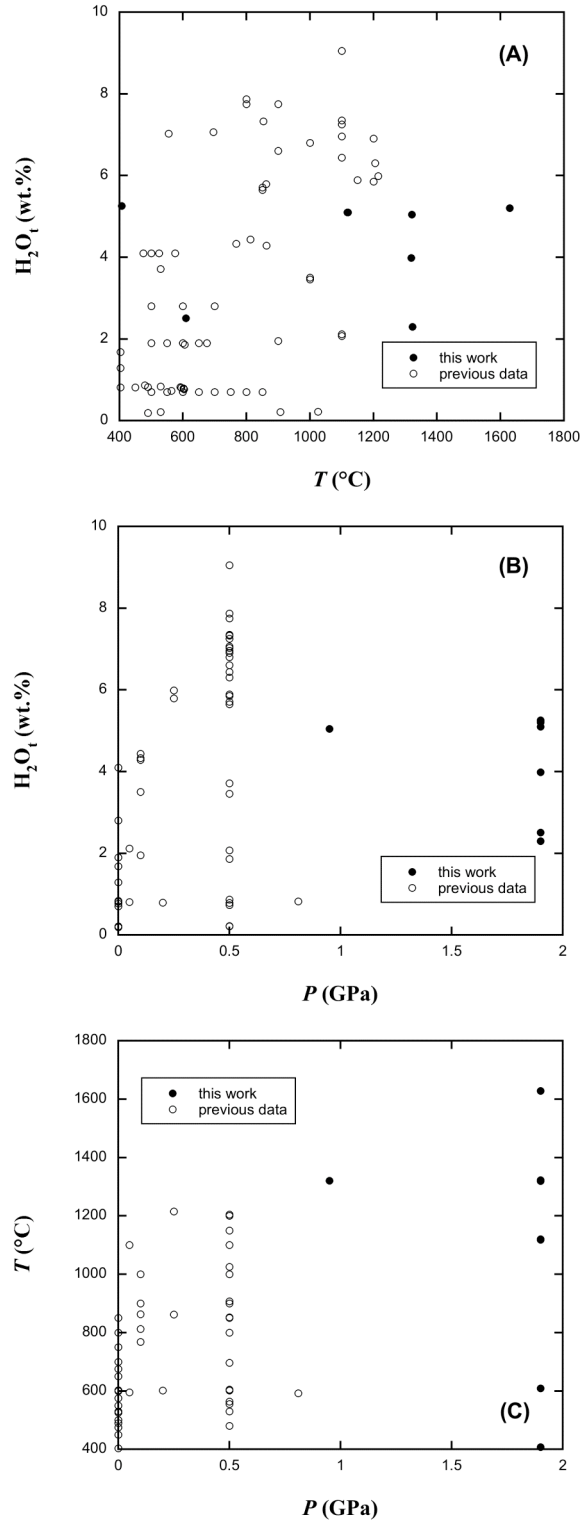
Fig. 2.3. Coverage of experimental conditions from this work (solid circles) and previous work (open circles) of Zhang et al. (1991), Nowak and Behrens (1997), Zhang and Behrens (2000), Okumura and Nakashima (2004), and Behrens et al. (2007).

21

$$\frac{\partial X}{\partial t} = \frac{\partial}{\partial x}\left(D_{H_2O_t}\frac{\partial X}{\partial x}\right), \tag{2-1}$$

where X is mole fraction of H_2O_t on a single oxygen basis (Stolper, 1982; Zhang, 1999b) and is calculated as $X = C/18.015/[C/18.015+(100-C)/32.49]$ with C being H_2O_t content in wt.%, t is time, x is distance, and $D_{H_2O_t}$ is H_2O_t diffusivity which depends on H_2O concentration (and therefore depends on x). A common approach for obtaining the concentration dependence of the diffusivity is to use the Boltzmann-Matano method. This method is independent of presumptions of the relation between diffusivity and concentration, but the precision of this method is not high (Zhang and Behrens, 2000). An alternative approach is to assume a diffusivity-concentration relation, and whether such an assumption is reasonable can be judged from the quality of the fitting. Because molecular H_2O (H_2O_m) and hydroxyl (OH) may contribute distinctly to H_2O diffusion, the mechanistic approach to H_2O diffusion is to consider the contribution of the two water species (H_2O_m and OH) separately:

$$\frac{\partial X}{\partial t} = \frac{\partial}{\partial x}\left(D_{H_2O_m}\frac{\partial X_m}{\partial x} + D_{OH}\frac{\partial X_{OH}/2}{\partial x}\right), \tag{2-2}$$

where $D_{H_2O_m}$ and X_m are diffusivity and mole fraction of molecular H_2O, and D_{OH} and X_{OH} are diffusivity and mole fraction of hydroxyl group. Zhang et al. (1991) and Zhang and Behrens (2000) concluded that H_2O_m is the dominating diffusion species, and OH is almost immobile. Then Eq. (2-2) reduces to

$$\frac{\partial X}{\partial t} = \frac{\partial}{\partial x}\left(D_{H_2O_m}\frac{\partial X_m}{\partial x}\right). \tag{2-3}$$

If the reaction $H_2O_m+O \rightleftharpoons 2OH$ is in equilibrium, X_m can be determined from X using Eq. (13) in Zhang (1999b). The equilibrium constant was determined by Zhang et al.

(1997b). By comparing Eqs. (2-1) and (2-3), one can find the relation between $D_{H_2O_t}$ and $D_{H_2O_m}$:

$$D_{H_2O_t} = D_{H_2O_m} \frac{dX_m}{dX} .$$

(2-4)

Zhang and Behrens (2000) proposed that molecular H_2O diffusivity depends exponentially on total H_2O content:

$$D_{H_2O_m} = D_0 \exp(aX),$$

(2-5)

where a is a parameter depending on temperature and pressure. They used a trial-and-error method to estimate the value of a. This model fits all the diffusion profiles well. Furthermore, diffusivity of molecular species such as CO_2 and Ar has been shown to depend on H_2O_t exponentially (Watson, 1991; Behrens and Zhang, 2001).

I also assume Eq. (2-5) in treating H_2O diffusion profiles. The program code of Zhang and Behrens (2000) is revised so that the parameter a is determined from the fitting rather than by trial and error. Because of this improvement, the uncertainty on the parameter a can also be evaluated (which was the main purpose of revising the code). Hence, in the new code, a and D_0 are to be determined by fitting the profile, among which a is largely determined by the shape of the diffusion profile, and D_0 largely by the length of the diffusion profile (and the value of a). In the new fitting, the Levenberg-Marquardt algorithm (Press et al., 1992) is adopted to calculate new values of the fitting parameters in each iteration until the sum of the squares of residuals is minimized.

The new fitting procedure was successfully applied to the six diffusion profiles acquired at >1100°C and all are well fit. Two other profiles (Rhy-DC06-8 and Rhy-DC06-9) are not sufficiently long compared to the spatial resolution of FTIR microscope

(~30 μm in terms of FWHM). Hence, they are likely distorted and prolonged by the convolution effect (Ganguly et al., 1988) and cannot be used to extract best-fit a. To maintain consistency and find the errors of the best-fit a values, the new fitting procedure was also applied to the profiles at 250-500 MPa in Zhang and Behrens (2000). All best-fit a values (Table 2.3) apparently form a linear trend with $1/T$ (Fig. 2.4A), without much dependence on pressure. A weighted linear regression yields

$$a=(-37.256\pm1.863)+\frac{75884\pm2286}{T},\qquad(2\text{-}6)$$

where T is in K. The above equation differs from the expression of a in Zhang and Behrens (2000), who noticed a dependence of a on pressure with data for a small pressure range. With a larger pressure coverage by combining this study and previous studies, the pressure dependence of a is within experimental uncertainty. With a values from Eq. (2-6), all diffusion profiles, including those reported in Zhang et al. (1991) and Zhang and Behrens (2000), are refit to find the best D_0.

For the two short profiles (Rhy-DC06-8 and Rhy-DC06-9), the fitting procedures differ from the other profiles, to examine the convolution effect. A convoluted profile is computed from the theoretical profile by assuming a Gaussian distribution of infrared signal with FWHM = 30 μm. The convoluted profile is then used to fit the measured profile. The excellent fitting (Fig. 2.2) further verifies the effect of convolution. Similar convoluting procedure is also tested on long profiles such as Rhy-DC07-12, and the difference is negligible and therefore not applied.

All fitting results are reported in Table 2.4. The precision of diffusion-couple experiments are generally better than dehydration experiments. Fits of profiles from this

Table 2.3

Best-fit a values from fitting profiles with the assumption of $D_{\text{H}_2\text{O}_\text{m}} = D_0\exp(aX)$

Run #	T (°C)	P (GPa)	t (s)	a	R^2	source
Rhy-DC07-12	1321	0.95	248	13.53±1.43	0.9998	1
Rhy-DC06-7	1629	1.9	128	6.46±1.86	0.9996	1
Rhy-DC06-6	1323	1.9	587	7.91±3.69	0.9997	1
Rhy-DC06-1	1319	1.9	252	9.04±3.80	0.9994	1
Rhy-DC07-14	1120	1.9	613	16.82±1.88	0.9996	1
Rhy-DC06-11	1118	1.9	624	17.74±3.07	0.9993	1
Rhy-DC1	900	0.5	120	31.76±8.49	0.9978	2
Rhy-DC3	696	0.5	720	39.42±4.99	0.9978	2
Rhy-DC4	853	0.5	240	32.18±4.79	0.9961	2
Rhy-DC5a	555	0.5	9090	55.35±0.58	0.9991	2
Rhy-DC9	1205	0.5	1060	17.48±1.15	0.9998	2
KS&3-D16P	530	0.5	68 520	60.24±7.30	0.9959	2
Rhy-DC10	862	0.25	1920	24.96±2.01	0.9985	2
Rhy-DC11	1215	0.25	1360	7.07±1.19	0.9993	2

Errors of parameter a are given at 2σ level. Source of data: (1) = this work; (2) = refit of data in Zhang and Behrens (2000).
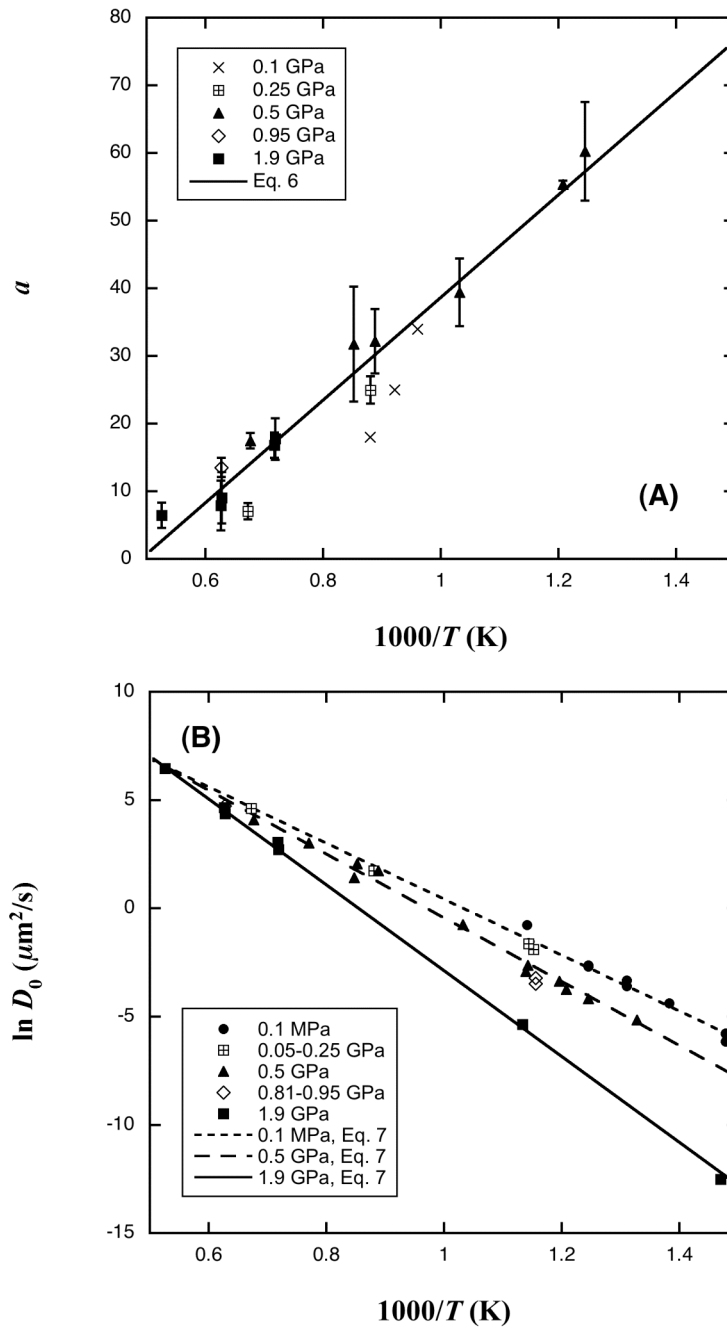
Fig. 2.4. (A) Best-fit *a* values (Table 2.3) from experiments of this work at 0.95-1.9 GPa and those of Zhang and Behrens (2000) at 0.25-0.5 GPa. The straight line is from Eq. (2-6). Three values at 0.1 GPa from Behrens et al. (2007) are also shown for comparison. (B) Best-fit $\ln D_0$ values reported in Table 2.4. Straight lines are from Eq. (2-7).

26

Table 2.4 Least-squares fitting results

Run #	T (°C)	P (MPa)	H_2O_t	$\ln D_0$	R^2	source
Dehydration experiments						
KS-D2	530	0.1	0.84	-2.69±0.21	0.9884	1
PD-D5	530	0.1	0.22	-2.62±0.15	0.9887	1
KS-D3	490	0.1	0.82	-3.59±0.10	0.9944	1
PD-D4	490	0.1	0.19	-3.33±0.23	0.9890	1
KS-D5A	450	0.1	0.82	-4.38±0.15	0.9889	1
3b-D4N	403	0.1	1.68	-5.78±0.15	0.9927	1
3b-D4	403	0.1	1.29	-5.80±0.08	0.9969	1
KS-D4A	403	0.1	0.81	-6.15±0.23	0.9866	1
KS-D14	603	0.1	0.77	-0.77±0.18	0.9778	2
KS-D13P	595	50	0.81	-1.90±0.09	0.9933	2
KS-D19P	601	200	0.79	-1.63±0.14	0.9822	2
KS-D18P.1	592	810	0.81	-3.22±0.10	0.9866	2
KS-D18P.2	592	810	0.83	-3.47±0.21	0.9782	2
KS-D12P	602	500	0.79	-2.63±0.08	0.9977	2
KS-D23P	563	500	0.74	-3.36±0.14	0.9884	2
KS-D24P	480	500	0.86	-5.15±0.11	0.9939	2
Rhy-D12P	605	500	1.86	-2.91±0.07	0.9979	2
SRhy-DAr1	907	500	0.21	1.43±0.19	0.9831	2
SRhy-DAr2	1025	500	0.22	3.02±0.10	0.9956	2
KS&3-D16P	530	500	3.72	-4.17±0.07	0.9958	2
Diffusion-couple experiments						
Rhy-DC1	900	500	7.7/0.1	2.05±0.12	0.9975	2
Rhy-DC3	696	500	7.1/0.2	-0.73±0.11	0.9975	2
Rhy-DC4	853	500	7.3/0.2	1.75±0.11	0.9960	2
Rhy-DC5a	555	500	7.0/0.1	-3.75±0.09	0.9984	2
Rhy-DC9	1205	500	6.3/0.2	4.09±0.04	0.9996	2
Rhy-DC10	862	250	5.8/0.1	1.74±0.06	0.9976	2
Rhy-DC11	1215	250	6.0/0.1	4.62±0.04	0.9980	2
Rhy-DC07-12	1321	950	5.0/0.2	4.73±0.03	0.9996	3
Rhy-DC06-1	1319	1900	4.0/0.2	4.37±0.05	0.9994	3
Rhy-DC06-6	1323	1900	2.3/0.2	4.65±0.03	0.9997	3
Rhy-DC06-7	1629	1900	5.2/0.2	6.47±0.05	0.9994	3
Rhy-DC06-8*	609	1900	2.5/0.2	-5.36±0.07	0.9991	3
Rhy-DC06-9*	407	1900	5.3/0.2	-12.52±0.08	0.9996	3
Rhy-DC06-11	1118	1900	5.1/0.2	2.72±0.05	0.9993	3
Rhy-DC07-14	1120	1900	5.1/0.2	3.05±0.04	0.9996	3

The fitting assumes that $D_{H_2O_m} = D_0\exp[(-37.256+75884/T)X]$ where D_0 is to be determined from fits. *: The theoretical profile is convoluted first and then used to fit experimental data (see text). Source of data: (1) = Zhang et al. (1991); (2) = Zhang and Behrens (2000); (3) = this work. Errors for $\ln D_0$ are from least squares fitting and are given at 2σ level.

work are plotted as solid curves together with data points in Fig. 2.2, and they match excellently.

D_0 values (in $\mu m^2/s$) in Table 2.4 are plotted in Fig. 2.4B. At a fixed pressure, the temperature dependence follows the Arrhenius relation despite crossing the glass transition. D_0 decreases from 0.1 MPa to 0.5 GPa to 1.9 GPa, and this negative pressure effect is more pronounced at low temperatures, but becomes minimal at >1200°C. Hence, at a given pressure, $\ln D_0 = \ln A - E_a/(RT)$, where E_a is the activation energy, R is the gas constant, and A is the pre-exponential factor. When the pressure dependence is examined, not only is the activation energy dependent on pressure, but also $\ln A$. Parameter D_0 can be fit as a function of temperature and pressure as follows:

$$\ln D_0 = (13.375 \pm 0.483) + (1.8875 \pm 0.5179)P$$
$$- \frac{(12939 \pm 489) + (3625.6 \pm 647.2)P}{T} \cdot \qquad (2\text{-}7)$$

where D_0 is in $\mu m^2/s$, T is in K, and P is in GPa. Eq. (2-7) reproduces all $\ln D_0$ data with a 2σ error of 0.49 and a maximum error of 0.63. If $\ln D_0$ was fit without the extra pressure term (the dependence of $\ln A$ on P), the 2σ error would be 1.35, too large to be tolerated. The activation energy (E_a) of D_0 increases from 108 ± 4 kJ/mol at 0.1 MPa to 123 ± 5 kJ/mol at 0.5 GPa to 165 ± 11 kJ/mol at 1.9 GPa.

The extra pressure term in addition to the pressure dependence of the activation energy may be explained in two ways. First, the extra term would result if the activation volume depends on temperature. Starting from Lasaga (1998),

$$\ln D = \ln A_0 - \frac{E_0 + P\Delta V_a}{RT}, \qquad (2\text{-}8)$$

we have:

$$\ln D = \ln A_0 - \frac{E_0 + P(\Delta V_0 - mRT)}{RT} = \ln A_0 + mP - \frac{E_0 + P\Delta V_0}{RT}, \qquad (2\text{-}9)$$

where P is pressure, A_0 is the pre-exponential factor at zero pressure, m is a coefficient, E_0 is the activation energy at zero pressure, and ΔV_a is the activation volume that is expressed as a linear function of temperature. Because the temperature range in H_2O diffusion studies is large (400-1600°C), the temperature dependence of the activation volume is needed to account for the data. The activation volume for H_2O_m diffusion at low H_2O_t can be calculated from $-RT\partial\ln D_0/\partial P$ using Eq. (2-7), and is 30±5 cm^3/mol at 0 K and linearly decreases to about 15 cm^3/mol at 965 K and to 0 at 1921 K. In comparison, Nogami and Tomozawa (1984) reported a huge activation volume of ~170 cm^3/mol at 465 K and ~72 cm^3/mol at 623 K for water diffusion in silica glass based on diffusion data in a small pressure range (<130 MPa).

Another way to explain the extra pressure term is to utilize the "compensation law" (Winchell, 1969; Lasaga, 1998), which states that $\ln A$ is positively and linearly related to the activation energy. Hence, a dependence of the activation energy on pressure would result in a dependence of $\ln A$ on pressure, as in Eq. (2-7).

Diffusivity vs. *T*, *P*, and *X*

In summary, by combining data from this work with that of Zhang et al. (1991) and Zhang and Behrens (2000), molecular H_2O diffusivity may be expressed as follows:

$$D_{H_2O_m} = D_0 \exp(aX), \qquad (2\text{-}10a)$$

with
$$D_0 = \exp\left(13.375 + 1.8875P - \frac{12939 + 3625.6P}{T}\right), \qquad (2\text{-}10b)$$

and
$$a = -37.256 + \frac{75884}{T}.$$
(2-10c)

where T is in K, P is in GPa, D is in $\mu m^2/s$, and X is mole fraction of H_2O_t on a single oxygen basis. From $D_{H_2O_m}$ above, total H_2O diffusivity can be obtained as follows (Zhang, 1999b):

$$D_{H_2O_t} = D_{H_2O_m} \frac{dX_m}{dX},$$
(2-11a)

with
$$\frac{dX_m}{dX} = \frac{16X}{b} - \frac{8X^2}{b^2}\left[8 - 2K + \frac{8K - 2K^2(1-2X) - 16KX}{\sqrt{K^2(1-2X)^2 + 16KX(1-X)}}\right],$$
(2-11b)

$$b = 8X + K(1-2X) + \sqrt{K^2(1-2X)^2 + 16KX(1-X)},$$
(2-11c)

and
$$K = \exp\left(1.876 - \frac{3110}{T}\right).$$
(2-11d)

This model can be used to calculate H_2O_m and H_2O_t diffusivity from 403-1629°C, 0-1.9 GPa, and 0.1-7.7 wt.% water content. In order to calculate total H_2O diffusivity using the above procedures, the H_2O_m diffusivity must be used in conjunction with the speciation model of Eq. (2-11d) (Zhang et al., 1997b), because unlike H_2O_t diffusivity, H_2O_m diffusivity cannot be directly extracted from diffusion profiles and its value depends on the expression of K. Since K at low pressures is used and it may not apply to high pressure, $D_{H_2O_m}$ from Eqs. (2-10a, b, and c) may not be accurate, but $D_{H_2O_t}$ is still accurate as long as self-consistency is maintained. If a new expression of K as a function of temperature and pressure is adopted in the future (Hui et al., 2008a), Eq. (2-11d) should still be used for calculation of $D_{H_2O_m}$ until new expression of $D_{H_2O_m}$ is obtained using new expressions of K.

The dependence of H_2O_t diffusivity on water content, temperature, and pressure is illustrated in Fig. 2.5. At low water content (<2 wt.%), $D_{H_2O_t}$ is roughly proportional to water content; this dependence becomes exponential as water content is above 2 wt.%. Temperature dependence is always Arrhenian, and the activation energy (E_a) increases with pressure and generally decreases with water content. At 1 wt.% H_2O_t, E_a increases from ~81 kJ/mol at 0.1 MPa to ~109 kJ/mol at 0.95 GPa to ~138 kJ/mol at 1.9 GPa; At 5 wt.% H_2O_t, E_a increases from ~46 kJ/mol at 0.1 MPa to ~74 kJ/mol at 0.95 GPa to ~103 kJ/mol at 1.9 GPa. Pressure reduces H_2O diffusion rate, and the negative pressure effect is more noticeable at low temperatures. For example, at 600°C H_2O_t diffusivity decreases by about one order of magnitude over 1 GPa, whereas at 1200°C it only decreases by a factor smaller than 2 over the same pressure range.

Because the above procedure to calculate $D_{H_2O_t}$ is fairly complicated, for convenience, the following explicit expression is provided to calculate $D_{H_2O_t}$ (in μm^2/s):

$$\ln\left(D_{H_2O_t}/X\right)=a_0+a_1X+a_2\sqrt{X}+a_3P-\frac{a_4+a_5X+a_6\sqrt{X}+a_7P}{T}, \qquad (2\text{-}12)$$

with $a_0 = 13.470$, $a_1 = -49.996$, $a_2 = 7.0827$, $a_3 = 1.8875$, $a_4 = 9532.3$, $a_5 = -91933$, $a_6 = 13403$, $a_7 = 3625.6$, where X is mole fraction of H_2O_t on a single oxygen basis, T is temperature in K, and P is pressure in GPa. Results from Eq. (2-12) agree with those from Eqs. (2-10a) to (2-11d) within 17%, which is smaller than the experimental error. Furthermore, Eq. (2-12) is independent of the speciation model.

When H_2O_t content is below 2 wt.%, $D_{H_2O_t}$ is approximately proportional to H_2O_t content, and the following simple equation is obtained for calculating $D_{H_2O_t}$:
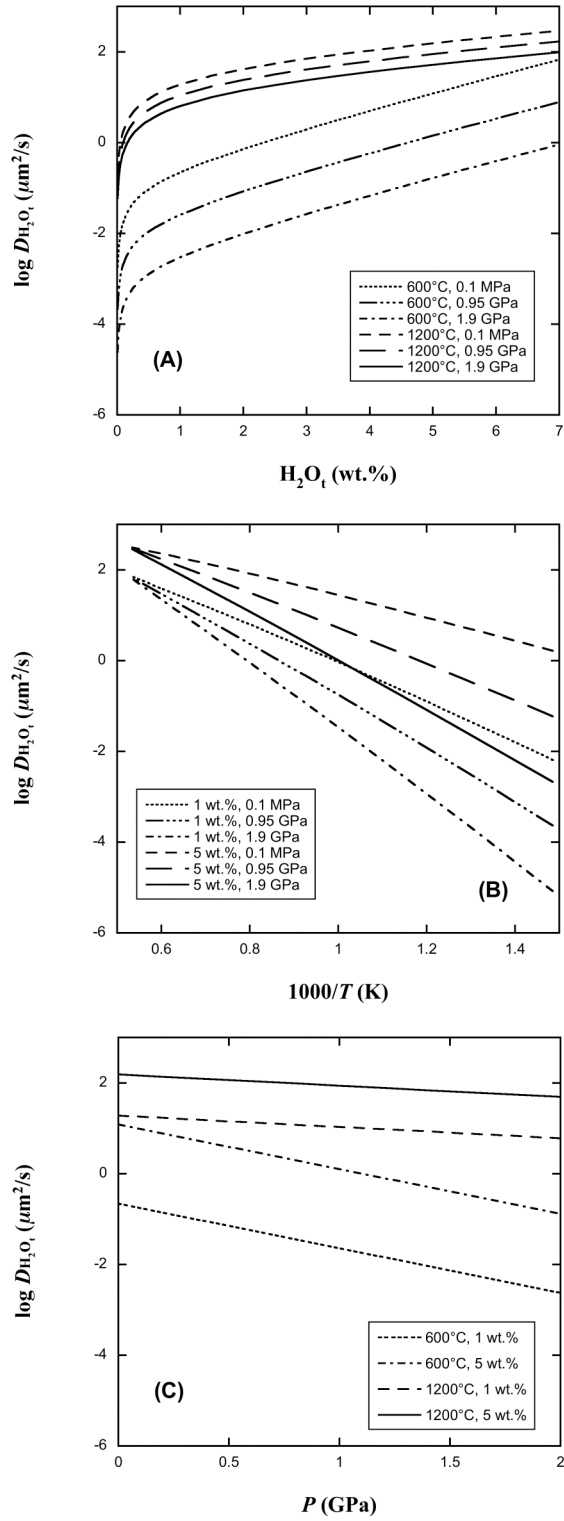
Fig. 2.5. The dependence of total H_2O diffusivity versus (A) water content, (B) temperature, and (C) pressure, respectively. H_2O_t diffusivity is linear with $1/T$ and P, but it first increases with H_2O_t content proportionally, and then exponentially with the transition at ~2 wt.%.

$$D_{H_2O_t} = D° \frac{X}{X_0} = D° \frac{C}{C_0} = \frac{C}{C_0} \exp\left(b_0 + b_1 P - \frac{b_2 + b_3 P}{T}\right), \quad (2\text{-}13)$$

where b_0 = 9.5279±0.0677, b_1 = 1.8875±0.0590, b_2 = 9698.5±74.2, and b_3 = 3625.6±64.7, C is water content in wt.%, and $D°$ is H_2O_t diffusivity at mole fraction of 0.01789 (X_0) or 1 wt.% (C_0).

Implication on melt structure

The decrease of H_2O diffusivity with increasing pressure may be explained as follows. Increasing pressure reduces free space in melt structure, and hence reduces the mobility of neutral molecular species such as H_2O_m. This negative pressure effect on diffusivity is consistent with the observation that viscosity of hydrous rhyolite increases with pressure (Hui et al., 2008b). Therefore, hydrous rhyolite behaves like a depolymerized melt, in which diffusion kinetics is slowed by pressure.

Results from this model lead to an activation volume of zero at 1648°C. Above this temperature, H_2O_m diffusivity would increase with increasing pressure. It is not clear whether there is qualitative change in the melt structure leading to a change in the diffusion behavior. Current experimental data have not covered such high temperatures and hence cannot verify the behavior. Such high temperatures are also much higher than normal temperatures those of rhyolitic melts but could apply momentarily to some impact melts.

The activation energy is lowered by increasing water content. This has been observed repeatedly (e.g., Karsten et al., 1982; Zhang et al., 1991; Zhang and Behrens, 2000; Behrens and Zhang, 2001), and may be attributed to increased porosity with more dissolved water. A lower activation energy at higher H_2O content is also consistent with

the observation that H_2O diffusivity increases more rapidly with water content at low temperatures.

Comparison with other data

In developing the model, some data in the literature was not included. Nowak and Behrens (1997) reported total H_2O diffusivity data at 800-1200°C, 50-500 MPa, and 0.5-6 wt.% water content also based on the diffusion-couple technique. Okumura and Nakashima (2004) investigated H_2O diffusivity <4.1 wt.% at room pressure based on dehydration with *in situ* FTIR. Behrens et al. (2007) studied H_2O diffusivity at 100 MPa from hydration experiments. In particular, Behrens et al. (2007) showed that their data are different from prediction by the model of Zhang and Behrens (2000) by a factor of 2, and attributed the difference to the uncertainty of the pressure effect in the model of Zhang and Behrens (2000). These experimental data are used to evaluate the applicability of my new model.

The comparison between data in Nowak and Behrens (1997) and Behrens et al. (2007) is straightforward. However, Okumura and Nakashima (2004) reported diffusion-out diffusivity, which is some average of $D_{H_2O_t}$ over a concentration range. To compare their data with $D_{H_2O_t}$ at a given H_2O concentration (the initial and maximum H_2O mole fraction, X_i), a conversion factor must be applied. For the case of proportionality between $D_{H_2O_t}$ and X_i, the correction factor is 0.347 (Wang et al., 1996). For the more general case to higher H_2O concentrations, this factor can be calculated from model profiles at a given temperature, i.e., given parameter of a, equilibrium constant K, and X_i. The mass

loss can be found from the model profile of H_2O mole fraction (X) vs. normalized distance ($\xi = x/\sqrt{4D_0 t}$) as

$$M = \int_0^\infty (X_i - X)d\xi. \tag{2-14}$$

It can be derived (Crank, 1975) that the diffusion-out diffusivity D_{out} obtained from mass loss is related to D_0 through

$$\frac{D_{out}}{D_0} = \pi \left(\frac{M}{X_i}\right)^2, \tag{2-15}$$

Combining Eqs. (2-4) and (2-5), $D_{H_2O_t}$ at X_i (D_{X_i}) is related to D_0 through

$$D_{X_i}/D_0 = \exp(aX_i) \cdot (dX_m/dX)_{X_i}. \tag{2-16}$$

Therefore we find the conversion factor as

$$D_{out}/D_{X_i} = \frac{\pi M^2}{X_i^2 \cdot \exp(aX_i) \cdot (dX_m/dX)_{X_i}}. \tag{2-17}$$

The conversion factor thus obtained depends somewhat on temperature, and is ~0.324 for 0.7 wt.%, 0.207-0.243 for 1.9 wt.%, and 0.146-0.198 for 2.8 wt.% H_2O_t, for the temperature range of Okumura and Nakashima (2004). Their H_2O_t diffusivities at 4.1 wt.% are not included in the comparison because they are similar to or even smaller than those at 2.8 wt.% at the same temperature, which is against the observed general trend of H_2O diffusivity.

In Fig. 2.6, these experimental data and calculations based on the new model are compared, indicating good inter-laboratory and multi-method consistency, and therefore demonstrating the reliability of the new model. The maximum difference is a factor of 2.3 between calculation and that of Nowak and Behrens (1997) using Boltzmann-Matano
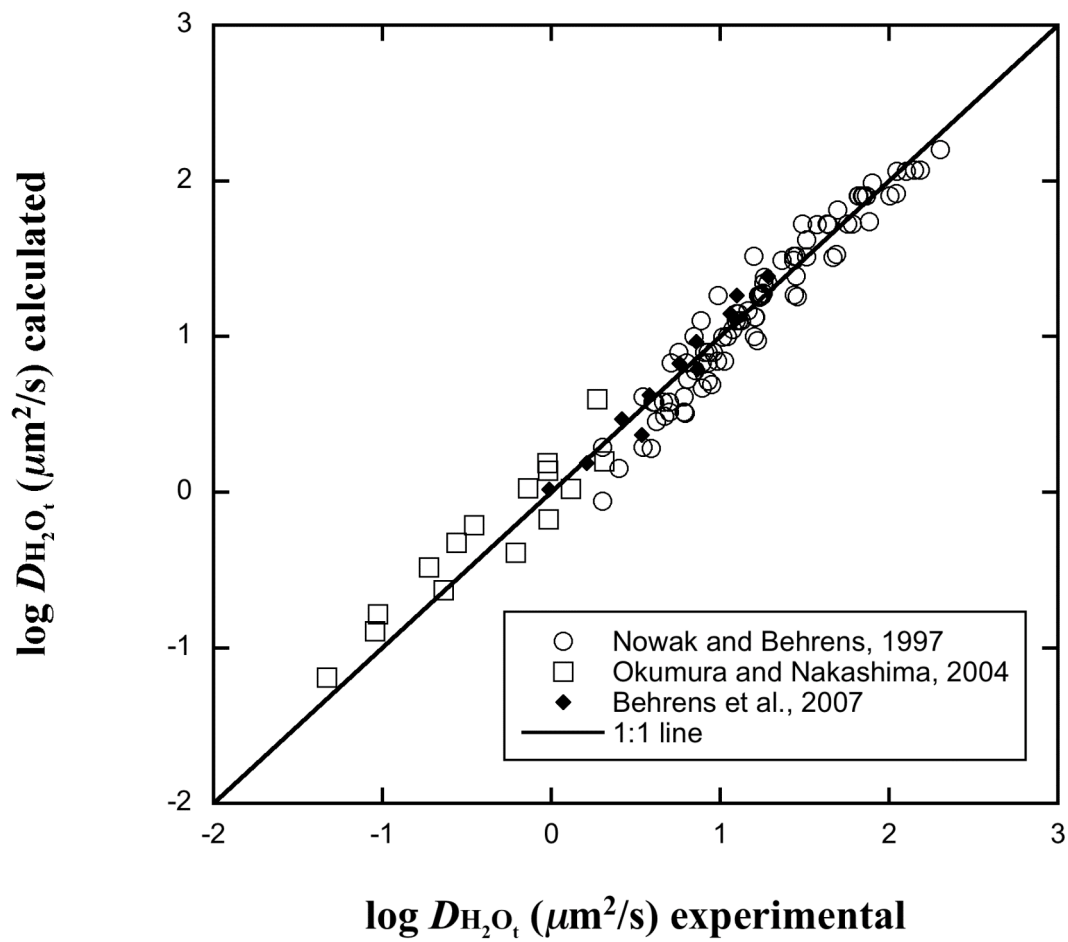
Fig. 2.6. Comparison between the new diffusivity expression and experimental data (Nowak and Behrens, 1997; Okumura and Nakashima, 2004; Behrens et al., 2007). The diffusion-out diffusivity of Okumura and Nakashima (2004) is converted to $D_{H_2O_t}$ (the data point at 500°C and 0.7 wt% H_2O_t is excluded due to species disequilibrium, Zhang et al., 2007).

method. Such a difference is expected because the precision of the Boltzmann-Matano method is not high. H_2O_t diffusivities at 1 wt.% H_2O_t from Behrens et al. (2007) are within a factor of 1.3, and those at 4 wt.% H_2O_t from Behrens et al. (2007) are within a factor of 1.6 with those predicted by my model. The differences are only slightly larger than the experimental and model uncertainty, and may be attributed to complications in hydration experiments (such as dissolution during the experiment and precipitation during quench). Resolving the pressure effect on H_2O diffusion is the main goal of this study. The agreement between the new H_2O diffusion model and previous experimental data including those of Behrens et al. (2007) suggests that the pressure effect is now well resolved.

Applicability of the Einstein or Eyring equation to molecular H_2O diffusion

The Einstein (1905) equation relates diffusivity of a neutral species in a liquid and the viscosity of the liquid, and is derived by considering molecular diffusion as Brownian motion in the liquid continuum. It takes the following form:

$$D = kT/(\eta L), \tag{2-18}$$

where D is diffusivity, k is the Boltzmann constant, T is temperature in K, η is viscosity, and L is a length scale and equals $6\pi r$ where r is the radius of the diffusing species. The equation can predict the diffusivity of Ar, Kr and Xe in water to within 30% (Jahne et al., 1987; Fig. 2.7A). It does not seem that the relation has been applied to silicate melts.

Fig. 2.7B compares experimental diffusivity of molecular H_2O and Ar with the calculated Einstein diffusivity. The latter is smaller than the experimental data by 5-15 orders of magnitude. Because the uncertainty in the diffusivities is less than a factor of 2,

37
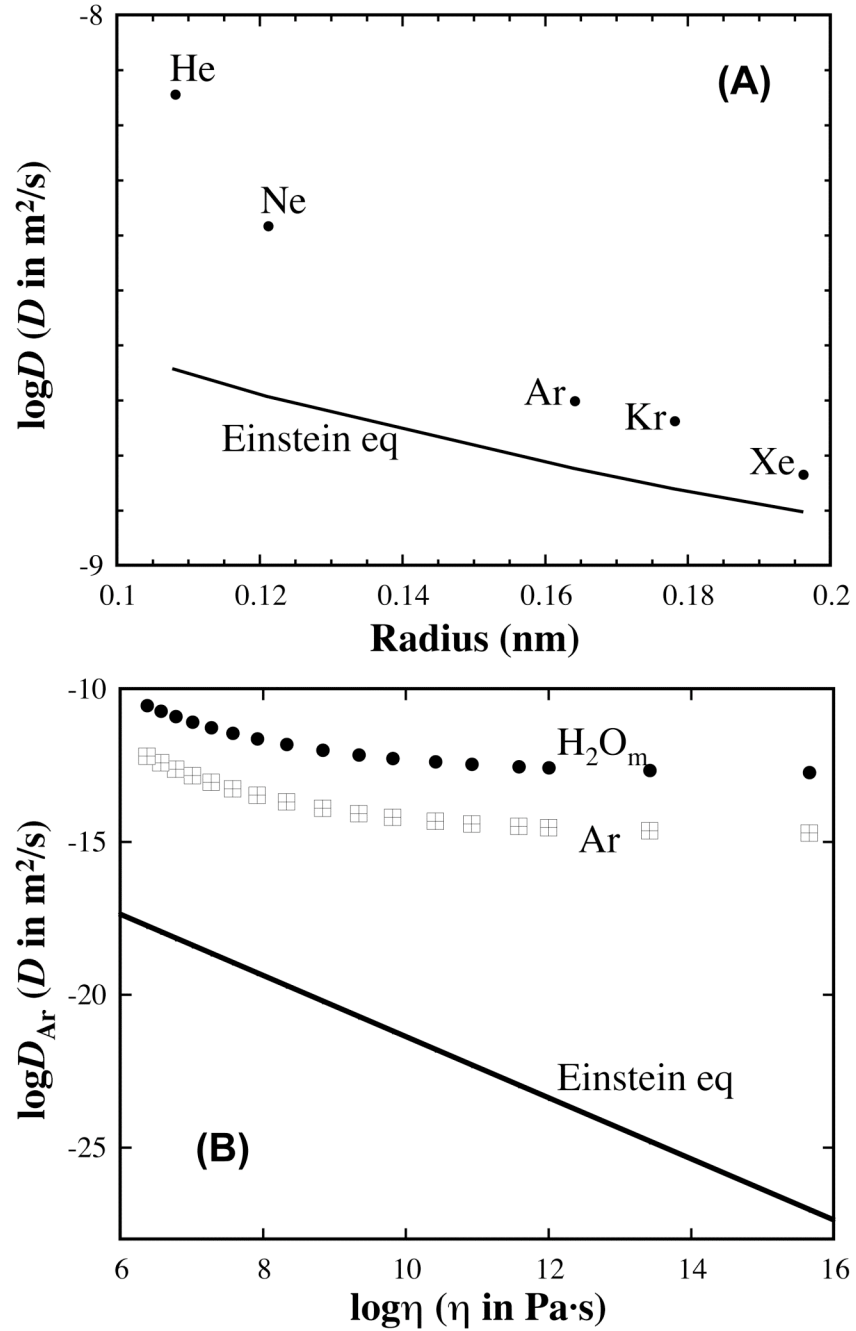
Fig. 2.7. (A) Noble gas diffusivity in water versus radius, and (B) H_2O_m and Ar diffusivity in rhyolitic melt versus viscosity of the melt at 600°C and 0.1-6.0 wt.% H_2O_t. Note the vertical scale difference in (A) and (B). Molecular H_2O diffusion data are from this study. Ar diffusion data are from Behrens and Zhang (2001). Viscosity of rhyolitic melts is from Zhang et al. (2003). Atomic radii of molecular H_2O and Ar are taken to be 0.137 nm and 0.164 nm respectively (Shannon, 1976; Zhang and Xu, 1995). The calculated Einstein diffusivity (solid line) for H_2O_m and Ar in rhyolitic melt are similar at this scale.

and that in the viscosities is less than a factor of 3, these uncertainties cannot explain the huge discrepancy of the Einstein equation. Therefore, the Einstein equation cannot predict diffusivity of molecular H_2O and Ar in rhyolitic melt. Not only do the values not match, but also the slope of $\log D$ versus $\log \eta$ is not -1. Furthermore, the slope is not even a constant (i.e., $\log D$ versus $\log \eta$ is not linear)! The failure of the Einstein equation is likely due to the large size of ionic clusters (such as SiO_4^{4-}, $Si_2O_7^{6-}$, etc.) in silicate melts, which are larger than molecular H_2O or Ar, meaning that the motion of the molecules in the melt cannot be treated as large molecules moving through a liquid continuum.

The Eyring equation (Glasstone, 1941) is based on the transition state theory and assumes that diffusion and viscous flow involve the same process. The equation has been shown to work for ^{18}O and ^{30}Si diffusion in some silicate melts (Shimizu and Kushiro, 1984; Lesher et al., 1996; Tinker and Lesher, 2001; Reid et al., 2003; Tinker et al., 2004), but does not work for, e.g., ^{18}O diffusion in hydrous rhyolitic melt (Behrens et al., 2007). It takes the same form as Eq. (2-18), but L is the jumping distance, which is often taken to be the diameter of the diffusing species. Hence, the difference between the Eyring and the Einstein equations is about a factor of 10. As can be seen from Figure 7B, a factor of 10 (or one order of magnitude) is not enough to reconcile the experimental and calculated diffusivities. Hence, the Eyring equation does not work here, which is expected because the process for viscous flow involves motion of the aluminosilicate network, but that of Ar and H_2O_m diffusion does not.

CONCLUSIONS

Water diffusion in rhyolite at 0.95-1.9 GPa and 407-1629°C is investigated to constrain the pressure dependence of H_2O diffusivity. High pressure results in a smaller diffusivity, which is attributed to decreased free space in the melt. This negative pressure effect indicates that the process of magma upwelling facilitates bubble growth not only thermodynamically (by reducing H_2O solubility), but also kinetically (by increasing H_2O diffusivity), although the latter effect is smaller. Based on a model that H_2O_m dominates water diffusion, two specific H_2O_t diffusivity expressions have been constructed: one for both low and high total H_2O contents (up to 7.7 wt.%), and the other simple form is applicable to low H_2O contents (up to 2 wt.%). All of the expressions are only applicable when species equilibrium is roughly maintained (Jambon et al., 1992), meaning relatively high temperatures and high H_2O_t contents. For example, at 500°C, H_2O_t needs to be ≥ 1 wt% for the diffusivities to be applicable. With this study, the pressure effect on H_2O diffusion in rhyolitic melt has been resolved so that H_2O diffusivity can be predicted from 0 to 2 GPa and from 400 to 1600°C. The use of these expressions is recommended for modeling bubble growth in and degassing from a rhyolitic melt, and the dynamics of H_2O-driven explosive rhyolitic eruptions, as well as H_2O transport in granitic magma chambers.

REFERENCES

Bartholomew, R.F., Schreurs, J.W.H., 1980. Wide-line NMR study of protons in hydrosilicate glasses of different water content. J. Non-Cryst. Sol. 38&39, 679-684.

Behrens, H., Nowak, M., 1997. The mechanisms of water diffusion in polymerized silicate melts. Contrib. Mineral. Petrol. 126, 377-385.

Behrens, H., Zhang, Y., 2001. Ar diffusion in hydrous silicic melts: implications for volatile diffusion mechanisms and fractionation. Earth Planet. Sci. Lett. 192, 363-376.

Behrens, H., Zhang, Y., Xu, Z., 2004. H_2O diffusion in dacitic and andesitic melts. Geochim. Cosmochim. Acta 68, 5139-5150.

Behrens, H., Zhang, Y., Leschik, M., Wiedenbeck, M., Heide, G., Frischat, G.H., 2007. Molecular H_2O as carrier for oxygen diffusion in hydrous silicate melts. Earth Planet. Sci. Lett. 254, 69-76.

Bose, K., Ganguly, J., 1995. Quartz-coesite transition revisited: reversed experimental determination at 500-1200°C and retrieved thermochemical properties. Am. Mineral. 80, 231-238.

Crank, J., 1975. The Mathematics of Diffusion. Oxford University Press, 414 p.

Delaney, J.R., Karsten, J.L., 1981. Ion microprobe studies of water in silicate melts: concentration-dependent water diffusion in obsidian. Earth Planet. Sci. Lett. 52, 191-202.

Einstein, A., 1905. The motion of small particles suspended in static liquids required by the molecular kinetic theory of heat. Ann. Phys. (in German) 17, 549-560.

Freda, C., Baker, D.R., Romano, C., Scarlato., P., 2003. Water diffusion in natural potassic melts. Geol. Soc. Spec. Publ. 213, 53-62.

Friedman, I., Long W., 1976. Hydration rate of obsidian. Science 191, 347-352.

Ganguly, J., Bhattacharya, R.N., Chakraborty, S., 1988. Convolution effect in the determination of compositional profiles and diffusion coefficients by microprobe step scans. Am. Mineral. 73, 901-909.

Glasstone, S., Laidler, K.J., Eyring, H., 1941. The Theory of Rate Processes. McGraw-Hill, New York, 611 pp.

Hui, H., Zhang, Y., Xu, Z., Behrens, H., 2008a. Pressure dependence of the speciation of dissolved H_2O in rhyolitic melt. Geochim. Cosmochim. Acta 72, 3229-3240.

Hui H., Zhang Y., Xu Z., Gaudio, P.D., Behrens H., 2008b. Pressure dependence of viscosity of rhyolitic melt. Geochim. Cosmochim. Acta, in press.

Jahne, B., Heinz, G., Dietrich, W., 1987. Measurement of the diffusion coefficients of sparingly soluble gases in water. J. Geophys. Res. C92, 10767-10776.

Jambon, A., 1979. Diffusion of water in a granitic melt: an experimental study. Carnegie Inst. Washington, Yearbook 78, 352-355.

Jambon, A., Zhang, Y., Stolper, E.M., 1992. Experimental dehydration of natural obsidian and estimation of D_{H_2O} at low water contents. Geochim. Cosmochim. Acta 56, 2931-2935.

Karsten, J.L., Holloway, J.R., Delaney, J.R., 1982. Ion microprobe studies of water in silicate melts: temperature-dependent water diffusion in obsidian. Earth. Planet. Sci. Lett. 59, 420-428.

Lapham, K.E., Holloway, J.R., Delaney, J.R., 1984. Diffusion of H_2O and D_2O in obsidian at elevated temperatures and pressures. J. Non-Cryst. Solids 67, 179-191.

Lasaga, A.C., 1998. Kinetic Theory in the Earth Sciences. Princeton University Press.

Lesher, C.E., Hervig, R.L., Tinker, D., 1996. Self diffusion of network formers (silicon and oxygen) in naturally occurring basaltic liquid. Geochim. Cosmochim. Acta 60, 405-413.

Liu, Y., Zhang, Y., 2000. Bubble growth in rhyolitic melt. Earth Planet. Sci. Lett. 181, 251-264.

Liu, Y., Zhang, Y., Behrens, H., 2004. H_2O diffusion in dacitic melts. Chem. Geol. 209, 327-340.

Newman, S., Stolper, E.M., Epstein, S., 1986. Measurement of water in rhyolitic glasses: calibration of an infrared spectroscopic technique. Am. Mineral. 71, 1527-1541.

Nogami, M., Tomozawa, M., 1984. Effect of stress on water diffusion in silica glass. J. Am. Ceram. Soc. 67, 151-154.

Nowak, M., Behrens, H., 1997. An experimental investigation on diffusion of water in haplogranitic melts. Contrib. Mineral. Petrol. 126, 365-376.

Okumura, S., Nakashima, S., 2004. Water diffusivity in rhyolitic glasses as determined by in situ IR spectrometry. Phys. Chem. Minerals 31, 183-189.

Okumura, S., Nakashima, S., 2006. Water diffusion in basaltic to dacitic glasses. Chem. Geol. 227, 70-82.

Orlova, G.P., 1962. The solubility of water in albite melts. Int. Geol. Rev. 6, 254-258.

Press, W.H., Teukolsky, S.A., Vetterling, W.T., Flannery, B.P., 1992. Numerical recipes in Fortran 77: the art of scientific computing, 2nd edition. Cambridge University Press. New York.

Reid, J.E., Suzuki, A., Funakoshi, K., Terasaki, H., Poe, B.T., Rubie, D.C., Ohtani, E., 2003. The viscosity of $CaMgSi_2O_6$ liquid at pressures up to 13 GPa. Phys. Earth Planet. Inter. 139, 45-54.

Shannon, R.D., 1976. Revised effective ionic radii and systematic studies of interatomic distances in halides and chalcogenides. Acta Crystallogr. A32, 751-767.

Shaw, H.R., 1974. Diffusion of H_2O in granitic liquids: I. Experimental data; II. Mass transfer in magma chambers. In: Hofmann, A.W., Giletti, B.J., Yoder, H.S., Yund, R.A. (Eds.), Geochemical Transport and Kinetics. Carnegie Inst. Washington Publ., Washington, DC, pp. 139-170.

Shimizu, N., Kushiro, I., 1984. Diffusivity of oxygen in jadeite and diopside melts at high pressures. Geochim. Cosmochim. Acta 48, 1295-1303.

Stolper, E.M., 1982. Water in silicate glasses: an infrared spectroscopic study. Contrib. Mineral. Petrol. 81, 1-17.

Tinker, D., Lesher, C.E., 2001. Self diffusion of Si and O in dacitic liquid at high pressures. Am. Mineral. 86, 1-13.

Tinker, D., Lesher, C.E., Baxter, G.M., Uchida, T., Wang, Y., 2004. High-pressure viscometry of polymerized silicate melts and limitations of the Eyring equation. Am. Mineral. 89, 1701-1708.

Wang, L., Zhang, Y. and Essene, E.J., 1996. Diffusion of the hydrous component in pyrope. Am. Mineral. 81, 706-718.

Wasserburg, G.J., 1988. Diffusion of water in silicate melts. J. Geol. 96, 363-367.

Watson, E.M., 1991. Diffusion of dissolved CO_2 and Cl in hydrous silicic to intermediate magmas. Geochim. Cosmochim. Acta 55, 1897-1902.

Winchell, P., 1969. The compensation law for diffusion in silicates. High Temp. Sci. 1, 200-215.

Withers, A.C., Behrens, H., 1999. Temperature-induced changes in the NIR spectra of hydrous albitic and rhyolitic glasses between 300 and 100 K. Phys. Chem. Minerals 27, 119-132.

Withers, A.C., Zhang, Y., Behrens, H., 1999. Reconciliation of experimental results on H_2O speciation in rhyolitic glass using in-situ and quenching techniques. Earth Planet. Sci. Lett. 173, 343-349.

Zhang, Y., 1999a. A criterion for the fragmentation of bubbly magma based on brittle failure theory. Nature 402, 648-650.

Zhang, Y., 1999b. H_2O in rhyolitic glasses and melts: measurement, speciation, solubility, and diffusion. Rev. Geophys. 37, 493-516.

Zhang, Y., Stolper, E.M., 1991. Water diffusion in basaltic melts. Nature 351, 306-309.

Zhang, Y., Xu, Z., 1995. Atomic radii of noble gas elements in condensed phases. Am. Mineral. 80, 670-675.

Zhang, Y., Behrens, H., 2000. H_2O diffusion in rhyolitic melts and glasses. Chem. Geol. 169, 243-262.

Zhang, Y., Stolper, E.M., Wasserburg, G.J., 1991. Diffusion of water in rhyolitic glasses. Geochim. Cosmochim. Acta 55, 441-456.

Zhang, Y., Stolper, E.M., Ihinger, P.D., 1995. Kinetics of the reaction $H_2O + O = 2OH$ in rhyolitic and albitic glasses: preliminary results. Am. Mineral. 80, 593-612.

Zhang Y., Jenkins, J., Xu, Z., 1997a. Kinetics of the reaction $H_2O + O = 2OH$ in rhyolitic glasses upon cooling: geospeedometry and comparison with glass transition. Geochim. Cosmochim. Acta 61, 2167-2173.

Zhang, Y., Belcher, R., Ihinger, P.D., Wang, L., Xu, Z., Newman, S., 1997b. New calibration of infrared measurement of dissolved water in rhyolitic glasses. Geochim. Cosmochim. Acta 61, 3089-3100.

Zhang, Y., Xu, Z., Behrens, H., 2000. Hydrous species geospeedometer in rhyolite: Improved calibration and application. Geochim. Cosmochim. Acta 64, 3347-3355.

Zhang, Y., Xu, Z., Liu, Y., 2003. Viscosity of hydrous rhyolitic melts inferred from kinetic experiments, and a new viscosity model. Am. Mineral. 88, 1741-1752.

Zhang, Y., Xu, Z., Zhu, M., Wang, H., 2007. Silicate melt properties and volcanic eruptions. Rev. Geophys. 45, RG4004, doi:10.1029/2006RG000216.

CHAPTER III

A GENERAL MODEL OF WATER DIFFUSIVITY IN DACITIC MELTS

ABSTRACT

H_2O diffusion in dacite was investigated at 0.48-0.95 GPa and 786-893 K in a piston-cylinder apparatus. The diffusion couple design was used, in which a nominally dry dacitic glass makes one half and is juxtaposed with a hydrous dacitic glass containing up to ~8 wt.% total water (H_2O_t). H_2O concentration profiles were measured on quenched glasses with infrared microscopy. The H_2O diffusivity in dacite increases rapidly with water content under experimental conditions, similar to previous measurements at the same temperature but at $P < 0.15$ GPa. However, compared with the low-pressure data, H_2O diffusion at high pressure is systematically slower. The H_2O diffusion profiles in dacite are modeled by assuming molecular H_2O (H_2O_m) is the diffusing species, whose diffusivity $D_{H_2O_m}$ (in μm^2/s) depends on T (in K), P (in GPa), and X (mole fraction of H_2O_t) within 786-1798 K, 0-1 GPa, and 0-8 wt.% H_2O_t:

$$D_{H_2O_m} = \exp\left(18.208 - 62.38X - \frac{19064 - 108882X + 1476.7P}{T}\right),$$

where $X = C/18.015/[C/18.015 + (100-C)/33.82]$, C is wt.% of H_2O_t, and 18.015 and 33.82 are the molar masses of H_2O and anhydrous dacite on a single oxygen basis. The above

equation can be combined with H_2O speciation model to calculate an apparent H_2O_t diffusivity:

$$D_{H_2O_t} = D_{H_2O_m}\left[1 + \frac{2X-1}{\sqrt{4X(X-1)(1-4/K)+1}}\right],$$

where K [$= \exp(1.49-2634/T)$] is the equilibrium constant of speciation reaction ($H_2O_m + O \rightleftharpoons 2OH$). Compared to H_2O diffusion in rhyolite, diffusivity in dacite is lower at intermediate temperatures but higher at superliquidus temperatures. This general H_2O diffusivity model can be applied to a broad range of geological conditions, including both magma chamber processes (degassing, mixing, etc.) and volcanic eruption dynamics from conduit to earth surface (such as bubble growth).

INTRODUCTION

Water diffusion in natural silicate melts has been extensively studied due to its importance in a variety of magmatic and volcanic processes (Zhang et al., 2007). For example, through diffusive transport of water, bubbles in magma can extract water from magma as nutrient for growth (e.g., Proussevitch and Sahagian, 1998; Liu and Zhang, 2000). Other relevant circumstances include magma dehydration, mixing, and fragmentation (e.g., Zhang, 1999; Martel et al., 2000). Furthermore, hydrous melts in the Earth's interior (Bercovici and Karato, 2003; Mierdel et al., 2007) may be heterogeneous in H_2O content due to dynamic processes such as mantle convection and slab subduction, and knowledge of H_2O diffusivity in these melts is valuable for assessing the time scale for re-homogenization of magma reservoirs.

Reported water diffusivity data has covered diverse melt compositions, including rhyolite (e.g., Zhang et al., 1991; Nowak and Behrens, 1997; Zhang and Behrens, 2000; Okumura and Nakashima, 2004; Behrens et al., 2007; Ni and Zhang, 2008), dacite (Liu et al., 2004a; Behrens et al., 2004; Okumura and Nakashima, 2006), andesite (Behrens et al., 2004; Okumura and Nakashima, 2006), basalt (Zhang and Stolper, 1991; Okumura and Nakashima, 2006), and trachyte (Freda et al., 2003). These contributions have established that the diffusivity of H_2O depends on temperature, pressure, water content, and chemical composition of the melt. However, a general H_2O diffusivity model that is applicable to a broad range of geological conditions is only available for rhyolite (Ni and Zhang, 2008). For other melts there are no data at high pressures and intermediate temperatures (773-973 K). The absence of experimental data and a general model makes it difficult to simulate the dynamics of volcanic eruptions.

Many arc volcanic eruptions have a dacitic bulk composition, such as the 1991 eruption of Mount Unzen (Holtz et al., 2005), although the composition of the residual melt is more silicic. There are andesitic eruptions with dacitic liquid composition as well, such as the 1968 eruption of Arenal Volcano (Szramek et al., 2006). Dacitic/granodioritic magma can also be present in deep reservoir and form granodiorite pluton (Vila et al., 2005). Several experimental studies have been carried out on water diffusion in dacite. Liu et al. (2004a) investigated the dehydration rate of hydrous dacitic glass containing 0.7-2.5 wt.% H_2O at 824-911 K and 0.1-145 MPa. Water diffusivity in dacite was found to increase with water content, more rapidly than in rhyolite. Under similar conditions (773-948 K and room pressure), Okumura and Nakashima (2006) monitored *in situ* the bulk water content of a thin dacite glass wafer undergoing

dehydration, and adopted a proportional correlation between diffusivity and water content (<1 wt.%). At high pressures (0.5-1.5 GPa), Behrens et al. (2004) measured H_2O diffusivity (up to 6 wt.% H_2O) at superliquidus temperatures (1458-1798 K) using a diffusion-couple technique. They demonstrated that H_2O diffusivity is roughly proportional to water content without much pressure effect.

Because previous experiments on H_2O diffusion in dacitic melts cover either intermediate temperature and low pressure (773-948 K, 0.1-145 MPa), or high temperature and high pressure (1458-1798 K, 0.5-1.5 GPa), the pressure effect is not well established. Zhang et al. (2007) ignored the pressure effect to combine the high and low temperature data. Furthermore, the data at intermediate temperatures only cover low H_2O concentration (up to 2.5 wt.%). In order to elucidate the pressure effect on H_2O diffusivity in dacite and construct H_2O diffusivity model over a wide range of H_2O content, temperature, and pressure, new diffusion-couple experiments at 786-893 K and 0.48-0.95 GPa were performed in a piston-cylinder apparatus. The acquired diffusivity data in this work together with previous data allow construction of a general model of H_2O diffusivity in dacitic melt, which can be applied to most geological circumstances. This work is one more crucial piece of continued efforts toward a comprehensive H_2O diffusivity model in natural silicate melts.

EXPERIMENTAL AND ANALYTICAL PROCEDURES

Starting Material

The diffusion couple is composed of an nominally anhydrous and a hydrous dacitic glass. The anhydrous dacite was produced by melting oxides and carbonates at 1873 K, and hydrous glasses were synthesized at 0.5 GPa and 1523-1623 K in an internally heated pressure vessel at University of Hannover, Germany. The method of synthesis was described in detail in Ohlhorst et al. (2001) and Behrens et al. (2004). No crystal or bubble are observed in all the end products. The nominally anhydrous glass contains 0.013 wt.% residual water (Table 3.1). Several pieces of hydrous glasses were prepared with 1.4-7.9 wt.% H_2O based on FTIR analyses, and the relative variation within each sample is less than 5%. All dacitic glasses were analyzed with a Cameca SX100 electron microprobe at the University of Michigan, and their anhydrous compositions are reported in Table 3.1. The compositions are close to the products of the 1980 Mount St. Helens (Gardner et al., 1995), the 1991 Pinatubo (Borisova et al., 2006), and the 1991 Unzen dacitic eruptions (Chen et al., 1993), and are also similar to samples used in previous H_2O diffusion studies (Liu et al., 2004a; Behrens et al., 2004; Okumura and Nakashima, 2006).

Diffusion Runs

Diffusion runs were performed in a 0.5″ end-loaded piston cylinder apparatus (PCA) at the University of Michigan. Considering the positive correlation between water diffusivity and water content, I always adopted a longer hydrous glass cylinder (2.6-3.0 mm length) than the anhydrous one (1.0-1.7 mm length) for the two halves of a diffusion couple. The cylinder pair of ~2.6 mm diameter were first placed in a graphite capsule of 4.5 mm diameter, with their polished surface in direct contact. The graphite capsule was

Table 3.1 Composition of starting dacitic glass (in wt.%) on anhydrous basis

	DRY-DC	DC1.4	Dac4	Dac5	Dac8
SiO_2	65.41	66.35	66.60	67.30	65.46
TiO_2	0.87	0.63	0.80	0.76	0.63
Al_2O_3	15.73	16.58	14.91	15.23	16.05
FeO_T	4.43	3.73	4.87	4.36	4.50
MnO	0.08	0.07	0.05	0.08	0.05
MgO	1.95	1.85	2.22	2.13	2.19
CaO	4.90	4.70	4.92	4.72	4.89
Na_2O	4.00	4.05	3.48	3.57	3.84
K_2O	2.51	2.72	2.51	2.44	2.55
Total	99.88	100.68	100.36	100.59	100.16
H_2O (IR)	0.013	1.42	4.91	5.49	7.85

A Cameca SX100 electron microprobe is used to make 5 analyses on each sample, with a scanning beam of 5 μm raster length,15 kV voltage, and 4 nA current. Oxide contents are reported on anhydrous basis by excluding water content measured with infrared spectrometry (calibrated by Yamashita et al., 1997 and Ohlhorst et al., 2001).

then enclosed in a gold tube of 5 mm diameter, which was welded on both ends. To ensure that convection does not contribute to the exchange of water, the gold capsule was always oriented to keep the hydrous half on top when placed into a crushable MgO rod. Outside the MgO rod was a graphite heater and then a $BaCO_3$ cell, together forming the entire sample assemblage.

The temperature during diffusion runs was measured by a type D thermocouple (Re_3W_{97}-$Re_{25}W_{75}$), which was separated from the gold capsule by an MgO wafer of 0.5 mm thickness. The calibrated temperature profile of the experimental charge (Hui et al., 2008) indicates that a temperature-dependent correction should be made in order to find the real temperature at the center of the charge (also the center of the dacite samples). After taking into account uncertainties in thermocouple and sample position and temperature fluctuation (typically within ±2 K), I estimate the overall error in temperature is estimated of about 10 K.

Experiments were carried out at 0.5 GPa and 1 GPa (nominal pressure) with a "piston-out" procedure. Real pressure of PCA used in this study is 5 to 6% lower than nominal pressure (Hui et al., 2008; Ni and Zhang, 2008). Due to imperfect pressure calibration as well as gauge imprecision and pressure fluctuation, the overall pressure uncertainty is approximately 50 MPa. To extend the pressure coverage, an experiment was conducted at 2 GPa and 873 K. However, the hydrous half crystallized, consistent with previous observations that increasing pressure increases the likelihood of crystallization (Hui et al., 2008; Ni and Zhang, 2008). Hence, no further experiments were conducted at > 1 GPa.

The experimental duration spanned 0.5-136 h, depending on temperature and maximum water content. Experiments were ended by turning off the heating power, and the initial cooling rate is roughly 80 K/s based on recorded thermal history. Table 3.2 lists the details of experimental conditions. These experiments fill the T-P-H_2O wt.% space not covered by previous works (Liu et al., 2004a; Behrens et al., 2004; Okumura and Nakashima, 2006), as displayed in Fig. 3.1, and they are necessary for resolving the pressure dependence of H_2O diffusivity, and hence for a quantitative understanding of how H_2O diffusivity depends on the controlling factors.

FTIR Analyses

Infrared analyses on doubly polished dacite glass wafers were performed at the University of Michigan using a Perkin-Elmer Spectrum GX FTIR spectrometer. Before diffusion experiments, bulk water contents in dacite wafers (Table 3.1) were analyzed using the FTIR with a NIR source, a CaF_2 beamsplitter, and an InSb detector cooled by liquid nitrogen. Infrared spectra were collected from 2000 to 9000 cm^{-1} wave numbers and 64-128 scans were accumulated for each analysis. The 3550 cm^{-1} MIR absorption band calibrated by Yamashita et al. (1997) was used to calculate the extremely low H_2O concentration in the nominally anhydrous dacite glass. For hydrous glasses, NIR bands at 5200 cm^{-1} (signifying H_2O molecules, or H_2O_m) and 4500 cm^{-1} (signifying hydroxyl group, or OH) are appropriate for obtaining the total water (H_2O_t) content (H_2O_m+OH) with the calibration by Ohlhorst et al. (2001). Two tangential lines (TT method) were used as baselines to determine absorption peak heights for all spectra.

Table 3.2 Experimental conditions

Run #	H_2O_t (I)[a] (wt.%)	T[b] (K)	P[c] (GPa)	t (s)	H_2O_t (E)[d] (wt.%)	thickness (μm)
Dac-DC05-12	0.01/7.9	893±10	0.95±0.05	1,825	0.01/7.7	264
Dac-DC05-13	0.01/5.5	892±10	0.95±0.05	54,000	0.01/5.3	203
Dac-DC05-14	0.01/7.9	840±10	0.95±0.05	10,800	0.01/7.7	215
Dac-DC06-15	0.01/5.5	842±10	0.95±0.05	144,000	0.01/5.7	191
Dac-DC06-17[e,f]	0.01/7.9	786±10	0.95±0.05	175,780	0.01/6.7	205
Dac-DC06-19[f]	0.01/4.9	893±10	0.48±0.05	185,400	0.01/4.0	206
Dac-DC06-21	0.01/1.4	842±10	0.95±0.05	489,600	0.01/1.4	173
Dac-DC06-22	0.01/5.5	791±10	0.95±0.05	252,000	0.02/5.8	157

[a] Initial water contents of the two halves measured by FTIR based on the calibration of Yamashita et al. (1997) and Ohlhorst et al. (2001).
[b] Effective temperature after considering axial thermal gradient in piston-cylinder apparatus.
[c] Effective pressure based on measured quartz-coesite transition against the phase boundary determined by Bose and Ganguly (1995).
[d] End minimum and maximum water contents measured at the flat regions of each diffusion profile. Nominal H_2O concentration is divided by a factor of 1.144 to account for baseline change in IR spectra after run.
[e] Heating power was disconnected after a duration of ~50 min and the capsule was reused.
[f] Long dwelling time caused noticeable water loss in the hydrous half.
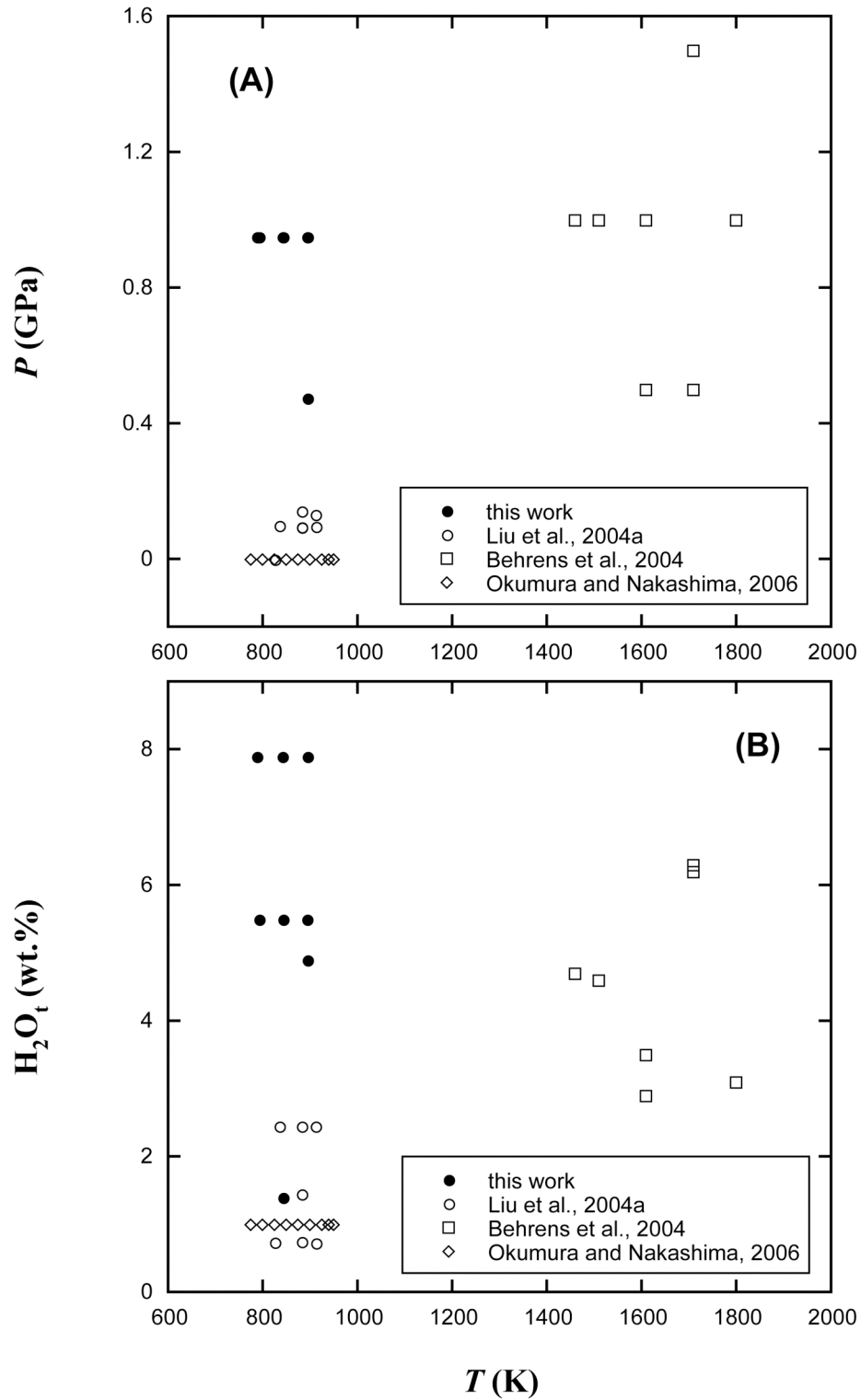
Fig. 3.1. Experimental conditions of this work and previous studies on H_2O diffusion in dacite: Liu et al. (2004a), Behrens et al. (2004), and Okumura and Nakashima (2006).

Each quenched capsule after a diffusion experimental run was mounted into epoxy resin and polished to reveal the central section of 160-260 μm thickness. No sign of crystallization in glass was observed under optical microscope for the reported runs. Typically one curved crack (roughly perpendicular to the cylinder axis) was developed in the glass, probably initiated during the rapid quenching. As the crack often lies outside the effective diffusion profile, it does not cause much problem in diffusivity determinations.

The post-experimental diffusion profiles were analyzed using the Autoimage system (with an MCT detector) of the FTIR. The aperture was 10 μm wide and 200 μm long on the focus plane of the microscope. However, the real spatial resolution is larger than aperture width. For example, the measurement of a step concentration profile yields a full width at half maximum (FWHM) of 30 μm (Ni and Zhang, 2008) for the case of a 20-μm wide aperture. The FWHM of 10-μm wide aperture is determined to be ~15 μm, and such spatial resolution is tolerable for most diffusion profiles, as manifested from the fact that the profiles change little upon further polishing. However, for two short profiles (<240 μm), Dac-DC05-12 and Dac-DC06-21, convolution effect may play an essential role, which will be discussed later. The IR spectra along diffusion profiles were collected and handled using a similar procedure for starting material IR analysis.

RESULTS

Diffusion profiles have been successfully acquired for eight experiments, whereas other runs failed due to power breakage or crystallization or poor contact between the

diffusion halves. For experiment Dac-DC06-17, power was shut down after sudden temperature fluctuation (±5 K at 773 K) was noticed, and the capsule was taken out and reused for a second run. In consideration of its long dwelling time, duration correction due to extra cooling and heating is negligible. The detailed experimental conditions are summarized in Table 3.2, and the measured H_2O_t concentration profiles are plotted with curve fits in Fig. 3.2. The species concentrations (H_2O_m and OH) are not used for modeling diffusivity because (a) they are less accurate than H_2O_t concentration (Ohlhorst et al., 2001); and (b) they may not represent equilibrium speciation at experimental conditions, especially at high H_2O_t.

As observed by Liu et al. (2004a) and Behrens et al. (2004), water content by IR analysis often shows a nominal increase of about 10-20% after diffusion runs. One might expect this effect is related to the change in redox state of iron ($Fe_2O_3 + H_2 = 2FeO + H_2O$) in the presence of the graphite capsule. However, Fe^{2+}/Fe_{tot} analyses on glasses before and after diffusion runs using a colorimetric technique (Schuessler et al., 2008) show only minor increase in ferrous iron (Table 3.3), which is equivalent to no more than 0.03 wt% H_2O_t increase. Furthermore, Behrens et al. (2004) demonstrated that redox state of iron has little influence on H_2O diffusion even in high-iron andesite (containing 7-8 wt.% FeO_t) at high temperatures (>1573 K). For experiments in dacite containing 4-5 wt% FeO_t, the influence of small change in Fe redox state is considered insignificant. Therefore, elevated nominal H_2O concentration is an artifact, possibly caused by the effect on the baseline of IR spectra (Liu et al., 2004a; Fig. 3.3) due to factors such as changing Fe^{2+} coordination. Accordingly, nominal total H_2O concentrations in diffusion
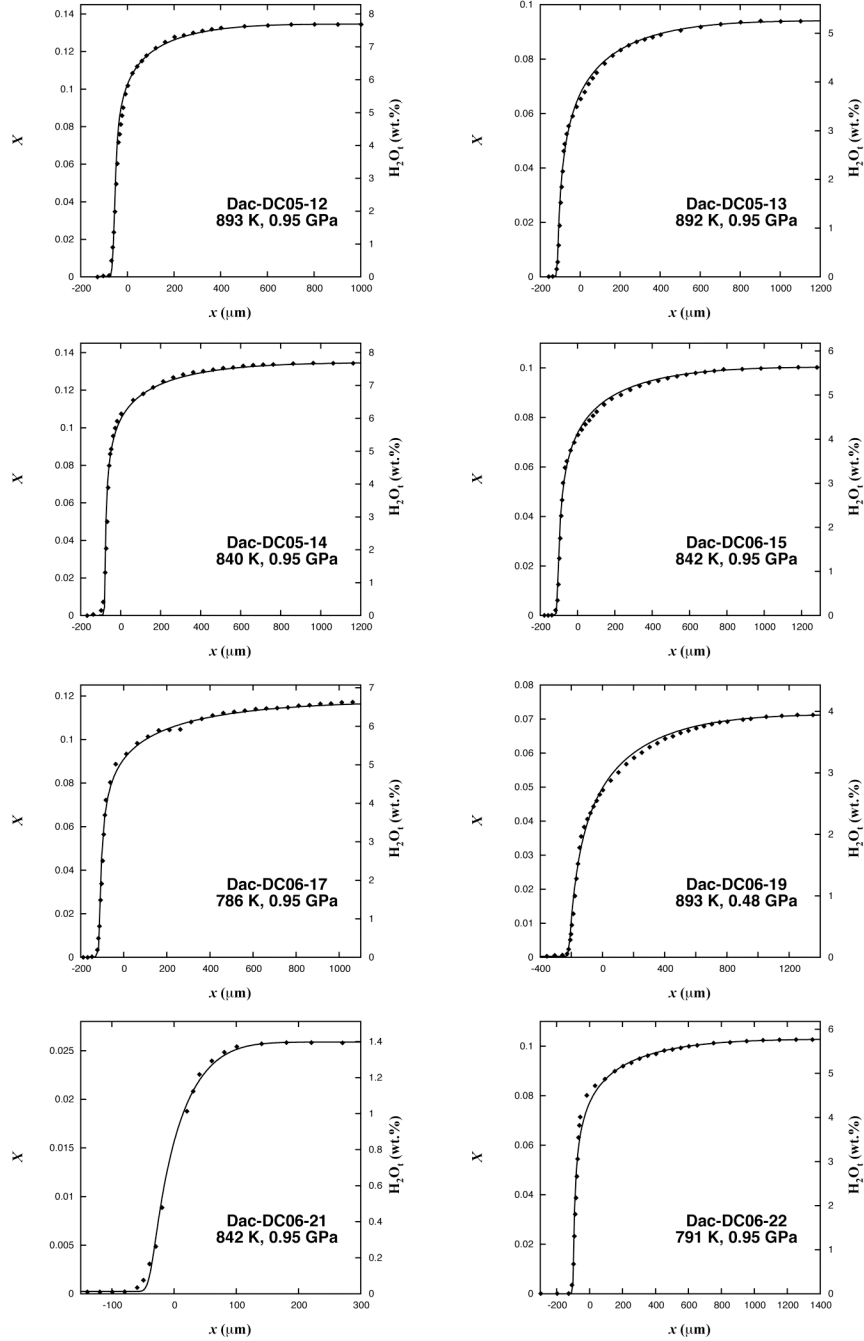
Fig. 3.2. H_2O_t concentration profiles in the diffusion-couples, with some data points outside the illustrated distance range for clarity. Fitting curves are also shown for comparison based on the model of $D_{H_2O_m} = D_0exp[(-62.38+108882/T)X]$, with results reported as lnD_0 in Table 3.5. Convolution effect is considered for the short profile of Dac-DC05-12 and Dac-DC06-21. See text for details.

Table 3.3

Ferrous iron quantification before (I) and after (E) heating and pressurization at 0.95 GPa

Run #	T (K)	H_2O (wt.%)	Fe^{2+}/Fe_{tot} (I)	Fe^{2+}/Fe_{tot} (E)
Dac-DC05-08	873	0.01	0.397±0.017	0.453±0.064
		1.1	0.796±0.021	0.812±0.030
Dac-DC05-10	873	0.01	0.389±0.014	0.432±0.046
		3.5	0.621±0.018	0.649±0.038
Dac-sp1	753	7.9	0.66±0.03	0.70±0.02

The colorimetric method by Vetere et al. (2008) was used and analyses results are reported with 2σ error.
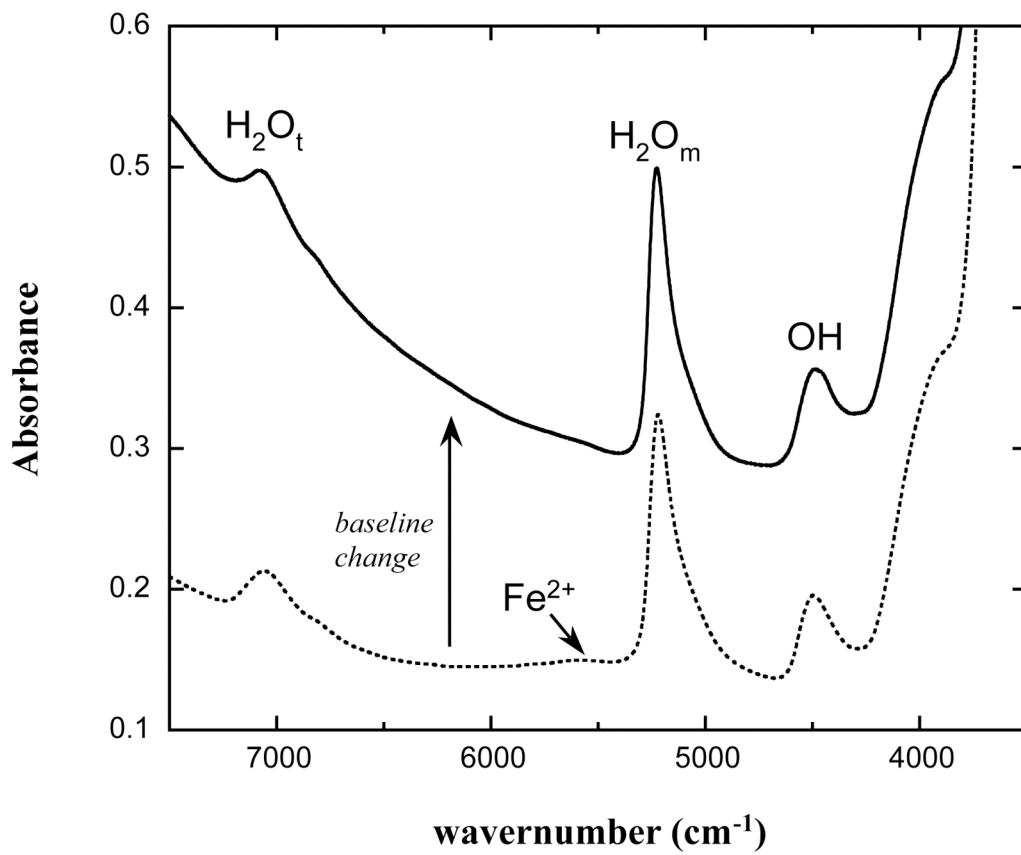
Fig. 3.3. FTIR baseline of Dac8 (dash curve) becomes steeper after diffusion run Dac-DC05-12 (solid curve).

profiles determined by NIR are divided by an averaged factor of 1.144 to be consistent with initial H_2O concentrations.

Experimental durations have been designed so that large regions maintain initial (and hence flat) water contents in both halves (meaning that diffusion in infinite medium applies). However, Dac-DC06-17 and Dac-DC06-19 show evident water loss in the hydrous half, which causes extra uncertainty in determining H_2O diffusivity. For other experiments, water gain or loss outside the flat regions was still observed, presumably due to water transport along container walls (Zhang and Behrens, 2000). These data points do not belong to effective diffusion profiles and are excluded in fitting.

DISCUSSION AND APPLICATION

Diffusion Mechanism and Modeling

Following previous workers (Zhang and Behrens, 2000; Liu et al., 2004a; Ni and Zhang, 2008), H_2O diffusion in silicate melts is treated as follows:

$$\frac{\partial X}{\partial t} = \frac{\partial}{\partial x}\left(D_{H_2O_m} \frac{\partial X_m}{\partial x} \right).$$

(3-1)

Here X is the mole fraction of total dissolved H_2O, and is related to H_2O percentage (C in wt.%) through $X=C/18.015/[C/18.015+(100-C)/33.82]$, where 18.015 and 33.82 are the molar masses of H_2O and anhydrous dacite on a single oxygen basis, respectively. X_m is the mole fraction of H_2O_m, t is time, x is distance, and $D_{H_2O_m}$ is H_2O_m diffusivity.

Despite the sluggishness of OH in motion during the process of H_2O diffusion, the concentration of OH still varies with time in response to the change in H_2O_m

concentration through the reaction $H_2O_m+O \rightleftharpoons 2OH$, in order to maintain equilibrium. The equilibrium constant K of this speciation reaction in dacite was reported by Liu et al. (2004b) using two different IR baselines (TT and GG). The TT expression of K was chosen in this study because (a) tangential baselines were adopted for water concentration determination in this study; (b) K from TT method lies between that of rhyolite (Zhang et al., 1997) and that of of andesite (Botcharnikov et al., 2006). [The intermediate K in dacite is in agreement with the observation that K decreases with silica content (Silver et al., 1990) and increases with NBO/T (and decreasing content of alkali earth elements) (Behrens and Yamashita, 2008).] Hence equilibrium constant K in dacite is assumed to be dependent on temperature as follows (Liu et al., 2004b):

$$\ln K = 1.49 - \frac{2634}{T},$$
(3-2)

where T is in K. One should note that the choice of the equation for water speciation affects the derived molecular H_2O diffusivity but has only negligible influence on the derived total H_2O diffusivity, and the latter is critical in calculating diffusion profiles.

The diffusivity of H_2O_m has been shown to increase rapidly with water content at temperatures below glass transition (such as 823 K) in rhyolite and dacite (Zhang and Behrens, 2000; Liu et al., 2004a; Ni and Zhang, 2008), which has led to the proposition of an exponential dependence:

$$D_{H_2O_m} = D_0 \exp(aX),$$
(3-3)

where D_0 and a are both constants at given T and P. Watson (1991) and Behrens and Zhang (2001) have described similar dependence on water content for CO_2 and Ar diffusivity, respectively.

The above diffusivity formulation (Eq. 3-3) combined with the speciation reaction formulation (Eq. 3-2) is used to solve the governing equation of H_2O diffusion (Eq. 3-1) and model the measured diffusion profiles. Parameter a should be constrained first. In this work multiple experiments have been carried out at the same T and P with samples containing different H_2O concentrations. If they can be fit well with roughly the same combination of D_0 and a, that is a good indication of model validity. This criterion has been successfully applied to the diffusion profiles at 0.95 GPa and three temperatures (Table 3.4), with the error of a estimated about 5 (e.g., 68±5 at 841 K). Fitting results show that a increases as temperature decreases, as also observed from the dehydration profiles of Liu et al. (2004a) and for rhyolitic melt (Ni and Zhang, 2008). The diffusion profiles from Behrens et al. (2004) were also refit to constrain parameter a in high temperature range, with a program allowing multivariate (D_0 and a) fitting and error analysis for a single profile (Ni and Zhang, 2008). The dependence of H_2O_m diffusivity on water content turns out to be much smaller at magmatic temperatures, and in some cases (above 1750 K) even negative a values are found. Because these temperatures are beyond typical magmatic temperatures, the validity of the negative a values was not explored further. The results of best-fit parameter a are summarized in Table 3.4 and are plotted in Fig. 3.4A, and they form a rough linear trend with $1000/T$ (with little pressure dependence), which can be fit (York, 1966) as

$$a=(-62.380\pm5.851)+\frac{108882\pm6185}{T}, \qquad (3\text{-}4)$$

where T is in K. By assuming Eq. (3-4), all diffusion profiles from Liu et al. (2004a), Behrens et al. (2004) and this work are fit again to constrain parameter D_0. Because the profiles of Dac-DC05-12 and Dac-DC06-21 are relatively short (240 µm and 130 µm,

62

Table 3.4 Best-fit *a* values using the model $D_{H_2O_m} = D_0 \exp(aX)$ and $\ln K = 1.49 - 2634/T$

Run #	T (K)	P (GPa)	a	R^2
Dac-DC05-12	~893	0.95	62±5	0.9928
Dac-DC05-13				0.9976
Dac-DC05-14	~841	0.95	68±5	0.9972
Dac-DC06-15				0.9978
Dac-DC06-17	~789	0.95	72±5	0.9941
Dac-DC06-22				0.9965

Refit from Liu et al. (2004a)

DC2B5	~911	~0.11	52±5	0.9983
DC53b2				0.9988
DC2B4				0.9973
DC1	881	~0.11	66±5	0.9951
DC53b1				0.9979

Refit from Behrens et al. (2004)

DacDC2	1608	1.0	7.1±10.0	0.9950
DacDC3	1708	0.5	-0.4±4.7	0.9954
			0.2±5.0	0.9961
DacDC5	1508	1.0	10.9±5.1	0.9966
DacDC6	1798	1.0	-8.6±12.3	0.9909
DacDC7	1458	1.0	17.2±6.0	0.9972
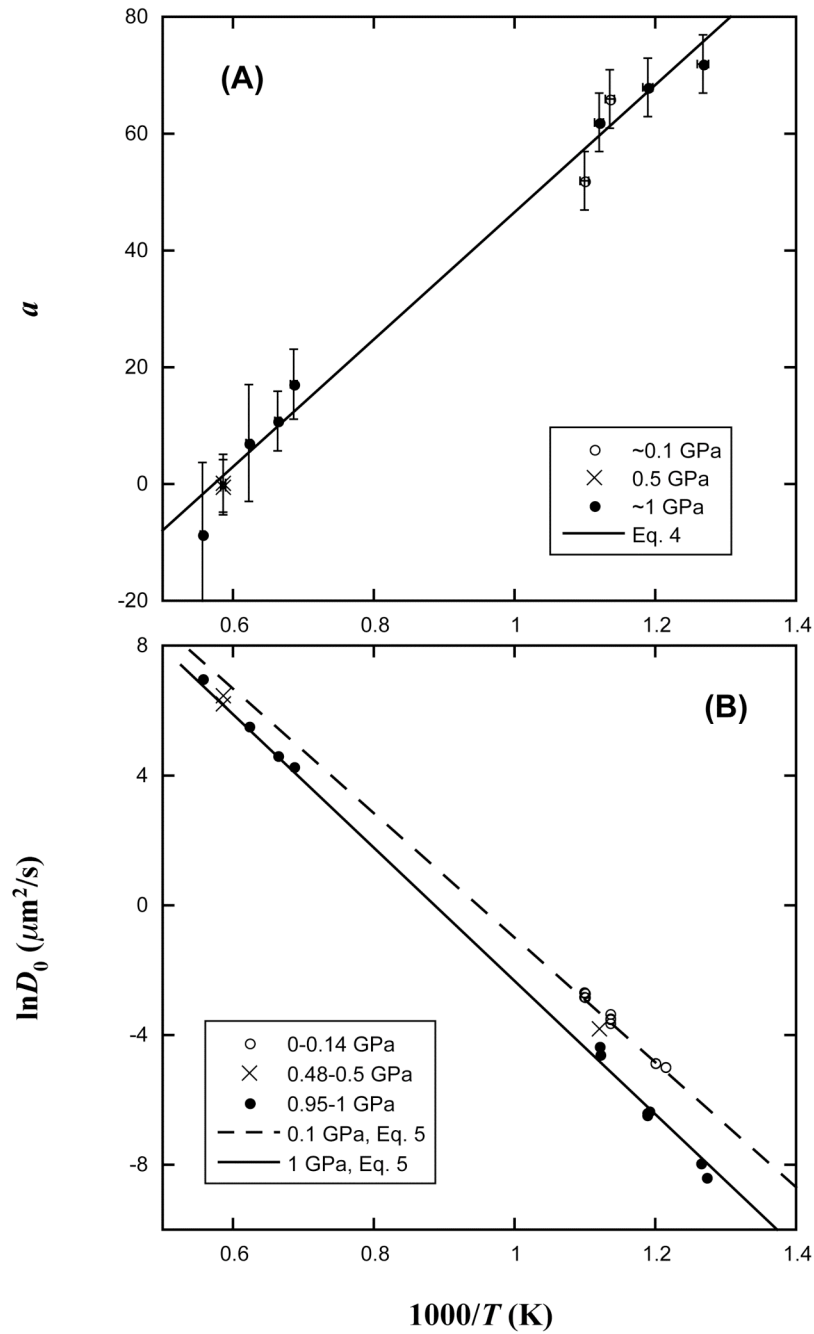
Fig. 3.4. Best-fit parameters using the model $D_{H_2O_m} = D_0 \exp(aX)$. (A) Parameter a from this work and from refits of data in Liu et al. (2004a) and Behrens et al. (2004). (B) $\ln D_0$ (Table 3.5) at various T and P assuming Eq. (3-4), indicating progressively negative pressure effect towards low T. Also shown are calculated $\ln D_0$ at 0.1 GPa (dash line) and 1 GPa (solid line) from Eq. (3-5).

respectively), they may have been considerably influenced by convolution effect. Therefore a convoluted profile is first computed by assuming that the spatial resolution of IR measurement is 15 μm, and then the new profile is used for fitting to find D_0.

The resulted D_0 values are reported in Table 3.5 and plotted in Fig. 3.4B. Furthermore, fitting curves have been compared with measured profiles in Fig. 3.2, showing fairly good matches. Although a pressure effect cannot be easily resolved in the high temperature range, at lower T, D_0 does show a systematic decrease from <0.15 GPa to ~1 GPa. The pressure dependence can be rationalized by a positive activation volume for H_2O_m diffusion, and an Arrhenius relation is appropriate to characterize both temperature and pressure dependences, resulting in

$$D_0 = \exp\left[(18.208\pm0.351) - \frac{(19064\pm303) + (1476.7\pm218.5)P}{T}\right]. \qquad (3\text{-}5)$$

where D_0 is in $\mu m^2/s$, T is in K, and P is in GPa. This regression reproduces most experimental $\ln D_0$ within an error of 0.4 (or a factor of 1.5 for D_0). A zero pressure activation energy E_a of 159 kJ/mol and a constant activation volume $\Delta V^{\ddagger}$ of 12±2 cm^3/mol (which is slightly lower than the molar volume of liquid water at ambient conditions) are implied based on this expression. H_2O_m diffusivity at a given T, P, and X can be calculated by combining Eqs. (3-3), (3-4) and (3-5):

$$D_{H_2O_m} = \exp\left(18.208 - 62.38X - \frac{19064 - 108882X + 1476.7P}{T}\right). \qquad (3\text{-}6)$$

$D_{H_2O_t}$ and T-P-X Dependence

H_2O_t diffusivity can be calculated from H_2O_m diffusivity through

Table 3.5

Fitting results of all H_2O diffusion profiles in dacite assuming

$D_{H_2O_m} = D_0 \exp[(-62.38 + 108882/T)X]$

Run #	T (K)	P (GPa)	H_2O_t	$\ln D_0$	R^2	source
Diffusion-couple						
DacDC3	1708	0.5	5.4	6.47±0.08	0.9953	2
				6.23±0.09	0.9961	2
DacDC2	1608	1.0	2.6	5.54±0.10	0.9950	2
DacDC5	1508	1.0	4.0	4.63±0.08	0.9966	2
DacDC6	1798	1.0	2.7	7.00±0.12	0.9906	2
DacDC7	1458	1.0	4.1	4.29±0.08	0.9970	2
Dac-DC06-22	791	0.95	5.8	-7.93±0.21	0.9958	3
Dac-DC06-17	786	0.95	6.7	-8.37±0.20	0.9950	3
Dac-DC06-15	842	0.95	5.7	-6.45±0.09	0.9982	3
Dac-DC05-14	840	0.95	7.7	-6.33±0.25	0.9936	3
Dac-DC06-21*	842	0.95	1.4	-6.38±0.14	0.9982	3
Dac-DC05-13	892	0.95	5.3	-4.58±0.10	0.9973	3
Dac-DC05-12*	893	0.95	7.7	-4.33±0.04	0.9937	3
Dac-DC06-19	893	0.48	4.0	-3.79±0.08	0.9978	3
Dehydration						
DC2A3	834	0.100	2.4	-4.83±0.06	0.9970	1
				-4.84±0.08	0.9950	1
DC2B4	881	0.143	2.5	-3.32±0.06	0.9979	1
DC2B5	910	0.133	2.6	-2.80±0.06	0.9978	1
				-2.68±0.07	0.9972	1
DC1	881	0.096	1.5	-3.46±0.08	0.9956	1
DC53b3	824	0.0001	0.8	-4.96±0.03	0.9994	1
				-4.95±0.08	0.9964	1
DC53b1	881	0.095	0.8	-3.61±0.05	0.9979	1
				-3.48±0.07	0.9974	1
DC53b2	911	0.097	0.8	-2.79±0.06	0.9976	1
				-2.65±0.05	0.9987	1

Source of data: [1]=Liu et al. (2004a); [2]=Behrens et al. (2004); [3]=this work.
* Fit with convoluted theoretical profile (see text).

$$D_{H_2O_t} = D_{H_2O_m} \frac{dX_m}{dX},$$ (3-7)

where dX_m/dX depends on equilibrium constant of the speciation reaction (Eq. 3-2) and H_2O_t mole fraction X as:

$$D_{H_2O_t} = D_{H_2O_m} \left[1 + \frac{2X-1}{\sqrt{4X(X-1)(1-4/K)+1}} \right].$$ (3-8)

The correlation between $D_{H_2O_t}$ and temperature, pressure, and water content is illustrated in Fig. 3.5. The $D_{H_2O_t}$ increases with temperature following an Arrhenius manner, and the activation energy depends strongly on water content and weakly on pressure. For example, E_a at 0.1 GPa decreases from 129 kJ/mol for 1 wt.% H_2O_t to 57 kJ/mol for 6 wt.% H_2O_t, whereas E_a at 1 wt.% increases by only 11 kJ/mol from 0.1 GPa to 1 GPa. Pressure reduces diffusivity more noticeably at low temperatures, by a factor of ~6 at 786-893 K over 1 GPa interval. The $D_{H_2O_t}$ also strongly depends on H_2O concentration, especially at low T where linear correlation can only hold at most to ~0.8 wt.%. Because H_2O diffusion is faster than the diffusion of most cations, bubbles are expected to grow more rapidly than crystals. On the other hand, H_2O diffusion is still not efficient for water migration over a large distance. For examples, at 1273 K and 0.2 GPa, diffusion distance of water after 100 years is only 1.3 m even at a high water content of 6 wt.%, far smaller than typical size of a magma chamber.

Okumura and Nakashima (2006) reported average diffusion-out H_2O diffusivity in dacitic glass. Their diffusivity from certain experiments was probably underestimated due to the curvature in absorbance versus $t^{1/2}$ plots. For comparison, new diffusion-out diffusivities were extracted from their original data by using the data with no more than
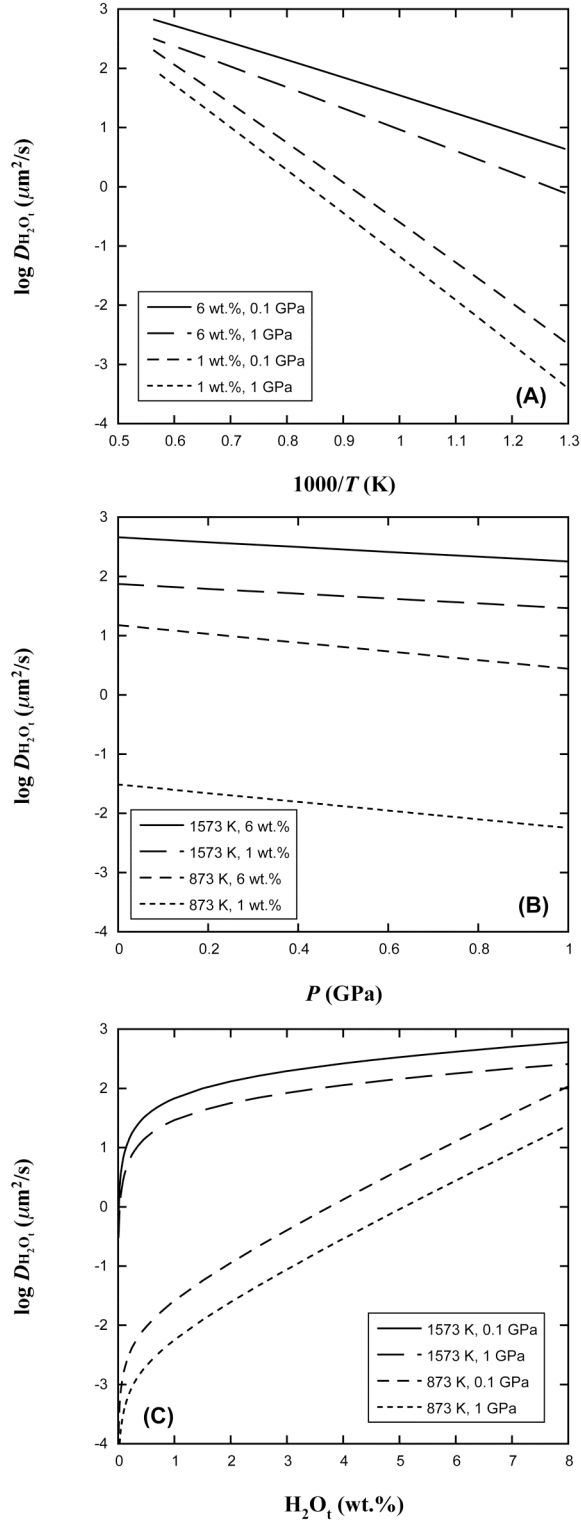
Fig. 3.5. H_2O_t diffusivity in dacite versus (A) temperature, (B) pressure, and (C) water content (Eq. 3-8). See text for detailed discussion.

20% dehydration, and then find $D_{H_2O_t}$ at 1 wt.% using the method described in Ni and Zhang (2008). Fig. 3.6 compares their results with the new diffusivity model and shows that there is general consistency (within a factor of 1.8, slightly larger than experimental and model uncertainty).

Comparison with H$_2$O diffusion in rhyolite

The P-T-H_2O_t dependence of H_2O diffusivity in dacite follows the same trend as those in rhyolite (Ni and Zhang, 2008), such as rapid increase with water concentration and negative pressure effect. Compared to rhyolite, H_2O diffusivity in dacite increases with water content more strongly at <1313 K but less strongly at >1313 K, as shown in the plot of parameter a vs. temperature (Fig. 3.7A). Furthermore, H_2O diffusivity in dacite shows a stronger dependence on temperature than in rhyolite. For example, at 0.1 GPa and 1 wt.% H_2O_t, the activation energy for H_2O diffusion in dacite is 129 kJ/mol, larger than that in rhyolite (84 kJ/mol, Ni and Zhang, 2008). The difference in E_a, likely due to lower ionic porosity in dacite, leads to a crossover of H_2O diffusivity at ~1253 K (Fig. 3.7B) below which $D_{H_2O_t}$ in dacite is smaller than in rhyolite. As pressure increases to 1.0 GPa, the crossover temperature increases to ~1323 K. Calculations show that when water content is below 5 wt.%, H_2O diffusion in dacite is always lower than that in rhyolite at <1173 K (Fig. 3.7C) and faster than that in rhyolite at >1323 K. Diffusivity in both melts becomes very similar at ≥5 wt.% H_2O, especially at 1.0 GPa (Fig. 3.7D). Pressure effect on H_2O diffusivity in rhyolite, about a factor of 10 over 1 GPa, is slightly larger than that in dacite.
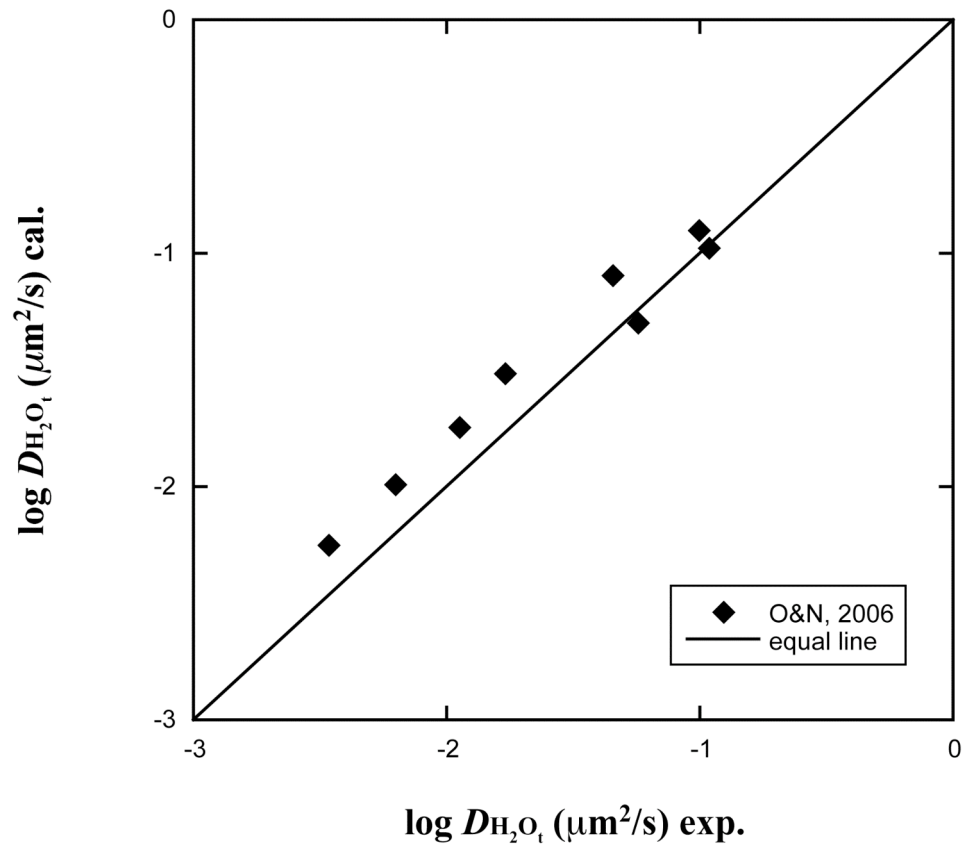
Fig. 3.6. Comparison of my new diffusivity model with the in situ study of Okumura and Nakashima (2006). Average diffusion-out diffusivity is extracted from the data of Okumura and Nakashima (2006) where the glass still retains 80 percent of its initial water, and then converted to diffusivity at 1 wt.% H_2O concentration.
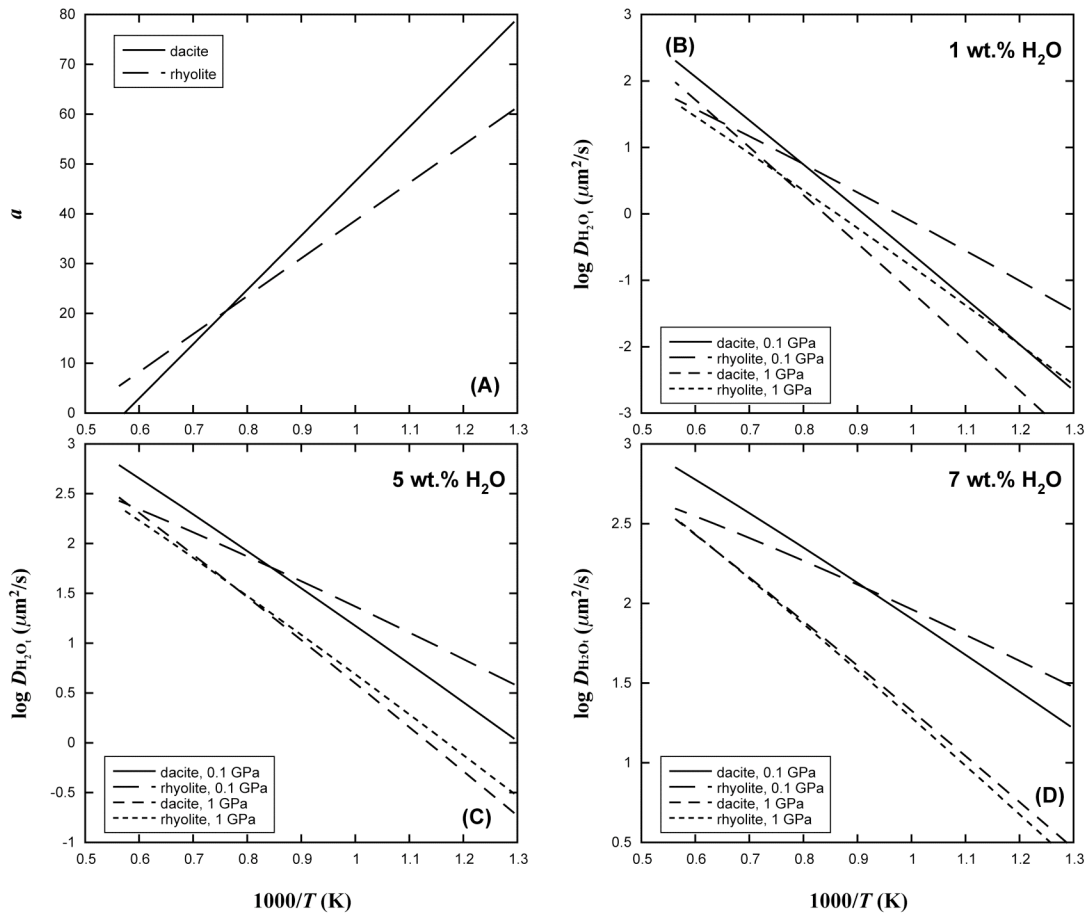
Fig. 3.7. Comparison of H_2O_t diffusivities in dacite (this study) and rhyolite (Ni and Zhang, 2008). H_2O_t diffusivity in dacite increases more strongly with water content at <1313 K (A) and temperature at 1 wt.% H_2O_t (B) and 5 wt.% H_2O_t (C) than that in rhyolite, but becomes similar as that in rhyolite at 7 wt.% (D). Note the difference in vertical scale of each plot. Crossover temperature of diffusivity in these two melts lies between 1173 K to 1323 K at <5 wt.% H_2O_t.

The viscosity of dacitic melt is less than that of rhyolite by more than one order of magnitude at 1 wt.% H_2O_t and $T >1073$ K based on calculations using the model of Hui and Zhang (2007). However, the diffusivity difference is within a factor of 3, which means that the inverse proportionality between diffusivity and viscosity (Einstein relation or Eyring relation) does not hold. Furthermore, because diffusivity in dacite may be smaller than that in rhyolite, even the inverse relation between diffusivity and viscosity may be violated.

Application to bubble growth in dacitic melt

Explosive volcanic eruptions are associated with the growth of water (with some CO_2) bubbles inside melts under water-oversaturated conditions. Bubble growth is controlled by the slower of two kinetic processes: viscous flow and water diffusion (Navon et al., 1998; Lensky et al., 2004). With established models of melt viscosity, water diffusivity and water solubility, the rate of bubble growth can be calculated (e.g., Proussevitch and Sahagian, 1998) and compared with experimental observations (e.g., Liu and Zhang, 2000).

The new H_2O diffusivity model in this study can be applied to simulate non-convective bubble growth in a melt with dacitic composition, with viscosity model of Hui and Zhang (2007) and solubility model of Zhang et al. (2007). Bubble growth model is from Proussevitch and Sahagian (1998), as modified by Liu and Zhang (2000). Simulation results for hydrous melts with 4 wt.% H_2O are illustrated in Fig. 3.8. At 50 MPa (in a volcanic conduit), H_2O diffusion is not efficient enough to keep high gas pressure in a bubble as it grows, therefore H_2O diffusion is the rate-determining process.
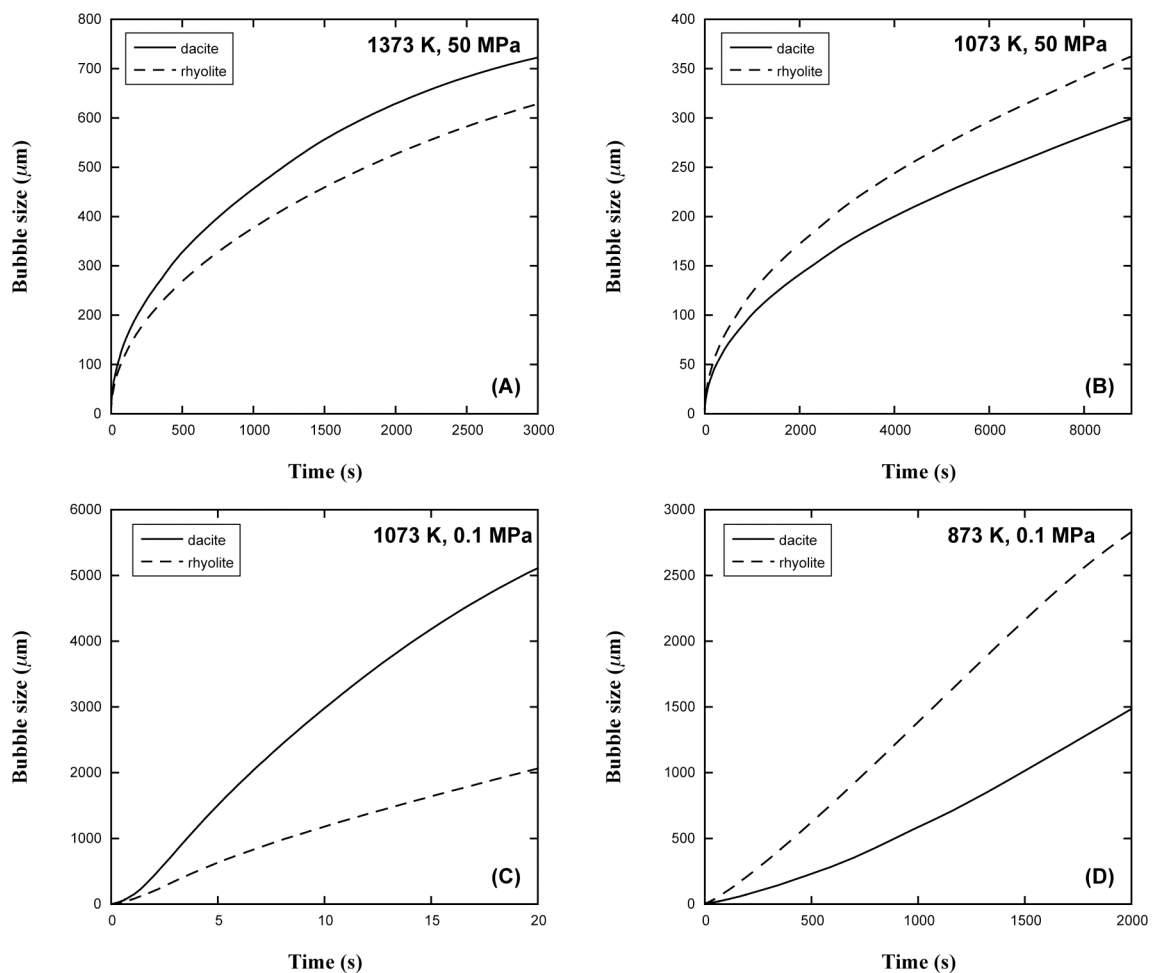
Fig. 3.8. Calculated bubble growth (initial bubble radius is 1 μm) using the model of Liu and Zhang (2000). Growth rate at 50 MPa is slow and controlled by H_2O diffusion (parabolic curve), therefore bubble size in dacite increases faster at 1373 K but slower at 1073 K than that in rhyolite. At 0.1 MPa viscosity plays a more important role: bubble growth in dacite is faster at 1073 K due to its lower viscosity whereas bubble growth in rhyolite is faster at 873 K because viscosity difference is minimal. For dacite, viscosity is from Hui and Zhang (2007) and H_2O diffusivity is from this study. For rhyolite, viscosity is from Zhang et al. (2003) and H_2O diffusivity is from Ni and Zhang (2008). H_2O solubility is from Zhang et al. (2007).

Bubble growth in dacite is faster at 1373 K (Fig. 3.8A) but slower at 1073 K (Fig. 3.8B) than that in rhyolite due to their H_2O diffusivity crossover. At ambient pressure, diffusion becomes much more efficient and viscosity starts to play a more effective role. Bubble growth is therefore much more rapid than at 50 MPa, and the growth curve is no longer parabolic. Furthermore, bubble growth in dacite is faster than in rhyolite by more than a factor of 2 due to the lower viscosity of dacitic melt, although H_2O diffusion in dacite is slower. In a lava dome at 873 K, the melt is more viscous and the growth curve becomes more concave (theoretically it should resemble an exponential function if growth is completely controlled by viscosity; Navon et al., 1998). However, because the viscosity of rhyolite and dacite is very close at 873 K, growth rate in rhyolite is faster again due to faster H_2O diffusion in rhyolite. Note that as bubble grows even larger, diffusion gradually takes control of the growth until bubble reaches their equilibrium size (Navon et al., 1998; Lensky et al., 2004).

CONCLUDING REMARKS

The experimental investigation on H_2O diffusion in dacite at 786-893 K and 0.48-0.95 GPa confirms that increasing pressure slows the rate of diffusive transport of H_2O. This negative pressure influence, as also observed in rhyolitic melt, is more prominent at low temperatures. Therefore, during the process of magma upwelling, reducing pressure helps the formation and growth of bubbles, and hence adds to the violence of explosive volcanic eruptions. Combined with previous studies under different *T-P* conditions, a general model of H_2O diffusivity in dacitic melts has been constructed. Dacite is the

second melt for which a general H_2O diffusion model is available, after rhyolitic melt. The new diffusivity model can applied to a variety of geological circumstances: 773-1773 K, 0-1 GPa, and 0-8 wt.% water content. The H_2O_m diffusivity based on this work and viscosity of hydrous dacite based on Hui and Zhang (2007) do not follow either Eyring relation or Einstein relation. Compared to rhyolite, H_2O diffusion in dacite shows a stronger dependence on temperature and water concentration, and its higher activation energy results in slower diffusion in dacite at T<1173 K but more rapid diffusion at T>1323 K than in rhyolite when H_2O_t <5 wt.%. This study provides important data towards a universal H_2O diffusivity model in felsic to basaltic calc-alkaline melts, and can be applied to both deep-seated magmatic processes and sub-surface volcanic eruptions.

REFERENCES

Behrens, H., Zhang, Y., 2001. Ar diffusion in hydrous silicic melts: implications for volatile diffusion mechanisms and fractionation. Earth Planet. Sci. Lett. 192, 363-376.

Behrens, H., Yamashita, S., 2008. Water speciation in hydrous sodium tetrasilicate and hexasilicate melts: constraints from high temperature NIR spectroscopy. Chem. Geol., in press.

Behrens, H., Zhang, Y., Xu, Z., 2004. H_2O diffusion in dacitic and andesitic melts. Geochim. Cosmochim. Acta 68, 5139-5150.

Behrens, H., Zhang, Y., Leschik, M., Wiedenbeck, M., Heide, G., Frischat, G.H., 2007. Molecular H_2O as carrier for oxygen diffusion in hydrous silicate melts. Earth Planet. Sci. Lett. 254, 69-76.

Bercovici, D., Karato S., 2003. Whole-mantle convection and the transition-zone water filter. Nature 425, 39-44.

Borisova, A.Y., Pichavant, M., Polvé, M., Wiedenbeck, M., Freydier, R., Candaudap, F., 2006. Trace element geochemistry of the 1991 Mt. Pinatubo silicic melts, Philippines: implications for ore-forming potential of adakitic magmatism. Geochim. Cosmochim. Acta 70, 3702-3716.

Bose, K., Ganguly, J., 1995. Quartz-coesite transition revisited: reversed experimental determination at 500-1200°C and retrieved thermochemical properties. Am. Mineral. 80, 231-238.

Botcharnikov, R.E., Behrens, H., Holtz, F., 2006. Solubility and speciation of C-O-H fluids in andesitic melt at T=1100-1300°C and P=200 and 500 MPa. Chem. Geol. 229, 125-143.

Chen, C.-H., Depaolo, D.J., Nakada, S., Shieh Y.-N., 1993. Relationship between eruption volume and neodymium isotopic composition at Unzen volcano. Nature 362, 831-834.

Freda, C., Baker, D.R., Romano, C., Scarlato, P., 2003. Water diffusion in natural potassic melts. Geol. Soc. Spec. Publ. 213, 53-62.

Gardner, J.E., Carey, S., Rutherford, M.J., Sigurdsson, H., 1995. Petrologic diversity in Mount St. Helens dacites during the last 4,000 years: implications for magma mixing. Contrib. Mineral. Petrol. 119, 224-238.

Holtz, F., Sato, H., Lewis, J., Behrens, H., Nakada, S., 2005. Experimental petrology of the 1991-1995 Unzen dacite, Japan. Part I: Phase relations, phase chemistry and pre-eruptive conditions. J. Petrol. 46, 319-337.

Hui, H. Zhang, Y., 2007. Toward a general viscosity equation for natural anhydrous and hydrous silicate melts. Geochim. Cosmochim. Acta 71, 403-416.

Hui, H., Zhang, Y., Xu, Z., Behrens, H., 2008. Pressure dependence of the speciation of dissolved H_2O in rhyolitic melts. Geochim. Cosmochim. Acta 72, 3229-3240.

Lensky, N.G., Navon, O., Lyakhovsky, V., 2004. Bubble growth during decompression of magma: experimental and theoretical investigation. J. Volcano. Geotherm. Res. 129, 7-22.

Liu, Y., Zhang, Y., 2000. Bubble growth in rhyolitic melt. Earth Planet. Sci. Lett. 181, 251-264.

Liu, Y., Zhang Y., Behrens, H., 2004a. H_2O diffusion in dacitic melts. Chem. Geol. 209, 327-340.

Liu, Y., Behrens, H., Zhang, Y., 2004b. The speciation of dissolved H_2O in dacitic melt. Am. Mineral. 89, 277-284.

Martel, C., Dingwell, D.B., Spieler, O., Pichavant, M., Wilke, M., 2000. Fragmentation of foamed silicic melts: an experimental study. Earth Planet. Sci. Lett. 178, 47-58.

Mierdel, K., Keppler, H., Smyth, J.R., Langenhorst, F., 2007. Water solubility in aluminous orthopyroxene and the origion of Earth's asthenosphere. Science 315, 364-368.

Navon, O., Chekhmir, A., Lyakhovsky, V., 1998. Bubble growth in highly viscous melts: theory, experiments and autoexplosivity of dome lavas. Earth Planet. Sci. Lett. 160, 763-776.

Ni, H., Zhang, Y., 2008. H_2O diffusion models in rhyolitic melt with new high pressure data. Chem. Geol. 250, 68-78.

Nowak, M., Behrens, H., 1997. An experimental investigation on diffusion of water in haplogranitic melts. Contrib. Mineral. Petrol. 126, 365-376.

Ohlhorst, S., Behrens, H., Holtz, F., 2001. Compositional dependence of molar absorptivities of near-infrared OH- and H_2O bands in rhyolitic to basaltic glasses. Chem. Geol. 174, 5-20.

Okumura, S., Nakashima, S., 2004. Water diffusivity in rhyolitic glasses as determined by in situ IR spectrometry. Phys. Chem. Minerals 31, 183-189.

Okumura, S., Nakashima, S., 2006. Water diffusion in basaltic to dacitic glasses. Chem. Geol. 227, 70-82.

Proussevitch, A.A., Sahagian, D.L., 1998. Dynamics and energetics of bubble growth in magmas: analytical formulation and numerical modeling. J. Geophys. Res. 103, 18223-18251.

Schuessler, J.A., Botcharnikov, R.E., Behrens, H., Misiti, V., Freda, C., 2008. Oxidation state of iron in hydrous phono-tephritic melts. Am. Mineral. 93, 1493-1504.

Silver, L.A., Ihinger, P.D., Stolper, E.M., 1990. The influence of bulk composition on the speciation of water in silicate glasses. Contrib. Mineral. Petrol. 104, 142-162.

Szramek, L., Gardner, J.E., Larsen, J., 2006. Degassing and microlite crystallization of basaltic andesite magma erupting at Arenal Volcano, Costa Rica. J. Volcanol. Geotherm. Res. 157, 182-201.

Vila, M., Pin, C., Enrique, P., Liesa, M., 2005. Telescoping of three distinct magmatic suites in an orogenic setting: generation of Hercynian igneous rocks of the Albera Massif (Eastern Pyrenees). Lithos 83, 97-127.

Watson, E.M., 1991. Diffusion of dissolved CO_2 and Cl in hydrous silicic to intermediate magmas. Geochim. Cosmochim. Acta 55, 1897-1902.

Yamashita, S., Kitamura, T., Kusakabe, M., 1997. Infrared spectroscopy of hydrous glasses of arc magma compositions. Geochem. J. 31, 169-174.

York, D., 1966. Least-squares fitting of a straight line. Can. J. Phys. 44, 1079-1086.

Zhang, Y., 1999. A criterion for the fragmentation of bubbly magma based on brittle failure theory. Nature 402, 648-650.

Zhang, Y., Behrens, H., 2000. H_2O diffusion in rhyolitic melts and glasses. Chem. Geol. 169, 243-262.

Zhang, Y., Stolper E.M., 1991. Water diffusion in a basaltic melt. Nature 351, 306-309.

Zhang, Y., Stolper, E.M., Wasserburg, G.J., 1991. Diffusion of water in rhyolitic glasses. Geochim. Cosmochim. Acta 55, 441-456.

Zhang, Y., Belcher, R., Ihinger, P.D., Wang, L., Xu, Z., Newman, S., 1997. New calibration of infrared measurement of dissolved water in rhyolitic glasses. Geochim. Cosmochim. Acta 61, 3089-3100.

Zhang Y., Xu Z., Liu, Y., 2003. Viscosity of hydrous rhyolitic melts inferred from kinetic experiments, and a new viscosity model. Am. Mineral. 88, 1741-1752.

Zhang, Y., Xu, Z., Zhu, M., Wang, H., 2007. Silicate melt properties and volcanic eruptions. Rev. Geophys. 45, RG4004, doi:10.1029/2006RG000216.

CHAPTER IV

WATER SPECIATION AND DIFFUSION IN HAPLOANDESITE

ABSTRACT

Water is an important volatile component in andesitic eruptions or deep-seated andesitic magma chambers. H_2O diffusion was studied by dehydrating haploandesitic melts containing ≤ 2.5 wt.% water content at 743-873 K and 0.1 GPa in cold-seal pressure vessels. FTIR microspectroscopy was utilized to measure species [molecular H_2O (H_2O_m) and hydroxyl group (OH)] and total H_2O (H_2O_t) concentration profiles on the quenched glasses from dehydration experiments. The equilibrium constant of H_2O speciation reaction $H_2O_m + O \rightleftharpoons 2OH$ in this Fe-free andesite varies with temperature as $\ln K = 1.547 - 2453/T$, indicating more OH is present in andesite than in rhyolite or dacite for a given water concentration. Water diffusivity at the experimental conditions depends strongly on H_2O concentration, contrary to previous H_2O diffusion data at 1608-1848 K. The diffusion profiles are consistent with the model that molecular H_2O is the diffusion species, and H_2O_m diffusivity (in $\mu m^2/s$) in haploandesite at 0.1 GPa can be formulated as

$$D_{H_2O_m} = \exp\left(14.986 - 13.905X - \frac{17974 - 73136X}{T}\right),$$

where T is temperature in K, and X is mole fraction of H_2O_t: $X = C/18.015/[C/18.015+(100-C)/33.84]$ with C being H_2O_t in wt.%. H_2O_t diffusivity can be expressed as:

$$D_{H_2O_t} = D_{H_2O_m}\left[1+\frac{2X-1}{\sqrt{4X(X-1)(1-4/K)+1}}\right].$$

By comparison with previous water diffusion studies, H_2O diffusivity at T <873 K in calc-alkaline silicate melts is found to increase with degree of polymerization: andesite < dacite < rhyolite, opposite from the trend at superliquidus temperatures.

INTRODUCTION

Water diffusion in felsic melts has been extensively studied (e.g., Shaw, 1974; Delaney and Karsten, 1981; Zhang et al., 1991a; Nowak and Behrens, 1997; Zhang and Behrens, 2000; Liu et al., 2004a; Behrens et al., 2004; Okumura and Nakashima, 2004, 2006; Behrens et al., 2007; Ni and Zhang, 2008; Ni et al., 2008; Behrens and Zhang, 2009; Wang et al., 2009) due to its importance in bubble growth and explosive volcanism. Molecular H_2O (H_2O_m), rather than hydroxyl (OH), has been shown to be the dominating diffusion species for water diffusion (Zhang et al., 1991a; Zhang and Behrens, 2000) and carrier of oxygen isotope diffusion (Zhang et al., 1991b; Behrens et al., 2007). Diffusivities of H_2O_m and total H_2O (H_2O_t) have been obtained for some melts as a function of temperature, water concentration and pressure (Ni and Zhang, 2008; Ni et al., 2008). These relations can be incorporated in modeling volcanic and magmatic processes. In general, H_2O_t diffusivity increases strongly with temperature and water

concentration (more strongly at lower temperatures), but decreases relatively slowly with pressure.

However, studies on water diffusion in intermediate to mafic melts are still scarce. Zhang and Stolper (1991) reported the first study in basalt at 1573-1773 K and 1 GPa, suggesting H_2O_t diffusivity is proportional to water content (C in wt.%). Freda et al. (2003) investigated water diffusion in trachyte at 1373-1673 K and 1 GPa, and demonstrated that H_2O diffusivity increases with water content. Behrens et al. (2004) found very weak dependence on water content in andesite at 1608-1848 K and 0.5-1.5 GPa. In treating the dehydration of basaltic and andesitic glasses at 673-948 K and 0.1 MPa with *in situ* infrared analysis, Okumura and Nakashima (2006) assumed proportional diffusivity ($D \propto C$) in basalt but constant diffusivity in andesite.

Andesitic magmas are characteristic of subduction zone environment and have widespread occurrences (Hess, 1989), although the liquid composition is often more silicic than total bulk composition (e.g., Szramek et al., 2006). Nonetheless, water-bearing andesitic liquid could be present in nonexplosive andesitic to basaltic eruptions (Lewis-Kenedi et al., 2005), as also shown by melt inclusions from Inamuradake scoria cone, Japan (Saito et al., 2001) or the presence of magnesian pargasitic amphibole from Mt. Shasta, USA (Grove et al., 2003). Therefore, information on water diffusion in andesite is important for interpreting the dynamics and history of these eruptions. Diffusive transport of water is also relevant to deep-seated magma chamber processes, such as magma mixing (Mora et al., 2002). Furthermore, H_2O diffusivity in andesite can be compared with that in rhyolite and dacite to unravel the correlation between diffusivity and melt composition or structure.

The presence of iron in andesite is expected to cause at least two major difficulties for infrared (IR) measurements: (a) baseline change in IR spectrum (Liu et al., 2004a; Ni et al., 2008) and (b) reduction of glass transparency. Haploandesite (Fe-free andesite) has been used as an analogue of andesitic composition in viscosity (Richet et al., 1996; Liebske et al., 2003; Vetere et al., 2006), H_2O or silicate solubility (Mysen and Wheeler, 2000a, 2000b), and melt structure studies (Mysen, 1999) to avoid Fe-induced complexities (such as redox alteration and crystallization). Fe-free andesite was also chosen in this study to represent andesitic composition. An experimental investigation on water speciation and diffusion in haploandesite is reported in this study. The results are discussed by comparison with water diffusivity in Fe-bearing andesite and water diffusivity models in other silicate melts.

EXPERIMENTAL TECHNIQUES

Starting material

The synthesis of hydrous haploandesite was part of the thesis work of Liu (2003) and generally follows the procedures of Liebske et al. (2003). In simulating an andesitic composition, Ca and Mg are used to replace Fe^{2+} while keeping the same Ca/Mg ratio, and Al is used to replace Fe^{3+}. That is, in terms of SiO_2 content, a haploandesite is similar to andesite in mole fraction but not in weight percentage. The compositions of synthesized hydrous haploandesite glasses (HAD1 and HAD2) are listed and are compared with other haploandesites in literature (Table 4.1). The haploandesite used in this study is similar to that reported in Richet et al. (1996), slightly more silicic than that

83

Table 4.1
Anhydrous composition and water content of haploandesitic glass in wt.%

	HAD1 (This study)	HAD2 (This study)	Richet et al. (1996)	Mandeville et al. (2002)	Liebske et al. (2003)	Vetere et al. (2006)
SiO_2	62.36	62.25	62.40	65.29	58.69	59.19
TiO_2	0.00	0.00	0.55	1.13	0.01	0.02
Al_2O_3	19.73	20.26	20.01	17.71	21.57	21.57
FeO_T	0.01	0.04	0.03	0.00	0.02	0.06
MnO	0.02	0.02	0.02	0.00	0.02	0.06
MgO	2.28	2.39	3.22	3.12	5.38	5.50
CaO	9.68	10.37	9.08	7.96	9.49	9.49
Na_2O	4.58	4.12	3.52	3.24	3.30	3.40
K_2O	0.99	0.96	0.93	1.47	1.57	1.79
P_2O_5	0.00	0.03	0.12	0.00	0.00	0.00
Total	99.65	100.44	99.88	99.92	100.05	101.08
H_2O (IR)	2.0	2.5				

Major oxide concentrations of HAD1 and HAD2 are determined by a Cameca SX100 electron microprobe using a scanning beam of 5 µm raster length, 15 kV voltage, and 4 nA current. Water content (C in wt.%) is measured by FTIR using the calibration of Vetere et al. (2006). The anhydrous concentrations are calculated by $C_i/(1-C/100)$ with C_i being raw oxide contents. The composition of haploandesite in literature is also listed for comparison.

of Liebske et al. (2003) and Vetere et al. (2006), but less silicic than that of Mandeville et al. (2002).

Dehydration experiments in cold-seal vessels

A preliminary dehydration experiment at 823 K in a 0.1 MPa horizontal tube furnace generated significant vesiculation in the glass. As a result, dehydration experiments were performed under pressure to avoid bubble formation. Seven dehydration runs were carried out in a rapid-quench TZM (Ti-Zr-Mo) cold-seal pressure vessel at the University of Michigan at 743-873 K and 100 MPa. Two of these runs failed due to crystallization or sample cracking, and hence are not reported. A piece of doubly polished hydrous glass (~2 mm size) was attached to a steel filler rod using chromel wire. The filler rod was inserted into the cold bottom of the vertical vessel, supported by a iron rod. The pressure vessel was then sealed, and purged and pressurized with prepurified Ar (99.995% purity). An external furnace was used to heat the top part of the vessel. After thermal steady state was reached, the sample assemblage (sample + steel rod + iron rod) was lifted into the hot spot with an electromagnet. A sheathed chromel-alumel thermocouple (at about the same level as the sample) was attached outside the vessel to monitor the temperature. Sample temperature was evaluated using lab-calibrated T (furnace)-T (sample) correlation (a type S thermocouple was originally used in the calibration), with an uncertainty of ~10 K. Pressure was manually controlled within 100±1 MPa in most of the dwelling time. After an experimental duration of 5 to 42 days, the magnetic field was annulled and the sample assemblage immediately

dropped to the cold Ar atmosphere and cooled down rapidly. The quench rate in this pressure vessel was estimated to be 100-200 K/s (Liu et al., 2004a).

In addition to the above experiments, experimental dehydration data from Liu (2003) on a similar andesite are included. Although three dehydration experiments were carried out in Liu (2003), a meaningful diffusion profile was obtained from only one run, whereas the other two runs are only used to constrain water speciation. In total, eight experiments are used to constrain speciation and six experiments are used to understand diffusion. The details of all dehydration experiments are summarized in Table 4.2.

Profile analyses using FTIR

Water concentration in starting hydrous glasses was measured in the N_2-purged main chamber of PerkinElmer Spectrum GX FTIR spectrometer at the University of Michigan. The spectrometer comprises a NIR source, a CaF_2 beamsplitter, and a liquid-nitrogen cooled InSb detector. The glass was analyzed by FTIR using an aperture of 531 μm diameter, and 128 scans were made over 7800 cm^{-1} to 2000 cm^{-1} for each analysis. Acquired infrared spectra were hand fit using the calibration of Vetere et al. (2006): absorption coefficient being 1.04 L/mol/cm for 5200 cm^{-1} H_2O_m band, and 0.92 L/mol/cm for 4500 cm^{-1} OH band. The summation of species concentrations gives total H_2O concentration, as reported in Table 4.1.

Quenched glasses from dehydration experiments, without any cracks, were polished to sections of ~200 μm thickness. An Autoimage infrared microscope with a MCT detector (also cooled by liquid nitrogen) was combined with the FTIR spectrometer to measure diffusion profiles on polished sections. A rectangular aperture of 10 μm by

Table 4.2
Experimental conditions of dehydration runs

Run #	T	P^a	t	K	a
	(K)	(MPa)	(s)		
HAD2C1	773±10	100±1	1173600	0.204±0.007	80±5
HAD2C2	743±10	100±1	3598200	0.172±0.004	85±5
HAD2C3	873±10	100±1	470400	0.298±0.012	70±5
HAD2C4	823±10	100±1	709200	0.223±0.005	75±5
HAD1A3	834±5	100±2	689315	0.239±0.008	
HAD1A1[b]	823±10	100±1	857400	0.239±0.005	
HAD2B1[c]	878±5	103 to 34	103975	0.288±0.007	
HAD2B2[c]	780±5	102±1	1554510	0.209±0.007	

[a] Pressure medium is prepuried Ar gas in dehydration runs.
[b] Run product shows partial crystallization.
[c] These two runs are only used to constrain H_2O speciation. Pressure dropped in HAD2B1.

200 μm was applied and a series of spectra were collected along the central axis of a sample. The acquired infrared spectra were handled in the same way as for starting materials.

Water concentration profiles were collected from six dehydration runs (Fig. 4.1), and the details of their experimental conditions are summarized in Table 4.2. Dehydration can be treated as diffusion problem in a semi-infinite medium because the center of the hydrous glasses still maintain their initial water concentration. Two diffusion profiles can be measured, one from each side, from a single dehydration run, and they are approximately identical, except that one run (HAD1A1) produced bubbles on one side of the sample.

RESULTS

The dehydration profiles are shown in Figs. 4.1 and 4.2. The concentration profiles are all long enough so that the convolution effect is not significant. As illustrated in Fig. 4.2, H_2O diffusion profiles in haploandesitic melt at 743-873 K cannot be fit by the error function (short-dashed curve in Fig. 4.2), in contrast to H_2O diffusion profiles at temperatures of 1608-1848 K and pressures of 0.5-1.5 GPa (Behrens et al., 2004). Therefore, the assumption of constant diffusivity to model H_2O dehydration data at 773-948 K (Okumura and Nakashima, 2006) is incorrect. The dependence of diffusivity on H_2O concentration is consistent with all available data for H_2O diffusion in silicate melts at temperatures of 700-900 K (Zhang et al., 1991a; Liu et al., 2004a; Okumura and Nakashima, 2004; Ni and Zhang, 2008; Ni et al., 2008).
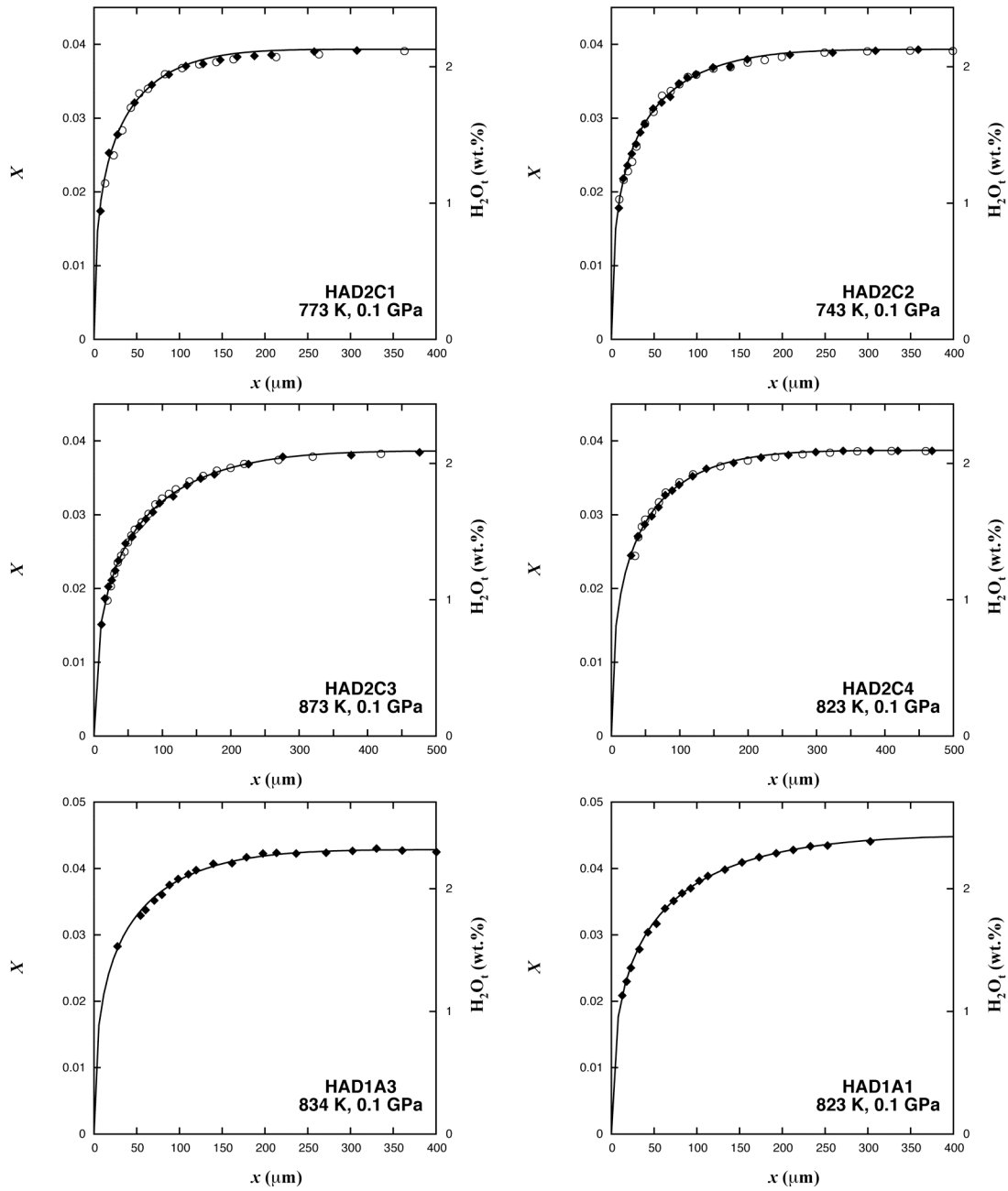
Fig. 4.1. Total H_2O concentration profiles from six dehydration experiments at 0.1 GPa. For the first four experiments, two profiles, one from each side, are plotted in filled diamonds and open circles, respectively. Some data points at large x are not shown for clarity. Solid curves are fits of filled diamonds assuming $D_{H_2O_m} = D_0 \exp[(-13.905 + 73136/T)X]$, with D_0 reported in Table 4.3.
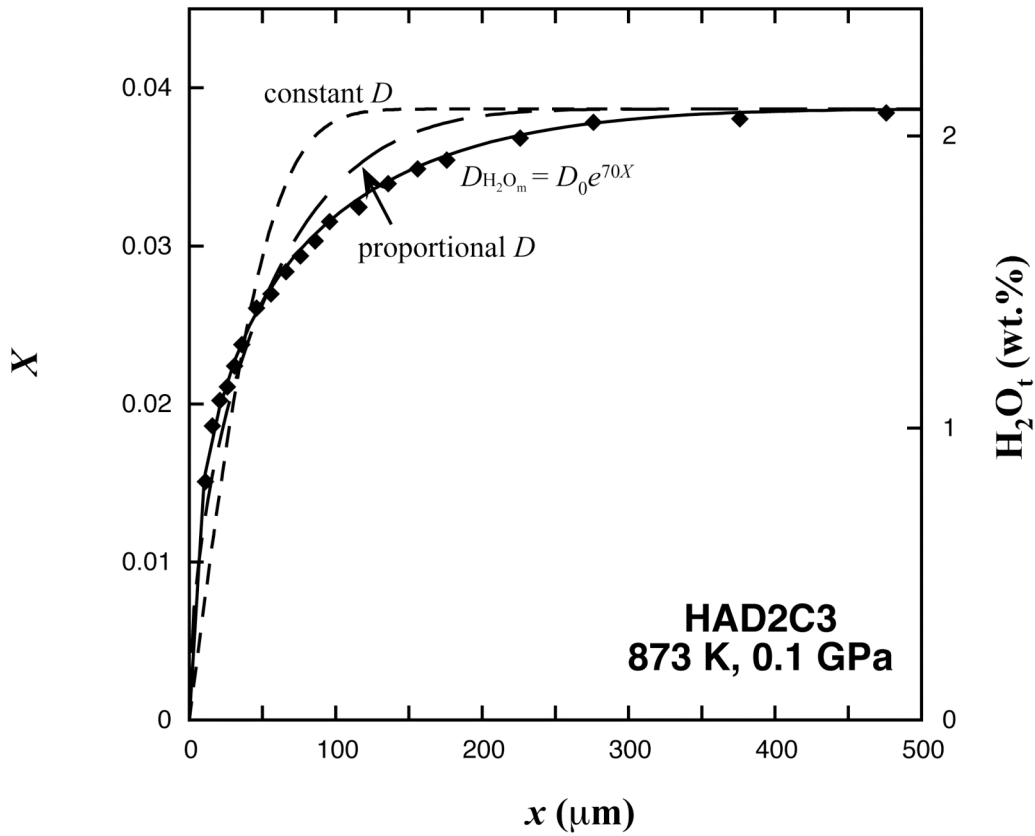
Fig. 4.2. Comparison of fitting quality using various models for HAD2C3. Constant diffusivity (short dash error function curve) or diffusivity proportional to H_2O concentration (long dash curve) yield significant mismatch, indicating the need of a stronger D vs. X correlation. Excellent fitting is achieved by assuming $D_{H_2O_m} = D_0 \exp(70X)$ for this profile.

By design and as shown by the experimental diffusion profiles (Figs. 4.1 and 4.2), H_2O_t in the center parts of the dehydration sections (large x in Figs. 4.1 and 4.2) is not affected by dehydration. Hence the center parts can be used to investigate the equilibrium of the species interconversion reaction:

$$H_2O_m + O \rightleftharpoons 2OH, \qquad (4.1)$$

where H_2O_m is molecular H_2O, OH is hydroxyl, and O is an anhydrous oxygen. The equilibrium constant for the above reaction is defined as:

$$K = \frac{[OH]^2}{[H_2O_m][O]} \qquad (4.2)$$

where brackets indicate mole fraction of each species on a single oxygen basis (Stolper, 1982; Zhang, 1999). The experimental data on the equilibrium constant K are shown in Table 4.2 and are plotted in Fig. 4.3. Because the experimental temperature is not very high, quench at 100-200 K/s is able to maintain the species concentrations at the experimental temperature (Zhang et al., 1995; Withers et al., 1999), as evidenced by well-defined trend between K and temperature (Fig. 4.3). The dependence of K on temperature can be modeled (York, 1966) as follows:

$$\ln K = 1.547 - \frac{2453}{T}, \qquad (4.3)$$

where T is temperature in K. The enthalpy of speciation reaction in haploandesite from the above equation is about 20 kJ/mol. As illustrated in Fig. 4.3, the equilibrium speciation in haploandesite is similar to that in Fe-bearing andesite (Botcharnikov et al., 2006). Furthermore, there is a consistent and systematic trend for the variation of K with anhydrous melt composition: K increases with the degree of melt depolymerization.
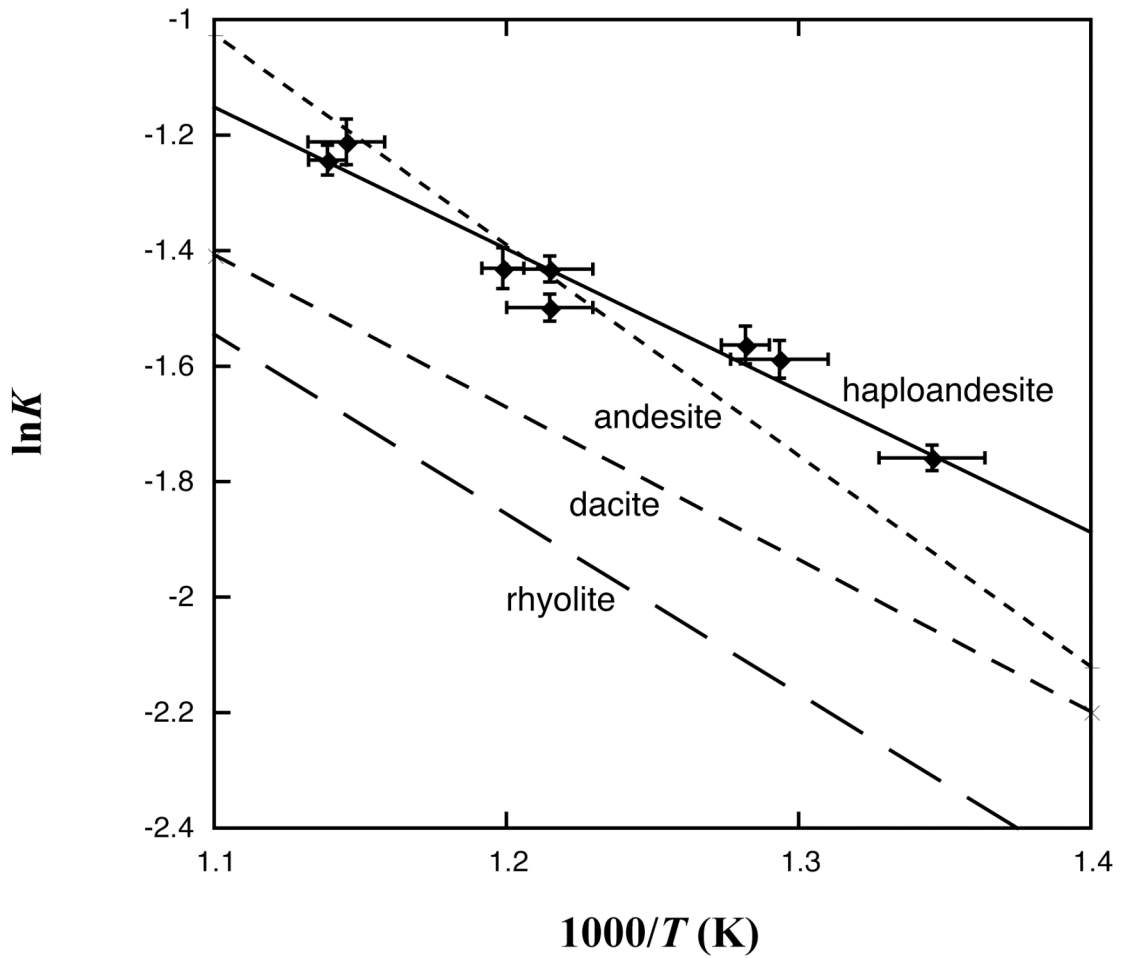
Fig. 4.3. Equilibrium constant K of water speciation reaction $H_2O_m + O \rightleftharpoons 2OH$ in rhyolite (Zhang et al., 1997), dacite (Liu et al., 2004b), andesite (Botcharnikov et al., 2006), and haploandesite from this work (Eq. 4-3). More OH is present in a more depolymerized melt at a given water content and temperature.

There is still debate on the mechanism of H_2O dissociation in aluminosilicate (Stolper, 1982; Mysen and Virgo, 1986; Kohn et al., 1992; Schmidt et al., 2001), but in hydrous calc-alkaline melts, replacing silicon and alkalis with aluminum and alkaline earth elements seem to destabilize H_2O molecules.

DISCUSSION

Modeling dehydration profiles

Simple diffusivity models, such as constant diffusivity or diffusivity proportional to H_2O_t concentration, were first tested to fit the dehydration profiles (Fig. 4.2). However, the significant mismatch between these simple models and experimental profiles indicates H_2O diffusivity increases with H_2O_t content more rapidly than the proportionality relation at our experimental conditions. For rhyolite, H_2O diffusivity is roughly proportional to H_2O_t at similar temperatures and with H_2O_t below 2 wt% (Zhang et al., 1991a; Zhang and Behrens, 2000; Behrens and Zhang, 2009). For dacite, the proportionality relation only holds when H_2O_t is below 0.8 wt% (Liu et al., 2004a; Ni et al., 2008). Our data indicate that the proportionality relation does not hold for haploandesite when H_2O_t is up to 2.0 wt% in a sample, similar to dacite but different from rhyolite. Strong correlation between diffusivity and H_2O concentration can be explained by H_2O_m being the dominating diffusion species ($D_{OH} << D_{H_2O_m}$) and $D_{H_2O_m}$ depending on water concentration exponentially (Zhang and Behrens, 2000; Liu et al., 2004a; Ni and Zhang, 2008; Ni et al., 2008; Wang et al., 2009). Thus H_2O diffusion in andesite follows:

$$\frac{\partial X}{\partial t} = \frac{\partial}{\partial x}\left(D_0 e^{aX} \frac{\partial X_m}{\partial x} \right). \tag{4.4}$$

Here t is time; x is distance; D_0 and a describe $D_{H_2O_m}$; X is the mole fraction of H_2O_t on a single oxygen basis: for hydrous haploandesite with C wt.% H_2O, $X = C/18.015/[C/18.015 + (100-C)/33.84]$ where 18.015 and 33.84 being the molar mass of H_2O and anhydrous haploandesite on one oxygen basis (Stolper, 1982) and X_m is the mole fraction of H_2O_m also on a single oxygen basis.

Eq. (4-3) is combined with Eq. (4-4) to fit measured concentration profiles to obtain the best-fit parameters D_0 and a. Among the six experiments, data for four experiments are suited to constrain the parameter a. The other two experiments are not used to constrain a because of inhomogeneity in starting glass (for HAD2A1) or missing profile in large H_2O_t concentration range (for HAD2A3). Best-fit parameter a from four experiments is found to increase with decreasing temperature (Table 4.2), and a linear regression (vs. $1/T$) results in (Fig. 4.4A)

$$a = -13.905 + \frac{73136}{T}, \tag{4.5}$$

where T is temperature in K. Compared to rhyolite, peralkaline rhyolite or dacite, parameter a in haploandesite is even larger at a given temperature, indicating $D_{H_2O_m}$ has an even stronger dependence on water concentration in haploandesite than in the more silicic melts. To maintain consistency, Eq. (4-5) was applied to refit all dehydration profiles and find D_0. The interface position Δx_0 is also allowed to vary to account for imperfect handling of sample surfaces. The fitting results are summarized in Table 4.3, and the calculated curves match the measured profiles excellently (Fig. 4.1). Determined $\ln D_0$ vs. $1/T$ define a linear trend as demonstrated in Fig. 4.4B (York, 1966):
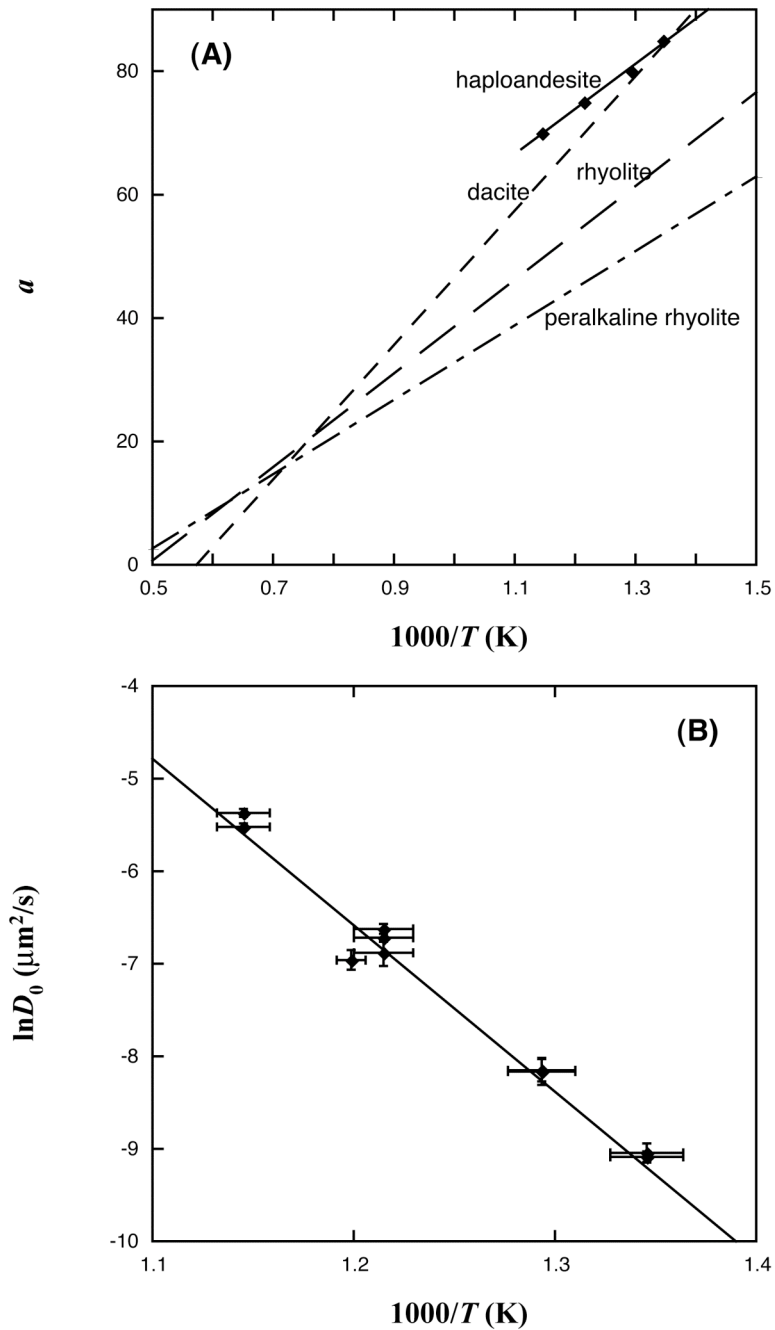
Fig. 4.4. (A) Parameter a in haploandesite (filled diamonds and solid line representing Eq. 4-5) using the model $D_{H_2O_m} = D_0\exp(aX)$ is higher than that in rhyolite (Ni and Zhang, 2008), peralkaline rhyolite (Wang et al., 2009), and dacite (Ni et al., 2008). (B) Arrhenius plot of $\ln D_0$ in haploandesite using the model $D_{H_2O_m} = D_0\exp[(-13.905+73136/T)X]$. The data of $\ln D_0$ are also reported in Table 4.3, and the solid curve is plotted from Eq. (4-6).

Table 4.3
Fitting results of dehydration experiments using the model
$D_{H_2O_m} = D_0\exp[(-13.905+73136/T)X]$

Run #	T (K)	H_2O_t (wt.%)	$\ln D_0$ ($\mu m^2/s$)	Δx_0	R^2
HAD2C1.1	773	2.0	-8.15±0.12	-2.8	0.9955
HAD2C1.2			-8.16±0.15	-3.9	0.9926
HAD2C2.1	743	2.0	-9.04±0.10	-0.9	0.9951
HAD2C2.2			-9.09±0.06	-1.5	0.9985
HAD2C3.1	873	2.0	-5.37±0.04	0.5	0.9991
HAD2C3.2			-5.52±0.04	1.4	0.9993
HAD2C4.1	823	2.0	-6.62±0.05	8.4	0.9988
HAD2C4.2			-6.88±0.14	3.3	0.9946
HAD1A3	834	2.5	-6.96±0.11	3.0	0.9928
HAD1A1	823	2.5	-6.72±0.04	-2.6	0.9990

Δx_0 is the adjustment of interface position.

$$\ln D_0 = 14.986 - \frac{17974}{T}, \tag{4.6}$$

where D_0 is in μm^2/s.

Therefore at 0.1 GPa and 743-873 K, H_2O_m diffusivity at $\leq$2.5 wt.% water concentration can be expressed by

$$D_{H_2O_m} = \exp\left(14.986 - 13.905X - \frac{17974 - 73136X}{T}\right), \tag{4.7}$$

where $D_{H_2O_m}$ is in μm^2/s. The activation energy for H_2O_m diffusion decreases from ~149 kJ/mol at zero water content to ~121 kJ/mol at 2.5 wt.% H_2O_t.

Total water (H_2O_t) diffusivity can be calculated through (Wang et al., 2009)

$$D_{H_2O_t} = D_{H_2O_m} \frac{dX_m}{dX} = D_{H_2O_m}\left[1 + \frac{2X-1}{\sqrt{4X(X-1)(1-4/K)+1}}\right]. \tag{4.8}$$

The activation energy for H_2O_t diffusion decreases from ~130 kJ/mol at 0.1 wt.% H_2O_t to ~115 kJ/mol at 2.5 wt.% H_2O_t. Fig. 4.5 plots H_2O_t diffusivity vs. water concentration at four different temperatures: H_2O_t diffusivity increases with water concentration proportionally at <0.7 wt.% H_2O_t, and then exponentially at higher H_2O_t.

Comparison with H_2O diffusion in Fe-bearing andesite

Using a dehydration method with *in situ* infrared analyses, Okumura and Nakashima (2006) measured average H_2O_t diffusivity in Fe-bearing andesite at atmospheric pressure and 773-948 K. Their mass-loss method cannot address the concentration dependence of H_2O diffusivity. In their treatment, they assumed that total H_2O diffusivity is independent of water content because the experiments at much higher
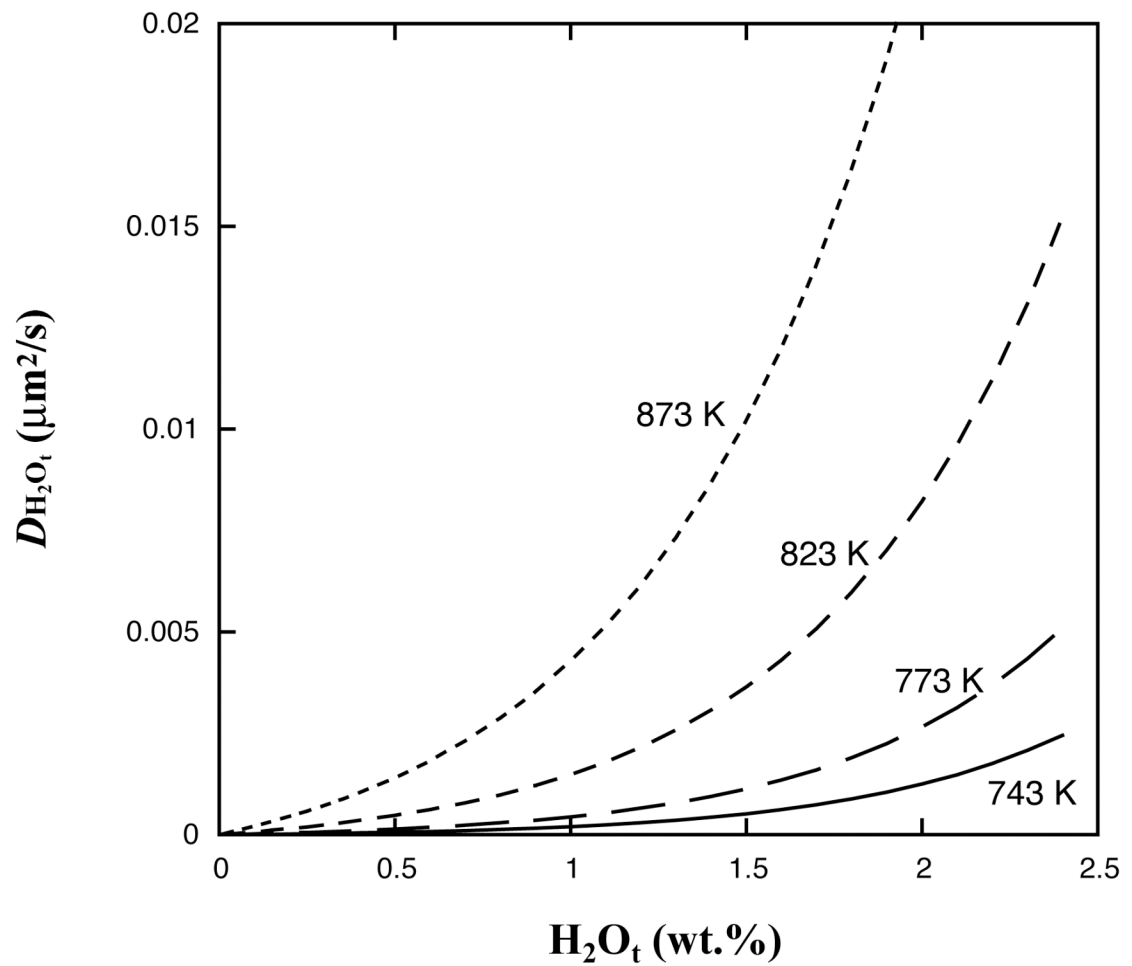
Fig. 4.5. The water concentration dependence of H_2O_t diffusivity at 0.1 GPa in haploandesite. H_2O_t diffusivity increases with H_2O_t concentration approximately proportionally up to H_2O_t <0.7 wt.%, and then more strongly at H_2O_t >0.7 wt.%.

temperatures (1523-1813 K) seem to indicate so (Behrens et al., 2004). However, on the basis of our results at similarly low temperatures, this assumption is not correct. Accordingly, their reported average diffusivity is converted to the diffusivity at initial water content (0.7 wt.%), and then compared to our diffusivity model at intermediate temperatures (Fig. 4.6). The two studies are different by a factor of 1.5-2.9 in diffusivity (or a difference of 0.40 to 1.05 in terms of $\ln D$), slightly larger than typical experimental error. Part of the differences may be attributed to pressure difference (0.1 MPa to 0.1 GPa) and part to compositional difference.

Comparison with H_2O diffusion in other melts

General models of water diffusivity have been constructed for rhyolite and dacite (Ni and Zhang, 2008; Ni et al., 2008). Behrens et al. (2004) reported H_2O_t diffusivity in Fe-bearing andesite at 1608-1848 K and 0.5-1.5 GPa using diffusion-couple technique. With respect to alkaline melts, Freda et al. (2003) studied H_2O diffusion in trachyte at 1373-1673 K and 1 GPa and Behrens and Zhang (2009) and Wang et al. (2009) investigated peralkaline rhyolite at 745-1516 K and 0.1-1.42 GPa. Fig. 4.7 illustrates the compositional dependence of water diffusivity from 0.5 wt.% to 2 wt.% water content. The compositional variation of the calc-alkaline andesite, dacite and rhyolite is represented by one single parameter: the cation mole fraction of Si (Table 4.4). Below 873 K, there is a positive correlation between H_2O diffusivity and silica content or degree of melt polymerization (andesite < dacite < rhyolite), and the diffusivity in rhyolite is higher than that in haploandesite by roughly two orders of magnitude, which has important implications on geological processes involving water transport in melts. For
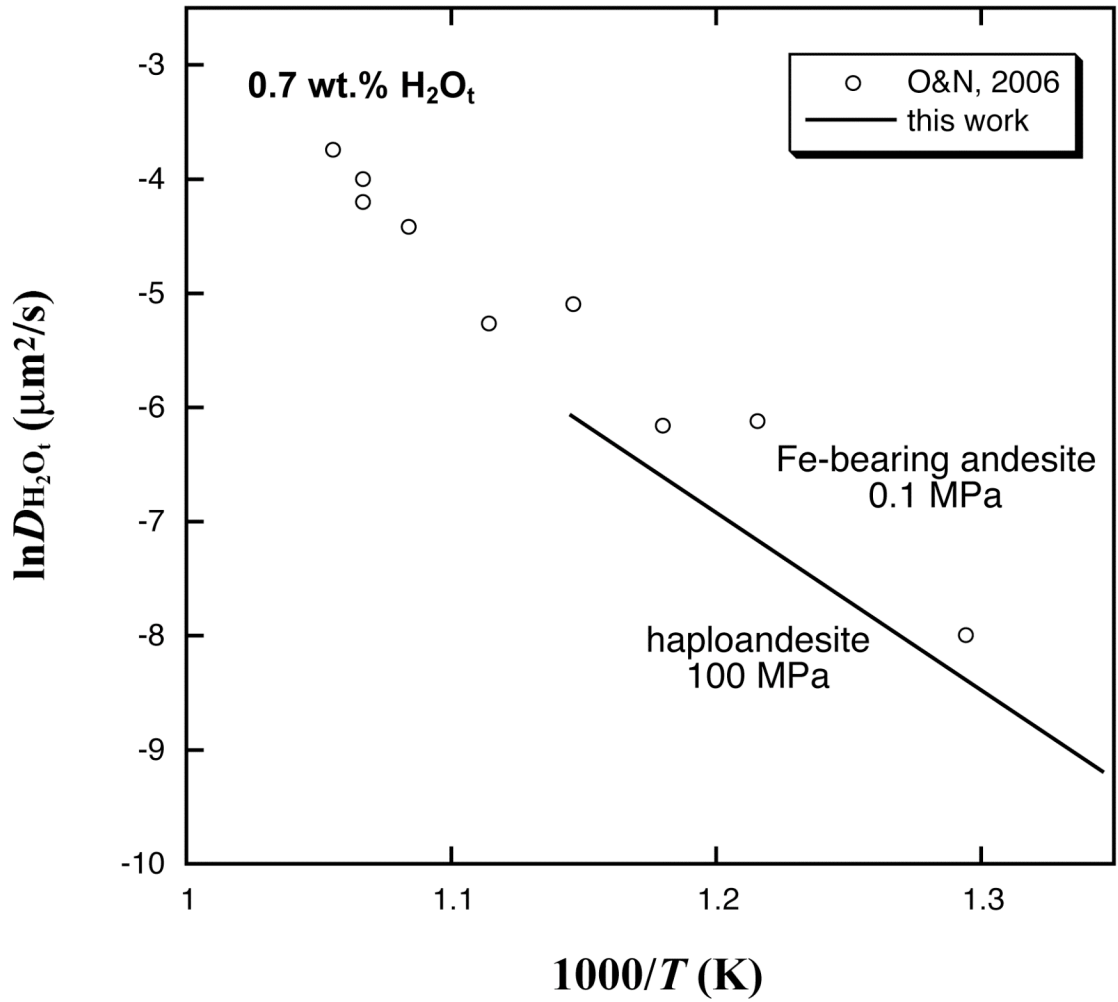
Fig. 4.6. Comparison between H_2O diffusivity at 0.7 wt.% H_2O_t in haploandesite and that in Fe-bearing andesite (Okumura and Nakashima, 2006). The small difference, within a factor of 1.5-2.9, is believed to be due to both composition difference and pressure difference.
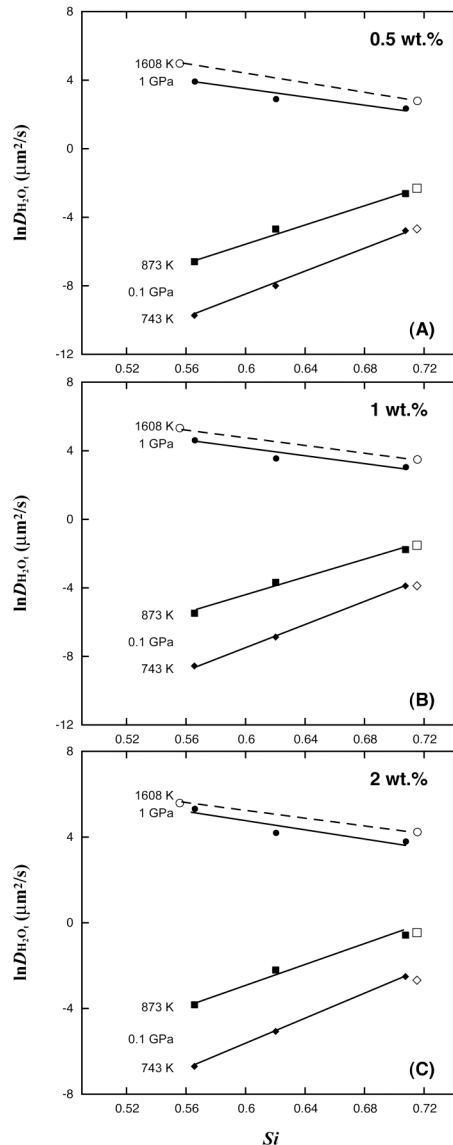
Fig. 4.7. The dependence of H_2O_t diffusivity on melt composition (cation mole fraction of Si) at (A) 0.5 wt.% H_2O_t; (B) 1 wt.% H_2O_t; and (C) 2 wt.%. H_2O_t diffusivity in various melts is compared at 1608 K and 1 GPa (circles), 873 K and 0.1 GPa (squares), and 743 K and 0.1 GPa (diamonds). Calc-alkaline melts are illustrated in solid symbols and lines, and peralkaline melts are illustrated in open symbols and dash lines. H_2O diffusivity at 743-873 K increases with degree of polymerization (andesite < dacite < rhyolite), but his trend is reversed at 1608 K. H_2O diffusivity in peralkaline melts (trachyte to peralkaline rhyolite) follows the same trend as calc-alkaline melts at intermediate T but is slightly higher than that in calc-alkaline melts at high T. Data sources: rhyolite (Ni and Zhang, 2008); dacite (Ni et al., 2008); andesite (Behrens et al., 2004; this study); peralkaline rhyolite (Wang et al., 2009); trachyte (Freda et al., 2003).

101

Table 4.4

Composition of rhyolite, dacite, and haploandesite in wt.% for Eq. (4-9)

	rhyolite[a]	dacite[b]	andesite
SiO_2	76.05	66.60	62.25
TiO_2	0.10	0.80	0.00
Al_2O_3	13.93	14.91	20.26
FeO_T	0.75	4.87	0.04
MnO	0.04	0.05	0.02
MgO	0.12	2.22	2.39
CaO	0.87	4.92	10.37
Na_2O	4.01	3.48	4.12
K_2O	4.22	2.51	0.96
P_2O_5	0.07	0.00	0.03
Total	100.16	100.36	100.44
Si	0.7072	0.6200	0.5654

[a] From Ni and Zhang (2008).
[b] From Ni et al. (2008).
[c] Cation mole fraction of Si.

example, at 773 K and 1 wt.% H$_2$O, water can travel to 60 μm in rhyolite but only 6 μm

in andesite in 1 day. This trend is opposite to the trend observed at superliquidus

temperatures (such as 1608 K; Fig. 4.7). However, at high temperatures, the diffusivities

are more similar: the diffusivity in andesite is only higher than that in rhyolite by about a

factor of five at 1608 K (Behrens et al., 2004; Ni and Zhang, 2008). The diffusivity

crossover is related to the higher activation energy for water diffusion in andesite than in

rhyolite, which can be explained by a lower ionic porosity in andesitic melt. It has been

demonstrated that reduced ionic porosity increases the activation energy for oxygen

diffusion in silicate minerals (Fortier and Giletti, 1989). Compared to calc-alkaline

melts, H$_2$O diffusion in alkaline melts (trachyte to peralkaline melts) follows the same

trend at intermediate temperatures but is only slightly faster (the diffusivities are within a

factor of two) at high temperatures. Behrens and Zhang (2009) showed that H$_2$O$_t$

diffusivity in peraluminous rhyolite is similar to that in "normal" metaluminous rhyolite.

Hence, the available data indicate that the most major effect on H$_2$O$_t$ diffusivity is SiO$_2$

content, not whether the melt is peralkaline, metaluminous, or peraluminous.

Based on this work (Eqs. 4-7 and 4-8) and studies of Ni and Zhang (2008) and Ni

et al. (2008), at 0.1 GPa and 743-873 K, total H$_2$O diffusivity in calc-alkaline andesitic,

dacitic and rhyolitic melts at <2.5 wt.% H$_2$O$_t$ can be modeled as

$$\ln(D_{\mathrm{H_2O_t}}/C)=22.505-16.481 Si-\frac{37135-630.17C-36163 Si}{T},\qquad (4.9)$$

where $D_{\mathrm{H_2O_t}}$ is H$_2$O$_t$ diffusivity in μm^2/s, C is water content in wt.%, Si is cation mole

fraction of Si, and T is temperature in K. This expression can reproduce $\ln D_{\mathrm{H_2O_t}}$ at 0.1 to

2.5 wt% H$_2$O$_t$ and 743-873 K to ±0.58. Interestingly, Eq. (4-9) also works well for

peralkaline rhyolite in this temperature range, even though previous work showed that H_2O diffusivity in peralkaline rhyolite is slightly higher than in metaluminous rhyolite (Behrens and Zhang, 2009; Wang et al., 2009).

H_2O_m diffusivity and viscosity

The Einstein (1905) equation is often used to address the relation between diffusivity (D) of a neutral species and viscosity (η):

$$D = \frac{kT}{\eta L}, \tag{4.10}$$

where k is the Boltzmann constant, T is temperature, and L equals $6\pi r$ with r being the radius of the diffusing species. The Eyring equation (Glasstone et al., 1941), which assumes diffusion and viscous flow involve the same process, follows similar form as Eq. (4-10) except that L is the jumping distance. If the Einstein or Eyring relation holds true, $\ln D$ vs. $\ln \eta$ would define a straight line with a slope of -1. However, it has been demonstrated that these relations underestimate ^{18}O or H_2O_m diffusivity in melts by many orders of magnitude (Behrens et al., 2007; Ni and Zhang, 2008).

Vetere et al. (2006) presented a viscosity model for hydrous andesite, based on which the Eyring equation predicts diffusivities 6-8 orders of magnitude lower than those evaluated from this work. Therefore the relation between H_2O_m diffusivity and melt viscosity significantly deviates from the Eyring equation. Fig. 4.8 shows that at $\ln \eta$ (η in Pa · s) <25, H_2O_m diffusivity is not much different from 773 K to 873 K, but at even larger viscosities, H_2O_m diffusivity increases with temperature. An empirical relation can be established as
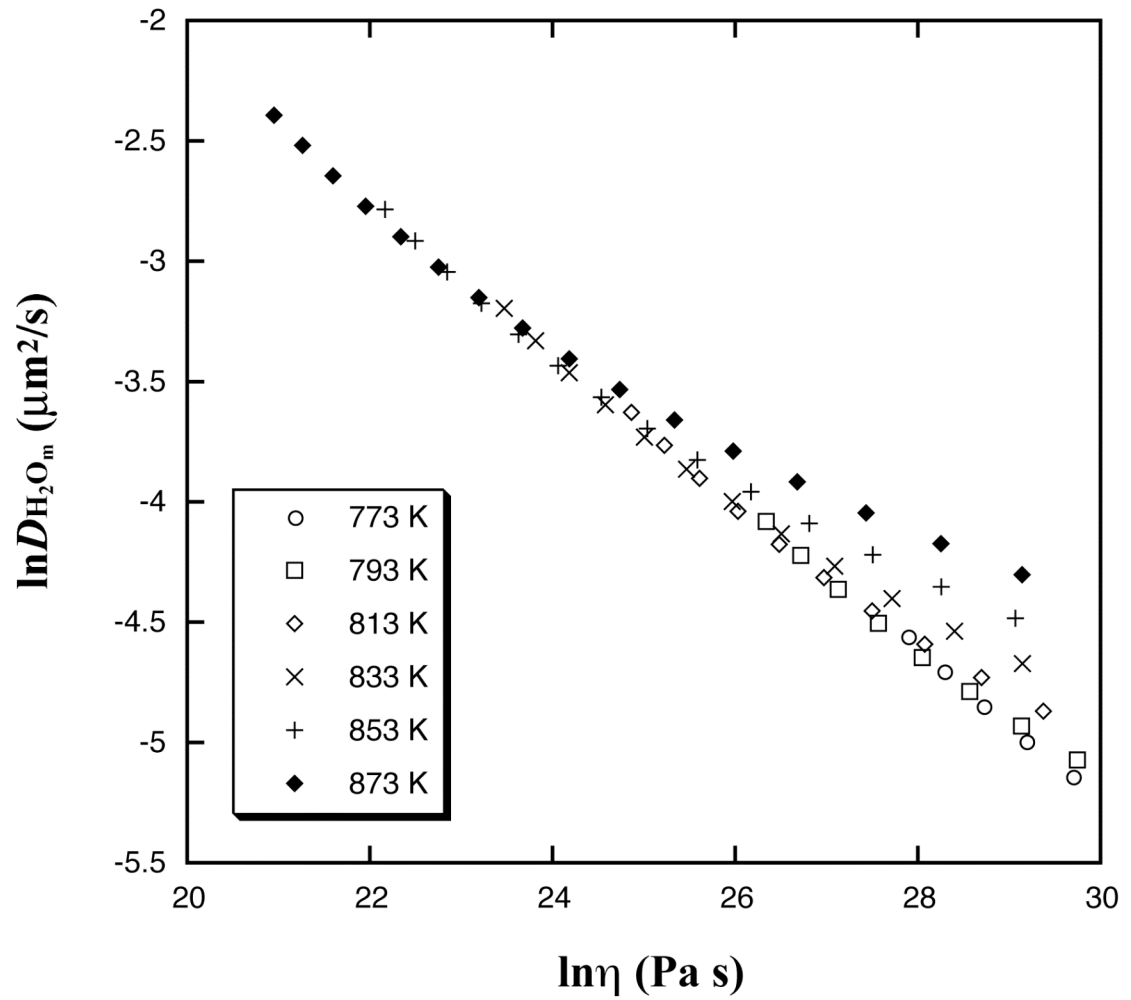
Fig. 4.8. H_2O_m diffusivity (this work) and viscosity (Vetere et al., 2006) in andesite show negative correlation but do not follow the Eyring equation. H_2O_m diffusivity at different temperatures scatters more as melt viscosity increases.

$$\ln D_{H_2O_m} = 0.50977 + (0.00028401T - 0.41515)\ln\eta + \frac{e^{35.259-0.029007T}}{\sqrt{\eta}}, \quad (4.11)$$

where $D_{H_2O_m}$ is in $\mu m^2/s$, T is in K, and η is viscosity of hydrous andesite in $Pa \cdot s$. The above equation can reproduce $\ln D_{H_2O_m}$ to ± 0.06.

Application to bubble growth

During magma upwelling in volcanic eruptions, originally dissolved water in melt may become saturated and water bubbles may grow inside the melt. The growth rate of bubbles depends on both melt viscosity and water diffusivity (Navon et al., 1998; Lensky et al., 2004). Fig. 4.9 shows the bubble growth curve at 873 K and 0.1 MPa in hydrous calc-alkaline melts with 2.5 wt.% H_2O, which is calculated from the code of Liu and Zhang (2000) modified from Proussevitch and Sahagian (1998). The H_2O diffusivity in andesite from this work is used assuming minimal change in H_2O diffusivity over 0.1 GPa. Because H_2O diffusivity becomes slower from rhyolite to dacite to andesite at the modeling conditions, bubble can grow from 10 μm to 575 μm in rhyolite in 3600 s, to 163 μm in dacite, but to only 26 μm in andesite during the same time period.

CONCLUDING REMARKS

Water speciation and diffusion in Fe-free andesite were examined at 743-873 K and 0.1 GPa using the dehydration method. There is more OH in andesite than in dacite or rhyolite at a given temperature and water content. H_2O diffusion profiles indicate strong dependence of H_2O_t diffusivity on its concentration, in contrary to previous water diffusion data in andesite at much higher temperatures. Hence, it cannot be assumed that
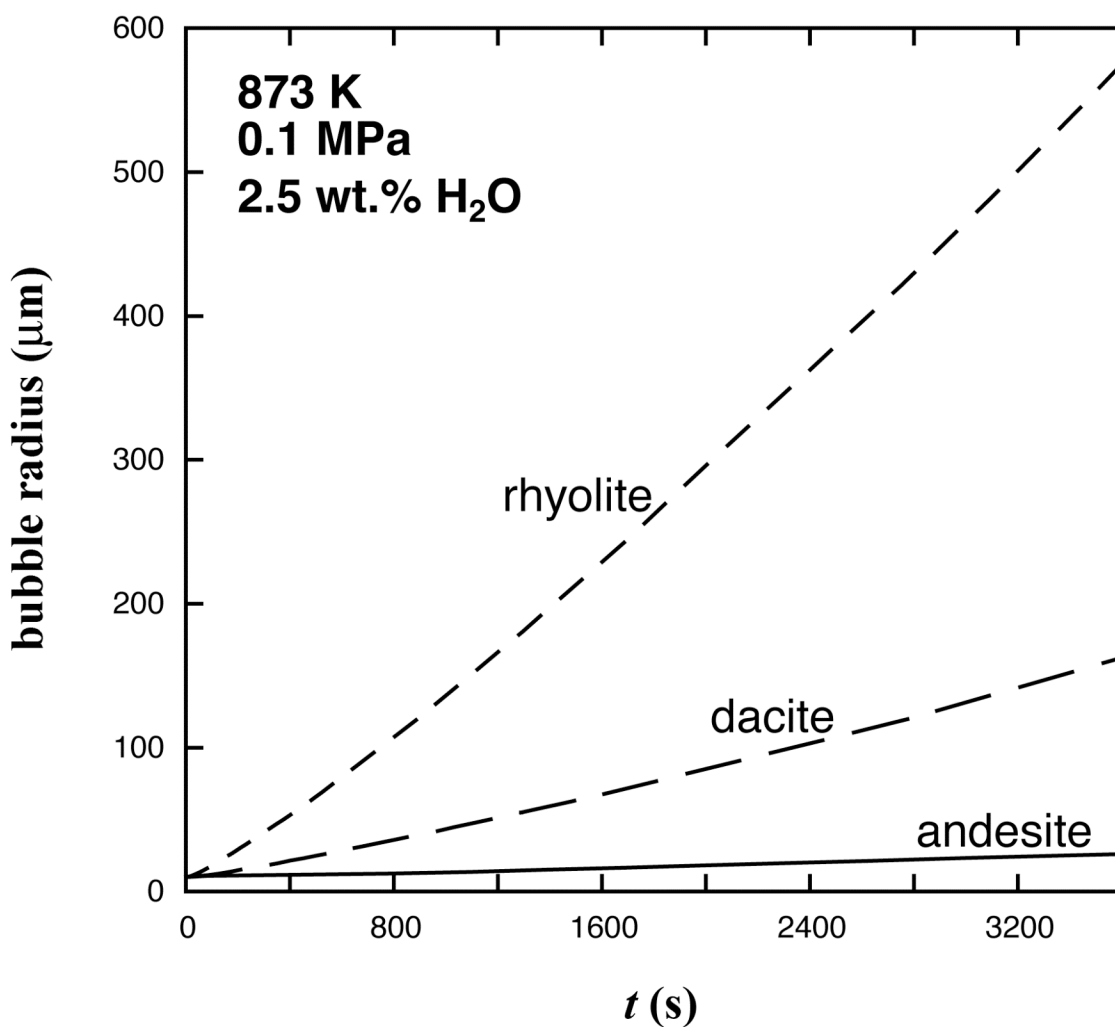
Fig. 4.9. Growth of a bubble with initial radius of 10 μm at 873 K and 0.1 MPa in three hydrous calc-alkaline melts using the model of Liu and Zhang (2000). The growth rate is determined by both melt viscosity and H_2O diffusivity. Bubble grows faster in rhyolite than in dacite than in andesite, which is caused by their difference in H_2O diffusivity. Diffusivity source: andesite (this work); dacite (Ni et al., 2008); rhyolite (Ni and Zhang, 2008). Viscosity source: andesite (Vetere et al., 2006); dacite (Hui and Zhang, 2007); rhyolite (Zhang et al., 2003). H_2O solubility is from Zhang et al. (2007).

H_2O_t diffusivity is independent of H_2O_t content at temperatures of 700-900 K. H_2O diffusion at the experimental conditions is dominated by molecular H_2O, similar to water diffusion in dacitic or rhyolitic melts. From andesite to dacite to rhyolite, at <2.5 wt.% H_2O, water diffusivity increases at T <873 K but decreases at superliquidus temperatures.

REFERENCES

Behrens, H., Zhang, Y., Xu, Z., 2004. H_2O diffusion in dacitic and andesitic melts. Geochim. Cosmochim. Acta 68, 5139-5150.

Behrens, H., Zhang, Y., 2009. H_2O diffusion in peralkaline to peraluminous rhyolitic melts. Contrib. Mineral. Petrol., in press.

Behrens, H., Zhang, Y., Leschik, M., Wiedenbeck, M., Heide, G., Frischat, G.H., 2007. Molecular H_2O as carrier for oxygen diffusion in hydrous silicate melts. Earth Planet. Sci. Lett. 254, 69-76.

Botcharnikov R.E., Behrens H., Holtz F., 2006. Solubility and speciation of C-O-H fluids in andesitic melt at T=1100-1300°C and P=200 and 500 MPa. Chem. Geol. 229, 125-143.

Delaney, J.R., Karsten, J.L., 1981. Ion microprobe studies of water in silicate melts: concentration-dependent water diffusion in obsidian. Earth Planet. Sci. Lett. 52, 191-202.

Einstein, A., 1905. The motion of small particles suspended in static liquids required by the molecular kinetic theory of heat. Ann. Phys. (in German) 17, 549-560.

Fortier, S.M., Giletti, B.J., 1989. An empirical model for predicting diffusion coefficients in silicate minerals. Science 245, 1481-1484.

Freda, C., Baker, D.R., Romano, C., Scarlato., P., 2003. Water diffusion in natural potassic melts. Geol. Soc. Spec. Publ. 213, 53-62.

Glasstone, S., Laidler, K.J., Eyring, H., 1941. The Theory of Rate Processes. McGraw-Hill, New York, 611 pp.

Grove, T.L., Elkins-Tanton, L.T., Parman, S.W., Chatterjee, N., Munterner, O., Gaetani, G.A., 2003. Fractional crystallization and mantle-melting controls on calc-alkaline differentiation trends. Contrib. Mineral. Petrol. 145, 515-533.

Hess, P.C., 1989. Origin of igneous rocks. Harvard University Press.

Hui, H., Zhang, Y., 2007. Toward a general viscosity equation for natural anhydrous and hydrous silicate melts. Geochim. Cosmochim. Acta 71, 403-416.

Kohn, S.C., Dupree, R., Mortuza, M.G., 1992. The interaction between water and aluminosilicate magmas. Chem. Geol. 96, 399-409.

Lensky, N.G., Navon, O., Lyakhovsky, V., 2004. Bubble growth during decompression of magma: experimental and theoretical investigation. J. Volcano. Geotherm. Res. 129, 7-22.

Lewis-Kenedi, C.B., Lange, R.A., Hall, C.M., Delgado-Granados, H., 2005. The eruptive history of the Tequila volcanic field, western Mexico: ages, volumes, and relative proportions of lava types. Bull. Volcanol. 67, 391-414.

Liebske, C., Behrens, H., Holtz, F., Lange, R.A., 2003. The influence of pressure and composition on the viscosity of andesitic melts. Geochim. Cosmochim. Acta 67, 473-485.

Liu Y., 2003. Water in rhyolitic and dacitic melts. Ph.D. dissertation, the University of Michigan.

Liu Y. and Zhang Y. (2000) Bubble growth in rhyolitic melt. Earth Planet. Sci. Lett. 181, 251-264.

Liu, Y., Zhang, Y., Behrens, H., 2004a. H_2O diffusion in dacitic melts. Chem. Geol. 209, 327-340.

Liu Y., Behrens H., Zhang Y., 2004b. The speciation of dissolved H_2O in dacitic melt. Am. Mineral. 89, 277-284.

Mandeville, C. W., Webster, J.D., Rutherford, M.J., Taylor, B.E., Timbal, A., Faure, K., 2002. Determination of molar absorptivities for infrared absorption bands of H_2O in andesitic glasses. Am. Mineral. 87, 813-821.

Mora, J.C., Macias, J.L., Saucedo, R., Orlando, A., Manetti, P., Vaselli, O., 2002. Petrology of the 1998-2000 products of Volcan de Colima, Mexico. J. Volcanol. Geotherm. Res. 117, 195-212.

Mysen, B.O., 1999. Structure and properties of magmatic liquids: from haplobasalt to haploandesite. Geochim. Cosmochim. Acta 63, 95-112.

Mysen, B.O., Virgo, D., 1986. Volatiles in silicate melts at high pressure and temperature. 1. Interaction between OH groups and Si^{4+}, Al^{3+}, Ca^{2+}, Na^+, and H^+. Chem. Geol. 57, 303-331.

Mysen, B.O., Wheeler, K., 2000a. Solubility behavior of water in haploandesitic melts at high pressure and high temperature. Am. Mineral. 85, 1128-1142.

Mysen, B.O., Wheeler, K., 2000b. Alkali aluminosilicate-saturated aqueous fluids in the earth's upper mantle. Geochim. Cosmochim. Acta 64, 4243-4256.

Navon, O., Chekhmir, A., Lyakhovsky, V., 1998. Bubble growth in highly viscous melts: theory, experiments and autoexplosivity of dome lavas. Earth Planet. Sci. Lett. 160, 763-776.

Ni, H., Zhang, Y., 2008. H_2O diffusion models in rhyolitic melt with new high pressure data. Chem. Geol. 250, 68-78.

Ni, H., Behrens, H., Zhang, Y., 2008. A general model of water diffusivity in dacitic melts. Geochim. Cosmochim. Acta, submitted.

Nowak, M., Behrens, H., 1997. An experimental investigation on diffusion of water in haplogranitic melts. Contrib. Mineral. Petrol. 126, 365-376.

Okumura, S., Nakashima, S., 2004. Water diffusivity in rhyolitic glasses as determined by in situ IR spectrometry. Phys. Chem. Minerals 31, 183-189.

Okumura, S., Nakashima, S., 2006. Water diffusion in basaltic to dacitic glasses. Chem. Geol. 227, 70-82.

Proussevitch, A.A., Sahagian, D.L., 1998. Dynamics and energetics of bubble growth in magmas: analytical formulation and numerical modeling. J. Geophys. Res. 103, 18223-18251.

Richet, P., Lejeune, A.-M., Holtz, F., Roux, J., 1996. Water and the viscosity of andesitic melts. Chem. Geol. 128, 185-197.

Schmidt, B.C., Riemer, T., Kohn, S.C., Holtz, F., Dupree, R., 2001. Structural implications of water dissolution in haplogranitic glasses from NMR spectroscopy: influence of total water content and mixed alkali effect. Geochim. Cosmochim. Acta 65, 2949-2964.

Shaw, H.R., 1974. Diffusion of H_2O in granitic liquids: I. Experimental data; II. Mass transfer in magma chambers. In: Hofmann, A.W., Giletti, B.J., Yoder, H.S., Yund, R.A. (Eds.), Geochemical Transport and Kinetics. Carnegie Inst. Washington Publ., Washington, DC, pp. 139-170.

Stolper, E.M., 1982. The speciation of water in silicate melts. Geochim. Cosmochim. Acta 46, 2609-2620.

Szramek, L., Gardner, J.E., Larsen, J., 2006. Degassing and microlite crystallization of basaltic andesite magma erupting at Arenal Volcano, Costa Rica. J. Volcanol. Geotherm. Res. 157, 182-201.

Saito, G., Kazahaya, K., Shinohara, H., Stimac, J., Kawanabe, Y., 2001. Variation of volatile concentration in a magma system of Satsuma-Iwojima volcano deduced from melt inclusion analyses. J. Volcanol. Geotherm. Res. 108, 11-31.

Vetere, F., Behrens, H., Holtz, F., Neuville, D.R., 2006. Viscosity of andesitic melts-new experimental data and a revised calculation model. Chem. Geol. 228, 233-245.

Wang, H., Xu, Z., Behrens, H., Zhang, Y., 2009. Water diffusion in Mount Changbai peralkaline rhyolitic melt. Contrib. Mineral. Petrol., in submission.

Withers, A.C., Zhang, Y., Behrens, H., 1999. Reconciliation of experimental results on H_2O speciation in rhyolitic glass using in-situ and quenching techniques. Earth Planet. Sci. Lett. 173, 343-349.

York, D., 1966. Least-squares fitting of a straight line. Can. J. Phys. 44, 1079-1086.

Zhang, Y., 1999. H_2O in rhyolitic glasses and melts: measurement, speciation, solubility, and diffusion. Rev. Geophys. 37, 493-516.

Zhang, Y., Stolper, E.M., 1991. Water diffusion in basaltic melts. Nature 351, 306-309.

Zhang, Y., Behrens, H., 2000. H_2O diffusion in rhyolitic melts and glasses. Chem. Geol. 169, 243-262.

Zhang, Y., Stolper, E.M., Wasserburg, G.J., 1991a. Diffusion of water in rhyolitic glasses. Geochim. Cosmochim. Acta 55, 441-456.

Zhang, Y., Stolper, E.M., Wasserburg, G.J., 1991b. Diffusion of a multi-species component and its role in oxygen and water transport in silicates. Earth Planet. Sci. Lett. 103, 228-240.

Zhang, Y., Stolper, E.M., Ihinger, P.D., 1995. Kinetics of the reaction $H_2O + O = 2OH$ in rhyolitic and albitic glasses: preliminary results. Am. Mineral. 80, 593-612.

Zhang, Y., Belcher, R., Ihinger, P.D., Wang, L., Xu, Z., Newman, S., 1997. New calibration of infrared measurement of dissolved water in rhyolitic glasses. Geochim. Cosmochim. Acta 61, 3089-3100.

Zhang, Y., Xu, Z., Liu, Y., 2003. Viscosity of hydrous rhyolitic melts inferred from kinetic experiments, and a new viscosity model. Am. Mineral. 88, 1741-1752.

Zhang, Y., Xu, Z., Zhu, M., and Wang, H., 2007. Silicate melt properties and volcanic eruptions. Rev. Geophys. 45, RG4004, doi:10.1029/2006RG000216.

CHAPTER V

OXYGEN ISOTOPE THERMOMETRY AND SPEEDOMETRY

ABSTRACT

Apparent equilibrium temperatures (T_{ae}) determined from oxygen isotope fractionation among coexisting minerals were suggested before to indicate the Dodson closure temperatures (T_c) of specific minerals when slow cooling causes significant diffusive retrogression and T_c is fairly below the peak temperature of metamorphism. The fast grain boundary (FGB) model was used to simulate the diffusive exchange of oxygen isotopes between coexisting minerals in a closed system during cooling, and investigate the behavior of the isotopic systems and the correspondence between T_{ae} and T_c. The simulations show that T_{ae} of most mineral pairs, even those with similar closure temperatures, does not necessarily represent closure temperature. However, in multi-mineralic rocks, T_{ae} of the pair with the largest isotopic fractionation (PLIF) is always confined between the closure temperatures of the two minerals. This finding has several important implications. First, T_{ae} of PLIF may be used to compare thermal history of rocks. Secondly, if the closure temperatures of PLIF are similar, T_{ae} would be a good approximation of T_c of both minerals, with little dependence on modal abundances of minerals. One such mineral pair is quartz and magnetite. For such a mineral pair,

two additional equations (one for each mineral) relate measured T_{ae}, diffusion property, and cooling rate. Therefore, if the diffusion property (including the cooling environment such as water fugacity) is known, the cooling rate may be estimated. On the other hand, if the cooling rate is independently determined, one may be able to use T_{ae} to infer the oxygen diffusivity, from which the fluid environment of the rock during cooling may be inferred if diffusivity as a function of water fugacity and other fluid conditions is experimentally quantified.

INTRODUCTION

"Reading" the thermal history of rocks from the mineral record is one of the basic aims of petrology. Oxygen isotope thermometry has been widely applied to obtain temperature information on plutonic and metamorphic rocks (Valley, 2001). In this approach, a temperature is calculated from bulk $\delta^{18}O$ values of two minerals using the equation relating equilibrium fractionation factor between the minerals to temperature. That is, the temperature is calculated as if the two minerals reached isotopic equilibrium at a temperature, hereafter referred to as the apparent equilibrium temperature, T_{ae}. [In stable isotope literature, this temperature was denoted sometimes as the apparent temperature T_{app} (e.g., Kohn and Valley, 1998a). Apparent equilibrium temperature T_{ae}, as in the literature of reaction kinetics (e.g., Skogby, 1992; Zhang, 1994; Zhang et al., 1997, 2000), is preferred because apparent temperature is not specific enough and could mean apparent formation temperature, apparent metamorphic temperature, apparent peak temperature, apparent alteration temperature, etc.] Due to continued mineral reactions,

recrystallization, or simply diffusive exchange between the minerals during retrograde process, the isotopic composition of minerals may be altered so that T_{ae} does not represent the equilibrium temperature and its meaning must be elucidated. A number of authors (Giletti, 1986; Eiler et al, 1992; Jenkin et al., 1994; Kohn and Valley, 1998a; Kohn, 1999) have developed increasingly more sophisticated models to investigate the behavior of oxygen isotope diffusive exchange upon cooling, realizing that T_{ae} is dependent on the modal abundances of minerals, in addition to other factors including cooling history, grain sizes, and oxygen fractionation and diffusion. There is no general relation between T_{ae} and cooling history and sometimes T_{ae} between two minerals does not even exist (in the case of reversed fractionation). Nonetheless, practitioners of oxygen isotope thermometry have continued to report T_{ae} between various mineral pairs as parameters obtainable from oxygen isotopes.

In order to understand the meaning of T_{ae}, it is instructive to relate the bulk T_{ae} between two minerals described above to the two bulk closure temperatures (T_c), each for one mineral. T_c of a mineral is a calculated parameter from the diffusion property, cooling rate, grain shape and size as follows (Dodson, 1973):

$$T_c = \frac{E}{R \ln \dfrac{GD_0 R T_c^2}{a^2 q E}}, \qquad (5\text{-}1)$$

where G is the geometry factor (55 for sphere, 27 for cylinder, and 8.7 for tablet), E and D_0 are the activation energy and the pre-exponential factor for diffusivity ($D = D_0 e^{-E/RT}$), R is the universal gas constant, and q is the cooling rate when the rock temperature was T_c. This formulation of T_c is independent of the onset peak temperature T_0 and is applicable only to systems that underwent sufficiently slow cooling. Otherwise the expression of

115

Ganguly and Tirone (1999) is appropriate. Closure temperature corresponds to the apparent equilibrium temperature between a bulk mineral grain and its surrounding infinite reservoir with constant isotopic composition.

Because T_{ae} is a measurable property, whereas T_c is a calculated parameter depending on diffusion property and cooling rate, if T_{ae} can be related to T_c, it would provide a relation between T_{ae} (measured property), diffusivity as a function of temperature (measured property but depending on cooling environment such as water fugacity) and cooling rate. This additional relation may be used to infer unknown information (such as cooling rate or cooling environment), or provide crosschecks of independently inferred parameters. Giletti (1986) extended the concept of closure temperature to closed-system oxygen isotope exchange by assuming that minerals with lower T_c than the mineral under consideration constitute an infinite reservoir so that Dodson's formulation is applicable. Eiler et al. (1992, 1993, 1994) established a Fast grain boundary (FGB) model to overcome the inconsistency of the former model, and found that T_{ae} is strongly dependent on modal abundances of minerals. Kohn and Valley (1998a, 1998b) proposed that T_{ae} between two minerals with similar T_c can be an indication of their T_c. In this work, the FGB model of Eiler et al. (1994) was used to examine the behavior of T_{ae} of different mineral pairs in several systems, with the goal to extract simple relations from the complicated systems, and to investigate possible applications of such relation in constraining thermal history or cooling conditions.

METHOD

The Fast grain boundary (FGB) model of Eiler et al. (1994) or its variation (Jenkin et al., 1994; Kohn and Valley, 1998a; Kohn, 1999) has been used to investigate the isotopic behavior of a multi-mineralic rock. This study follows these authors and use the FGB model to further examine the isotopic evolution in every mineral of multi-mineralic rocks during cooling, with the special aim to examine if there are simple and useful behaviors for subset of mineral pairs. Since this study is focusing on effects caused by diffusive exchange of oxygen isotopes, complexities such as fluid alteration or recrystallization are not taken into consideration here.

The FGB code was obtained from John Eiler. The cooling history (temperature T vs. time t) of the rock is assumed to be asymptotic:

$$T = \frac{T_0}{1 + t/\tau},$$
(5-2)

where T_0 is the onset temperature, and τ is the time constant for the rock to cool from T_0 to $T_0/2$. Oxygen isotope fractionation factors of common rock-forming minerals relative to quartz, and diffusivities as well as oxygen concentrations in the minerals are summarized in Table 5.1.

The fractionation factors were determined primarily from carbonate-exchange experiments (Clayton et al., 1989; Chiba et al., 1989; Zheng et al., 1994; Fortier and Lüttage, 1995; Chacko et al., 1996), with the rest from empirical evaluations (Kohn and Valley, 1998a; Valley et al., 2003). For the asymptotic cooling history (Eq. 5-2), the equilibrium fractionation between any two minerals (i.e., fractionation between the

117

surfaces of two minerals assuming fast grain boundary diffusion and hence surface equilibrium) depends on time as a parabolic function:

$$\Delta_{i-j}(t) = \frac{A_i - A_j}{T^2} = \frac{A_i - A_j}{T_0^2}\left(1 + \frac{t}{\tau}\right)^2,$$

(5-3)

where A_i/T^2 is the fractionation factor between quartz and mineral i.

A large dataset of oxygen diffusivities is available from hydrothermal exchange experiments at 100 MPa water pressure, and limited data under anhydrous conditions can also be found in the literature (Table 5.1). Diffusivities under hydrothermal conditions, plotted with diffusivities in quartz, magnetite and olivine under anhydrous condition for comparison (Fig. 5.1), are used in the following simulations. For asymptotic cooling, diffusivity decreases exponentially with time:

$$\ln D(t) = \ln D_0 - \frac{E}{RT} = \left(\ln D_0 - \frac{E}{RT_0}\right) - \frac{E}{\tau RT_0}t.$$

(5-4)

The FGB model is used to trace the evolution of $\delta^{18}O$ of minerals and calculate apparent equilibrium temperatures from ultimate "frozen" fractionations using the following input: (a) cooling history (Eq. 5-2), (b) fractionation factors as a function of temperature (Eq. 5-3, Table 5.1), (c) diffusivities as a function of temperature (Eq. 5-4, Table 5.1), and (d) oxygen concentration (Table 5.1), modal abundance and grain size of each mineral.

SIMULATION RESULTS AND DISCUSSION

Eiler et al. (1992, 1993) showed that for a bimineralic rock, T_{ae} varies between T_c of the two coexisting minerals, dependent on their modal abundance. If the two minerals

118

Table 5.1. Oxygen isotope fractionation factors and diffusivities of minerals

	A	Fluid cond. (MPa)	D_0 (m²/s)	E (J/mol)	Ref.	Orie.	G	O conc. (mol/m³)
Quartz	0	H_2O, 100	2.90×10^{-05}	243000	1	$//\,c$	8.7	88,145
		O_2, 0.1	2.95×10^{-11}	221000	2			
		CO_2, 10	2.10×10^{-12}	159000	3			
Calcite	0.38	H_2O, 100	7.00×10^{-09}	173000	4	~isotr.	55	81,235
		CO_2, 100	7.50×10^{-07}	242000	5			
Albite	0.94	H_2O, 100	2.31×10^{-13}	89119	6	~isotr.	55	79,944
Muscovite	1.5	H_2O, 100	7.70×10^{-09}	163176	7	$\perp c$	27	85,221
Anorthite	1.99	H_2O, 100	1.39×10^{-11}	109621	6	~isotr.	55	79,373
		O_2, 0.1	1.00×10^{-09}	236000	8			
		$CO-CO_2$, 0.1	8.40×10^{-13}	162000	9			
Phlogopite	2.16	H_2O, 100	1.40×10^{-08}	175728	7	$\perp c$	27	80,187
Biotite	2.4	H_2O, 100	9.10×10^{-10}	142256	7	$\perp c$	27	77,771
Apatite	2.51	H_2O, 100	9.00×10^{-09}	205016	10	$//\,c$	8.7	81,454
Hornblend	2.6	H_2O, 100	1.00×10^{-11}	171544	11	$//\,c$	8.7	88,235
Tremolite	2.6	H_2O, 100	2.00×10^{-12}	163176	11	$//\,c$	8.7	87,944
Zircon	2.64	H_2O, <1000	5.50×10^{-12}	210200	12	~isotr.	55	101,885
		dry, 0.1	1.33×10^{-04}	448300	12			
Almandine	2.71	H_2O, 100	6.00×10^{-09}	301000	13	isotr.	55	104,058
Diopside	2.75	H_2O, 100	1.50×10^{-10}	226000	14	$//\,c$	8.7	90,785
		$CO-CO_2$, 0.1	4.30×10^{-04}	457000	9			
Titanite	3.66	H_2O, 100	2.05×10^{-12}	180000	15	~isotr.	55	89,702
		dry, 0.1	3.03×10^{-08}	276000	15			
Forsterite	3.67	O_2, 0.02	5.90×10^{-08}	377800	16	~isotr.	55	91,638
Rutile	4.69	H_2O, 100	2.00×10^{-05}	330000	17	$\perp c$	27	106,270
		dry, 0.1	1.50×10^{-07}	258000	17			
Magnetite	6.29	H_2O, 100	3.50×10^{-10}	188280	18	isotr.	55	89,847
		dry, empiric.	4.30×10^{-11}	211000	19			

Fractionation factors are from Clayton et al. (1989) for albite, anorthite, and calcite; Chiba et al. (1989) for diopside, forsterite, and magnetite; Zheng et al. (1994) for tremolite; Fortier and Lüttge (1995) for apatite; Chacko et al. (1996) for muscovite, phlogopite, and rutile; Kohn and Valley (1998a) for biotite and hornblende; and Valley et al. (2003) for zircon, almandine, and titanite. Diffusivities references are: 1. Farver and Yund (1991); 2. Dennis (1984); 3. Sharp et al. (1991); 4. Farver (1994); 5. Labotka et al. (2000); 6. Giletti et al. (1978); 7. Fortier and Giletti (1991); 8. Elphick et al. (1988); 9. Ryerson and Mckeegan (1994); 10. Farver and Giletti (1989); 11. Farver and Giletti (1985); 12. Watson and Cherniak (1997); 13. Coghlan (1990); 14. Farver (1989); 15. Zhang et al. (2006); 16. Hallwig et al. (1982); 17. Moore et al. (1998); 18. Giletti and Hess (1988); and 19. Sharp (1991). Oxygen concentrations are calculated as v/V, where v is the stoichiometric coefficient of oxygen and V is the molar volume of one mineral (Robie and Hemingway, 1995).
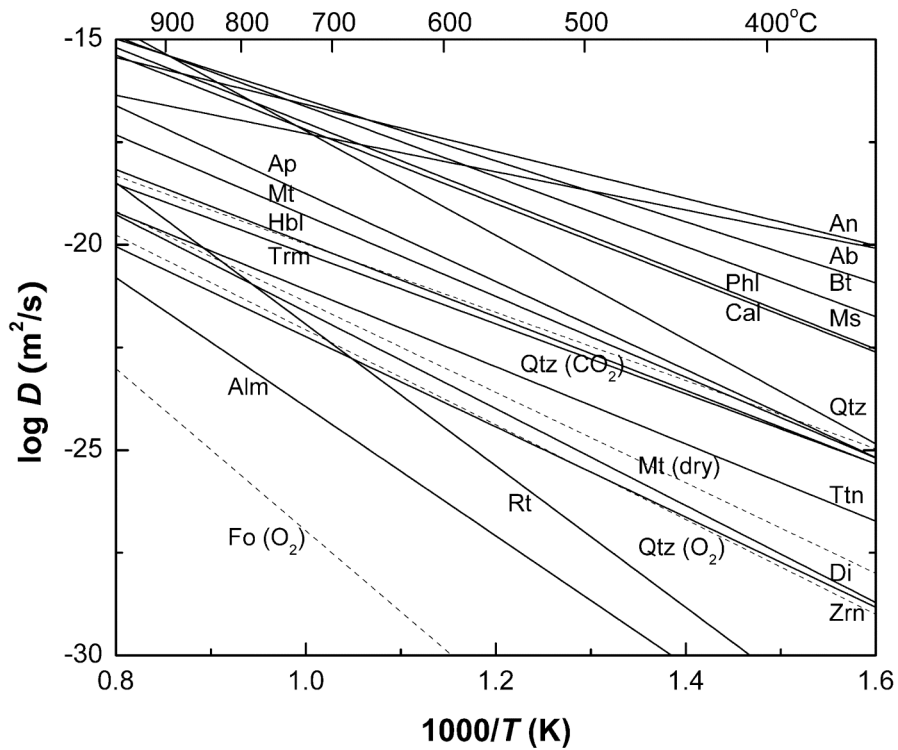
Fig. 5.1. Arrhenius plot of oxygen diffusivity in common rock-forming minerals under hydrothermal condition $P(H_2O)=100$ MPa (solid line) as well as oxygen diffusivity in quartz, magnetite, and olivine under anhydrous conditions (dash line). References can be found from the note of Table 5.1.

happen to have similar T_c, the two T_c values and T_{ae} will all be similar, and the apparent equilibrium temperature will be a good approximation of closure temperatures of both minerals. However, only a few types of rocks can be treated as bimineralic, such as quartz-calcite marbles. Furthermore, for rocks that are bimineralic, such as a gabbro containing only pyroxene and plagioclase, the two minerals may have very different oxygen isotope diffusivity and hence very different T_c values. These difficulties significantly hinder this simple idea to relate T_{ae} and T_c. Therefore, the FGB model was used to investigate the behavior of T_{ae} in rocks that have three or four minerals.

Fig. 5.2 illustrates how T_{ae} varies with modal abundances of minerals in a hypothetical rock containing quartz, albite and magnetite. All minerals have a uniform grain size of 1 mm. This rock was cooled from 750°C to 50°C in 160 million years (cooling rate at 600°C is 10°C/Myr), which results in closure temperature of 505°C for quartz, 219°C for albite, and 526°C for magnetite from Eq. (5-1). In this and the following simulations, "100%" of a mineral means that abundances of all other minerals are 10^{-7} (because there must be some finite amount of other minerals so that T_{ae} can be calculated). First examine T_{ae} of quartz-magnetite pair (Fig. 5.2a). At nearly pure quartz T_{ae} is 519°C, approximating T_c of magnetite; and T_{ae} at nearly pure magnetite is 503°C, approximating T_c of quartz. (T_{ae} values from numerical simulations may differ from those calculated from Eq. (5-1) by a few degrees because both methods are approximate.) Throughout the mineral abundance triangular diagram, quartz-magnetite T_{ae} lies between these two T_c values (503 to 519°C). In contrast, T_{ae} of quartz-albite (Fig. 5.2b) lies between the T_c values of quartz and albite (503 to 217°C) only when magnetite abundance is very low. Elsewhere in the triangle, T_{ae} is outside the T_c range (open circles

121
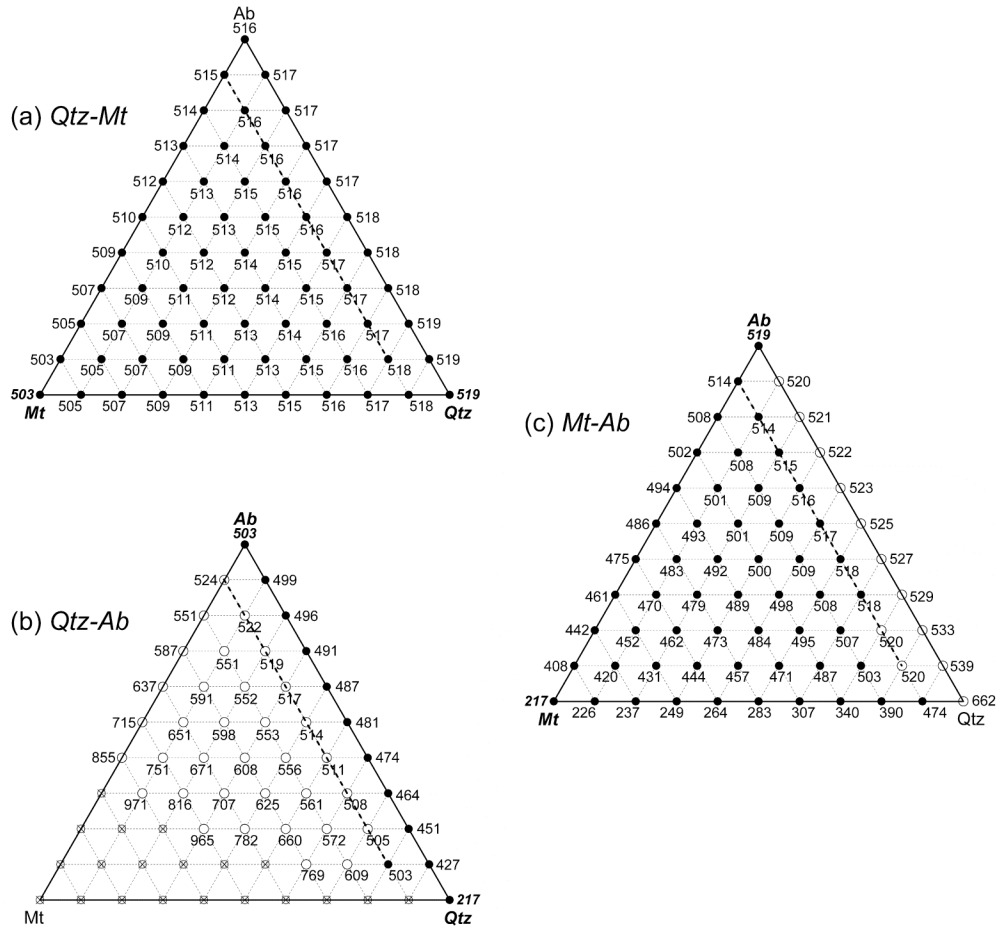
Fig. 5.2. Simulated apparent equilibrium temperature (in °C) of three mineral pairs in a quartz-albite-magnetite "granite" using the FGB model with asymptotic cooling $T = T_0/(1+t/\tau)$ with $T_0 = 1023$ K and $\tau = 74$ Myrs, the grain size of 1 mm for all three minerals, and fractionation factors and diffusivities from Table 5.1. (a) quartz-magnetite; (b) quartz-albite; (c) magnetite-albite. Solid circles represent T_{ae}'s that are constrained by the closure temperature range of the corresponding mineral pair (503-519°C, 217-503°C, and 217-519°C, respectively). Open circles represent those not constrained, and open circles with cross inside represent reversed isotopic composition. The dash lines indicate the compositions at which T_{ae} values of all three pairs are similar.

122

in Fig. 5.2b), or is not defined at all (open circles with crosses in Fig. 5.2b) because isotopic fractionation is reversed. In a large part of the triangle, T_{ae} is above the T_c range: not only might the T_{ae} value be accidentally the same as the peak temperature 750°C, but also it could be well above the peak temperature. Therefore, a mineral pair with higher T_{ae} values does not mean that the pair preserves the peak temperature information. The complex behavior of T_{ae} between quartz and albite is similar to previous results (Eiler et al., 1992, 1993) and is due to the relatively small fractionation between quartz and albite but large difference in their T_c, which makes T_{ae} easily disturbed by exchange with magnetite. The third pair in the system, magnetite-albite pair (Fig. 5.2c) yields T_{ae} outside the T_c range near quartz-albite border, especially near pure quartz.

In summary, T_{ae} between quartz and albite is not constrained by the T_c values of the two minerals, nor is T_{ae} between albite and magnetite. Only for quartz and magnetite, the pair with the largest isotopic fractionation (PLIF), is T_{ae} constrained by the T_c values of the two minerals. The two minerals also happen to have similar oxygen diffusivity and hence similar T_c values. Therefore, the overall variation of quartz-magnetite T_{ae} in the whole mineral abundance space is small (within 20°C), and T_{ae} is a good approximation for T_c values of both quartz and magnetite at any modal abundance of the three minerals.

A second noteworthy feature in Fig. 5.2 is that when the abundance of magnetite is ~10% (the line inside the triangles in Fig. 5.2), all three pairs yield similar T_{ae} (503-524°C). However, these apparently consistent temperatures are very different from the onset temperature 750°C. Therefore, even if different mineral pairs show similar T_{ae} values, it cannot be taken for granted that such a temperature corresponds to the peak temperature at which they reached equilibrium. Such false isotherm among coexisting

123

minerals has been reported in the Whitestone meta-anorthosite, Ontario (Sharp and Moecher, 1994).

It was suggested by Kohn and Valley (1998a) that T_{ae} of two minerals with similar T_c would also be a good proxy of T_c, with examples such as coexisting amphiboles (cummingtonite and hornblende), pyroxenes (orthopyroxene and clinopyroxene) and micas (biotite and muscovite). Based on this hypothesis, Kohn and Valley (1998b) interpreted the observed oxygen isotope partition between the two amphiboles Δ(Cum-Hbl) = 0.94 as equilibrium fractionation at closure temperature of amphiboles (~575°C). To evaluate the general applicability of their hypothesis, the fractionation between the two amphiboles in a hornblende-cummingtonite-albite amphibolite was investigated (Fig. 5.3). A fractionation factor $A_{Cum-Hbl}$ of approximately 0.7 is estimated from the observed fractionation (Kohn and Valley, 1998b). Therefore, albite-hornblende, instead of cummingtonite-hornblende, is the pair with the largest fractionation (PLIF) in this system. Because oxygen diffusivity in cummingtonite is currently not available, the diffusivity in tremolite (Table 5.1) was used. Cooling history and grain sizes can be found in the caption, resulting in ΔT_c = 10°C between hornblende and amphibole in Fig. 5.3a and ΔT_c = 44°C in Fig. 5.3b. Simulated T_{ae} between cummingtonite and hornblende is not constrained (shown as open circles) by their closure temperatures 542-552°C (Fig. 5.3a) and 542-586°C (Fig. 5.3b) when albite is higher than 20 vol.%. The departure of the minimum T_{ae} from the range defined by the two T_c values increases as $|\Delta T_c|$ increases. When ΔT_c = 10°C, the minimum T_{ae} is 527°C, 15°C below the minimum T_c of 542°C. In contrast, when ΔT_c = 44°C, the minimum T_{ae} is 51°C below the minimum T_c of 542°C. The fractionation between the two amphiboles is therefore disturbed by their exchange
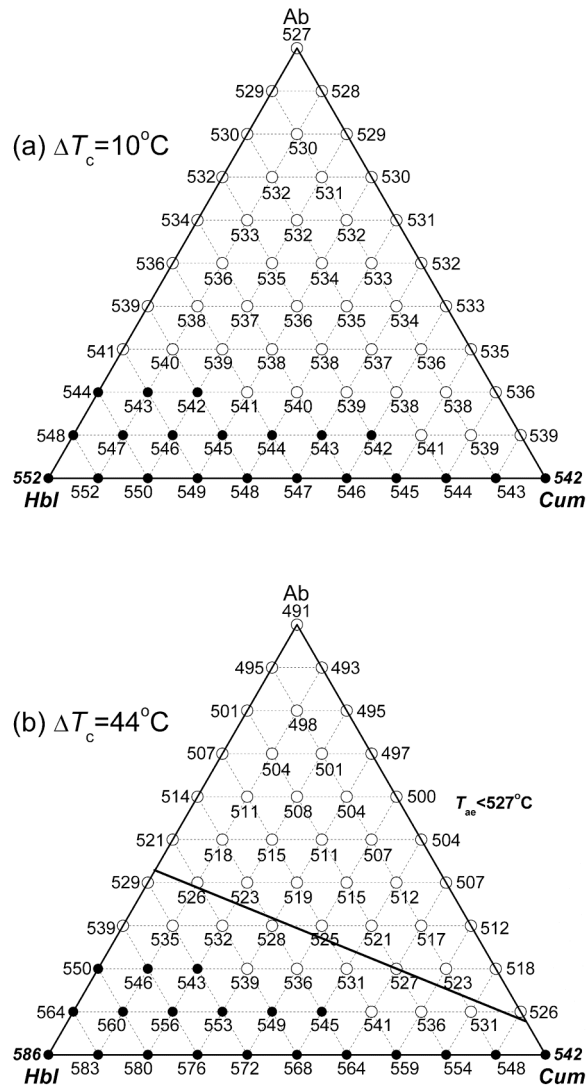
Fig. 5.3. Simulated apparent equilibrium temperatures (in °C) of cummingtonite-hornblende in an albite-cummingtonite-hornblende "amphibolite". The system cools from 750°C to 50°C in 350 Myrs. Grain size is 1 mm for albite and 0.5 mm for hornblende. Solid circles represent T_{ae}'s that are constrained by the closure temperature range, and open circles are not. *a,* cummingtonite grain is 0.5 mm, ΔT_c (cummingtonite-hornblende) is 10°C; *b,* 0.8 mm cummingtonite, and $\Delta T_c = 44$°C. Solid line indicates the isotherm of 527°C.

with albite, the mineral with fast diffusion and lower T_c (200°C). Such exchange results in a T_{ae} outside the range of two T_c values. Therefore, the hypothesis of Kohn and Valley (1998a) is correct when the two T_c values are identical, but becomes increasingly less reliable as ΔT_c increases.

To compare PLIF with similar T_c and non-PLIF with similar T_c, a quartz-magnetite-biotite-muscovite system is examined (Fig. 5.4 and 5.5), in which the quartz-magnetite pair has similar T_c's and also the largest fractionation, and biotite-muscovite pair has similar T_c's but smaller fractionation. Cooling history and grain sizes are given in the caption. Muscovite and biotite have similar T_c values (336°C and 293°C), and quartz and magnetite also have similar closure temperatures (477°C and 526°C). The closure temperatures of muscovite and biotite are close to the values Kohn and Valley (1998a) used in their discussion. Furthermore, the differences in T_c of the two pairs are also similar. The T_{ae} of quartz and magnetite (Fig. 5.4a), the pair with the largest oxygen isotope fractionation, lies exactly between the closure temperatures of quartz and magnetite. In contrast, T_{ae} between the two micas is not well constrained between the closure temperatures of the two micas (Fig. 5.5), although at most compositions T_{ae} is not very far off the T_c range and may still be used as approximation of T_c. The performance of muscovite-biotite is better than that of cummingtonite-hornblende due to two factors. First, the fractionation between muscovite and biotite is larger than that of the two amphiboles. Secondly, oxygen diffusion in amphiboles is much slower than diffusion in the coexisting albite, whereas here oxygen diffusion in micas is faster in micas than in quartz or magnetite. Therefore after quartz and magnetite roughly become "closed", biotite and muscovite still have the ability to "tune" the partition of oxygen isotopes and
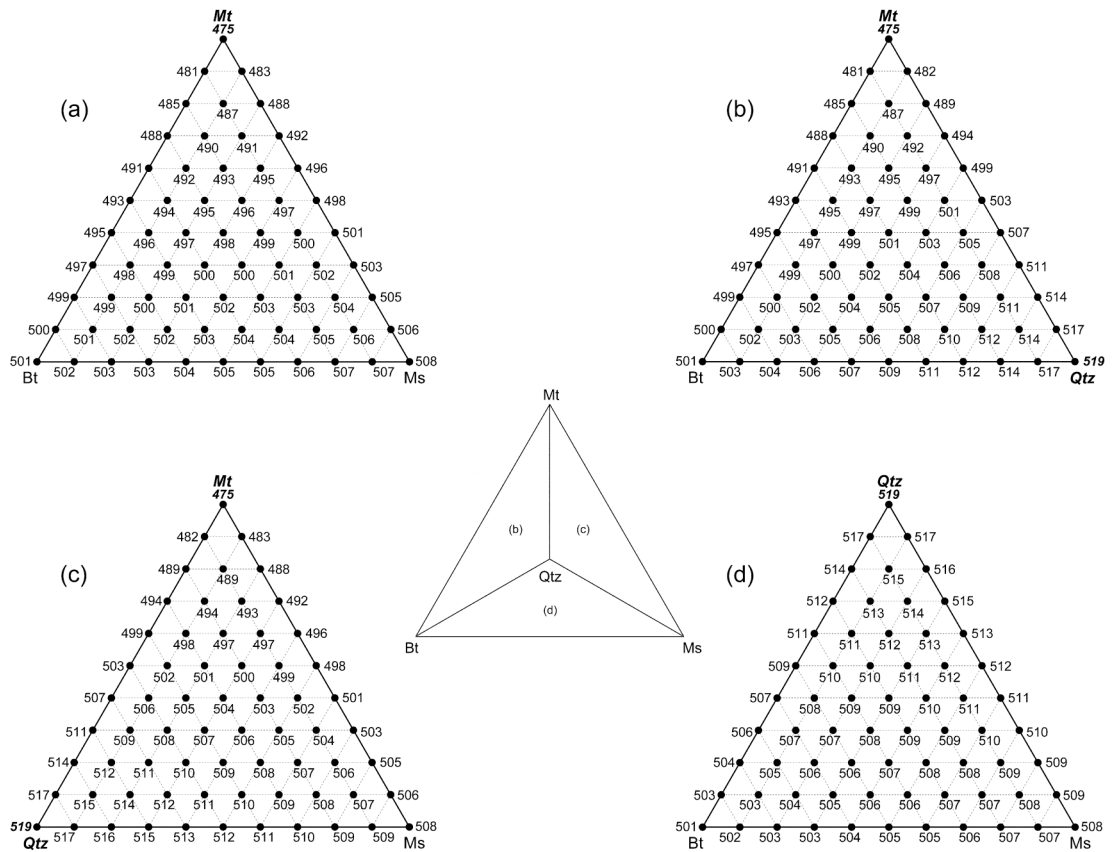
Fig. 5.4. Apparent equilibrium temperatures (in °C) of quartz-magnetite in a quartz-magnetite-biotite-muscovite system, illustrated in four ternary subsystems: *a,* magnetite-biotite-muscovite; *b,* quartz-magnetite-biotite; *c,* quartz-magnetite-muscovite; *d,* quartz-biotite-muscovite. T_{ae} is constrained within the T_c range without exception. Same cooling history as Fig. 5.2, and the grain size of 0.5 mm for all minerals but magnetite (1 mm).
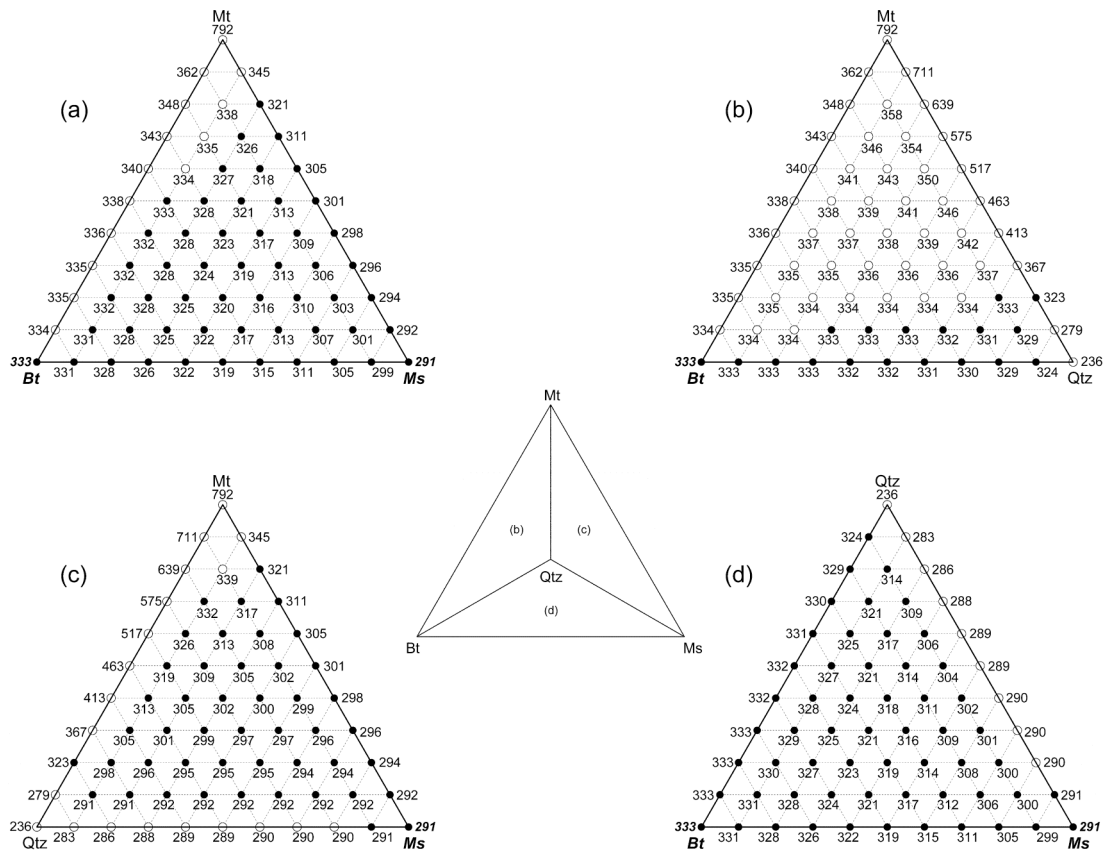
Fig. 5.5. Apparent equilibrium temperature (in °C) of biotite-muscovite in the same system as in Fig. 5.4. In contrast to quartz-magnetite, T_{ae} of the mica pair is not strictly constrained by their closure temperatures (291-333°C), with maximum of 792°C and minimum of 236°C.

generate a T_{ae} that is not far off their T_c, whereas the influence of albite on the fractionation between the amphiboles is lasting.

Some calculated evolution paths of $\delta^{18}O$ versus T of each mineral in the system (Fig. 5.6) can further illustrate the difference in the influence of other minerals on PLIF and non-PLIF. Because the largest effect is when the abundance of the mineral pair in consideration is very low, trace amount of the mineral pair in a third mineral was examined. Fig. 5.6a considers the quartz-magnetite-albite system when trace amount quartz and magnetite reside in an albite. The equilibrium fractionations at the closure temperature of magnetite (519°C) and that of quartz (503°C) are indicated by two short-dashed vertical lines. The frozen-in fractionation (from which T_{ae} is calculated) is denoted by the thin solid vertical line. Because quartz and magnetite are the pair with the largest fractionation, as temperature decreases, $\delta^{18}O$ of quartz only goes one direction - upward, and $\delta^{18}O$ of magnetite only goes downward. The length of the solid vertical line always lies in between the two dashed vertical lines; i.e., the frozen-in fractionation between quartz and magnetite always lies in between the equilibrium fractionations at their closure temperatures. Hence, even for the case of trace amounts of quartz and magnetite in almost pure albite, T_{ae} between quartz and magnetite is still between their T_c's. In the case of trace amount biotite and muscovite in a quartz (Fig. 5.6b), the frozen-in fractionation between the two micas is larger than the equilibrium fractionation at either of the two T_c values, and therefore T_{ae} is smaller than both T_c's. When the third mineral is magnetite (Fig. 5.6c), the frozen-in fractionation between the two micas is smaller than the equilibrium fractionation at either T_c, and therefore T_{ae} is larger than both
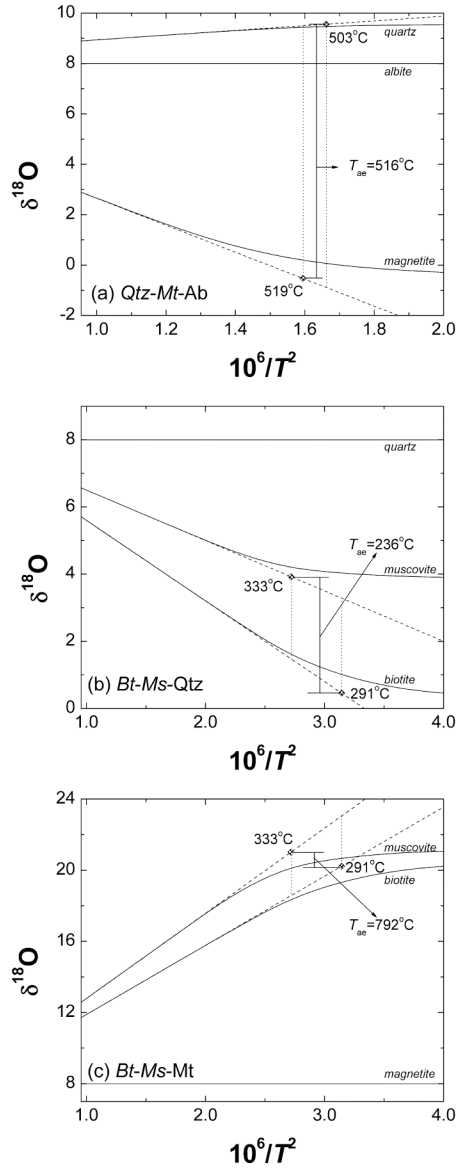
Fig. 5.6. Calculated isotopic evolution path of each mineral during cooling to show the effect of the third mineral on the oxygen isotope fractionation and T_{ae} of a mineral pair with similar T_c's. *a*, quartz-magnetite (PLIF) in albite: T_{ae} between quartz and magnetite in nearly pure albite is 516°C, between the closure temperatures of quartz and magnetite (503-519°C); *b*, biotite-muscovite (non-PLIF) in quartz: T_{ae} between biotite and muscovite in nearly pure quartz is 236°C, lower than the T_c range (291-333°C); *c*, biotite-muscovite in magnetite: T_{ae} between biotite and magnetite in nearly pure magnetite is 792°C, higher than the T_c range (291-333°C). Solid lines show the real evolution of $\delta^{18}O$ of minerals, and dash lines show $\delta^{18}O$ in equilibrium with the third mineral. Diamonds and solid vertical lines show the frozen-in $\delta^{18}O$ and fractionations, whereas dash vertical lines show equilibrium fractionation.

T_c's. It is apparent that the offset from equilibrium fractionations grows when the fractionation of the mineral pair is smaller and the difference in their T_c is larger.

In summary, the mineral pair with the largest isotopic fractionation (PLIF) is robust in constraining T_{ae} to be within their closure temperatures. Furthermore, if PLIF also happen to have similar T_c values, T_{ae} will be a good proxy of T_c of both minerals no matter how abundant the minerals are. One such pair is quartz and magnetite. Two minerals with similar closure temperature does not necessarily yield T_{ae} similar to T_c, which depends on (a) oxygen diffusion relative to each other (difference in T_c); (b) modal abundances of minerals; (c) oxygen isotope fractionation between the two minerals; and (d) oxygen diffusion relative to other minerals.

APPLICATIONS

The principle of oxygen isotope thermometry requires that isotopic compositions of minerals were "quenched", such as during the rapid cooling of volcanic rocks. For the slow cooling of plutonic and metamorphic rocks, successful oxygen isotope thermometry has been accomplished with minerals that are immune to alteration, such as refractory accessory minerals (RAM), such as zircon, which are resistant to oxygen diffusion (Valley, 2001), or the dominant mineral (> 90 vol.%) which can maintain its initial $\delta^{18}O$ due to mass balance. Otherwise the measured $\delta^{18}O$ values of minerals are different from the initial equilibrium values and the meaning of T_{ae} is not immediately clear.

The results of the simulations using the FGB model of Eiler et al. (1992, 1993, 1994) help to interpret diffusion-reset isotopic fractionation between mineral pairs. The

mineral pair with the largest isotopic fractionation (PLIF) is unique, in that their T_{ae} is always bracketed by their closure temperatures no matter how modal abundances of minerals vary! The T_{ae} between other mineral pairs may be high or low or in between (depending on mineral proportions), but the meaning cannot be gauged simply and requires efforts to decode. Furthermore, PLIF allows one to deduce the closure temperature of the two minerals when they approximately equal. Therefore, it provides two additional relations, one for each mineral, between measurable properties, cooling history, and cooling environment (because diffusivities depend on cooling environment). Below, some applications are discussed using insight gained from the simulations about the mineral pair with the largest isotopic fractionation.

Thermal history of rocks

Many authors reported oxygen isotope data in ultra-high pressure (UHP) metamorphic rocks in China (e.g., Zheng et al., 1998; Fu et al., 1999). The mineral pair with the largest oxygen isotope fractionation is quartz-rutile in UHP eclogite as long as rutile is present. Hence, T_{ae} based on this mineral pair has some meaning: it lies between the closure temperatures of quartz and rutile and does not exceed the peak temperature if equilibrium was reached between the two minerals at the peak temperature. The T_{ae} between other mineral pairs do not have much meaning, and could be above the peak temperature or very low. For example, Zheng et al. (1999) carried out a systematic study on east Dabie UHP eclogites from the so-called "hot" zone to "cold" zone (Okay, 1993), and calculated T_{ae} between many mineral pairs, but T_{ae} varies widely and the systematics is not obvious. Detailed examination of their data show that although T_{ae} based on other

mineral pairs may vary widely (from 385°C to >1000°C for quartz and omphacite), T_{ae}

between quartz and rutile in eclogites in any location only varies in a narrow range. This

is consistent with the simulation results above. The mineral abundances do not vary that

much from Bixiling eclogites to Huangzhen eclogites. Therefore, T_{ae} between quartz and

rutile may be used to investigate thermal history of the eclogites from "hot" zone to

"cold" zone. Fig. 5.7 shows how T_{ae} between quartz and rutile varies systematically with

distance from Bixiling ("hot" zone), to Wumiao ("hot" zone); to Maowu ("hot" zone); to

Hualiangting ("hot" zone); and to Huangzhen ("cold" zone). The gradual decrease of T_{ae}

from Bixiling to Huangzhen based on oxygen isotope thermometry is consistent with the

trend from "hot" to "cold" based on cation thermometry (Okay, 1993), but there is no

sharp boundary. The presence or absence of diamond and coesite (Okay, 1993) in these

regions suggest that different metamorphic grade coupled with different cooling rates

likely caused the difference in oxygen isotope fractionation between quartz and rutile.

Unfortunately, because diffusivities in quartz and rutile are not similar, no matter whether

it is "dry" or "wet", using T_{ae} to approximate T_c's of quartz and rutile would result in

large errors. Hence, cooling rate cannot be inferred.

Inference of cooling rate

By converting Eq. (5-1), the cooling rate at T_c may be expressed as:

$$q = \frac{GRT_c^2 D(T_c)}{a^2 E},\qquad(5\text{-}5)$$

where $D(T_c)$ is diffusivity of ^{18}O at temperature of T_c. Therefore, if oxygen isotope

diffusivity has been determined accurately, cooling rate can be calculated by using T_{ae} as
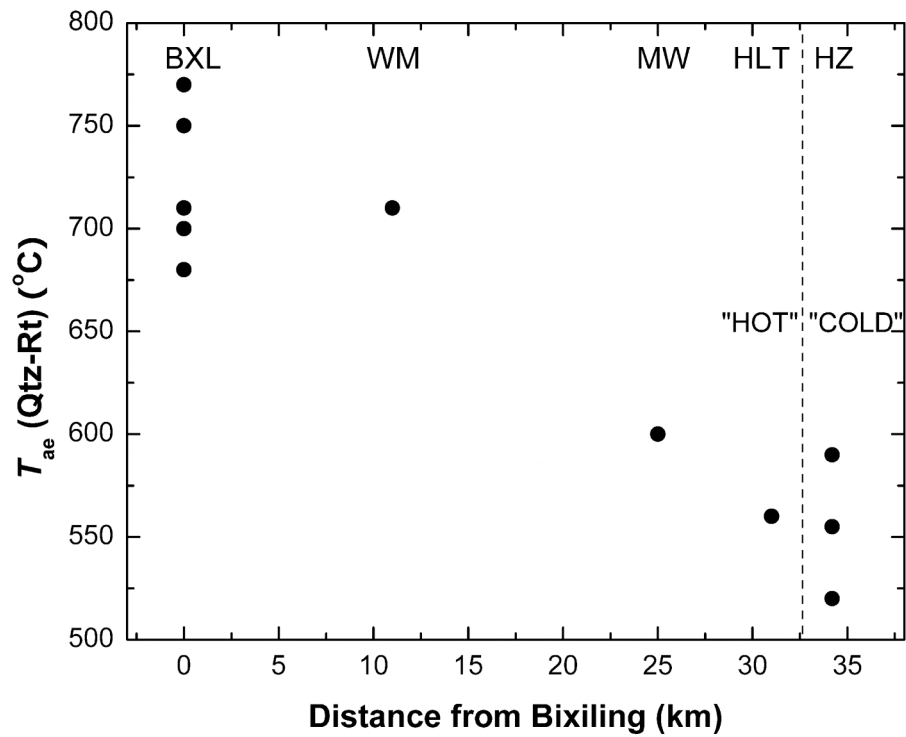
Fig. 5.7. The variation of the apparent equilibrium temperature between quartz and rutile in east Dabie ultra-high pressure eclogites as a function of distance from Bixiling. Data are from Zheng et al. (1999). Dash line shows the boundary between "hot" zone and "cold" zone defined by Okay (1993). Abbreviation of location names: BXL = Bixiling; WM = Wumiao; MW = Maowu; HLT = Hualiangting; HZ = Huangzhen. The distance is projected on a line connecting Bixiling and Huangzhen.

proxy of T_c of both minerals. Whether the two cooling rates calculated from each mineral are consistent can be used to back inspect the validity of the approximation.

The San Jose tonalite is a 108 km^2 pluton of ~105 Ma, belonging to the Jurassic to Cretaceous Peninsular Ranges batholith of northern Baja California, Mexico (Johnson et al., 2003). The oxygen isotopes of a sample from the central portion of the pluton with $Plag_{62.3}Hbl_{9.6}Bt_{5.95}Qtz_{17.1}Mt_{2.6}$ were examined (Taylor and Epstein, 1962; Taylor, 1968) and interpreted (Giletti, 1986) to have experienced a cooling rate of 100-200°C/Myr ($141 \overset{\times}{\div} 1.4$°C/Myr). The same isotopic data was re-interpreted to estimate cooling rate as follows. Based on the measured $\delta^{18}O$ of the largest fractionated pair, 9.7‰ for quartz and 2.0‰ for magnetite, and the calibration of Chiba et al. (1989), a T_{ae} of 633°C was obtained. Due to the presence of hydrous minerals, the real diffusivity is assumed to be identical to that determined from experiments at 1 kbar water pressure. The grain size is 2.0 mm for quartz and 0.5 mm for magnetite (Giletti, 1986). Assuming T_c's of both quartz and magnetite are the same as T_{ae} (633°C), a cooling rate of 556 (from quartz) to 1247°C/Myr (from magnetite) is estimated for San Jose tonalite, or $(830 \overset{\times}{\div} 1.5)$°C/Myr from Eq. (5-5), which is about 6 times higher than the former estimate (Giletti, 1986).

Assuming heat conduction only (i.e., ignoring convection and latent heat during magma crystallization) for a spherical pluton, adopting a heat diffusivity of 0.8 mm^2/s for both the pluton and its country rock (Lasaga, 1998), the cooling rate at the center of the pluton is calculated for different pluton size based on three-dimensional heat conduction of spherical symmetry (Table 5.2). My cooling rate estimate suggests that the largest cross section area of San Jose pluton was 120 to 260 km^2, 1.1 to 2.4 times the 108 km^2, while previous cooling rate estimate would require that the largest cross section area of

135

Table 5.2. Cooling rate for San Jose tonalite based on heat conduction model

Pluton size	Radius	6.1	9.1	15.2	21.5
	Area	116	260	726	1452
Cooling rate		1247	556	200	100

Calculation is based on 3-dimensional heat conduction of spherical symmetry. The solidus temperature of the pluton is assumed to be 1000°C, and the initial temperature of the country rock is estimated to be 213°C based on the intrusion pressure (~ 2.3 kbar, Johnson et al., 2003) and an assumed 25°C/km geotherm.

San Jose pluton be 7 to 14 times the 108 km^2. If the exposed area of the pluton of 108 km^2 is not much smaller than the largest cross section area, my estimate is more reasonable. If thermal convection is considered, then cooling rate at the center of the pluton would be greater than the pure conductive cooling rate, which would favor the higher cooling rate inferred in this work than that of Giletti (1986). The low estimate of cooling rate by Giletti (1986) is probably due to the inconsistency in considering diffusion and mass balance.

Thermochronology is the typical and preferred method for inferring cooling rate. However, in the absence of thermochronological data, my method can provide a rough estimate of the cooling rate. Future improvements on analytical techniques would reduce uncertainty in isotope ratios, fractionation factors and diffusivities, and improve the accuracy of the method.

Estimation of oxygen isotope diffusivity and fluid conditions

In addition to the inference of cooling rate with known diffusivity, if the cooling history of a rock has been established based on thermochronology, empirical oxygen isotope diffusivity can be estimated by rewriting Eq. (5-5) as

$$D(T_c) = \frac{a^2 Eq}{GRT_c^2}.$$ (5-6)

Because there are errors in estimating q (a factor of ~2), a (a factor <2) and E (a factor <2), the estimate of $D(T_c)$ is likely to have an uncertainty of ~10. Oxygen diffusivity in a mineral depends strongly on the fluid condition such as H_2O fugacity (Farver and Yund, 1991), likely because molecular water is the diffusing species (Zhang et al., 1991; McConnell, 1995; Behrens et al., 2007). Diffusivity estimated using Eq. (5-6) may hence

be compared with oxygen diffusivity under different fluid conditions to constrain the fluid environment of the rock during cooling. Below is an example.

The Adirondack Mountains are part of the Grenville Province. The peak temperature at Lyon Mountain, NE Adirondack Highlands is ~725°C (Bohlen et al., 1985) at >1.0 Ga followed by cooling at 1-4°C/Myr (Mezger et al., 1991). Sample AF665, collected by Eiler et al. (1993) from Lyon Mountain, contains quartz, magnetite, albite, clinopyroxene, and some accessory minerals. Oxygen isotope fractionation between quartz (7.97‰) and magnetite (-0.87‰) shows a reset temperature of 572°C, which may be used as proxy for T_c's of quartz and magnetite. Using the average cooling rate of $(2 \overset{\times}{\div} 2)$°C/Myr, with grain size of ~0.3 mm for both quartz and magnetite (Eiler et al., 1993), the oxygen isotope diffusivity at $T_c = 572$°C is estimated to be 2.5×10^{-23} m^2/s for quartz and 2.9×10^{-24} m^2/s for magnetite based on Eq. (5-6) if the activation energy at 1 kbar hydrothermal conditions is adopted. Because $D(T_c)$ in Eq. (5-6) is proportional to the activation energy, uncertainty in the activation energy only leads to small errors (such as a factor of 2) in $D(T_c)$.

In order to infer the cooling environment of the rock, the above inferred oxygen isotope diffusivities were compared with experimental or empirical oxygen diffusivities under different fluid conditions (Fig. 5.8). The calculated diffusivity in magnetite is roughly identical to the empirical diffusivity of Sharp (1991) when the water fugacity is low. Similarly, the calculated diffusivity in quartz is lower than the values when water or CO_2 fugacity is high, but is higher than the value at 1 bar oxygen gas pressure. Therefore, the oxygen isotope data indicates that this rock cooled under dry conditions when the
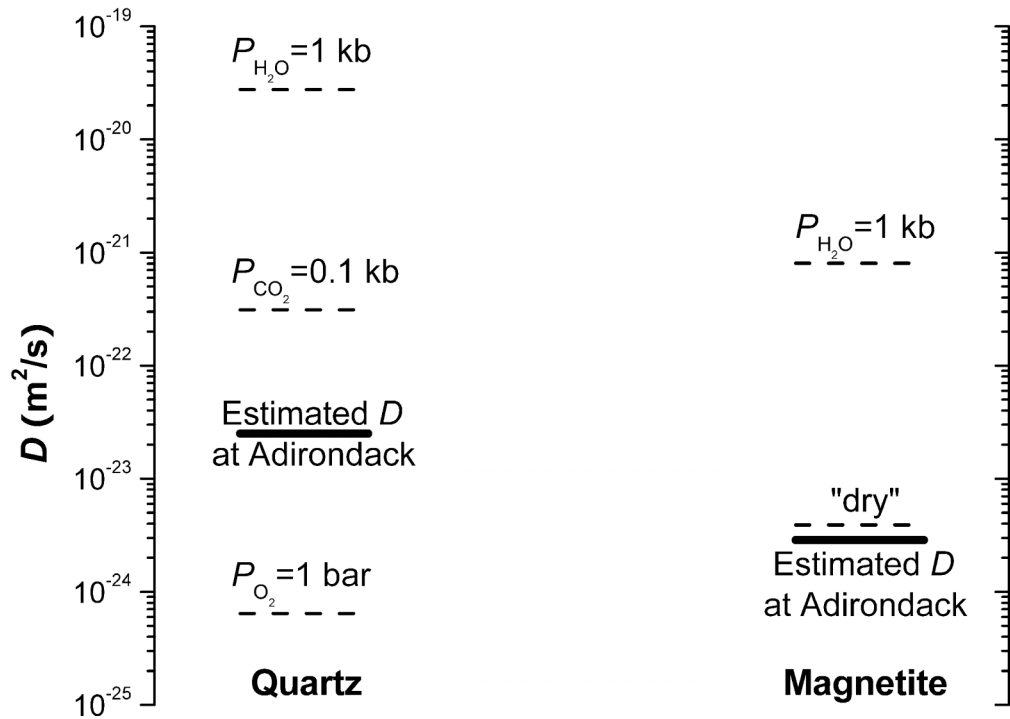
Fig. 5.8. Inferred oxygen isotope diffusivities compared with experimental or empirical diffusivities under various fluid conditions. Oxygen isotope diffusivity in quartz (left-hand side) and magnetite (right-hand side) at 572°C under various fluid conditions are shown by dashed segments. "Dry" oxygen diffusivity is empirically estimated diffusivity in magnetite hosted in a calcite marble (Sharp, 1991). The heavy solid segments are estimated oxygen isotope diffusivities in quartz and magnetite in sample AF665 from the Adirondack (Eiler et al., 1993) at 572°C (which is T_{ae} based on oxygen isotopic ratios in quartz and magnetite and used as proxy of T_c) and the thermochronologically estimated cooling rate of $2 \overset{\times}{\div} 2$ °C/Myr (Mezger et al., 1991).

temperature was about 572°C, consistent with the petrological observations of Eiler et al. (1993).

Evaluation of closed system vs. open system behavior

The previous discussion on the mineral pair with the largest isotopic fractionation (PLIF) is based on the assumption that the rock can be treated as a closed system during its cooling history. Open system behavior would be different. The presence of a fluid and the importance of fluid-rock interaction in stable isotopes have been addressed by many authors (e.g., Baumgartner and Valley, 2001). In terms of the significance in interpreting T_{ae}, a fluid phase is an extra phase in the system. Hence the conclusion that T_{ae} of PLIF lies between the two T_c values must include this extra phase. If the equilibrium oxygen isotopic ratio of the fluid phase lies between ratios of other minerals, i.e., if the PLIF is a mineral pair, then T_{ae} of the mineral pair is between the two T_c values. For example, T_{ae} of quartz-magnetite is still between their T_c's even in presence of water, because magnetite is depleted in ^{18}O relative to water, while quartz is enriched in ^{18}O relative to water at temperatures below 800°C (Fig. 5.9).

In some open systems, the pair with the largest isotopic fractionation may be a mineral (such as quartz) and water. Because the isotopic ratio of water is not frozen in by a rock, T_{ae} between a mineral and water cannot be calculated. T_{ae} of the "apparent PLIF", i.e., two minerals, may not have any meaning. An example of simulation is as follows. In a quartz-albite-muscovite system, quartz and muscovite are the PLIF. In the presence of water, quartz and water are the PLIF. The calibration $\Delta = 3.306 \times 10^6/T^2$-2.71 by Zhang et al. (1989) for quartz and water was adopted, because when it is combined with the
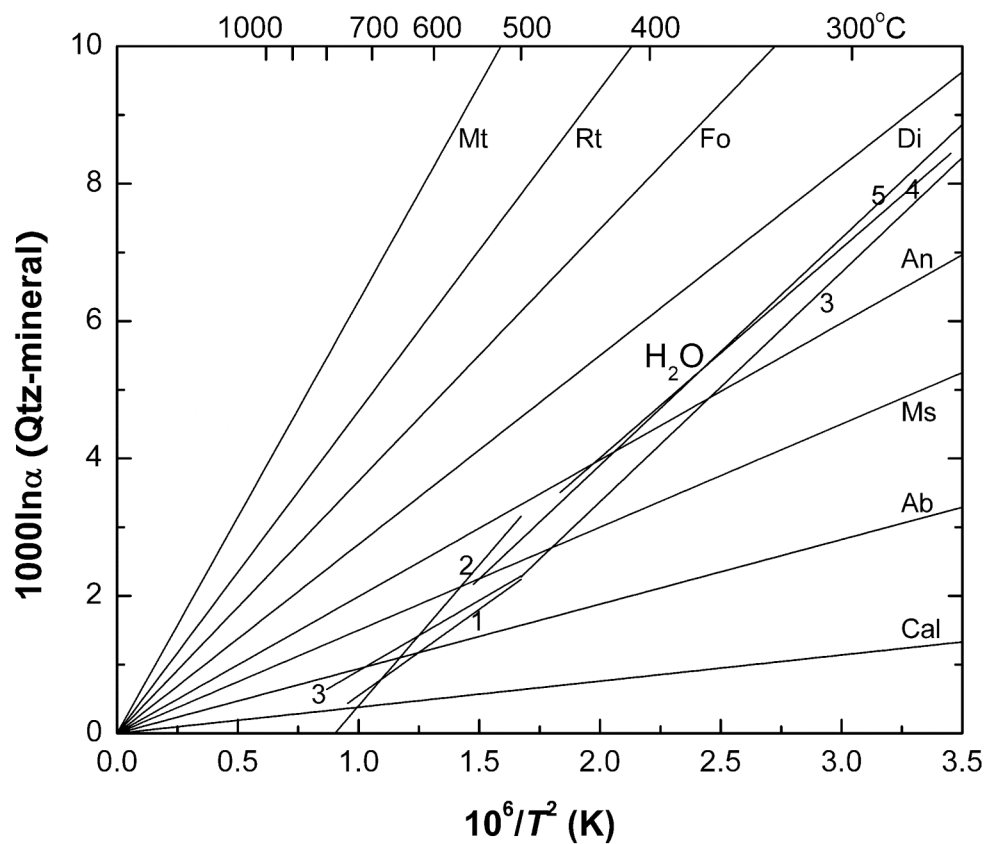
Fig. 5.9. Oxygen isotope fractionation between quartz and water (segments 1-5), and between quartz and other minerals (Table 5.1). References are: (1) Clayton et al. (1972); (2) Bottinga and Javoy (1973); (3) Matsuhisa et al. (1979); (4) Matthews and Beckinsale (1979); (5) Zhang et al. (1989).

141

fractionation between quartz and muscovite (Table 5.1), the result is in agreement with the evaluation $\Delta = 1.90 \times 10^6/T^2 - 3.10$ of muscovite-H_2O fractionation (Bottinga and Javoy, 1973). For cooling from 1000°C to 50°C in 160 Myrs and 0.5 mm mineral grains, T_c of quartz is 477°C and T_c of muscovite is 336°C, $\Delta^{18}O$ of quartz-water and muscovite-water is 3.16‰ and 2.16‰, i.e., the equilibrium fractionation at their respective T_c. The fractionation between quartz and muscovite thus results in an extremely high T_{ae} of 947°C, obviously beyond their T_c range. The above complexity may be used to our advantage, to identify fluid involvement. If the fractionation between the mineral pair of PLIF is not large and may be smaller than the fractionation between a fluid and a mineral, and if T_{ae} between the PLIF is unrealistically high or low, it might imply fluid involvement during cooling of the rock.

CONCLUDING REMARKS

From this work and previous publications, the meaning of T_{ae} based on oxygen isotope thermometry between a pair of minerals is summarized below. Minerals with extremely slow oxygen diffusion (T_c is higher than peak temperature) and the mineral of high abundant minerals (> 90 vol.%) may preserve their initial oxygen isotopic composition, which can be used to infer the peak temperature (Valley, 2001). The composition of other minerals have been altered through diffusive exchange during slow cooling. For a two-mineral system, T_{ae} between the two minerals is between the closure temperatures of the two minerals. For a system with three or more minerals, T_{ae} of the mineral pair with the largest isotopic fractionation (PLIF) is between the closure

temperatures of the two minerals. If diffusivities of such a mineral pair are similar, T_{ae} would be a good approximation of the closure temperatures of the two minerals. One such mineral pair is quartz and magnetite. Other minerals with similar closure temperatures may show a T_{ae} that represents T_c, but do not have to be.

Since apparent equilibrium temperature depends on mineral abundances, it is difficult to use oxygen isotopes to infer thermal history or diffusion kinetics at first glance. Nonetheless, the mineral pair with the largest fractionation may provide consistent apparent equilibrium temperatures for discussion of thermal history of rocks. Furthermore, quartz and magnetite pair may provide not only consistent T_{ae}'s, but also two additional equations (one for each mineral) relating T_{ae}, cooling rate, and diffusion properties. This additional relation may be applied to estimate cooling rate if diffusion properties and cooling environment are known, or to constrain the fluid environment (which affects the diffusion properties) if cooling rate is independently determined. In the case of open system (such as presence of water), T_{ae} of the PLIF may deviate from their T_c range when PLIF are both enriched in ^{18}O than the extra phase.

The relations developed for the mineral pair with the largest fractionation may be more useful in the future when oxygen fractionation factors and oxygen isotopic diffusivity are better measured as a function of temperature, pressure and fluid fugacity. Furthermore, the method in principle can be applied to other exchange reactions, such as Fe-Mg exchange reactions between ferromagnesian minerals. In such cases, T_{ae} for the mineral pair with the largest difference in Fe^{2+}/Mg ratio would be constrained to be within the two closure temperatures.

REFERENCES

Baumgartner, L.P., Valley, J.W., 2001. Stable isotope transport and contact metamorphic fluid flow. Rev. Mineral. Geochem. 43, 415-467.

Behrens, H., Zhang, Y., Leschik, M., Wiedenbeck, M., Heide, G., Frischat, G.H., 2007. Molecular H_2O as carrier for oxygen diffusion in hydrous silicate melts. Earth Planet. Sci. Lett. 254, 69-76.

Bohlen, S.R., Valley, J.W., Essene, E.J., 1985. Metamorphism in the Adirondacks. I. Petrology, pressure and temperature. J. Petrol. 26, 971-992.

Bottinga, Y., Javoy, M., 1973. Comments on oxygen isotope geothermometry. Earth Planet. Sci. Lett. 20, 250-265.

Chacko, T., Hu, X., Mayeda, T.K., Clayton, R.N., Goldsmith, J.R., 1996. Oxygen isotope fractionations in muscovite, phlogopite, and rutile. Geochim. Cosmochim. Acta 60, 2595-2608.

Chiba, H., Chacko, T., Clayton, R.N., Goldsmith, J.R., 1989. Oxygen isotope fractionations involving diopside, forsterite, magnetite, and calcite: application to geothermometry. Geochim. Cosmochim. Acta 53, 2985-2995.

Clayton, R. N., O'Neil, J.R., Mayeda, T.K., 1972. Oxygen isotope exchange between quartz and water. J. Geophys. Res. B77, 3057-3067.

Clayton, R.N., Goldsmith, J.R., Mayeda, T.K., 1989. Oxygen isotope fractionation in quartz, albite, anorthite, and calcite. Geochim. Cosmochim. Acta 53, 725-733.

Coghlan, R.A.N., 1990. Studies in diffusional transport: grain boundary transport of oxygen in feldspar, diffusion of oxygen, strontium and the REE's in garnet, and thermal histories of granitic intrusions in south-central Maine using oxygen isotopes. Ph. D. dissertation, Brown University, Providence, RI.

Dennis, P.F., 1984. Oxygen self diffusion in quartz. Prog. Exp. Petrol., NERC Publ. D. 25, 260-265.

Dodson, M.H., 1973. Closure temperature in cooling geochronological and petrological systems. Contrib. Mineral. Petrol. 40, 259-274.

Eiler, J.M., Baumgartner, L.P., Valley, J.W., 1992. Intercrystalline stable isotope diffusion: a fast grain boundary model. Contrib. Mineral. Petrol. 112, 543-557.

Eiler, J.M., Valley, J.W., Baumgartner, L.P., 1993. A new look at stable isotope thermometry. Geochim. Cosmochim. Acta 57, 2571-2583.

Eiler, J.M., Baumgartner, L.P., Valley, J.W., 1994. Fast grain boundary: a Fortran-77 program for calculating the effects of retrograde interdiffusion of stable isotopes. Computers Geosci. 20, 1415-1434.

Elphick, S.C., Graham, C.M., Dennis, P.F., 1988. An ion microprobe study of anhydrous oxygen diffusion in anorthite: a comparison with hydrothermal data and some geological implications. Contrib. Mineral. Petrol. 100, 490-495.

Farver, J.R., 1989. Oxygen self-diffusion in diopside with application to cooling rate determinations. Earth Planet. Sci. Lett. 92, 386-396.

Farver, J.R., 1994. Oxygen self-diffusion in calcite: dependence on temperature and water fugacity. Earth Planet. Sci. Lett. 121, 575-587.

Farver, J.R., Giletti, B.J., 1985. Oxygen diffusion in amphiboles. Geochim. Cosmochim. Acta 49, 1403-1411.

Farver, J.R., Giletti, B.J., 1989. Oxygen and strontium diffusion kinetics in apatite and potential applications to thermal history determinations. Geochim. Cosmochim. Acta 53, 1621-1631.

Farver, J.R., Yund, R.A., 1991. Oxygen diffusion in quartz: dependence on temperature and water fugacity. Chem. Geol. 90, 55-70.

Fortier, S.M., Giletti, B.J., 1991. Volume self-diffusion of oxygen in biotite, muscovite, and phlogopite micas. Geochim. Cosmochim. Acta 55, 1319-1330.

Fortier, S.M., Lüttge, A., 1995. An experimental calibration of the temperature dependence of oxygen isotope fractionation between apatite and calcite at high temperatures (350-800°C). Chem. Geol. 125, 281-290.

Fu, B., Zheng, Y.-F., Wang, Z., Xiao, Y., Gong, B., Li, S., 1999. Oxygen and hydrogen isotope geochemistry of gneisses associated with ultrahigh pressure eclogites at Shuanghe in the Dabie Mountains. Contrib. Mineral. Petrol. 134, 52-66.

Ganguly, J., Tirone, M., 1999. Diffusion closure temperature and age of a mineral with arbitrary extent of diffusion: theoretical formulation and applications. Earth. Planet. Sci. Lett. 170, 131-140.

Giletti, B.J., 1986. Diffusion effects on oxygen isotope temperatures of slowly cooled igneous and metamorphic rocks. Earth Planet. Sci. Lett. 77, 218-228.

Giletti, B.J., Hess, K.C., 1988. Oxygen diffusion in magnetite. Earth Planet. Sci. Lett. 89, 115-122.

Giletti, B.J., Semet, M.P., Yund, R.A., 1978. Studies in diffusion –III. Oxygen in feldspars: an ion microprobe determination. Geochim. Cosmochim. Acta 42, 45-57.

Hallwig, D., Schachtner, R., Sockel, H.G., 1982. Diffusion of magnesium, silicon and oxygen in Mg_2SiO_4 and formation of the compound in the solid state. *In* Dyrek, K., Habor, J, and Nowotry J., eds. Reactivity in solids. Proc. Int'l Symp. (9th), p. 166-169.

Jenkin, G.R.T., Farrow C.M., Fallick, A.E., Higgins, D., 1994. Oxygen isotope exchange and closure temperatures in cooling rocks. J. Metamorphic Geol. 12, 221-235.

Johnson, S.E., Fletcher, J.M., Fanning, C.M., Vernon, R.H., Paterson, S.R., Tate, M. C., 2003. Structure, emplacement and lateral expansion of the San Jose tonalite pluton, Peninsular Ranges batholith, Baja California, Mexico. J. Struct. Geol. 25, 1933-1957.

Kohn, M.J., 1999. Why most "dry" rocks should cool "wet". Am. Mineral. 84, 570-580.

Kohn, M.J., Valley, J.W., 1998a. Obtaining equilibrium oxygen isotope fractionations from rocks: theory and examples. Contrib. Mineral. Petrol. 132, 209-224.

Kohn, M.J., Valley, J.W., 1998b. Oxygen isotope geochemistry of the amphiboles: isotope effects of cation substitutions in minerals. Geochim. Cosmochim. Acta 62, 1947-1958.

Labotka, T.C., Cole, D.R., Riciputi, L.R., 2000. Diffusion of C and O in calcite at 100 MPa. Am. Mineral. 85, 488-494.

Lasaga, A.C., 1998. Kinetic theory in the earth sciences. Princeton University Press, Princeton, New Jersey, 430 p.

Matsuhisa, Y., Goldsmith, J.R., Clayton, R.N., 1979. Oxygen isotopic fractionation in the system quartz-albite-anorthite-water. Geochim. Cosmochim. Acta 43, 1131-1140.

Matthews, A., Beckinsale, R.D., 1979. Oxygen isotope equilibration systematics between quartz and water. Am. Mineral. 64, 232-240.

McConnell, J.D.C., 1995. The role of water in oxygen isotope exchange in quartz. Earth Planet. Sci. Lett. 136, 97-107.

Mezger, K., Rawnsley, C.M., Bohlen, S.R., Hanson, G.N., 1991. U-Pb garnet, sphene, monazite, and rutile ages: implications for the duration of high-grade metamorphism and cooling histories, Adirondack Mts., New York. J. Geol. 99, 415-428.

Moore, D.K., Cherniak, D.J., Watson, E.B., 1998. Oxygen diffusion in rutile from 750 to 1000 °C and 0.1 to 1000 MPa. Am. Mineral. 83, 700-711.

Okay, A.I., 1993. Petrology of a diamond and coesite-bearing metamorphic terrain: Dabie Shan, China. Eur. J. Mineral. 5, 659-675.

146

Robie, R.A., Hemingway, B.S., 1995. Thermodynamics properties of minerals and related substances at 298.15 K and 1 bar (10^5 pascals) pressure and at higher temperatures. U.S. Geol. Survey Bull. 2131.

Ryerson, F.J., Mckeegan, K.D., 1994. Determination of oxygen self-diffusion in åkermanite, anorthite, diopside, and spinel: implications for oxygen isotopic anomalies and the thermal histories of Ca-Al-rich inclusions. Geochim. Cosmochim. Acta 58, 3713-3734.

Sharp, Z.D., 1991. Determination of oxygen diffusion rates in magnetite from natural isotopic variations. Geology 19, 653-656.

Sharp, Z.D., Moecher, D.P., 1994. O-isotope variations in a porphyroclastic meta-anorthosite: diffusion effects and false isotherms. Am. Mineral. 79, 951-959.

Sharp, Z.D., Giletti, B.J., Yoder, H.S. Jr., 1991. Oxygen diffusion rates in quartz exchanged with CO_2. Earth Planet. Sci. Lett. 107, 339-348.

Skogby, H., 1992. Order-disorder kinetics in orthopyroxenes of ophiolite origin. Contrib. Mineral. Petrol. 109, 471-478.

Taylor, H.P. Jr., Epstein, S., 1962. Relationship between $^{18}O/^{16}O$ ratios in coexisting minerals of igneous and metamorphic rocks. Geol. Soc. Am. Bull. 73, 461-480.

Taylor, H.P. Jr., 1968. The oxygen isotope geochemistry of igneous rocks. Contrib. Mineral. Petrol. 19, 1-71.

Valley, J.W., 2001. Stable isotope thermometry at high temperatures. Rev. Miner. Geochem. 43, 365-413.

Valley, J.W., Bindeman, I.N., Peck, W.H., 2003. Empirical calibration of oxygen isotope fractionation in zircon. Geochim. Cosmochim. Acta 67, 3257-3266.

Watson, E.B., Cherniak, D.J., 1997. Oxygen diffusion in zircon. Earth Planet. Sci. Lett. 148, 527-544.

Zhang, L., Liu, J., Zhou, H., Chen, Z., 1989. Oxygen isotope fractionation in the quartz-water-salt system. Econ. Geol. 84, 1643-1650.

Zhang, X.Y., Cherniak, D.J., Watson E.B., 2006. Oxygen diffusion in titanite: lattice diffusion and fast-path diffusion in single crystals. Chem. Geol. 235, 105-123.

Zhang, Y., 1994. Reaction kinetics, geospeedometry, and relaxation theory. Earth Planet. Sci. Lett. 122, 373-391.

Zhang, Y., Stolper, E.M., Wasserburg, G.J., 1991. Diffusion of a multi-species component and its role in oxygen and water transport in silicates. Earth Planet. Sci. Lett. 103, 228-240.

Zhang, Y., Jenkins, J., Xu, Z., 1997. Kinetics of the reaction $H_2O + O = 2OH$ in rhyolitic glasses upon cooling: geospeedometry and comparison with glass transition. Geochim. Cosmochim. Acta 61, 2167-2173.

Zhang, Y., Xu, Z., Behrens, H., 2000. Hydrous species geospeedometer in rhyolite: improved calibration and application. Geochim. Cosmochim. Acta 64, 3347-3355.

Zheng, Y.-F., Meta, P., Satir, M., 1994. Oxygen isotope fractionation between calcite and tremolite: an experimental study. Contrib. Mineral. Petrol. 118, 249-255.

Zheng, Y.-F., Fu, B., Li, Y., Xiao, Y., Li, S., 1998. Oxygen and hydrogen isotope geochemistry of ultrahigh-pressure eclogites from the Dabie Mountains and the Sulu terrane. Earth Planet. Sci. Lett. 155, 113-129.

Zheng, Y.-F., Fu, B., Xiao, Y., Li, Y., Gong, B., 1999. Hydrogen and oxygen isotope evidence for fluid-rock interactions in the stages of pre- and post-UHP metamorphism in the Dabie Mountains. Lithos 46, 677-693.

CHAPTER VI

CONCLUSION

Water is an essential volatile component in volcanic eruptions and magmatic processes, and its presence can significantly change the physicochemical states of silicate melts. The transport properties of H_2O are of interests to igneous petrologists. H_2O diffusion is crucial for understanding bubble growth, magma degassing, and magma fragmentation. H_2O diffusivity depends on temperature, water concentration, pressure and melt composition. This dissertation is a systematic investigation on H_2O diffusion in a series of calc-alkaline silicate melts, including rhyolite, dacite, and andesite.

In Chapter II, H_2O diffusion in rhyolite at 680-1902 K, 0.95-1.9 GPa, and 0.2-5.2 wt.% H_2O_t was studied using a diffusion-couple method in a piston-cylinder apparatus. Diffusion profiles, measured by FTIR microspectroscopy, are consistent with the model that H_2O_m is the dominating diffusion species and $D_{H_2O_m} = D_0\exp(aX)$. The Levenberg-Marquardt algorithm was adopted to evaluate the best a parameter and its associated error. Previous diffusion-couple and dehydration profiles at low pressures are re-treated, and a general H_2O_m diffusivity model that is applicable to 676-1902 K, 0-1.9 GPa, and 0-7.7 wt.% H_2O is constructed in the form of

$$D_{H_2O_m} = \exp\left(13.375 - 37.256X + 1.8875P - \frac{12939 - 75884X + 3625.6P}{T}\right),$$

where $D_{H_2O_m}$ is H_2O_m diffusivity in $\mu m^2/s$, X is mole fraction of total H_2O and $X =$ $C/18.015/[C/18.015+(100-C)/32.49]$ with C being water content in wt.%, P is pressure in GPa, and T is temperature in K. H_2O_t diffusivity can be calculated from $D_{H_2O_t} = D_{H_2O_m}(dX_m/dX)$ as

$$D_{H_2O_t} = D_{H_2O_m}\left[1+\frac{2X-1}{\sqrt{4X(X-1)(1-4/K)+1}}\right],$$

where $K\ [= \exp(1.876\text{-}3110/T)]$ is the equilibrium constant of speciation reaction $(H_2O_m+O \rightleftharpoons 2OH)$. At low water concentration ($C < 2$ wt.%), $D_{H_2O_t}$ can be expressed as

$$D_{H_2O_t} = \frac{C}{C_0}\exp\left(9.5279+1.8875P-\frac{9698.5+3625.6P}{T}\right),$$

where C_0 is 1 wt.%. Pressure has a negative effect on H_2O diffusion in rhyolite, increasingly so towards a lower temperature. All literature data are demonstrated to be consistent with the this general model of H_2O diffusivity in rhyolite.

In Chapter III, H_2O diffusion in dacite at 786-893 K and 0.48-0.95 GPa with 0-8 wt.% H_2O was investigated in a piston-cylinder apparatus. H_2O diffusivity in dacite increases rapidly with water content under experimental conditions, but is systematically lower than previous measurements at P <0.15 GPa. H_2O diffusion profiles in dacite can also be modeled by assuming molecular H_2O (H_2O_m) is the diffusing species, whose diffusivity $D_{H_2O_m}$ (in $\mu m^2/s$) depends on T (in K), P (in GPa), and X (mole fraction of H_2O_t) within 786-1798 K, 0-1 GPa, and 0-8 wt.% H_2O_t as follows:

$$D_{H_2O_m} = \exp\left(18.208-62.38X-\frac{19064-108882X+1476.7P}{T}\right),$$

where $X = C/18.015/[C/18.015+(100-C)/33.82]$, C is wt% of H_2O_t, and 18.015 and 33.82 are the molar masses of H_2O and anhydrous dacite on a single oxygen basis. The above equation can be combined with H_2O speciation model $K = \exp(1.49-2634/T)$ to calculate an apparent H_2O_t diffusivity. Compared to H_2O diffusion in rhyolite, diffusivity in dacite is lower at intermediate temperatures but higher at superliquidus temperatures.

In Chapter IV, water speciation and diffusion in hydrous haploandesite with ≤ 2.5 wt.% water content were examined from dehydration experiments at 743-873 K and 0.1 GPa in rapid-quench cold-seal pressure vessels. Equilibrium H_2O speciation at experimental conditions was preserved, and the equilibrium constant of speciation reaction $H_2O_m+O \rightleftharpoons 2OH$ in this Fe-free andesite is determined to be:

$$\ln K = 1.473 - \frac{2403}{T},$$

where T is temperature in K. Equilibrium constant K increases from rhyolite to dacite to haploandesite. More OH is found in haploandesite than in rhyolite or dacite at a given water concentration and temperature. Water diffusivity at the experimental conditions depends strongly on H_2O concentration, contrary to previous H_2O diffusivity data at 1608-1848 K. The diffusion profiles are consistent with the model that molecular H_2O is the diffusion species, and H_2O_m diffusivity (in μm^2/s) in haploandesite at 0.1 GPa can be formulated as

$$D_{H_2O_m} = \exp\left(14.948 - 13.905X - \frac{17947 - 73136X}{T}\right),$$

where T is temperature in K, and X is mole fraction of H_2O_t. H_2O diffusivity at $T < 873$ K in calc-alkaline silicate melts increases with degree of polymerization: andesite < dacite < rhyolite, opposite from the trend at superliquidus temperatures. At 0.1 GPa and 743-873

K, total H_2O diffusivity in calc-alkaline andesitic, dacitic and rhyolitic melts at <2.5 wt.% H_2O_t can be modeled as

$$\ln(D_{H_2O_t}/C) = 22.342 - 16.241Si - \frac{37019 - 630.17C - 35993Si}{T},$$

where $D_{H_2O_t}$ is H_2O_t diffusivity in $\mu m^2/s$, C is water content in wt.%, Si is cation mole fraction of Si, and T is temperature in K.

The diffusivity models presented in Chapter II to Chapter IV can be used to model various magmatic and volcanic processes, such as bubble growth in explosive volcanic eruptions. However, there still is room for improvement in future. For example, for H_2O diffusion in andesite at superliquidus temperatures, previously reported weak dependence of H_2O_t diffusivity on water content is still not well understood.

In Chapter V, for oxygen isotope exchange between coexisting minerals during slow cooling, the mineral pair with the largest isotopic fractionation (PLIF) was found to always confine their apparent equilibrium temperature (T_{ae}) within their Dodson closure temperatures (T_c). On the other hand, the T_{ae} of other mineral pairs may not have much geological meaning. The PLIF approach can be used to understand the thermal history of plutonic and metamorphic rocks. One good example of PLIF is quartz and magnetite, which have similar oxygen diffusivity (therefore similar T_c) but very different fractionation property ($\delta^{18}O$ of quartz is higher than most minerals, whereas $\delta^{18}O$ of magnetite is lower than most minerals). Therefore T_{ae} of quartz-magnetite is a good proxy of their T_c, which can then be used to estimate cooling rate or oxygen diffusivity if one of them is independently determined.

APPENDICES

FTIR SPECTRA OF STARTING GLASSES

The spectra of doubly polished starting glasses were collected with 64-128 scans in the N_2-purged main chamber of PerkinElmber Spectrum GX (NIR source + CaF_2 beamsplitter + InSb detector). There is a red filter and a pinhole of 531 μm diameter in the beam path between the spectrometer and sample. H_2O_t concentration (c) and thickness of sample (d) are shown in each figure.

Fig. A.1 FTIR spectra of Starting glasses used in Chapter II

Rhy5

c=5.2 wt.%
d=2.876 mm

Fig. A.2 FTIR spectra of starting glasses used in Chapter III

DC1.4

c=1.4 wt.%
d=0.506 mm

Dac4

c=4.9 wt.%
d=0.639 mm
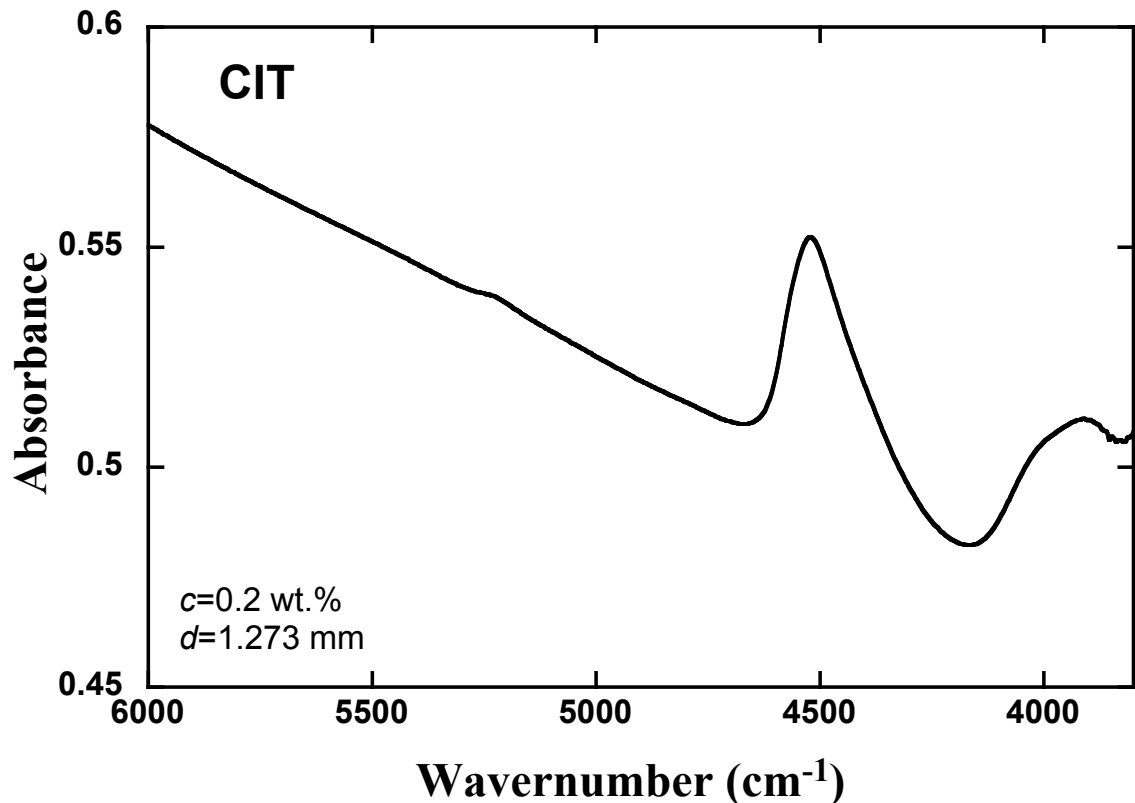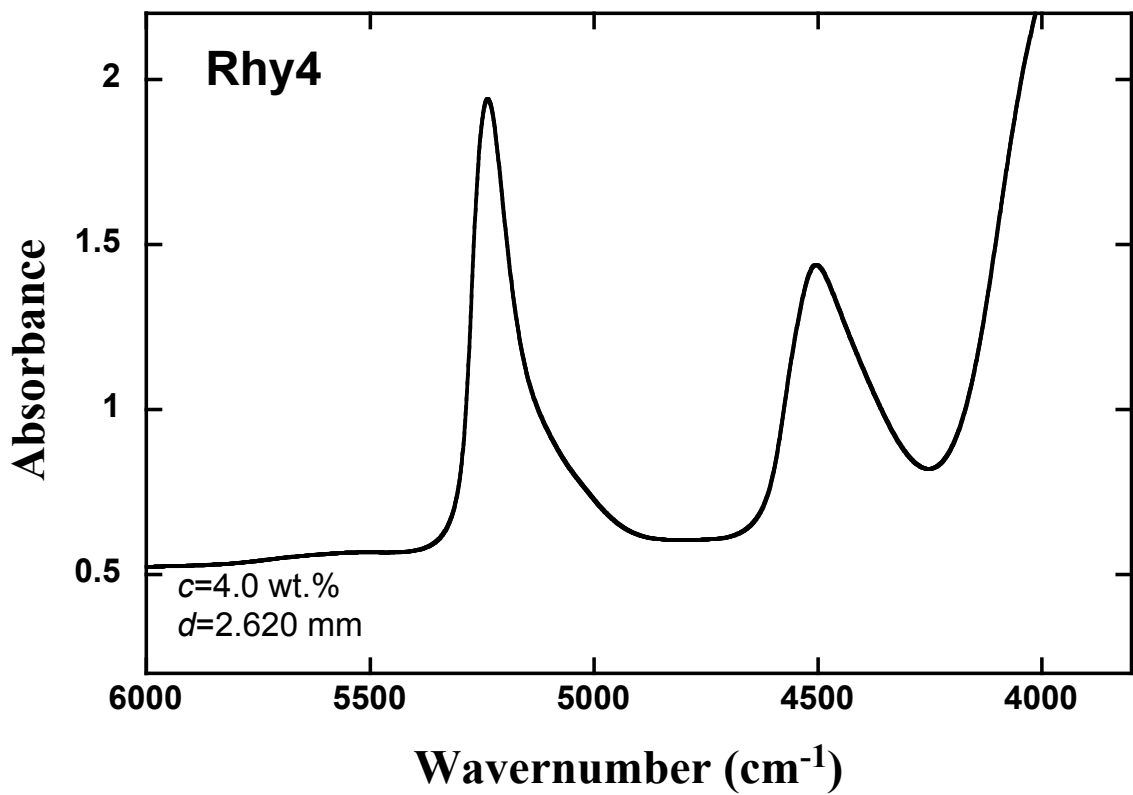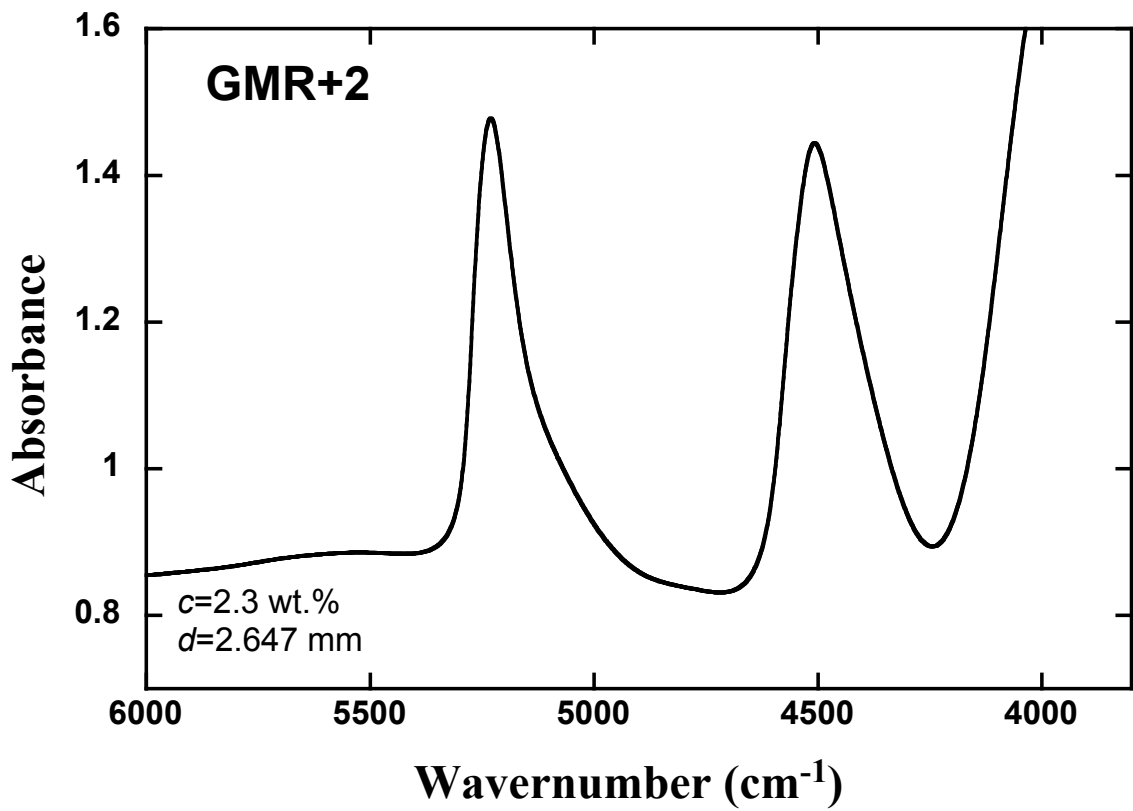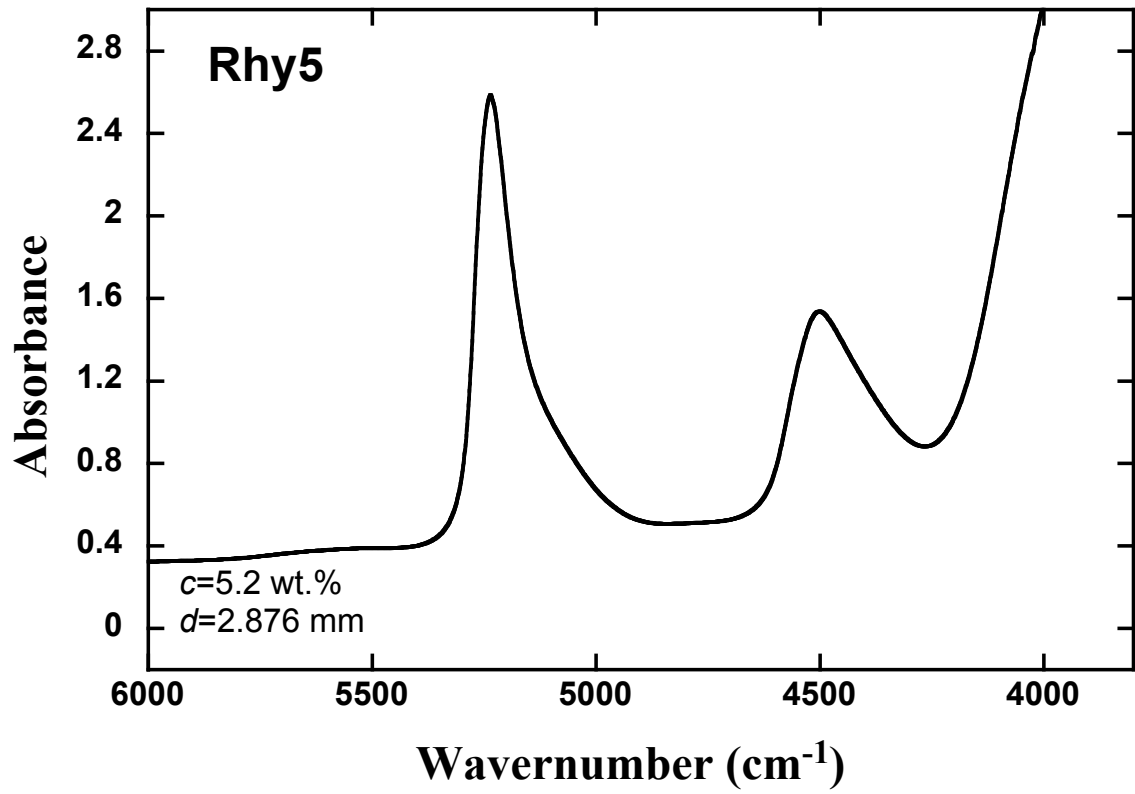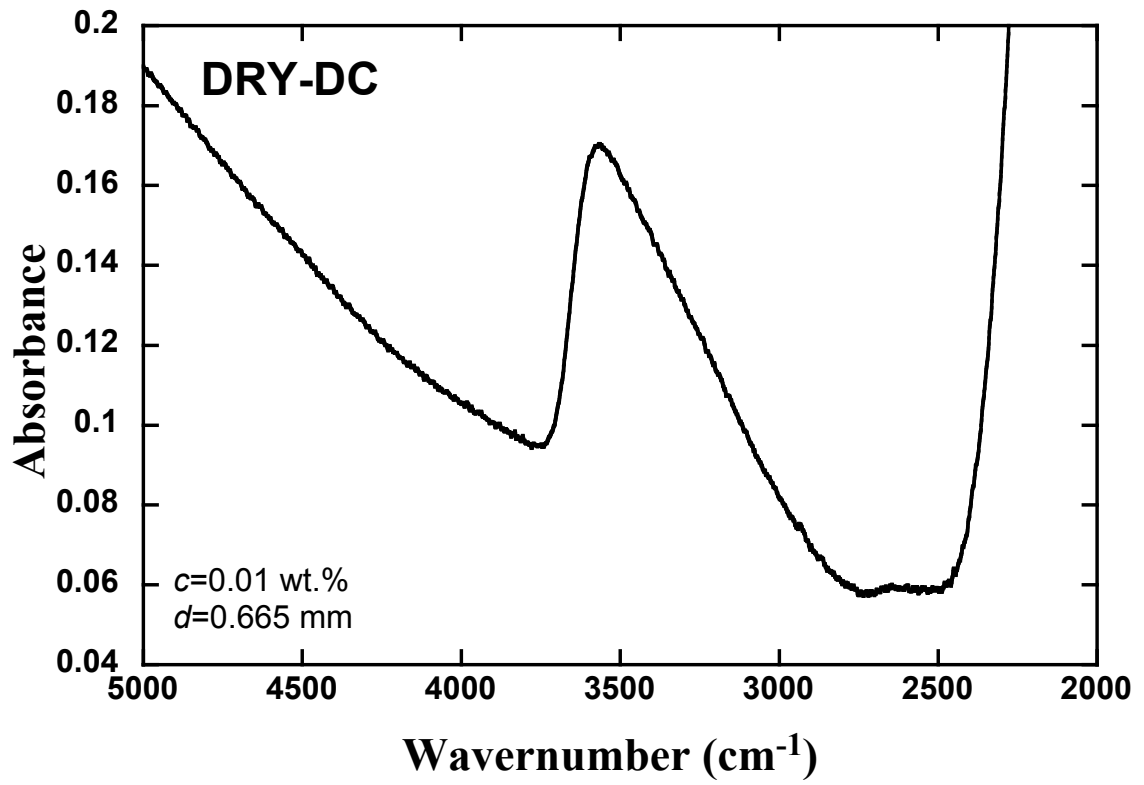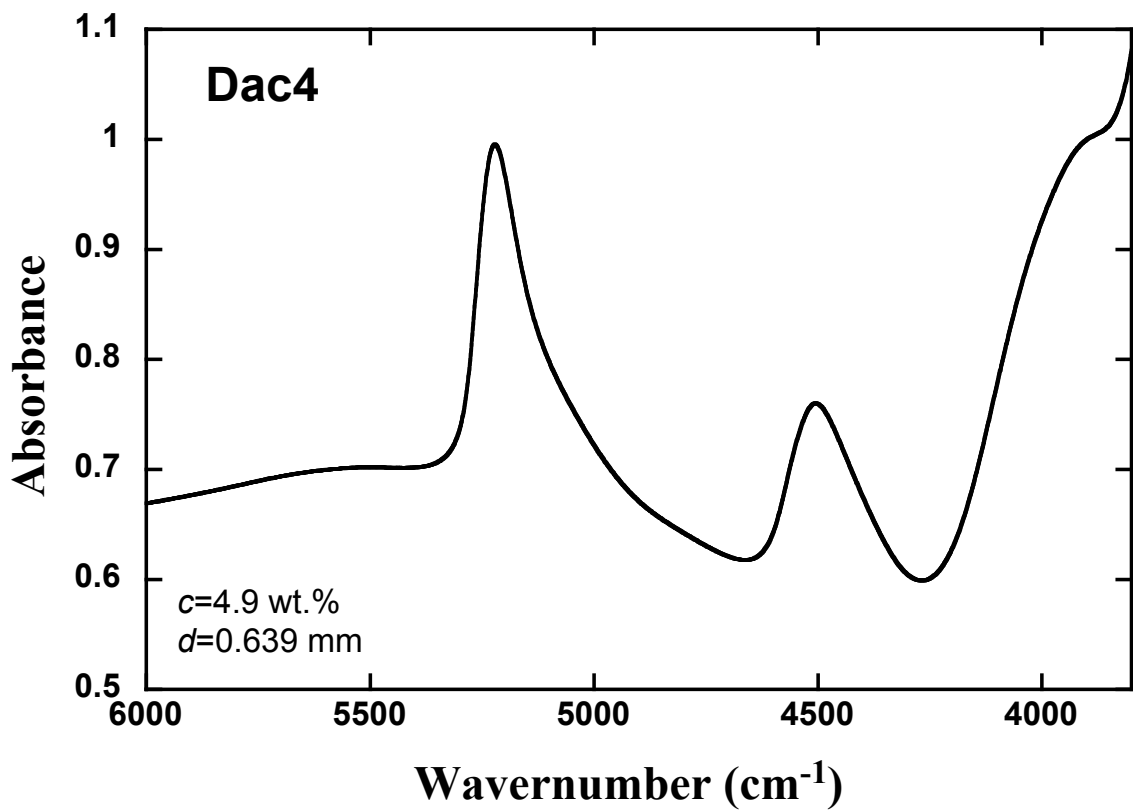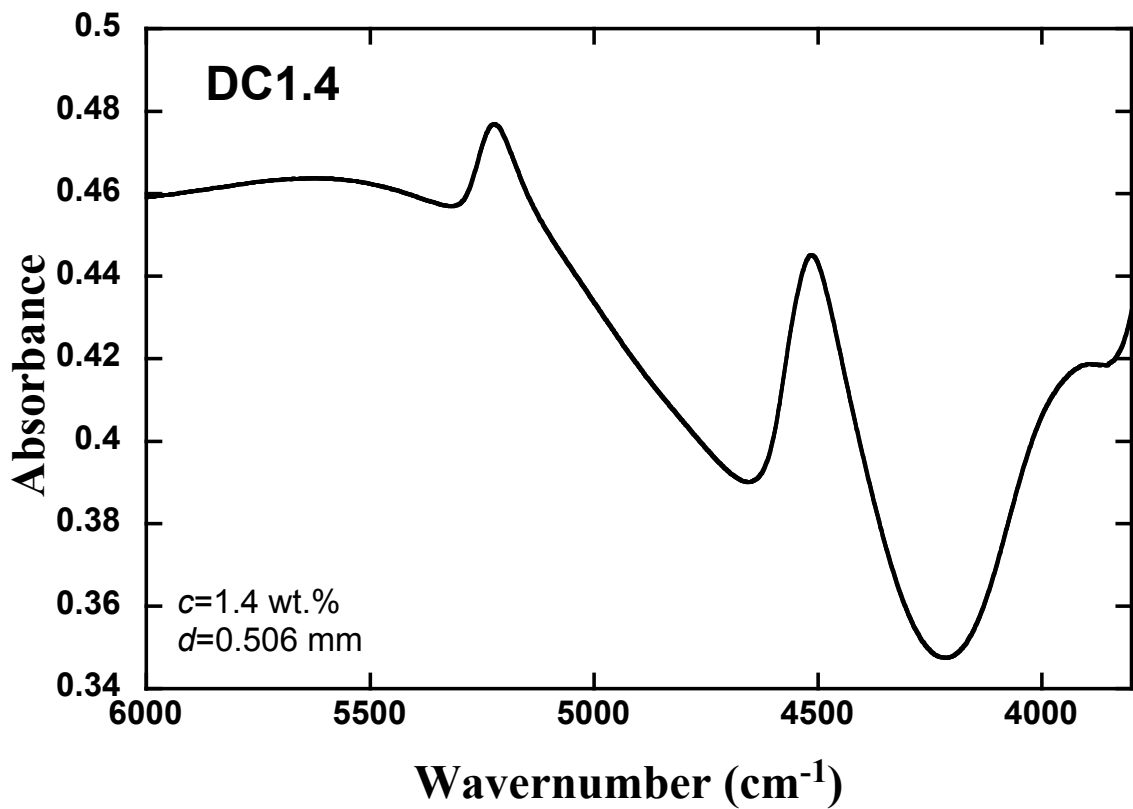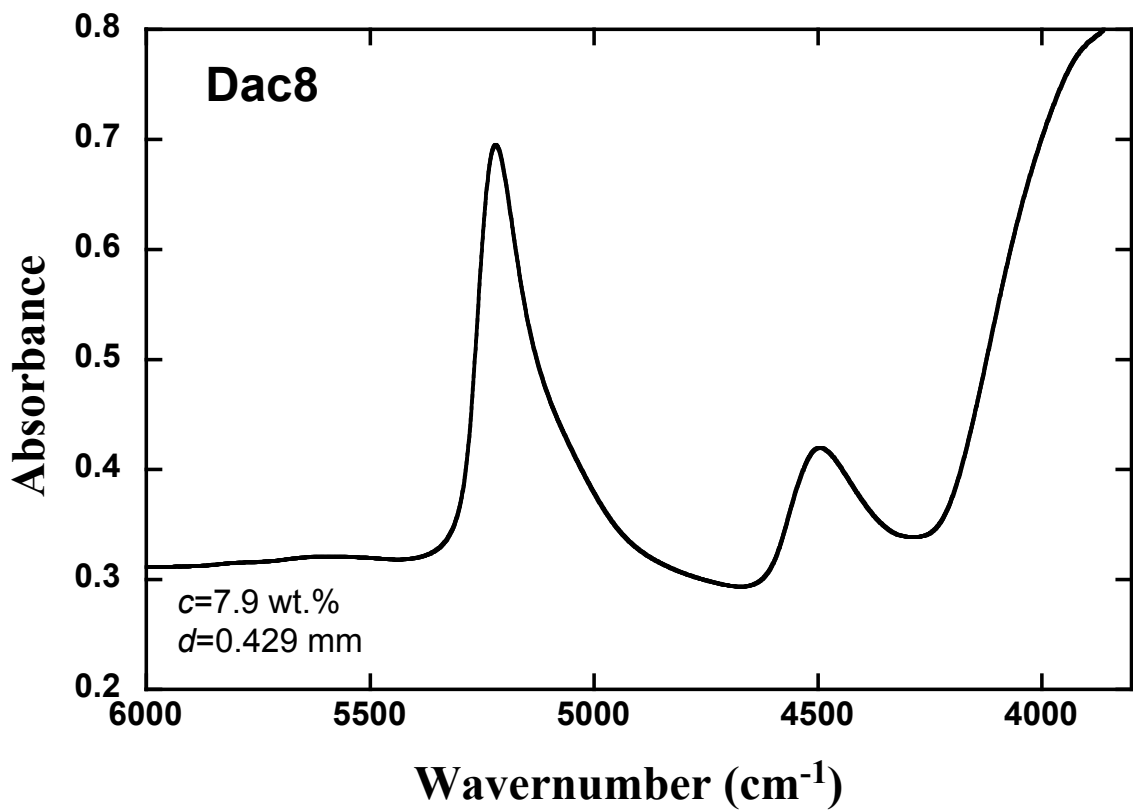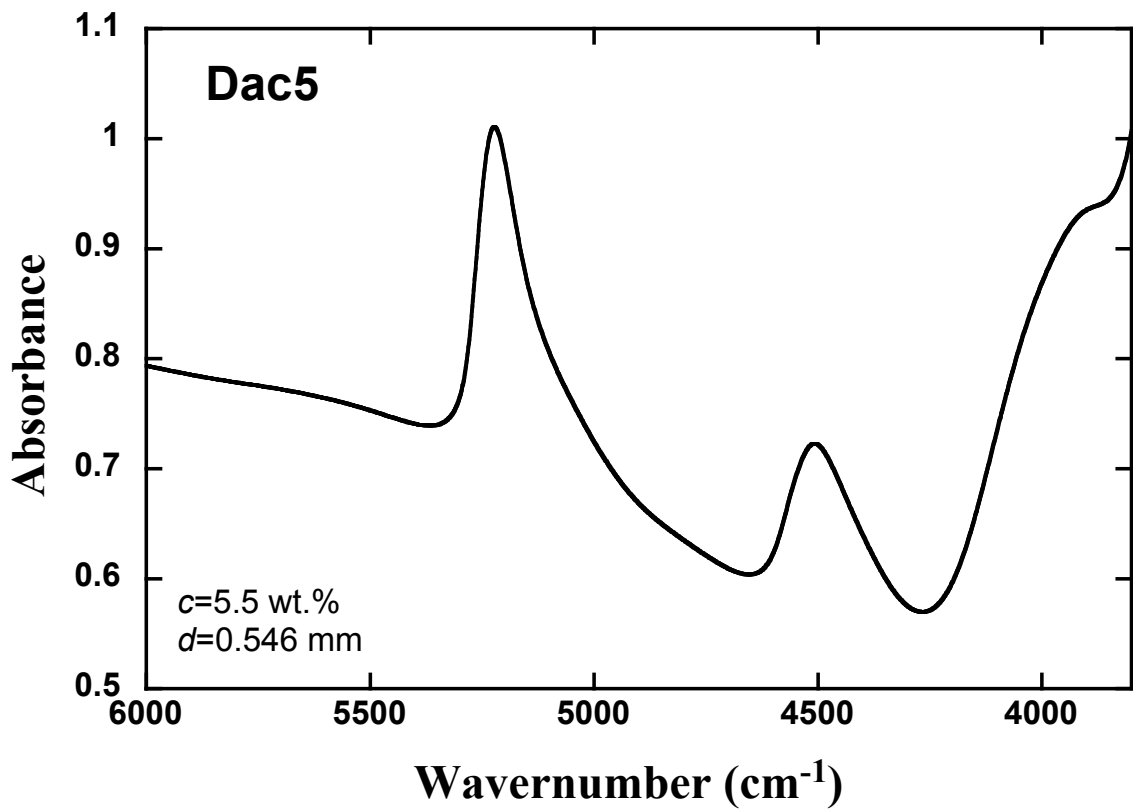
Fig. A.3 FTIR spectra of starting glasses used in Chapter IV

HAD2

c=2.0 wt.%
d=1.845 mm

HAD1

c=2.5 wt.%
d=1.743 mm
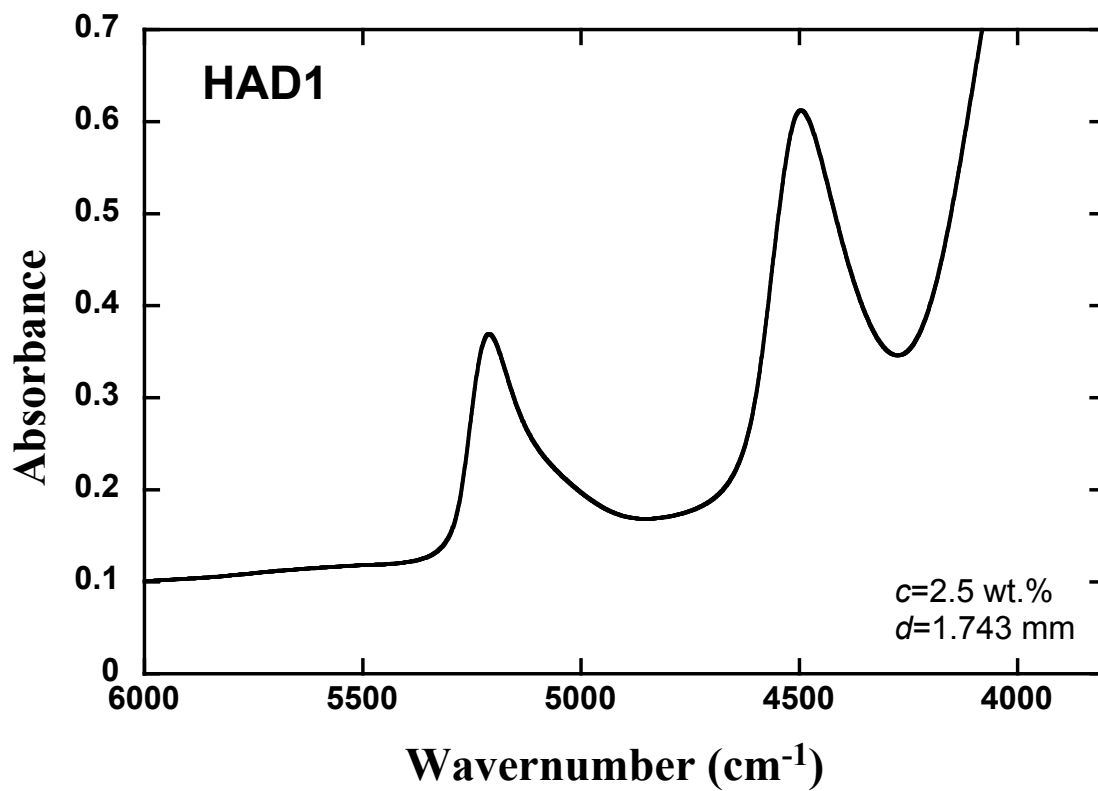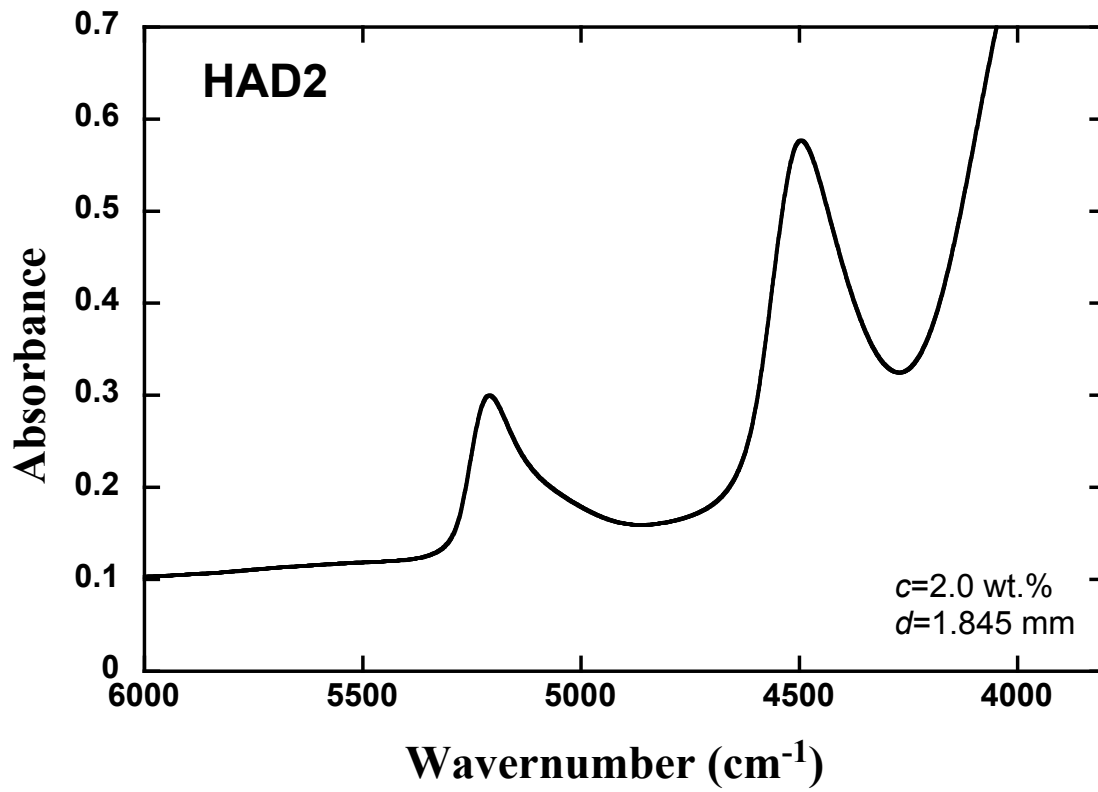
APPENDIX B

DATA TABLE OF DIFFUSION PROFILES IN CHAPTER II

FTIR spectra of the diffusion profiles in rhyolite were fit using the calibration of Withers and Behrens (1999): two straight baselines, absorption coefficient being 1.66 L/mol/cm for the 5200 cm^{-1} H_2O_m band and 1.41 L/mol/cm for the 4500 cm^{-1} OH band.

Table B.1 Diffusion profile of Rhy-DC06-1

x (μm)	A_{5200}	A_{4500}	A_{3550}	d (mm)	H_2O_m (wt.%)	OH (wt.%)	H_2O_t (wt.%)	$X_{H_2O_t}$
-800	0.0000	0.0083		0.204	0.00	0.22	0.22	0.00394
-700	0.0000	0.0085		0.205	0.00	0.22	0.22	0.00401
-600	0.0000	0.0086		0.206	0.00	0.22	0.22	0.00402
-500	0.0000	0.0088		0.207	0.00	0.23	0.23	0.00408
-400	0.0000	0.0088		0.208	0.00	0.23	0.23	0.00406
-350	0.0000	0.0088		0.208	0.00	0.23	0.23	0.00406
-300	0.0000	0.0087		0.208	0.00	0.22	0.22	0.00403
-280	0.0000	0.0089		0.208	0.00	0.23	0.23	0.00412
-260	0.0000	0.0086		0.208	0.00	0.22	0.22	0.00399
-240	0.0000	0.0090		0.208	0.00	0.23	0.23	0.00416
-218	0.0000	0.0105		0.208	0.00	0.27	0.27	0.00487
-198	0.0000	0.0114		0.208	0.00	0.29	0.29	0.00526
-178	0.0011	0.0126		0.208	0.02	0.33	0.35	0.00627
-158	0.0018	0.0160		0.208	0.04	0.41	0.45	0.00810
-140	0.0031	0.0208		0.217	0.07	0.52	0.58	0.01042
-120	0.0059	0.0279		0.217	0.12	0.69	0.82	0.01463
-100	0.0104	0.0347		0.217	0.22	0.86	1.08	0.01934
-80	0.0175	0.0421		0.217	0.37	1.05	1.42	0.02529
-60	0.0255	0.0483		0.217	0.54	1.21	1.75	0.03105
-40	0.0339	0.0529		0.217	0.72	1.32	2.04	0.03623
-20	0.0435	0.0570		0.217	0.93	1.43	2.35	0.04165
0	0.0502	0.0592		0.217	1.07	1.48	2.56	0.04516
20	0.0567	0.0609		0.217	1.21	1.53	2.74	0.04834
40	0.0625	0.0625		0.217	1.33	1.57	2.91	0.05121
60	0.0679	0.0638		0.217	1.45	1.61	3.06	0.05387
80	0.0727	0.0648		0.217	1.56	1.63	3.19	0.05611
100	0.0771	0.0655		0.217	1.65	1.65	3.31	0.05809
150	0.0861	0.0669		0.217	1.85	1.69	3.54	0.06205
200	0.0919	0.0676		0.217	1.98	1.71	3.69	0.06457
250	0.0962	0.0683		0.217	2.07	1.73	3.80	0.06646
300	0.0988	0.0689		0.217	2.13	1.74	3.87	0.06770
350	0.1007	0.0691		0.217	2.17	1.75	3.92	0.06854
400	0.1020	0.0692		0.217	2.20	1.75	3.95	0.06906
450	0.1025	0.0691		0.217	2.21	1.75	3.96	0.06919
650	0.1036	0.0694		0.217	2.23	1.76	3.99	0.06973
830	0.1038	0.0694		0.217	2.24	1.76	4.00	0.06983
1050	0.1035	0.0690		0.216	2.24	1.76	4.00	0.06985
1201	0.1023	0.0681		0.214	2.23	1.75	3.99	0.06964
1400	0.1007	0.0676		0.212	2.22	1.75	3.97	0.06945
1450	0.1005	0.0676		0.212	2.21	1.75	3.97	0.06935

Table B.2 Diffusion profile of Rhy-DC06-6

x (μm)	A_{5200}	A_{4500}	A_{3550}	d (mm)	H_2O_m (wt.%)	OH (wt.%)	H_2O_t (wt.%)	$X_{H_2O_t}$
-1030	0.0000	0.0088		0.230	0.00	0.20	0.20	0.00369
-930	0.0000	0.0083		0.232	0.00	0.19	0.19	0.00343
-770	0.0000	0.0088		0.238	0.00	0.20	0.20	0.00355
-530	0.0000	0.0091		0.240	0.00	0.20	0.20	0.00367
-430	0.0000	0.0091		0.240	0.00	0.20	0.20	0.00367
-280	0.0000	0.0090		0.241	0.00	0.20	0.20	0.00359
-250	0.0000	0.0098		0.242	0.00	0.22	0.22	0.00392
-230	0.0000	0.0105		0.242	0.00	0.23	0.23	0.00420
-210	0.0000	0.0124		0.242	0.00	0.27	0.27	0.00492
-190	0.0000	0.0145		0.242	0.00	0.32	0.32	0.00577
-170	0.0000	0.0176		0.242	0.00	0.39	0.39	0.00700
-150	0.0020	0.0214		0.242	0.04	0.48	0.51	0.00920
-130	0.0033	0.0261		0.242	0.06	0.58	0.64	0.01151
-110	0.0061	0.0313		0.242	0.12	0.70	0.81	0.01454
-90	0.0082	0.0346		0.242	0.15	0.77	0.92	0.01654
-70	0.0107	0.0384		0.242	0.20	0.85	1.06	0.01888
-50	0.0142	0.0389		0.242	0.27	0.87	1.14	0.02032
-30	0.0154	0.0441		0.247	0.29	0.96	1.25	0.02231
0	0.0217	0.0442		0.248	0.40	0.96	1.36	0.02435
10	0.0236	0.0455		0.248	0.44	0.99	1.43	0.02545
30	0.0256	0.0483		0.248	0.47	1.05	1.53	0.02717
50	0.0282	0.0502		0.248	0.52	1.09	1.62	0.02879
100	0.0328	0.0532		0.248	0.61	1.16	1.77	0.03144
110	0.0339	0.0538		0.248	0.63	1.18	1.80	0.03207
130	0.0357	0.0560		0.248	0.66	1.22	1.89	0.03352
150	0.0374	0.0573		0.248	0.69	1.25	1.95	0.03456
170	0.0391	0.0582		0.248	0.73	1.27	2.00	0.03548
190	0.0405	0.0591		0.248	0.75	1.29	2.05	0.03631
210	0.0417	0.0597		0.248	0.78	1.31	2.08	0.03691
230	0.0427	0.0602		0.248	0.79	1.32	2.11	0.03746
250	0.0436	0.0606		0.248	0.81	1.33	2.14	0.03790
270	0.0443	0.0610		0.248	0.82	1.34	2.16	0.03829
290	0.0454	0.0622		0.251	0.83	1.35	2.18	0.03865
490	0.0491	0.0637		0.251	0.90	1.38	2.28	0.04044
530	0.0499	0.0637		0.251	0.92	1.38	2.30	0.04068
690	0.0494	0.0640		0.250	0.91	1.39	2.30	0.04080
920	0.0497	0.0640		0.251	0.91	1.39	2.30	0.04076
1130	0.0492	0.0632		0.248	0.92	1.38	2.30	0.04074
1310	0.0488	0.0630		0.247	0.91	1.39	2.30	0.04069
1390	0.0486	0.0626		0.246	0.91	1.38	2.29	0.04063

Table B.3 Diffusion profile of Rhy-DC06-7

x (μm)	A_{5200}	A_{4500}	A_{3550}	d (mm)	H_2O_m (wt.%)	OH (wt.%)	H_2O_t (wt.%)	$X_{H_2O_t}$
-920	0.0000	0.0092		0.246	0.00	0.20	0.20	0.00359
-820	0.0000	0.0092		0.246	0.00	0.20	0.20	0.00359
-570	0.0000	0.0091		0.247	0.00	0.20	0.20	0.00357
-520	0.0000	0.0093		0.247	0.00	0.20	0.20	0.00362
-370	0.0000	0.0101		0.248	0.00	0.22	0.22	0.00394
-320	0.0000	0.0114		0.248	0.00	0.25	0.25	0.00445
-270	0.0000	0.0175		0.250	0.00	0.37	0.37	0.00673
-240	0.0022	0.0233		0.250	0.04	0.50	0.54	0.00970
-220	0.0044	0.0282		0.250	0.08	0.61	0.69	0.01232
-200	0.0073	0.0338		0.250	0.13	0.73	0.86	0.01543
-180	0.0121	0.0418		0.250	0.22	0.90	1.12	0.02009
-160	0.0174	0.0478		0.250	0.32	1.03	1.35	0.02411
-140	0.0239	0.0533		0.250	0.44	1.15	1.59	0.02835
-120	0.0312	0.0584		0.250	0.57	1.27	1.84	0.03268
-100	0.0394	0.0629		0.250	0.73	1.37	2.09	0.03710
-80	0.0488	0.0671		0.250	0.90	1.46	2.36	0.04181
-60	0.0565	0.0701		0.250	1.04	1.53	2.57	0.04544
-30	0.0677	0.0725		0.250	1.26	1.58	2.84	0.05002
20	0.0857	0.0742		0.251	1.59	1.62	3.20	0.05630
40	0.0923	0.0746		0.251	1.71	1.63	3.34	0.05864
60	0.0977	0.0754		0.251	1.81	1.65	3.46	0.06070
200	0.1326	0.0826		0.253	2.45	1.80	4.25	0.07417
240	0.1415	0.0837		0.253	2.62	1.83	4.45	0.07745
280	0.1485	0.0841		0.253	2.76	1.84	4.59	0.07988
330	0.1556	0.0846		0.253	2.89	1.85	4.74	0.08237
380	0.1614	0.0851		0.253	3.00	1.86	4.86	0.08439
430	0.1660	0.0855		0.253	3.09	1.87	4.96	0.08604
630	0.1753	0.0861		0.253	3.27	1.89	5.16	0.08930
880	0.1770	0.0855		0.253	3.30	1.88	5.17	0.08960
990	0.1776	0.0861		0.253	3.31	1.89	5.20	0.09003
1180	0.1776	0.0861		0.253	3.31	1.89	5.20	0.09003
1230	0.1776	0.0857		0.252	3.32	1.89	5.21	0.09021
1480	0.1753	0.0851		0.250	3.31	1.89	5.20	0.08996
1530	0.1755	0.0852		0.250	3.31	1.89	5.20	0.09007

Table B.4 Diffusion profile of Rhy-DC06-8

x (μm)	A_{5200}	A_{4500}	A_{3550}	d (mm)	H_2O_m (wt.%)	OH (wt.%)	H_2O_t (wt.%)	$X_{H_2O_t}$
-240	0.0000	0.0094		0.249	0.00	0.20	0.20	0.00363
-85	0.0000	0.0094		0.249	0.00	0.20	0.20	0.00362
-75	0.0000	0.0104		0.249	0.00	0.22	0.22	0.00403
-65	0.0011	0.0102		0.249	0.02	0.22	0.24	0.00431
-55	0.0020	0.0105		0.249	0.04	0.23	0.26	0.00473
-45	0.0031	0.0127		0.250	0.06	0.27	0.33	0.00590
-40	0.0030	0.0148		0.251	0.06	0.32	0.37	0.00667
-35	0.0042	0.0172		0.250	0.08	0.37	0.45	0.00801
-30	0.0066	0.0199		0.251	0.12	0.43	0.55	0.00979
-20	0.0103	0.0273		0.251	0.19	0.59	0.77	0.01384
-10	0.0150	0.0355		0.251	0.27	0.76	1.04	0.01853
0	0.0222	0.0443		0.251	0.41	0.95	1.36	0.02423
10	0.0289	0.0513		0.251	0.53	1.11	1.63	0.02910
20	0.0337	0.0555		0.251	0.62	1.20	1.81	0.03226
30	0.0387	0.0603		0.251	0.71	1.30	2.01	0.03573
40	0.0418	0.0626		0.251	0.77	1.35	2.12	0.03760
50	0.0445	0.0644		0.251	0.82	1.39	2.21	0.03919
60	0.0462	0.0654		0.251	0.85	1.42	2.26	0.04011
70	0.0482	0.0665		0.251	0.89	1.44	2.33	0.04122
80	0.0499	0.0676		0.251	0.92	1.46	2.38	0.04217
100	0.0518	0.0686		0.251	0.95	1.49	2.44	0.04317
120	0.0530	0.0693		0.251	0.98	1.50	2.48	0.04380
140	0.0534	0.0695		0.251	0.98	1.51	2.49	0.04403
170	0.0538	0.0699		0.251	0.99	1.51	2.51	0.04430
200	0.0540	0.0699		0.251	0.99	1.51	2.51	0.04435
260	0.0541	0.0699		0.251	1.00	1.52	2.51	0.04440
550	0.0541	0.0699		0.251	1.00	1.52	2.51	0.04440

Table B.5 Diffusion profile of Rhy-DC06-9

x (μm)	A_{5200}	A_{4500}	A_{3550}	d (mm)	H_2O_m (wt.%)	OH (wt.%)	H_2O_t (wt.%)	$X_{H_2O_t}$
-200	0.0000	0.0093		0.240	0.00	0.21	0.21	0.00375
-100	0.0000	0.0094		0.240	0.00	0.21	0.21	0.00376
-80	0.0000	0.0094		0.240	0.00	0.21	0.21	0.00378
-60	0.0000	0.0097		0.240	0.00	0.22	0.22	0.00389
-40	0.0021	0.0104		0.240	0.04	0.23	0.27	0.00488
-30	0.0044	0.0143		0.240	0.08	0.32	0.40	0.00725
-20	0.0137	0.0218		0.240	0.26	0.49	0.75	0.01344
-10	0.0363	0.0348		0.240	0.69	0.78	1.48	0.02634
10	0.1227	0.0637		0.245	2.34	1.43	3.77	0.06591
20	0.1401	0.0679		0.245	2.68	1.53	4.21	0.07337
30	0.1519	0.0712		0.245	2.91	1.61	4.51	0.07857
40	0.1629	0.0728		0.245	3.12	1.64	4.77	0.08281
50	0.1694	0.0760		0.245	3.25	1.72	4.97	0.08624
60	0.1719	0.0770		0.245	3.31	1.74	5.05	0.08750
70	0.1738	0.0777		0.245	3.34	1.76	5.10	0.08838
90	0.1768	0.0784		0.245	3.40	1.78	5.18	0.08964
110	0.1780	0.0784		0.245	3.43	1.78	5.20	0.09003
130	0.1788	0.0787		0.245	3.44	1.78	5.23	0.09044
150	0.1795	0.0790		0.245	3.46	1.79	5.25	0.09079
170	0.1800	0.0790		0.245	3.47	1.79	5.26	0.09096
220	0.1803	0.0795		0.246	3.46	1.80	5.25	0.09090
270	0.1807	0.0797		0.246	3.46	1.80	5.26	0.09108

Table B.6 Diffusion profile of Rhy-DC06-11

x (µm)	A_{5200}	A_{4500}	A_{3550}	d (mm)	H_2O_m (wt.%)	OH (wt.%)	H_2O_t (wt.%)	$X_{H_2O_t}$
-560	0.0000	0.0106		0.244	0.00	0.23	0.23	0.00420
-360	0.0000	0.0109		0.244	0.00	0.24	0.24	0.00431
-210	0.0000	0.0105		0.244	0.00	0.23	0.23	0.00416
-160	0.0000	0.0175		0.245	0.00	0.38	0.38	0.00690
-110	0.0122	0.0327		0.245	0.23	0.72	0.95	0.01692
-100	0.0142	0.0379		0.245	0.27	0.83	1.10	0.01964
-90	0.0198	0.0450		0.245	0.37	0.99	1.36	0.02431
-80	0.0240	0.0489		0.245	0.45	1.08	1.53	0.02722
-60	0.0387	0.0611		0.245	0.73	1.35	2.08	0.03692
-50	0.0451	0.0636		0.245	0.85	1.41	2.26	0.04001
-40	0.0511	0.0663		0.245	0.96	1.47	2.44	0.04309
-30	0.0579	0.0682		0.245	1.09	1.52	2.61	0.04609
-10	0.0684	0.0692		0.245	1.29	1.54	2.83	0.04998
40	0.0961	0.0748		0.245	1.83	1.67	3.50	0.06139
50	0.1015	0.0773		0.245	1.93	1.73	3.66	0.06415
70	0.1104	0.0799		0.245	2.10	1.79	3.90	0.06818
90	0.1170	0.0816		0.245	2.23	1.83	4.07	0.07102
110	0.1228	0.0822		0.245	2.35	1.85	4.20	0.07319
130	0.1281	0.0828		0.245	2.45	1.86	4.31	0.07518
150	0.1322	0.0827		0.245	2.53	1.86	4.39	0.07651
170	0.1364	0.0827		0.245	2.61	1.86	4.47	0.07789
270	0.1509	0.0850		0.245	2.90	1.92	4.82	0.08361
280	0.1521	0.0847		0.245	2.92	1.91	4.83	0.08388
430	0.1607	0.0843		0.245	3.09	1.91	5.00	0.08663
540	0.1644	0.0854		0.245	3.16	1.93	5.09	0.08826
680	0.1656	0.0855		0.246	3.17	1.93	5.10	0.08837
800	0.1659	0.0861		0.247	3.16	1.93	5.10	0.08835
1090	0.1647	0.0852		0.245	3.17	1.93	5.10	0.08831
1190	0.1641	0.0851		0.244	3.17	1.93	5.10	0.08840

Table B.7 Diffusion profile of Rhy-DC07-12

x (µm)	A_{5200}	A_{4500}	A_{3550}	d (mm)	H_2O_m (wt.%)	OH (wt.%)	H_2O_t (wt.%)	$X_{H_2O_t}$
-680	0.0000	0.0103		0.248	0.00	0.22	0.22	0.00399
-300	0.0000	0.0096		0.248	0.00	0.21	0.21	0.00374
-280	0.0000	0.0097		0.248	0.00	0.21	0.21	0.00378
-260	0.0000	0.0102		0.248	0.00	0.22	0.22	0.00396
-240	0.0000	0.0108		0.248	0.00	0.23	0.23	0.00421
-220	0.0000	0.0129		0.248	0.00	0.28	0.28	0.00500
-200	0.0011	0.0164		0.248	0.02	0.35	0.37	0.00674
-180	0.0030	0.0226		0.248	0.06	0.49	0.54	0.00977
-160	0.0068	0.0307		0.248	0.13	0.66	0.79	0.01417
-140	0.0127	0.0393		0.248	0.23	0.85	1.09	0.01947
-120	0.0223	0.0486		0.248	0.41	1.06	1.47	0.02621
-100	0.0313	0.0550		0.248	0.58	1.20	1.78	0.03164
-80	0.0412	0.0600		0.248	0.77	1.31	2.08	0.03688
-60	0.0514	0.0643		0.248	0.96	1.41	2.37	0.04190
-40	0.0613	0.0675		0.248	1.14	1.48	2.63	0.04640
-20	0.0724	0.0702		0.248	1.35	1.55	2.90	0.05112
0	0.0806	0.0720		0.248	1.51	1.59	3.10	0.05447
20	0.0885	0.0734		0.248	1.66	1.62	3.28	0.05765
40	0.0958	0.0745		0.248	1.80	1.65	3.44	0.06044
60	0.1026	0.0753		0.248	1.93	1.67	3.59	0.06299
80	0.1100	0.0763		0.248	2.07	1.69	3.76	0.06580
130	0.1232	0.0780		0.248	2.32	1.73	4.05	0.07081
180	0.1341	0.0790		0.248	2.53	1.76	4.29	0.07480
230	0.1429	0.0799		0.248	2.70	1.78	4.48	0.07804
280	0.1501	0.0807		0.248	2.84	1.80	4.64	0.08068
330	0.1559	0.0811		0.248	2.95	1.81	4.76	0.08273
380	0.1594	0.0815		0.248	3.02	1.82	4.84	0.08408
430	0.1625	0.0817		0.248	3.08	1.82	4.91	0.08514
480	0.1648	0.0818		0.248	3.13	1.83	4.96	0.08596
580	0.1671	0.0820		0.248	3.17	1.83	5.01	0.08678
680	0.1683	0.0822		0.248	3.20	1.84	5.03	0.08724
780	0.1688	0.0825		0.248	3.20	1.84	5.05	0.08750
880	0.1688	0.0823		0.248	3.20	1.84	5.05	0.08745
980	0.1681	0.0822		0.247	3.21	1.84	5.05	0.08754
1380	0.1672	0.0820		0.246	3.20	1.85	5.05	0.08753

Table B.8 Diffusion profile of Rhy-DC07-14

x (µm)	A_{5200}	A_{4500}	A_{3550}	d (mm)	H_2O_m (wt.%)	OH (wt.%)	H_2O_t (wt.%)	$X_{H_2O_t}$
-990	0.0000	0.0084		0.238	0.00	0.19	0.19	0.00340
-790	0.0000	0.0091		0.242	0.00	0.20	0.20	0.00361
-490	0.0000	0.0094		0.244	0.00	0.21	0.21	0.00373
-390	0.0000	0.0094		0.246	0.00	0.20	0.20	0.00369
-190	0.0000	0.0130		0.248	0.00	0.28	0.28	0.00506
-170	0.0028	0.0168		0.248	0.05	0.36	0.41	0.00745
-150	0.0061	0.0211		0.248	0.11	0.46	0.57	0.01024
-140	0.0112	0.0282		0.248	0.21	0.61	0.82	0.01467
-130	0.0159	0.0335		0.248	0.29	0.73	1.02	0.01824
-120	0.0207	0.0384		0.248	0.38	0.83	1.22	0.02172
-110	0.0264	0.0423		0.248	0.49	0.92	1.41	0.02514
-100	0.0321	0.0459		0.248	0.59	1.00	1.60	0.02841
-90	0.0387	0.0499		0.248	0.72	1.09	1.81	0.03211
-80	0.0437	0.0531		0.248	0.81	1.16	1.97	0.03500
-70	0.0492	0.0555		0.248	0.91	1.22	2.13	0.03777
-60	0.0548	0.0556		0.248	1.02	1.22	2.24	0.03964
-40	0.0697	0.0600		0.248	1.30	1.32	2.62	0.04624
-30	0.0758	0.0642		0.248	1.42	1.41	2.83	0.04990
-20	0.0820	0.0666		0.248	1.53	1.47	3.00	0.05284
-10	0.0856	0.0678		0.248	1.60	1.49	3.10	0.05449
0	0.0879	0.0691		0.248	1.65	1.52	3.17	0.05578
70	0.1127	0.0784		0.250	2.10	1.72	3.83	0.06699
110	0.1243	0.0806		0.250	2.33	1.78	4.10	0.07161
130	0.1296	0.0816		0.250	2.43	1.80	4.22	0.07369
170	0.1384	0.0828		0.250	2.60	1.83	4.42	0.07706
210	0.1462	0.0836		0.250	2.75	1.85	4.59	0.07988
250	0.1511	0.0840		0.250	2.84	1.86	4.70	0.08163
270	0.1533	0.0833		0.250	2.88	1.84	4.72	0.08208
390	0.1624	0.0849		0.250	3.06	1.88	4.94	0.08568
430	0.1654	0.0855		0.250	3.12	1.90	5.01	0.08691
470	0.1670	0.0857		0.250	3.15	1.90	5.05	0.08746
510	0.1679	0.0858		0.250	3.16	1.90	5.07	0.08782
560	0.1689	0.0857		0.250	3.18	1.90	5.08	0.08811
610	0.1694	0.0858		0.250	3.19	1.90	5.10	0.08831
710	0.1696	0.0857		0.250	3.20	1.90	5.10	0.08831
890	0.1693	0.0852		0.249	3.20	1.90	5.10	0.08838
1070	0.1685	0.0851		0.248	3.20	1.90	5.10	0.08843
1370	0.1671	0.0846		0.246	3.20	1.91	5.11	0.08852

APPENDIX C

DATA TABLE OF DIFFUSION PROFILES IN CHAPTER III

FTIR spectra of the diffusion profiles in dacite were fit using the calibration of Ohlhorst et al. (2001): two straight baselines, absorption coefficient being 1.13 L/mol/cm for the 5200 cm^{-1} H$_2$O$_m$ band and 0.96 L/mol/cm for the 4500 cm^{-1} OH band. To account for change in baseline shape during the experiment (see text Chapter III for explanation), the sum of species concentrations after experiments (meaning all profiles in this Appendix) is divided by a factor of 1.144 to find H$_2$O$_t$ concentration. Some spectra at low H$_2$O$_t$ were fit using the calibration of Yamashita et al. (1997) for 3550 cm^{-1} H$_2$O$_t$ band (68 L/mol/cm).

Table C.1 Diffusion profile of Dac-DC05-12

x (μm)	A_{5200}	A_{4500}	A_{3550}	d (mm)	H_2O_m (wt.%)	OH (wt.%)	H_2O_t (wt.%)	$X_{H_2O_t}$
-130			0.0318	0.265			0.01	0.00024
-105			0.1026	0.265			0.04	0.00077
-80			0.1398	0.265			0.06	0.00104
-70	0.0115	0.0096		0.265	0.28	0.27	0.48	0.00893
-65	0.0219	0.0162		0.265	0.53	0.46	0.86	0.01601
-60	0.0358	0.0219		0.265	0.86	0.62	1.30	0.02404
-55	0.0555	0.0290		0.264	1.35	0.83	1.90	0.03500
-50	0.0826	0.0384		0.264	2.01	1.10	2.72	0.04974
-45	0.1021	0.0458		0.264	2.50	1.32	3.33	0.06056
-40	0.1229	0.0534		0.264	3.01	1.54	3.98	0.07192
-35	0.1314	0.0558		0.264	3.23	1.61	4.23	0.07622
-30	0.1423	0.0584		0.264	3.50	1.69	4.54	0.08149
-25	0.1516	0.0609		0.264	3.74	1.77	4.81	0.08616
-20	0.1603	0.0629		0.264	3.96	1.83	5.06	0.09033
-10	0.1753	0.0667		0.264	4.34	1.94	5.49	0.09766
0	0.1846	0.0689		0.264	4.57	2.01	5.75	0.10212
20	0.1995	0.0712		0.264	4.95	2.08	6.15	0.10873
40	0.2091	0.0712		0.264	5.20	2.08	6.37	0.11235
60	0.2175	0.0708		0.264	5.41	2.07	6.54	0.11528
80	0.2250	0.0708		0.264	5.60	2.08	6.71	0.11809
120	0.2370	0.0699		0.264	5.91	2.05	6.96	0.12213
160	0.2455	0.0699		0.264	6.13	2.05	7.15	0.12530
200	0.2539	0.0689		0.264	6.35	2.03	7.32	0.12801
240	0.2564	0.0689		0.264	6.41	2.03	7.38	0.12894
280	0.2598	0.0689		0.264	6.50	2.03	7.46	0.13021
320	0.2628	0.0689		0.264	6.58	2.03	7.52	0.13131
360	0.2651	0.0689		0.264	6.63	2.03	7.57	0.13216
400	0.2664	0.0694		0.264	6.67	2.05	7.62	0.13286
500	0.2686	0.0684		0.263	6.75	2.02	7.67	0.13374
600	0.2698	0.0684		0.263	6.78	2.03	7.70	0.13419
700	0.2701	0.0682		0.262	6.82	2.03	7.73	0.13467
800	0.2696	0.0677		0.261	6.83	2.02	7.74	0.13477
900	0.2693	0.0677		0.261	6.82	2.02	7.73	0.13468
1000	0.2686	0.0672		0.260	6.83	2.01	7.73	0.13470

Table C.2 Diffusion profile of Dac-DC05-13

x (μm)	A_{5200}	A_{4500}	A_{3550}	d (mm)	H_2O_m (wt.%)	OH (wt.%)	H_2O_t (wt.%)	$X_{H_2O_t}$
-160			0.0259	0.203			0.01	0.00025
-140			0.0377	0.203			0.02	0.00037
-120	0.0017	0.0037		0.203	0.05	0.13	0.16	0.00307
-115	0.0028	0.0070		0.203	0.09	0.26	0.30	0.00565
-110	0.0061	0.0145		0.203	0.19	0.53	0.63	0.01181
-105	0.0137	0.0201		0.203	0.43	0.74	1.03	0.01905
-100	0.0228	0.0265		0.203	0.72	0.98	1.49	0.02749
-95	0.0304	0.0297		0.203	0.96	1.10	1.80	0.03323
-90	0.0356	0.0349		0.203	1.12	1.30	2.12	0.03894
-85	0.0458	0.0389		0.203	1.45	1.45	2.53	0.04640
-80	0.0484	0.0411		0.203	1.53	1.53	2.68	0.04900
-70	0.0531	0.0434		0.203	1.68	1.62	2.89	0.05270
-60	0.0572	0.0448		0.203	1.82	1.67	3.05	0.05559
-40	0.0621	0.0469		0.203	1.97	1.75	3.26	0.05923
-20	0.0693	0.0467		0.203	2.20	1.75	3.45	0.06266
0	0.0740	0.0476		0.203	2.36	1.78	3.62	0.06553
20	0.0783	0.0482		0.203	2.50	1.81	3.76	0.06809
40	0.0825	0.0503		0.204	2.62	1.88	3.93	0.07102
60	0.0849	0.0520		0.204	2.70	1.94	4.06	0.07317
80	0.0884	0.0524		0.204	2.81	1.96	4.17	0.07514
120	0.0942	0.0533		0.204	3.00	2.00	4.37	0.07855
160	0.0986	0.0546		0.204	3.14	2.05	4.54	0.08144
200	0.1027	0.0547		0.204	3.27	2.05	4.65	0.08349
240	0.1059	0.0550		0.204	3.38	2.06	4.76	0.08521
280	0.1092	0.0551		0.205	3.47	2.06	4.83	0.08650
320	0.1118	0.0552		0.206	3.53	2.05	4.88	0.08739
360	0.1142	0.0553		0.207	3.59	2.05	4.93	0.08819
400	0.1163	0.0558		0.208	3.64	2.06	4.98	0.08910
500	0.1201	0.0563		0.209	3.74	2.06	5.08	0.09070
600	0.1233	0.0566		0.210	3.83	2.07	5.15	0.09197
700	0.1253	0.0566		0.210	3.89	2.07	5.21	0.09298
800	0.1268	0.0567		0.210	3.94	2.07	5.26	0.09374
900	0.1283	0.0563		0.210	3.99	2.06	5.28	0.09419
1000	0.1286	0.0558		0.210	3.99	2.04	5.27	0.09404
1100	0.1286	0.0559		0.210	3.99	2.04	5.28	0.09410

Table C.3 Diffusion profile of Dac-DC05-14

x (μm)	A_{5200}	A_{4500}	A_{3550}	d (mm)	H_2O_m (wt.%)	OH (wt.%)	H_2O_t (wt.%)	$X_{H_2O_t}$
-270			0.0300	0.215			0.01	0.00028
-220			0.0300	0.215			0.01	0.00028
-170			0.0299	0.215			0.01	0.00028
-140			0.0929	0.215			0.05	0.00085
-100	0.0037	0.0021		0.216	0.11	0.07	0.16	0.00296
-90	0.0070	0.0073		0.216	0.21	0.25	0.40	0.00750
-80	0.0266	0.0185		0.216	0.79	0.64	1.25	0.02317
-75	0.0453	0.0259		0.217	1.34	0.90	1.95	0.03599
-70	0.0685	0.0320		0.217	2.03	1.12	2.75	0.05024
-65	0.0944	0.0430		0.217	2.81	1.51	3.78	0.06835
-60	0.1137	0.0489		0.218	3.39	1.71	4.46	0.08011
-55	0.1234	0.0520		0.218	3.68	1.83	4.82	0.08624
-50	0.1277	0.0533		0.218	3.81	1.88	4.97	0.08893
-40	0.1391	0.0566		0.218	4.17	1.99	5.39	0.09591
-30	0.1463	0.0583		0.218	4.39	2.06	5.63	0.10009
-20	0.1529	0.0596		0.218	4.59	2.11	5.85	0.10377
0	0.1607	0.0603		0.218	4.83	2.13	6.09	0.10770
60	0.1752	0.0606		0.217	5.30	2.16	6.52	0.11493
110	0.1791	0.0627		0.216	5.45	2.25	6.73	0.11833
160	0.1852	0.0628		0.215	5.67	2.27	6.94	0.12176
210	0.1905	0.0632		0.214	5.87	2.29	7.13	0.12494
260	0.1951	0.0632		0.214	6.01	2.29	7.26	0.12703
310	0.1989	0.0628		0.214	6.13	2.28	7.36	0.12859
360	0.2020	0.0625		0.214	6.23	2.27	7.43	0.12982
410	0.2044	0.0615		0.214	6.31	2.24	7.47	0.13041
460	0.2064	0.0613		0.214	6.37	2.23	7.52	0.13121
510	0.2082	0.0613		0.214	6.43	2.23	7.57	0.13202
560	0.2095	0.0607		0.214	6.47	2.21	7.59	0.13234
610	0.2107	0.0602		0.213	6.54	2.20	7.64	0.13316
660	0.2117	0.0602		0.213	6.57	2.20	7.67	0.13362
710	0.2123	0.0602		0.213	6.59	2.20	7.68	0.13389
760	0.2129	0.0598		0.213	6.61	2.18	7.69	0.13395
860	0.2137	0.0600		0.213	6.63	2.19	7.71	0.13442
960	0.2139	0.0592		0.212	6.67	2.17	7.73	0.13470
1060	0.2139	0.0590		0.212	6.67	2.17	7.73	0.13459
1160	0.2133	0.0584		0.211	6.69	2.15	7.73	0.13461

Table C.4 Diffusion profile of Dac-DC06-15

x (μm)	A_{5200}	A_{4500}	A_{3550}	d (mm)	H_2O_m (wt.%)	OH (wt.%)	H_2O_t (wt.%)	$X_{H_2O_t}$
-180			0.0240	0.191			0.01	0.00025
-160			0.0249	0.191			0.01	0.00026
-140			0.0321	0.191			0.02	0.00033
-120	0.0000	0.0037		0.191	0.00	0.14	0.12	0.00234
-110	0.0030	0.0074		0.191	0.10	0.29	0.34	0.00637
-105	0.0080	0.0132		0.191	0.27	0.52	0.69	0.01280
-100	0.0175	0.0217		0.191	0.58	0.85	1.26	0.02330
-95	0.0251	0.0280		0.191	0.84	1.11	1.70	0.03141
-90	0.0366	0.0326		0.191	1.23	1.29	2.20	0.04046
-85	0.0456	0.0352		0.191	1.54	1.39	2.56	0.04684
-80	0.0541	0.0390		0.191	1.82	1.55	2.95	0.05378
-70	0.0621	0.0421		0.191	2.10	1.68	3.30	0.05997
-60	0.0652	0.0437		0.191	2.20	1.74	3.45	0.06255
-40	0.0715	0.0453		0.191	2.42	1.80	3.69	0.06688
-20	0.0759	0.0468		0.191	2.57	1.87	3.88	0.07014
0	0.0799	0.0484		0.191	2.71	1.93	4.06	0.07319
20	0.0827	0.0493		0.191	2.81	1.97	4.18	0.07526
40	0.0846	0.0511		0.191	2.88	2.05	4.30	0.07741
60	0.0859	0.0527		0.191	2.92	2.11	4.40	0.07905
80	0.0879	0.0541		0.191	2.99	2.16	4.51	0.08093
100	0.0902	0.0547		0.191	3.07	2.19	4.60	0.08252
140	0.0941	0.0561		0.191	3.20	2.25	4.77	0.08541
180	0.0978	0.0568		0.191	3.33	2.28	4.91	0.08779
230	0.1011	0.0573		0.192	3.43	2.29	5.00	0.08935
280	0.1042	0.0580		0.192	3.54	2.32	5.12	0.09136
330	0.1068	0.0584		0.192	3.63	2.33	5.21	0.09294
380	0.1090	0.0586		0.192	3.70	2.34	5.29	0.09424
430	0.1112	0.0588		0.193	3.76	2.34	5.33	0.09500
480	0.1130	0.0589		0.193	3.82	2.35	5.39	0.09604
530	0.1147	0.0588		0.193	3.88	2.34	5.44	0.09685
580	0.1163	0.0593		0.194	3.92	2.35	5.48	0.09751
630	0.1173	0.0597		0.194	3.95	2.36	5.52	0.09819
680	0.1186	0.0592		0.194	3.99	2.35	5.54	0.09859
730	0.1193	0.0593		0.194	4.02	2.35	5.57	0.09903
780	0.1203	0.0595		0.194	4.05	2.36	5.60	0.09962
880	0.1216	0.0594		0.195	4.08	2.34	5.61	0.09976
980	0.1221	0.0594		0.195	4.09	2.34	5.63	0.10001
1080	0.1229	0.0594		0.195	4.12	2.34	5.65	0.10038
1180	0.1232	0.0593		0.195	4.13	2.34	5.66	0.10049
1280	0.1230	0.0594		0.195	4.12	2.34	5.65	0.10044

Table C.5 Diffusion profile of Dac-DC06-17

x (μm)	A_{5200}	A_{4500}	A_{3550}	d (mm)	H_2O_m (wt.%)	OH (wt.%)	H_2O_t (wt.%)	$X_{H_2O_t}$
-190			0.0254	0.200			0.01	0.00025
-170			0.0240	0.200			0.01	0.00024
-150			0.0512	0.200			0.03	0.00051
-125	0.0029	0.0035		0.200	0.09	0.13	0.19	0.00364
-120	0.0075	0.0083		0.200	0.24	0.31	0.48	0.00895
-115	0.0137	0.0122		0.200	0.44	0.46	0.78	0.01453
-110	0.0269	0.0207		0.200	0.86	0.78	1.43	0.02650
-105	0.0370	0.0247		0.200	1.18	0.93	1.85	0.03405
-100	0.0511	0.0301		0.200	1.64	1.14	2.43	0.04456
-95	0.0685	0.0356		0.200	2.21	1.35	3.11	0.05664
-90	0.0813	0.0397		0.200	2.63	1.51	3.62	0.06553
-85	0.0914	0.0428		0.200	2.96	1.63	4.01	0.07244
-65	0.1006	0.0487		0.200	3.27	1.86	4.48	0.08053
-40	0.1162	0.0572		0.210	3.60	2.09	4.97	0.08894
10	0.1238	0.0590		0.210	3.85	2.16	5.25	0.09358
60	0.1317	0.0612		0.210	4.10	2.24	5.54	0.09853
110	0.1374	0.0618		0.210	4.28	2.26	5.72	0.10155
160	0.1425	0.0626		0.210	4.44	2.30	5.89	0.10440
210	0.1411	0.0599		0.205	4.51	2.25	5.91	0.10466
260	0.1374	0.0634		0.205	4.39	2.38	5.92	0.10490
310	0.1418	0.0656		0.205	4.53	2.47	6.12	0.10826
360	0.1447	0.0658		0.205	4.63	2.48	6.21	0.10972
410	0.1467	0.0667		0.205	4.70	2.51	6.30	0.11126
460	0.1485	0.0671		0.205	4.75	2.53	6.37	0.11235
510	0.1494	0.0674		0.205	4.78	2.54	6.40	0.11292
560	0.1502	0.0677		0.205	4.81	2.55	6.44	0.11350
610	0.1514	0.0680		0.205	4.85	2.56	6.48	0.11422
660	0.1518	0.0671		0.204	4.89	2.54	6.50	0.11448
710	0.1525	0.0668		0.204	4.91	2.53	6.51	0.11466
760	0.1528	0.0661		0.203	4.95	2.52	6.52	0.11494
810	0.1528	0.0665		0.202	4.97	2.55	6.57	0.11574
860	0.1531	0.0667		0.202	4.98	2.55	6.59	0.11597
910	0.1533	0.0667		0.201	5.01	2.57	6.62	0.11660
960	0.1539	0.0664		0.201	5.03	2.55	6.63	0.11673
1010	0.1543	0.0659		0.200	5.07	2.55	6.66	0.11725
1060	0.1548	0.0658		0.200	5.09	2.54	6.67	0.11739

Table C.6 Diffusion profile of Dac-DC06-19

x (μm)	A_{5200}	A_{4500}	A_{3550}	d (mm)	H_2O_m (wt.%)	OH (wt.%)	H_2O_t (wt.%)	$X_{H_2O_t}$
-510			0.0374	0.270			0.01	0.00027
-460			0.0368	0.270			0.01	0.00027
-410			0.0370	0.270			0.01	0.00027
-360			0.0634	0.270			0.02	0.00046
-310			0.0970	0.270			0.04	0.00071
-260			0.1085	0.270			0.04	0.00079
-230			0.1214	0.200			0.06	0.00120
-220			0.2570	0.200			0.14	0.00254
-210			0.5370	0.201			0.28	0.00528
-205			0.7078	0.201			0.37	0.00695
-200	0.0043	0.0122		0.201	0.13	0.45	0.51	0.00960
-190	0.0064	0.0160		0.202	0.20	0.59	0.69	0.01294
-180	0.0104	0.0213		0.202	0.33	0.79	0.98	0.01816
-170	0.0146	0.0262		0.202	0.46	0.97	1.25	0.02326
-160	0.0192	0.0298		0.203	0.60	1.11	1.49	0.02763
-150	0.0243	0.0335		0.203	0.77	1.24	1.76	0.03238
-140	0.0265	0.0374		0.204	0.83	1.38	1.94	0.03566
-120	0.0303	0.0390		0.204	0.95	1.44	2.09	0.03847
-100	0.0339	0.0402		0.205	1.06	1.48	2.22	0.04077
-80	0.0368	0.0407		0.205	1.15	1.50	2.32	0.04251
-60	0.0399	0.0414		0.205	1.25	1.53	2.43	0.04445
-40	0.0425	0.0420		0.205	1.33	1.55	2.52	0.04615
-20	0.0452	0.0429		0.205	1.42	1.59	2.62	0.04800
0	0.0478	0.0434		0.206	1.49	1.59	2.70	0.04930
50	0.0518	0.0447		0.206	1.62	1.65	2.85	0.05209
100	0.0560	0.0458		0.207	1.74	1.68	2.99	0.05447
150	0.0598	0.0468		0.207	1.86	1.71	3.13	0.05690
200	0.0627	0.0475		0.207	1.96	1.74	3.23	0.05879
250	0.0655	0.0478		0.207	2.04	1.75	3.32	0.06032
300	0.0680	0.0485		0.207	2.12	1.78	3.41	0.06192
350	0.0700	0.0488		0.207	2.18	1.79	3.48	0.06306
400	0.0720	0.0494		0.207	2.25	1.81	3.55	0.06437
450	0.0735	0.0494		0.207	2.30	1.82	3.59	0.06511
500	0.0752	0.0497		0.207	2.35	1.83	3.65	0.06610
550	0.0761	0.0500		0.207	2.38	1.84	3.69	0.06672
600	0.0773	0.0502		0.207	2.42	1.85	3.73	0.06744
650	0.0784	0.0504		0.207	2.45	1.85	3.76	0.06805
700	0.0792	0.0507		0.207	2.48	1.87	3.80	0.06864
750	0.0800	0.0510		0.207	2.50	1.88	3.83	0.06919
800	0.0805	0.0509		0.207	2.52	1.87	3.84	0.06939

Table C.6 continued

x (μm)	A_{5200}	A_{4500}	A_{3550}	d (mm)	H_2O_m (wt.%)	OH (wt.%)	H_2O_t (wt.%)	$X_{H_2O_t}$
900	0.0815	0.0511		0.207	2.55	1.88	3.87	0.06997
950	0.0820	0.0511		0.207	2.56	1.88	3.89	0.07022
1050	0.0827	0.0516		0.207	2.59	1.90	3.92	0.07083
1150	0.0829	0.0513		0.206	2.61	1.90	3.94	0.07110
1250	0.0832	0.0515		0.206	2.62	1.91	3.95	0.07136
1350	0.0833	0.0514		0.206	2.62	1.90	3.95	0.07136

Table C.7 Diffusion profile of Dac-DC06-21

x (µm)	A_{5200}	A_{4500}	A_{3550}	d (mm)	H_2O_m (wt.%)	OH (wt.%)	H_2O_t (wt.%)	$X_{H_2O_t}$
-240			0.0214	0.177			0.01	0.00024
-190			0.0215	0.177			0.01	0.00024
-140			0.0215	0.177			0.01	0.00024
-120			0.0215	0.177			0.01	0.00024
-100			0.0214	0.177			0.01	0.00024
-80			0.0246	0.177			0.01	0.00027
-60			0.0616	0.177			0.04	0.00069
-50			0.1299	0.177			0.08	0.00145
-40			0.2800	0.177			0.17	0.00313
-30	0.0018	0.0056		0.177	0.06	0.24	0.26	0.00492
-20	0.0020	0.0112		0.177	0.07	0.47	0.48	0.00891
20	0.0085	0.0189		0.169	0.32	0.84	1.01	0.01882
30	0.0089	0.0214		0.169	0.34	0.95	1.12	0.02088
40	0.0117	0.0214		0.169	0.44	0.95	1.22	0.02260
60	0.0129	0.0224		0.169	0.49	0.99	1.30	0.02400
80	0.0139	0.0228		0.169	0.52	1.01	1.34	0.02489
100	0.0142	0.0233		0.169	0.54	1.04	1.38	0.02547
140	0.0143	0.0237		0.169	0.54	1.05	1.39	0.02576
180	0.0142	0.0239		0.169	0.54	1.06	1.40	0.02588
220	0.0145	0.0237		0.169	0.55	1.05	1.40	0.02589
270	0.0142	0.0239		0.169	0.54	1.06	1.40	0.02585
320	0.0143	0.0238		0.169	0.54	1.06	1.40	0.02587
370	0.0142	0.0239		0.169	0.54	1.06	1.40	0.02589
420	0.0142	0.0240		0.169	0.54	1.07	1.40	0.02592

Table C.8 Diffusion profile of Dac-DC06-22

x (μm)	A_{5200}	A_{4500}	A_{3550}	d (mm)	H_2O_m (wt.%)	OH (wt.%)	H_2O_t (wt.%)	$X_{H_2O_t}$
-400			0.0795	0.479			0.02	0.00033
-300			0.0745	0.479			0.02	0.00031
-200			0.0779	0.479			0.02	0.00032
-130			0.0221	0.157			0.01	0.00028
-110	0.0013	0.0037		0.157	0.05	0.18	0.20	0.00376
-100	0.0085	0.0085		0.157	0.35	0.41	0.66	0.01226
-95	0.0173	0.0155		0.157	0.70	0.74	1.27	0.02346
-90	0.0251	0.0205		0.157	1.02	0.98	1.75	0.03235
-85	0.0336	0.0219		0.157	1.37	1.05	2.12	0.03895
-80	0.0430	0.0252		0.157	1.76	1.22	2.60	0.04763
-75	0.0517	0.0272		0.157	2.12	1.31	3.00	0.05469
-70	0.0607	0.0309		0.157	2.50	1.50	3.49	0.06334
-65	0.0671	0.0320		0.157	2.77	1.55	3.77	0.06825
-60	0.0693	0.0346		0.157	2.86	1.68	3.97	0.07163
-20	0.0751	0.0412		0.157	3.11	2.01	4.47	0.08035
30	0.0785	0.0436		0.157	3.25	2.13	4.70	0.08425
90	0.0793	0.0465		0.157	3.29	2.27	4.86	0.08695
150	0.0823	0.0482		0.157	3.42	2.35	5.04	0.09013
200	0.0849	0.0488		0.157	3.52	2.38	5.16	0.09218
250	0.0869	0.0489		0.157	3.61	2.39	5.24	0.09354
300	0.0887	0.0496		0.157	3.69	2.43	5.34	0.09520
350	0.0904	0.0497		0.157	3.76	2.43	5.41	0.09637
400	0.0916	0.0497		0.157	3.81	2.43	5.46	0.09712
450	0.0931	0.0502		0.157	3.87	2.46	5.54	0.09845
500	0.0939	0.0501		0.157	3.91	2.46	5.56	0.09890
550	0.0948	0.0502		0.157	3.95	2.46	5.60	0.09955
600	0.0957	0.0503		0.157	3.98	2.47	5.64	0.10019
650	0.0963	0.0503		0.157	4.01	2.47	5.66	0.10059
750	0.0975	0.0505		0.157	4.06	2.48	5.72	0.10148
850	0.0980	0.0505		0.157	4.08	2.48	5.73	0.10177
950	0.0988	0.0505		0.157	4.12	2.47	5.76	0.10227
1050	0.0994	0.0505		0.157	4.14	2.47	5.78	0.10264
1150	0.0997	0.0505		0.157	4.16	2.47	5.80	0.10283
1250	0.1000	0.0503		0.157	4.17	2.47	5.80	0.10287
1350	0.0999	0.0504		0.157	4.16	2.47	5.80	0.10288

APPENDIX D

DATA TABLE OF DIFFUSION PROFILES IN CHAPTER IV

FTIR spectra of the diffusion profiles in haploandesite were fit using the calibration of Vetere et al. (2006): two straight baselines, absorption coefficient being 1.04 L/mol/cm for the 5200 cm^{-1} H$_2$O$_m$ band and 0.92 L/mol/cm for the 4500 cm^{-1} OH band.

Table D.1 Diffusion profile of HAD2C1

x (μm)	A_{5200}	A_{4500}	A_{3550}	d (mm)	H_2O_m (wt.%)	OH (wt.%)	H_2O_t (wt.%)	$X_{H_2O_t}$
10	0.0078	0.0173		0.201	0.27	0.67	0.94	0.01745
20	0.0105	0.0259		0.201	0.36	1.01	1.37	0.02534
30	0.0126	0.0275		0.201	0.43	1.07	1.50	0.02781
50	0.0164	0.0302		0.201	0.56	1.17	1.74	0.03215
70	0.0180	0.0321		0.201	0.62	1.25	1.87	0.03456
90	0.0192	0.0330		0.201	0.66	1.29	1.95	0.03597
110	0.0198	0.0341		0.201	0.68	1.33	2.01	0.03710
130	0.0201	0.0342		0.201	0.69	1.33	2.03	0.03740
150	0.0207	0.0345		0.201	0.71	1.34	2.06	0.03795
170	0.0209	0.0348		0.201	0.72	1.36	2.08	0.03835
190	0.0208	0.0351		0.201	0.72	1.37	2.09	0.03848
210	0.0210	0.0352		0.201	0.72	1.37	2.09	0.03862
260	0.0211	0.0356		0.201	0.73	1.39	2.12	0.03906
310	0.0216	0.0357		0.202	0.74	1.39	2.13	0.03921
410	0.0216	0.0362		0.203	0.74	1.40	2.13	0.03932
610	0.0218	0.0363		0.204	0.74	1.39	2.13	0.03934
810	0.0217	0.0361		0.203	0.74	1.39	2.13	0.03935
1010	0.0218	0.0360		0.203	0.74	1.39	2.13	0.03935
1210	0.0219	0.0356		0.202	0.75	1.38	2.13	0.03934
1410	0.0216	0.0353		0.200	0.75	1.38	2.13	0.03933
1510	0.0215	0.0349		0.199	0.75	1.38	2.13	0.03919
1610	0.0212	0.0343		0.198	0.74	1.36	2.10	0.03875
1660	0.0209	0.0338		0.197	0.74	1.35	2.08	0.03839
1710	0.0205	0.0332		0.195	0.73	1.34	2.06	0.03807
1730	0.0204	0.0328		0.195	0.72	1.32	2.04	0.03771
1750	0.0202	0.0326		0.195	0.72	1.31	2.03	0.03739
1770	0.0198	0.0323		0.195	0.70	1.30	2.00	0.03689
1790	0.0192	0.0316		0.195	0.68	1.27	1.95	0.03606
1810	0.0175	0.0305		0.195	0.62	1.22	1.84	0.03408
1820	0.0173	0.0298		0.195	0.61	1.20	1.81	0.03345
1830	0.0160	0.0284		0.195	0.57	1.14	1.70	0.03153
1840	0.0136	0.0263		0.195	0.48	1.05	1.54	0.02846
1850	0.0113	0.0236		0.194	0.40	0.95	1.35	0.02507
1860	0.0081	0.0213		0.194	0.29	0.86	1.14	0.02128

Table D.2 Diffusion profile of HAD2C2

x (μm)	A_{5200}	A_{4500}	A_{3550}	d (mm)	H_2O_m (wt.%)	OH (wt.%)	H_2O_t (wt.%)	$X_{H_2O_t}$
10	0.0084	0.0204		0.211	0.27	0.75	1.03	0.01911
15	0.0095	0.0233		0.211	0.31	0.86	1.17	0.02174
20	0.0106	0.0241		0.211	0.34	0.89	1.23	0.02291
25	0.0115	0.0251		0.211	0.37	0.93	1.30	0.02419
30	0.0138	0.0261		0.211	0.45	0.96	1.42	0.02626
40	0.0162	0.0285		0.211	0.53	1.06	1.58	0.02936
50	0.0183	0.0290		0.211	0.60	1.07	1.67	0.03094
60	0.0196	0.0310		0.211	0.64	1.15	1.79	0.03313
70	0.0206	0.0311		0.211	0.67	1.15	1.83	0.03378
80	0.0211	0.0319		0.211	0.69	1.18	1.88	0.03468
90	0.0222	0.0325		0.211	0.73	1.20	1.93	0.03569
100	0.0224	0.0327		0.211	0.74	1.21	1.95	0.03598
120	0.0231	0.0333		0.211	0.76	1.24	2.00	0.03683
140	0.0234	0.0334		0.211	0.77	1.24	2.01	0.03703
160	0.0236	0.0341		0.211	0.77	1.27	2.04	0.03764
180	0.0236	0.0346		0.211	0.77	1.28	2.06	0.03798
200	0.0239	0.0349		0.211	0.78	1.30	2.08	0.03840
250	0.0242	0.0355		0.211	0.79	1.32	2.11	0.03899
300	0.0243	0.0357		0.211	0.80	1.32	2.12	0.03917
350	0.0244	0.0358		0.211	0.80	1.33	2.13	0.03926
400	0.0245	0.0359		0.212	0.80	1.33	2.13	0.03922
500	0.0249	0.0360		0.213	0.81	1.32	2.13	0.03932
600	0.0246	0.0361		0.213	0.80	1.33	2.13	0.03930
700	0.0248	0.0363		0.213	0.81	1.33	2.14	0.03947
800	0.0248	0.0361		0.213	0.81	1.33	2.13	0.03933
900	0.0248	0.0361		0.213	0.81	1.33	2.13	0.03933
1000	0.0251	0.0363		0.215	0.81	1.32	2.13	0.03930
1100	0.0251	0.0361		0.214	0.81	1.32	2.13	0.03933
1200	0.0249	0.0362		0.214	0.81	1.32	2.13	0.03928
1300	0.0249	0.0362		0.214	0.81	1.32	2.13	0.03931
1400	0.0245	0.0363		0.213	0.80	1.34	2.14	0.03938
1500	0.0246	0.0359		0.212	0.80	1.33	2.13	0.03934
1550	0.0243	0.0359		0.212	0.80	1.33	2.12	0.03917
1600	0.0242	0.0357		0.212	0.79	1.32	2.11	0.03893
1650	0.0241	0.0354		0.212	0.79	1.31	2.09	0.03864
1700	0.0234	0.0350		0.212	0.77	1.29	2.06	0.03800
1720	0.0230	0.0339		0.212	0.75	1.25	2.01	0.03704
1740	0.0229	0.0339		0.212	0.75	1.25	2.00	0.03692
1760	0.0221	0.0332		0.212	0.72	1.23	1.95	0.03599
1770	0.0218	0.0328		0.212	0.71	1.21	1.92	0.03552

Table D.2 continued

x (µm)	A_{5200}	A_{4500}	A_{3550}	d (mm)	H_2O_m (wt.%)	OH (wt.%)	H_2O_t (wt.%)	$X_{H_2O_t}$
1780	0.0211	0.0323		0.212	0.69	1.19	1.88	0.03474
1790	0.0196	0.0309		0.212	0.64	1.14	1.78	0.03292
1800	0.0190	0.0304		0.212	0.62	1.12	1.74	0.03217
1810	0.0181	0.0299		0.212	0.59	1.10	1.69	0.03133
1820	0.0160	0.0287		0.212	0.52	1.06	1.58	0.02922
1825	0.0151	0.0278		0.212	0.49	1.02	1.52	0.02810
1830	0.0140	0.0265		0.212	0.45	0.98	1.43	0.02653
1835	0.0127	0.0257		0.212	0.41	0.94	1.36	0.02522
1840	0.0113	0.0246		0.212	0.37	0.91	1.27	0.02363
1845	0.0101	0.0231		0.212	0.33	0.85	1.18	0.02186
1850	0.0081	0.0190		0.212	0.26	0.70	0.96	0.01786

Table D.3 Diffusion profile of HAD2C3

x (µm)	A_{5200}	A_{4500}	A_{3550}	d (mm)	H_2O_m (wt.%)	OH (wt.%)	H_2O_t (wt.%)	$X_{H_2O_t}$
10	0.0048	0.0179		0.212	0.16	0.66	0.81	0.01516
15	0.0061	0.0220		0.212	0.20	0.81	1.00	0.01870
20	0.0068	0.0237		0.212	0.22	0.87	1.09	0.02029
25	0.0069	0.0249		0.212	0.23	0.91	1.14	0.02118
30	0.0080	0.0259		0.212	0.26	0.95	1.21	0.02249
35	0.0086	0.0273		0.212	0.28	1.00	1.28	0.02384
45	0.0097	0.0297		0.212	0.32	1.09	1.41	0.02614
55	0.0104	0.0305		0.212	0.34	1.12	1.46	0.02705
65	0.0114	0.0316		0.212	0.37	1.16	1.53	0.02844
75	0.0121	0.0325		0.212	0.39	1.20	1.59	0.02946
85	0.0127	0.0333		0.212	0.41	1.23	1.64	0.03040
95	0.0134	0.0345		0.212	0.44	1.27	1.71	0.03162
115	0.0145	0.0351		0.213	0.47	1.29	1.76	0.03253
135	0.0155	0.0364		0.213	0.50	1.34	1.84	0.03403
155	0.0160	0.0374		0.213	0.52	1.37	1.89	0.03495
175	0.0166	0.0377		0.213	0.54	1.38	1.92	0.03552
225	0.0175	0.0392		0.214	0.57	1.43	2.00	0.03691
275	0.0181	0.0401		0.214	0.59	1.47	2.05	0.03791
375	0.0181	0.0404		0.214	0.59	1.48	2.07	0.03813
475	0.0183	0.0411		0.215	0.59	1.50	2.09	0.03851
575	0.0184	0.0410		0.215	0.59	1.49	2.09	0.03853
675	0.0184	0.0412		0.215	0.59	1.50	2.10	0.03868
875	0.0184	0.0418		0.217	0.59	1.51	2.10	0.03867
1075	0.0183	0.0413		0.215	0.59	1.51	2.10	0.03865
1275	0.0183	0.0411		0.214	0.59	1.51	2.10	0.03869
1375	0.0183	0.0409		0.214	0.59	1.50	2.09	0.03855
1475	0.0183	0.0406		0.214	0.59	1.49	2.08	0.03836
1575	0.0183	0.0401		0.214	0.59	1.47	2.06	0.03797
1625	0.0174	0.0402		0.214	0.56	1.47	2.03	0.03754
1675	0.0170	0.0397		0.214	0.55	1.45	2.00	0.03698
1695	0.0166	0.0393		0.214	0.54	1.44	1.97	0.03646
1715	0.0163	0.0390		0.214	0.53	1.43	1.95	0.03609
1735	0.0157	0.0384		0.214	0.51	1.41	1.91	0.03536
1755	0.0153	0.0377		0.214	0.50	1.38	1.87	0.03462
1775	0.0146	0.0368		0.214	0.47	1.34	1.81	0.03354
1785	0.0143	0.0361		0.214	0.46	1.32	1.78	0.03292
1795	0.0140	0.0354		0.214	0.45	1.29	1.75	0.03230
1805	0.0136	0.0346		0.214	0.44	1.26	1.70	0.03150
1815	0.0121	0.0337		0.213	0.39	1.24	1.63	0.03021
1825	0.0116	0.0326		0.213	0.38	1.19	1.57	0.02908

Table D.3 continued

x (μm)	A_{5200}	A_{4500}	A_{3550}	d (mm)	H_2O_m (wt.%)	OH (wt.%)	H_2O_t (wt.%)	$X_{H_2O_t}$
1835	0.0111	0.0315		0.213	0.36	1.15	1.51	0.02808
1840	0.0107	0.0307		0.213	0.35	1.13	1.47	0.02729
1845	0.0102	0.0298		0.213	0.33	1.09	1.42	0.02635
1850	0.0095	0.0285		0.213	0.31	1.04	1.35	0.02511
1855	0.0095	0.0277		0.213	0.31	1.01	1.32	0.02454
1860	0.0094	0.0265		0.213	0.30	0.97	1.27	0.02362
1865	0.0087	0.0248		0.213	0.28	0.91	1.19	0.02212
1870	0.0071	0.0237		0.213	0.23	0.87	1.10	0.02042
1875	0.0060	0.0219		0.213	0.19	0.80	0.99	0.01849

Table D.4 Diffusion profile of HAD2C4

x (μm)	A_{5200}	A_{4500}	A_{3550}	d (mm)	H_2O_m (wt.%)	OH (wt.%)	H_2O_t (wt.%)	$X_{H_2O_t}$
20	0.0092	0.0234		0.186	0.34	0.98	1.32	0.02452
30	0.0100	0.0261		0.186	0.37	1.09	1.46	0.02714
40	0.0110	0.0272		0.186	0.41	1.14	1.55	0.02873
50	0.0117	0.0282		0.187	0.43	1.18	1.61	0.02983
60	0.0131	0.0286		0.187	0.48	1.20	1.68	0.03106
70	0.0139	0.0300		0.187	0.52	1.25	1.77	0.03271
80	0.0148	0.0302		0.188	0.54	1.26	1.80	0.03331
90	0.0154	0.0307		0.188	0.57	1.28	1.84	0.03410
110	0.0164	0.0313		0.188	0.61	1.30	1.91	0.03527
130	0.0178	0.0317		0.189	0.65	1.31	1.97	0.03629
170	0.0182	0.0324		0.189	0.67	1.34	2.01	0.03709
210	0.0188	0.0331		0.190	0.69	1.36	2.05	0.03781
250	0.0189	0.0334		0.190	0.69	1.38	2.07	0.03815
290	0.0192	0.0337		0.190	0.70	1.39	2.09	0.03854
330	0.0192	0.0339		0.190	0.70	1.40	2.10	0.03871
370	0.0191	0.0342		0.191	0.69	1.40	2.10	0.03872
410	0.0192	0.0344		0.192	0.69	1.41	2.10	0.03871
460	0.0193	0.0344		0.192	0.70	1.40	2.10	0.03871
510	0.0193	0.0347		0.193	0.69	1.41	2.10	0.03875
560	0.0195	0.0350		0.195	0.69	1.41	2.10	0.03871
610	0.0194	0.0351		0.195	0.69	1.41	2.10	0.03872
710	0.0195	0.0350		0.195	0.69	1.41	2.10	0.03871
910	0.0195	0.0348		0.194	0.69	1.41	2.10	0.03874
1110	0.0196	0.0347		0.194	0.70	1.40	2.10	0.03876
1210	0.0196	0.0346		0.194	0.70	1.40	2.10	0.03869
1310	0.0195	0.0345		0.193	0.70	1.40	2.10	0.03873
1360	0.0192	0.0345		0.192	0.69	1.41	2.10	0.03875
1410	0.0195	0.0342		0.192	0.70	1.40	2.10	0.03873
1460	0.0192	0.0342		0.191	0.70	1.40	2.10	0.03874
1510	0.0190	0.0343		0.191	0.69	1.41	2.10	0.03870
1550	0.0190	0.0341		0.191	0.69	1.40	2.09	0.03852
1590	0.0189	0.0338		0.191	0.69	1.39	2.08	0.03829
1630	0.0189	0.0332		0.190	0.69	1.37	2.06	0.03794
1670	0.0185	0.0328		0.190	0.68	1.35	2.03	0.03745
1710	0.0180	0.0325		0.191	0.65	1.33	1.99	0.03668
1750	0.0174	0.0319		0.192	0.63	1.30	1.93	0.03559
1770	0.0164	0.0315		0.193	0.59	1.28	1.87	0.03450
1790	0.0156	0.0304		0.193	0.56	1.23	1.79	0.03312
1800	0.0148	0.0294		0.193	0.53	1.19	1.72	0.03180
1810	0.0137	0.0285		0.193	0.49	1.16	1.65	0.03047

Table D.4 continued

x (µm)	A_{5200}	A_{4500}	A_{3550}	d (mm)	H_2O_m (wt.%)	OH (wt.%)	H_2O_t (wt.%)	$X_{H_2O_t}$
1820	0.0129	0.0279		0.193	0.46	1.13	1.59	0.02945
1825	0.0124	0.0270		0.193	0.44	1.09	1.54	0.02850
1830	0.0114	0.0258		0.192	0.41	1.05	1.46	0.02708
1835	0.0100	0.0235		0.191	0.36	0.96	1.32	0.02452

Table D.5 Diffusion profile of HAD2A1

x (μm)	A_{5200}	A_{4500}	A_{3550}	d (mm)	H_2O_m (wt.%)	OH (wt.%)	H_2O_t (wt.%)	$X_{H_2O_t}$
15	0.0082	0.0234		0.212	0.27	0.86	1.13	0.02093
20	0.0097	0.0252		0.212	0.31	0.93	1.24	0.02304
25	0.0106	0.0274		0.212	0.34	1.01	1.35	0.02509
35	0.0132	0.0291		0.212	0.43	1.07	1.50	0.02789
45	0.0148	0.0316		0.212	0.48	1.16	1.64	0.03046
55	0.0157	0.0326		0.212	0.51	1.20	1.71	0.03173
65	0.0170	0.0349		0.212	0.55	1.29	1.84	0.03401
75	0.0184	0.0353		0.212	0.60	1.30	1.90	0.03517
85	0.0188	0.0366		0.212	0.61	1.35	1.97	0.03632
95	0.0193	0.0374		0.212	0.63	1.38	2.01	0.03709
105	0.0202	0.0382		0.212	0.66	1.41	2.07	0.03820
115	0.0208	0.0387		0.212	0.68	1.43	2.11	0.03892
135	0.0217	0.0393		0.212	0.71	1.45	2.16	0.03987
155	0.0224	0.0403		0.212	0.73	1.49	2.22	0.04097
175	0.0233	0.0407		0.212	0.76	1.51	2.27	0.04177
195	0.0234	0.0414		0.212	0.77	1.53	2.30	0.04234
215	0.0239	0.0418		0.212	0.78	1.55	2.33	0.04285
235	0.0245	0.0421		0.212	0.80	1.56	2.36	0.04341
255	0.0246	0.0421		0.212	0.81	1.56	2.36	0.04351
305	0.0250	0.0426		0.212	0.82	1.58	2.40	0.04413

Table D.6 Diffusion profile of HAD2A3

x (µm)	A_{5200}	A_{4500}	A_{3550}	d (mm)	H_2O_m (wt.%)	OH (wt.%)	H_2O_t (wt.%)	$X_{H_2O_t}$
24	0.0147	0.0303		0.221	0.46	1.07	1.53	0.02832
51	0.0163	0.0360		0.221	0.51	1.27	1.78	0.03297
57	0.0165	0.0371		0.221	0.52	1.31	1.83	0.03380
67	0.0179	0.0381		0.221	0.56	1.35	1.91	0.03523
76	0.0190	0.0385		0.221	0.60	1.36	1.96	0.03612
85	0.0203	0.0396		0.221	0.63	1.40	2.04	0.03756
95	0.0211	0.0402		0.221	0.66	1.42	2.09	0.03846
107	0.0215	0.0410		0.221	0.67	1.45	2.12	0.03918
116	0.0224	0.0412		0.222	0.70	1.46	2.16	0.03981
136	0.0230	0.0421		0.222	0.72	1.49	2.21	0.04076
158	0.0232	0.0421		0.222	0.73	1.49	2.22	0.04086
175	0.0243	0.0425		0.222	0.76	1.50	2.27	0.04173
194	0.0246	0.0432		0.222	0.77	1.53	2.30	0.04231
210	0.0249	0.0431		0.222	0.78	1.52	2.30	0.04241
233	0.0249	0.0430		0.222	0.78	1.52	2.30	0.04230
268	0.0247	0.0434		0.222	0.77	1.53	2.30	0.04242
299	0.0253	0.0434		0.222	0.79	1.53	2.32	0.04271
327	0.0256	0.0436		0.222	0.80	1.54	2.34	0.04305
357	0.0250	0.0438		0.223	0.78	1.54	2.32	0.04276
397	0.0253	0.0432		0.223	0.79	1.52	2.31	0.04253
447	0.0253	0.0435		0.223	0.79	1.53	2.32	0.04267
497	0.0253	0.0442		0.223	0.79	1.56	2.34	0.04311
597	0.0257	0.0438		0.224	0.80	1.54	2.33	0.04295
697	0.0256	0.0442		0.224	0.79	1.55	2.34	0.04305
797	0.0256	0.0440		0.225	0.79	1.54	2.33	0.04287
897	0.0260	0.0440		0.225	0.80	1.54	2.34	0.04302
897	0.0251	0.0442		0.225	0.78	1.54	2.32	0.04264

APPENDIX E

DATA TABLE OF ADDITIONAL HAPLOANDESITE PROFILES

FTIR spectra of the diffusion profiles in haploandesite were fit using the calibration of Vetere et al. (2006): two straight baselines, absorption coefficient being 1.04 L/mol/cm for the 5200 cm^{-1} H_2O_m band and 0.92 L/mol/cm for the 4500 cm^{-1} OH band and Mandeville et al. (2002): straight baseline, absorption coefficient being 69.21 L/mol/cm for the 3550 cm^{-1} H_2O_t band. The composition of starting anhydrous glass SA-D2 is 58.46% SiO_2, 1.65% TiO_2, 16.23% Al_2O_3, 6.59% MgO, 12.53% CaO, and 4.46% K_2O in weight percentage. The composition of starting hydrous glass HAD2 can be found in Table 4.1. The diffusion profiles from these experiments are not included in Chapter IV because of the inconsistency in diffusivities extracted from dehydration data and from diffusion couple data (tentatively attributed to the chemical compositions of the two halves on anhydrous basis are different).

Table E.1 Diffusion profile of HAD-DC1 (823 K, 0.1 GPa, 1281600 s, cold-seal vessel)

x (µm)	A_{5200}	A_{4500}	A_{3550}	d (mm)	H_2O_m (wt.%)	OH (wt.%)	H_2O_t (wt.%)	$X_{H_2O_t}$
-480			0.0142	0.218			0.01%	0.00013
-380			0.0134	0.218			0.01%	0.00012
-280			0.0133	0.218			0.01%	0.00012
-180			0.0141	0.218			0.01%	0.00012
-130			0.0166	0.218			0.01%	0.00015
-100			0.0194	0.218			0.01%	0.00017
-80			0.0289	0.218			0.01%	0.00026
-70			0.0580	0.218			0.03%	0.00051
-60	0.0008	0.0026		0.218	0.03%	0.09%	0.12%	0.00224
-50	0.0013	0.0041		0.218	0.04%	0.15%	0.19%	0.00351
-40	0.0017	0.0077		0.218	0.05%	0.27%	0.33%	0.00611
-30	0.0033	0.0121		0.218	0.11%	0.43%	0.53%	0.00998
-20	0.0057	0.0166		0.218	0.18%	0.59%	0.77%	0.01441
-10	0.0080	0.0205		0.218	0.25%	0.73%	0.98%	0.01829
0	0.0104	0.0262		0.218	0.33%	0.94%	1.27%	0.02352
10	0.0125	0.0297		0.218	0.40%	1.06%	1.46%	0.02704
20	0.0141	0.0324		0.218	0.45%	1.16%	1.61%	0.02977
30	0.0159	0.0351		0.218	0.50%	1.26%	1.76%	0.03259
40	0.0168	0.0365		0.218	0.53%	1.31%	1.85%	0.03411
60	0.0178	0.0386		0.218	0.57%	1.38%	1.95%	0.03604
80	0.0186	0.0395		0.218	0.59%	1.42%	2.01%	0.03711
100	0.0195	0.0403		0.218	0.62%	1.45%	2.07%	0.03814
140	0.0207	0.0406		0.218	0.66%	1.46%	2.12%	0.03903
180	0.0215	0.0405		0.218	0.68%	1.46%	2.14%	0.03946
220	0.0212	0.0408		0.218	0.67%	1.47%	2.14%	0.03948
270	0.0211	0.0409		0.218	0.67%	1.47%	2.14%	0.03949
320	0.0214	0.0407		0.218	0.68%	1.46%	2.14%	0.03951
420	0.0214	0.0408		0.218	0.68%	1.47%	2.15%	0.03961
520	0.0216	0.0405		0.218	0.69%	1.46%	2.14%	0.03949
620	0.0214	0.0406		0.218	0.68%	1.46%	2.14%	0.03947

Table E.2 Diffusion profile of HAD-DC2 (1584 K, 0.95 GPa, 326 s, Piston-cylinder)

x (μm)	A_{5200}	A_{4500}	A_{3550}	d (mm)	H_2O_m (wt.%)	OH (wt.%)	H_2O_t (wt.%)	$X_{H_2O_t}$
-620			0.0206	0.216			0.01%	0.00018
-570			0.0209	0.216			0.01%	0.00019
-520			0.0266	0.216			0.01%	0.00024
-470			0.0402	0.216			0.02%	0.00036
-450			0.0429	0.216			0.02%	0.00038
-430			0.0622	0.216			0.03%	0.00056
-410			0.0781	0.216			0.04%	0.00070
-390			0.0991	0.216			0.05%	0.00088
-370			0.1254	0.216			0.06%	0.00112
-350			0.1582	0.216			0.08%	0.00141
-330			0.1982	0.216			0.09%	0.00177
-310			0.2471	0.216			0.12%	0.00221
-290			0.3052	0.216			0.15%	0.00272
-270			0.3810	0.216			0.18%	0.00340
-250			0.4547	0.216			0.22%	0.00406
-230			0.5404	0.216			0.26%	0.00482
-210			0.6330	0.216			0.30%	0.00565
-190			0.7347	0.216			0.35%	0.00656
-170			0.8397	0.216			0.40%	0.00749
-150			0.9460	0.216			0.45%	0.00844
-130			1.0505	0.216			0.50%	0.00937
-110			1.1469	0.216			0.55%	0.01023
-90	0.0020	0.0162		0.218	0.06%	0.58%	0.64%	0.01196
-70	0.0026	0.0177		0.218	0.08%	0.63%	0.71%	0.01326
-50	0.0032	0.0191		0.218	0.10%	0.68%	0.78%	0.01460
-30	0.0038	0.0206		0.218	0.12%	0.73%	0.86%	0.01594
-10	0.0046	0.0224		0.218	0.14%	0.80%	0.94%	0.01756
10	0.0054	0.0243		0.218	0.17%	0.87%	1.04%	0.01937
30	0.0065	0.0261		0.218	0.21%	0.93%	1.14%	0.02117
50	0.0074	0.0277		0.218	0.23%	0.99%	1.22%	0.02270
70	0.0086	0.0295		0.218	0.27%	1.05%	1.33%	0.02462
90	0.0096	0.0308		0.218	0.30%	1.10%	1.40%	0.02605
110	0.0106	0.0327		0.218	0.34%	1.17%	1.51%	0.02795
130	0.0112	0.0341		0.218	0.35%	1.22%	1.58%	0.02919
150	0.0120	0.0354		0.218	0.38%	1.27%	1.65%	0.03051
170	0.0129	0.0367		0.218	0.41%	1.32%	1.72%	0.03192
190	0.0138	0.0379		0.218	0.44%	1.36%	1.80%	0.03324
210	0.0145	0.0387		0.218	0.46%	1.39%	1.85%	0.03418
230	0.0150	0.0392		0.218	0.48%	1.41%	1.88%	0.03480
250	0.0154	0.0398		0.218	0.49%	1.43%	1.92%	0.03543

Table E.2 continued

x (μm)	A_{5200}	A_{4500}	A_{3550}	d (mm)	H_2O_m (wt.%)	OH (wt.%)	H_2O_t (wt.%)	$X_{H_2O_t}$
270	0.0160	0.0405		0.218	0.51%	1.45%	1.96%	0.03620
290	0.0165	0.0411		0.218	0.53%	1.47%	2.00%	0.03693
340	0.0185	0.0404		0.218	0.59%	1.45%	2.04%	0.03767
360	0.0189	0.0405		0.218	0.60%	1.46%	2.06%	0.03799
380	0.0186	0.0412		0.218	0.59%	1.48%	2.07%	0.03820
450	0.0190	0.0410		0.218	0.61%	1.47%	2.08%	0.03832
490	0.0193	0.0412		0.218	0.61%	1.48%	2.09%	0.03859
530	0.0195	0.0410		0.218	0.62%	1.47%	2.09%	0.03857
580	0.0191	0.0415		0.218	0.61%	1.49%	2.10%	0.03877
630	0.0193	0.0410		0.217	0.62%	1.48%	2.09%	0.03862
680	0.0191	0.0411		0.217	0.61%	1.48%	2.09%	0.03860
730	0.0190	0.0411		0.217	0.61%	1.48%	2.09%	0.03857
780	0.0188	0.0407		0.215	0.61%	1.48%	2.09%	0.03855
830	0.0189	0.0405		0.215	0.61%	1.48%	2.09%	0.03851

Table E.3 Diffusion profile of HAD-DC3 (818 K, 0.95 GPa, 2026320 s, Piston-cylinder)

x (µm)	A_{5200}	A_{4500}	A_{3550}	d (mm)	H_2O_m (wt.%)	OH (wt.%)	H_2O_t (wt.%)	$X_{H_2O_t}$
-100			0.0264	0.220			0.01%	0.00023
-80			0.0264	0.220			0.01%	0.00023
-60			0.0304	0.220			0.01%	0.00027
-50			0.0417	0.220			0.02%	0.00037
-40			0.0721	0.220			0.03%	0.00063
-30			0.1279	0.220			0.06%	0.00112
-20	0.0000	0.0053		0.220	0.00%	0.19%	0.19%	0.00349
-10	0.0040	0.0119		0.220	0.13%	0.42%	0.54%	0.01016
0	0.0089	0.0186		0.220	0.28%	0.66%	0.94%	0.01744
10	0.0167	0.0324		0.220	0.52%	1.15%	1.67%	0.03101
20	0.0191	0.0349		0.220	0.60%	1.24%	1.84%	0.03402
30	0.0204	0.0359		0.220	0.64%	1.28%	1.92%	0.03542
40	0.0216	0.0369		0.220	0.68%	1.31%	1.99%	0.03679
50	0.0225	0.0376		0.220	0.71%	1.34%	2.05%	0.03780
60	0.0228	0.0380		0.220	0.72%	1.35%	2.07%	0.03820
70	0.0228	0.0384		0.220	0.72%	1.37%	2.08%	0.03845
80	0.0231	0.0385		0.220	0.73%	1.37%	2.10%	0.03867
90	0.0229	0.0388		0.220	0.72%	1.38%	2.10%	0.03879
100	0.0230	0.0389		0.221	0.72%	1.38%	2.10%	0.03878
120	0.0231	0.0393		0.222	0.72%	1.39%	2.11%	0.03888
140	0.0227	0.0395		0.222	0.71%	1.39%	2.10%	0.03880
160	0.0225	0.0395		0.221	0.71%	1.40%	2.11%	0.03885
180	0.0225	0.0390		0.220	0.71%	1.39%	2.10%	0.03871
200	0.0225	0.0390		0.220	0.71%	1.39%	2.10%	0.03868

Table E.4 Diffusion profile of HAD-DC4 (1785 K, 0.95 GPa, 105 s, Piston-cylinder)

x (μm)	A_{5200}	A_{4500}	A_{3550}	d (mm)	H_2O_m (wt.%)	OH (wt.%)	H_2O_t (wt.%)	$X_{H_2O_t}$
-550			0.0944	0.225			0.04%	0.00081
-500			0.0965	0.225			0.04%	0.00083
-450			0.1279	0.225			0.06%	0.00110
-350			0.2637	0.225			0.12%	0.00226
-325			0.3312	0.225			0.15%	0.00284
-300			0.3999	0.225			0.18%	0.00343
-280			0.4799	0.225			0.22%	0.00411
-260			0.5525	0.225			0.25%	0.00473
-240			0.6376	0.225			0.29%	0.00546
-220			0.7290	0.225			0.33%	0.00625
-200			0.8271	0.225			0.38%	0.00708
-180			0.9315	0.225			0.43%	0.00798
-160			1.0398	0.225			0.48%	0.00891
-140			1.1443	0.225			0.52%	0.00980
-120			1.2466	0.225			0.57%	0.01067
-100			1.3370	0.225			0.61%	0.01145
-80	0.0023	0.0175		0.225	0.07%	0.60%	0.67%	0.01256
-60	0.0029	0.0188		0.225	0.09%	0.65%	0.74%	0.01379
-40	0.0033	0.0194		0.220	0.10%	0.68%	0.79%	0.01467
40	0.0059	0.0268		0.220	0.18%	0.95%	1.13%	0.02110
50	0.0064	0.0284		0.225	0.20%	0.98%	1.18%	0.02193
60	0.0071	0.0289		0.225	0.22%	1.00%	1.22%	0.02263
80	0.0079	0.0305		0.225	0.24%	1.06%	1.30%	0.02409
100	0.0089	0.0324		0.225	0.27%	1.12%	1.39%	0.02586
120	0.0098	0.0337		0.225	0.30%	1.17%	1.47%	0.02724
140	0.0108	0.0344		0.225	0.33%	1.19%	1.52%	0.02827
160	0.0116	0.0357		0.225	0.35%	1.24%	1.59%	0.02953
180	0.0127	0.0368		0.225	0.39%	1.28%	1.67%	0.03085
200	0.0132	0.0376		0.225	0.41%	1.31%	1.71%	0.03171
240	0.0144	0.0390		0.225	0.44%	1.36%	1.80%	0.03329
280	0.0161	0.0395		0.225	0.50%	1.37%	1.87%	0.03453
320	0.0170	0.0398		0.225	0.52%	1.39%	1.91%	0.03526
360	0.0175	0.0405		0.225	0.54%	1.41%	1.95%	0.03598
400	0.0181	0.0406		0.225	0.56%	1.41%	1.97%	0.03641
440	0.0185	0.0410		0.225	0.57%	1.43%	1.99%	0.03682
480	0.0191	0.0410		0.225	0.59%	1.43%	2.02%	0.03720
600	0.0188	0.0413		0.225	0.58%	1.44%	2.02%	0.03721
650	0.0189	0.0413		0.225	0.58%	1.44%	2.02%	0.03727
700	0.0192	0.0412		0.225	0.59%	1.44%	2.03%	0.03739
750	0.0190	0.0412		0.225	0.58%	1.44%	2.02%	0.03727

Table E.4 continued

x (μm)	A_{5200}	A_{4500}	A_{3550}	d (mm)	H_2O_m (wt.%)	OH (wt.%)	H_2O_t (wt.%)	$X_{H_2O_t}$
800	0.0190	0.0412		0.225	0.58%	1.44%	2.02%	0.03727
900	0.0186	0.0414		0.225	0.57%	1.44%	2.01%	0.03719

APPENDIX F

QUICKBASIC SUBROUTINE FOR EXTRACTING THE BEST *a* and D_0

Previous routines (developed in Zhang et al., 1991a, 1991b, Zhang and Stolper, 1991; Zhang and Behrens, 2000) use trial-and-error method to fit a diffusion profile: parameter *a* is first designated and a theoretical profile is calculated; the calculated profile is then used to fit a measured profile for D_0 (or $4D_0t$); the above procedure is repeated until the least squares are reached.

This subroutine uses Levenberg-Marquardt algorithm to realize trivariate fitting (*a*, D_0, and interface adjustment Δx_0). It assumes H_2O_m is the dominant diffusion species and $D_{H_2O_m} = D_0\exp(aX)$. The speciation model is integrated inside the program so that the equilibrium constant *K* is calculated from the input temperature (the code below is for rhyolite). The new subroutine is much less time-consuming and allows evaluating the uncertainties in the parameters.

```
6500      REM fit data to constant D(H2O)
          Pre#=.0000000001#
          PRINT "this part is modified by Huaiwei in 2007"
          PRINT "this assumes D(H2O)=D0*exp(aX) and D(OH)=0"
          PRINT "this calculates and fits X(data) vs x profile by a, D0, and x0"
          PRINT "X(data)=F((x+x0)/√4D0t)"
          PRINT "F is the calculated function and depends a"
6505        PRINT "   0=exit this part"
          PRINT "   1=calculate dif profile and fit to get D"
          PRINT "   2=change relative precision of Chi.sq (default 1D-10)"
6510      INPUT "    What is your choice?  (0,1,2)",Any%
          IF Any%<0 OR Any%>2 THEN 6510
          ON Any%+1 GOTO 6000,6550,6530
6530      INPUT "Relative precision for calculating Chi.sq?",Pre#
          IF Pre#=0 THEN Pre#=.0000000001#
          GOTO 6505


6550      REM Data information and fitting parameters
          CLS
          PRINT "Relative precision is",Pre#
          Nv%=3
6553      INPUT "Which column is x (µm) or x/2√Dt in original data matrix?",K1%
          IF K1%<=0 OR K1%>Column% THEN 6553
6555      INPUT "which column is the profile to be fit?",K2%
          IF K2%<=0 OR K2%>Column% THEN 6555
          Choice%=0
6567      PRINT "You can choose to minimize ∑(yi-yi.c)^2 or ∑[(yi-yi.c)/ei]^2"
          PRINT "   0=minimizing absolute errors ∑(yi-yi.c)^2"
          PRINT "   1=minimizing relative errors ∑[(yi-yi.c)/ei]^2"
          INPUT "What is your choice?",Choice%
          IF Choice%=1 THEN
6568        PRINT "   which column in the original matrix stores error?"
            INPUT K.err%
            IF K.err%<=0 OR K.err%>Column% THEN 6568
          END IF
          linshi=(D#(Row%,K1%)-D#(1,K1%))/6#
          linshi=linshi*linshi
          INPUT "initial guess for exponential factor a? (0-100)",aexp#
          INPUT "step of a to calculate differential? (0.1)",astep#
          INPUT "initial guess for x0 in µm/√s or µm? (e.g., 5)",X0#
6570      PRINT "initial guess for D0 or 4Dt (in µm2/s or µm2) can be";linshi;
          INPUT "  change to what?", Dh2o#
          IF Dh2o#<=0 THEN 6570
          REM calculation parameters
          DIM W3#(20),Xp(4),Nx%(20),V$(9),Wp#(12)
          REM W3#(1)=C1@-∞; W3#(2)=C1@∞; W3#(3)=dx; W3#(4)=dt/(dx*dx)
          REM W3#(5)=time to end; W3#(6)=DOH/DH2Om=0
          REM W3#(7)=equilibrium constant; W3#(8)=old t; W3#(9)=new t
          REM W3#(10)=exponential factor a
          V$(1)="x/sqrt(4D0t)" : V$(2)="XH2Ot" : V$(3)="XH2Om"
          V$(4)=" old x/sqrt(4D0t)" : V$(5)="old x(B)" : Nx%(17)=20
          W3#(6)=0# : Opt%=0
          INPUT "Temperature in celsis?",W3#(7)
```

```
        W3#(7)=W3#(7)+273.15#
        W3#(7)=EXP(1.876#-3110#/(W3#(7)))
        PRINT "Equilibrium constant (Zhang et al., 1997) is ",W3#(7)
        linshi=(D#(1,K2%)+D#(2,K2%)+D#(3,K2%))/3#
        linshi1=(D#(Row%,K2%)+D#(Row%-1,K2%)+D#(Row%-2,K2%))/3#
6580    PRINT "Concentrations at x=-∞ and x=∞ can be";linshi;"and";linshi1
        INPUT "  change to what?",W3#(1),W3#(2)
        IF W3#(1)<0 OR W3#(2)<0 THEN GOTO 6580
        IF W3#(1)=W3#(2) THEN PRINT " the conc. profile is flat" : GOTO 6580
6590    INPUT "Minimum number of space steps in calculation? (suggest: 100)",Nmin%
        IF Nmin%<=2 THEN Nmin%=50
        IF Nmin%/2<>INT(Nmin%/2) THEN Nmin%=Nmin%+1
        N%=6*Nmin% : Nx%(6)=N%-1 : Nmid%=3*Nmin% : Nx%(18)=Nmid%
        REM if Nmin%=50, then row 1 to 149 stores the LHS (x<0)
        REM row 150 Nx%(18) stores the midpoint
        REM and row 151 to 299 stores the RHD (x>0), Nx%(6)=299
6600    Xp(1)=.00001 : Xp(2)=.00001
        INPUT "dx=?    (suggest 0.01)",W3#(3)
        IF W3#(3)<=0 THEN W3#(3)=.01#
        Round%=1
        Iter%=1
        Lambda#=.125#
        PRINT "File name for intermediate results?"
        B$="intermediate results"
        File2$=FILES$(0,B$)
        IF File2$="" THEN File2$="crap.csv"
        OPEN "O",#1,File2$
        PRINT#1,B$
        PRINT#1,"Round #";",  ";"Iter #";",  ";"a";",  ";"4Dt or D(H2O)";",  ";" X0";",  ";"Chi.sq";",
";"Lambda"
        DIM W1#(N%-1,5),water#(N%-1,6),water1#(N%-1,6),water2#(N%-1,6)
        REM W1#: 1st column=x; 2nd=new C; 3rd=old C
        REM water: 1st=normalized x; 2nd=new C; 4th=old normalized x; 5th=old C
        DIM D.tem#(N%-1,6),D1.tem#(N%-1,6),D2.tem#(N%-1,6)
        DIM Fd#(Row%,3),Fp#(Row%,1),X1#(3,4),XA#(3,3),Fdold#(Row%,3),Fpold#(Row%,1)
        DIM Plot#(Row%,2),X2#(3,4)
        Test=0#
6650    Pse!=1E-10
        PRINT ""
        PRINT ""
        PRINT ""
        PRINT ""
        PRINT ""
        PRINT "Fitting begins."
        PRINT "It takes long time to fit one profile. Please be patient."
        PRINT "Time step is determined to be a quarter of dx*dx/exp(aX)."
        Nx%(16)=1000
        Round%=1
        Iter%=1
        Lambda#=.125#
6670    REM loop
        REM calculation of theoretical profiles
        PRINT "ROUND";Round%
```

```
        W3#(10)=aexp#
        Xt#=W3#(1)
        IF W3#(2)>W3#(1) THEN Xt#=W3#(2)
        W3#(4)=.25#/EXP(W3#(10)*Xt#)
        tstep#=W3#(4)*W3#(3)*W3#(3)
        PRINT "Time step of this round is";tstep#
        W3#(5)=1999#*W3#(4)*W3#(3)*W3#(3)
6672    PRINT "Print concentration at zero after 100 time steps."
        PRINT "Plot calculated diffusion profile after 1000 time steps."
        PRINT "Calculation ends after 2000 time steps."
6673    CALL Water.Forward(W1#(),W3#(),water#(),Xp(),Wp#(),V$(),Nx%(),Morder%,Opt%)
        Nf%=Nx%(1) : NL1%=Nmid%-Nf%+1 : NR1%=Nmid%+Nf%-1
        CALL Find.end.rows(water#(),2,NL1%,Nmid%,NR1%,Pse!,Iend1%,Iend2%)
        Rtem%=Iend2%-Iend1%+1
        FOR I%=1 TO Rtem%
          FOR J%=1 TO 5
            D.tem#(I%,J%)=water#(I%+Iend1%-1,J%)
          NEXT J%
        NEXT I%
        W3#(10)=aexp#-astep# : CALL
Water.Forward(W1#(),W3#(),water1#(),Xp(),Wp#(),V$(),Nx%(),Morder%,Opt%)
        Nf%=Nx%(1) : NL1%=Nmid%-Nf%+1 : NR1%=Nmid%+Nf%-1
        CALL Find.end.rows(water1#(),2,NL1%,Nmid%,NR1%,Pse!,Iend1%,Iend2%)
        R1tem%=Iend2%-Iend1%+1
        FOR I%=1 TO R1tem%
          FOR J%=1 TO 5
            D1.tem#(I%,J%)=water1#(I%+Iend1%-1,J%)
          NEXT J%
        NEXT I%
        W3#(10)=aexp#+astep# : CALL
Water.Forward(W1#(),W3#(),water2#(),Xp(),Wp#(),V$(),Nx%(),Morder%,Opt%)
        Nf%=Nx%(1) : NL1%=Nmid%-Nf%+1 : NR1%=Nmid%+Nf%-1
        CALL Find.end.rows(water2#(),2,NL1%,Nmid%,NR1%,Pse!,Iend1%,Iend2%)
        R2tem%=Iend2%-Iend1%+1
        FOR I%=1 TO R2tem%
          FOR J%=1 TO 5
            D2.tem#(I%,J%)=water2#(I%+Iend1%-1,J%)
          NEXT J%
        NEXT I%
        dx#=D.tem#(2,1)-D.tem#(1,1)
        dx1#=D1.tem#(2,1)-D1.tem#(1,1)
        dx2#=D2.tem#(2,1)-D2.tem#(1,1)
        Dh2o1#=SQR(Dh2o#)
6680    REM now calculate how good the fit is (value of function is interpolated using the tabulated
function)
        variance#=0
        FOR I%=1 TO Row%
          Xt#=(D#(I%,K1%)+X0#)/Dh2o1#
          I0%=INT(1+(Xt#-D.tem#(1,1))/dx#)
          I1%=INT(1+(Xt#-D1.tem#(1,1))/dx1#)
          I2%=INT(1+(Xt#-D2.tem#(1,1))/dx2#)
          IF I0%>=Rtem% THEN
            Fptem#=D#(I%,K2%)-D.tem#(Rtem%,2)
```

```
    IF Choice%=1 THEN Fptem#=Fptem#/D#(I%,K.err%)
   Fdtem#=0 : Fdtem1#=0# : Fdtem2#=0#
ELSE
  IF I0%<1 THEN
    Fptem#=D#(I%,K2%)-D.tem#(1,2)
    IF Choice%=1 THEN Fptem#=Fptem#/D(I%,K.err%)
    Fdtem#=0 : Fdtem1#=0# : Fdtem2#=0#
  ELSE
   IF I0%=1 THEN I0%=2
   Xt0#=Xt#-D.tem#(I0%-1,1)
   Xt1#=Xt#-D.tem#(I0%,1)
   Xt2#=Xt#-D.tem#(I0%+1,1)
   value#=.5#*Xt1#*Xt2#*D.tem#(I0%-1,2)
   value#=value#-Xt0#*Xt2#*D.tem#(I0%,2)
   value#=value#+.5#*Xt0#*Xt1#*D.tem#(I0%+1,2)
   value#=value#/(dx#*dx#)
   Fptem#=D#(I%,K2%)-value#
   IF Choice%=1 THEN Fptem#=Fptem#/D#(I%,K.err%)
   Fdtem1#=.5#*(Xt1#+Xt2#)*D.tem#(I0%-1,2)
   Fdtem1#=Fdtem1#-(Xt0#+Xt2#)*D.tem#(I0%,2)
   Fdtem1#=Fdtem1#+.5#*(Xt0#+Xt1#)*D.tem#(I0%+1,2)
   Fdtem1#=Fdtem1#/(dx#*dx#)
   Fdtem2#=-Fdtem1#/Dh2o1#
   Fdtem1#=Xt#*Fdtem1#/(Dh2o#+Dh2o#)
   IF I1%>=R1tem% THEN value1#=D1.tem#(R1tem%,2)
   IF I1%<1 THEN value1#=D1.tem#(1,2)
   IF I1%>=1 AND I1%<R1tem% THEN
      IF I1%=1 THEN I1%=2
      Xt0#=Xt#-D1.tem#(I1%-1,1)
      Xt1=Xt#-D1.tem#(I1%,1)
      Xt2=Xt#-D1.tem#(I1%+1,1)
      value1#=.5#*Xt1#*Xt2#*D1.tem#(I1%-1,2)
      value1#=value1#-Xt0#*Xt2#*D1.tem#(I1%,2)
      value1#=value1#+.5#*Xt0#*Xt1#*D1.tem#(I1%+1,2)
      value1#=value1#/(dx1#*dx1#)
   END IF
   IF I2%>=R2tem% THEN value2#=D2.tem#(R2tem%,2)
   IF I2%<1 THEN value2#=D2.tem#(1,2)
   IF I2%>=1 AND I2%<R2tem% THEN
      IF I2%=1 THEN I2%=2
      Xt0#=Xt#-D2.tem#(I2%-1,1)
      Xt1#=Xt#-D2.tem#(I2%,1)
      Xt2#=Xt#-D2.tem#(I2%+1,1)
      value2#=.5#*Xt1#*Xt2#*D2.tem#(I2%-1,2)
      value2#=value2#-Xt0#*Xt2#*D2.tem#(I2%,2)
      value2#=value2#+.5*Xt0#*Xt1#*D2.tem#(I2%+1,2)
      value2#=value2#/(dx2#*dx2#)
   END IF
   Fdtem#=(value1#-value2#)/(astep#+astep#)
  END IF
END IF
Fp#(I%,1)=Fptem#
variance#=variance#+Fp#(I%,1)*Fp#(I%,1)
```

```
        Fd#(I%,1)=Fdtem#
        Fd#(I%,2)=Fdtem1#
        Fd#(I%,3)=Fdtem2#
        IF Choice%=1 THEN
          Fd#(I%,1)=Fd#(I%,1)/D(I%,K.err%)
          Fd#(I%,2)=Fd#(I%,2)/D(I%,K.err%)
          Fd#(I%,3)=Fd#(I%,3)/D(I%,K.err%)
        END IF
      NEXT I%
      IF Round%=1 THEN
          aexpold#=aexp#
          Dh2oold#=Dh2o#
          X0old#=X0#
          FOR I%=1 TO Row%
            Fdold#(I%,1)=Fd#(I%,1)
            Fdold#(I%,2)=Fd#(I%,2)
            Fdold#(I%,3)=Fd#(I%,3)
            Fpold#(I%,1)=Fp#(I%,1)
          NEXT I%
          varianceold#=variance#
          PRINT#1,1;", ";1;", ";aexp#;", ";Dh2o#;", ";X0#;", ";variance#;", ";Lambda#
      ELSE
          IF variance#<=varianceold# THEN
              Lambda#=Lambda#*.125
              Iter%=Iter%+1
              PRINT#1,Round%;", ";Iter%;", ";aexp#;", ";Dh2o#;", ";X0#;", ";variance#;",
";Lambda#
              IF ABS(variance#-varianceold#)<Pre#*varianceold# THEN
                  CLOSE #1
                  GOTO 6686
              END IF
              aexpold#=aexp#
              Dh2oold#=Dh2o#
              X0old#=X0#
              FOR I%=1 TO Row%
                Fdold#(I%,1)=Fd#(I%,1)
                Fdold#(I%,2)=Fd#(I%,2)
                Fdold#(I%,3)=Fd#(I%,3)
                Fpold#(I%,1)=Fp#(I%,1)
              NEXT I%
              varianceold#=variance#
          ELSE
              Lambda#=Lambda#*64#
              PRINT#1,Round%;", ";Iter%;", ";aexp#;", ";Dh2o#;", ";X0#;", ";variance#;",
";Lambda#
              aexp#=aexpold#
              Dh2o#=Dh2oold#
              X0#=X0old#
              FOR I%=1 TO Row%
                Fd#(I%,1)=Fdold#(I%,1)
                Fd#(I%,2)=Fdold#(I%,2)
                Fd#(I%,3)=Fdold#(I%,3)
                Fp#(I%,1)=Fpold#(I%,1)
```

```
                NEXT I%
                variance#=varianceold#
             END IF
          END IF
6685    Delta0=SQR(variance#/(Row%-3))
           Opt1%=1 : CALL
Least.square(Fd#(),Fp#(),X1#(),XA#(),Row%,Nv%,Opt1%,Test,Lambda#)
        Deltaa=X1#(1,1)
        DeltaD=X1#(2,1)
        Deltax0=X1#(3,1)
        aexp#=aexp#-X1#(1,1)
        Dh2o#=Dh2o#-X1#(2,1)
        X0#=X0#-X1#(3,1)
        CLS
        PRINT "a=";aexp#;"4Dt or D(H2O)=";Dh2o#;" X0=";X0#;" std err on wAf(i): ";Delta0
        Round%=Round%+1
        GOTO 6670
6686    PRINT "Calculate profile and errors for finalized a:";aexp#
        W3#(10)=aexp#
        Xt#=W3#(1)
        IF W3#(2)>W3#(1) THEN Xt#=W3#(2)
        W3#(4)=.25#/EXP(W3#(10)*Xt#)
        tstep#=W3#(4)*W3#(3)*W3#(3)
        PRINT "Time step of the final round";Round%;"is";tstep#
        W3#(5)=1999#*W3#(4)*W3#(3)*W3#(3)
        PRINT "Print concentration at zero after 100 time steps"
        PRINT "Plot calculated diffusion profile after 1000 time steps"
        PRINT "Calculation ends after 2000 time steps"
        CALL Water.Forward(W1#(),W3#(),water#(),Xp(),Wp#(),V$(),Nx%(),Morder%,Opt%)
        Nf%=Nx%(1) : NL1%=Nmid%-Nf%+1 : NR1%=Nmid%+Nf%-1
        CALL Find.end.rows(water#(),2,NL1%,Nmid%,NR1%,Pse!,Iend1%,Iend2%)
        Rtem%=Iend2%-Iend1%+1
        DIM Final#(Rtem%,6)
        FOR I%=1 TO Rtem%
           FOR J%=1 TO 5
              Final#(I%,J%)=water#(I%+Iend1%-1,J%)
           NEXT J%
        NEXT I%
        Delta0=SQR(variance#/(Row%-3))
        Lambda#=0
           Opt1%=1 : CALL
Least.square(Fd#(),Fp#(),X1#(),XA#(),Row%,Nv%,Opt1%,Test,Lambda#)
        REM Print and plot results
        Tem1=Delta0*SQR(X1#(1,2))
        PRINT "a=";aexp#;"±";Tem1
        Tem2=Delta0*SQR(X1#(2,3))
        PRINT "4Dt or D(H2O)=";Dh2o#;"±";Tem2
        Tem3=Delta0*SQR(X1#(3,4))
        PRINT "X0=";X0#;"±";Tem3
6690    Dh2o1#=SQR(Dh2o#)
        Y1=0 : Y2=0
        FOR I%=1 TO Row%
        Y0=D#(I%,K2%) : Y1=Y1+Y0 : Y2=Y2+Y0*Y0
```

```
          NEXT I%
          R2=1-variance#/(Y2-Y1*Y1/Row%)
          INPUT "Title for the diagram(s)?",A$
          FOR I%=1 TO Row%
             Plot#(I%,1)=(D#(I%,K1%)+X0#)/Dh2o1#
             Plot#(I%,2)=D#(I%,K2%)
          NEXT I%
          DIM V2$(2) : V2$(1)="x/2√(Dt)" : V2$(2)=Variable$(K2%)
          Xmin=Plot#(1,1) : Xmax=Plot#(Row%,1)
          IF Xmin<.1*Xmax AND Xmin>0 THEN Xmin=0
          Ymin=Final#(1,2) : Ymax=Final#(Rtem%,2)
          IF Plot#(Row%,2)<Plot#(1,2) THEN Ymin=Final#(Rtem%,2) : Ymax=Final#(1,2)
          CALL
Plot.Data(Plot#(),V2$(),A$,1,2,1,Row%,3!,7.5,9!,6!,Xmin,Xmax,Ymin,Ymax,1.5,"F",0,1)
          CALL
Plot.Data(Final#(),V2$(),"",1,2,1,Rtem%,3!,7.5,9!,6!,Xmin,Xmax,Ymin,Ymax,1.5,"F",1,2)
          Posi=170 : IF Plot#(Row%,2)<Plot#(1,2) THEN Posi=100
          CALL MOVETO (220,Posi)
          PRINT "a=";aexp#;"±";Tem1
          CALL MOVETO (220,Posi+15)
          PRINT "D(H2O) or 4Dt=";Dh2o#;"±";Tem2
          CALL MOVETO(220,Posi+30)
          PRINT "X0=";X0#;"±";Tem3
          CALL MOVETO(220,Posi+45)
          PRINT "single r*r≈";R2
          CALL MOVETO(5,255)
          PRINT "std. error for w";Variable$(K2%);" is ";Delta0
6691    REM Store Data
          DIM Huaiwei(Rtem%,6)
          PRINT "File name?"
          A$="calc water dif profile"
          File$=FILES$(0,A$)
          IF File$="" THEN File$="junk.csv"
          OPEN "O",#1,File$
          PRINT#1,A$;
          Sum=0
          FOR I%=Nx%(1)-1 TO 2 STEP -2
           Sum=Sum+(water#(I%+1,2)+4#*water#(I%,2)+water#(I%-1,2)-
6#*W3#(1))*(water#(I%+1,1)-water#(I%-1,1))/6#
          NEXT I%
          Sum=Sum/(W3#(2)-W3#(1)) : Sum=Sum*Sum*3.141593
          Xt1=W3#(1) : Xt2=W3#(2) : Xt3=W3#(3) : Xt4=W3#(9) : Xt5=W3#(8) : Xt6=W3#(6)
          Xt7=W3#(7) : Xt8=W3#(4)*W3#(3)*W3#(3) : Xt9=W3#(10) : Xt10=Dh2o# : Xt11=X0# :
Xt12=astep#
          PRINT#1, "   D(OH)/D(H2O)=";0;"    DH2Om=D0*exp(a*XH2Ot); a=";Xt9;"±";Tem1
          PRINT#1,Rtem%;",  ";6
          PRINT#1,"ID#"; ",  "; V$(1); ",  ";V$(2); ",  "; V$(3); ",  "; V$(4); ",  "; V$(5)
          FOR I%=1 TO Rtem%
          PRINT#1,I%+(Iend1%-1)-Nmid%;",  ";
          FOR J%=1 TO 4
          Huaiwei(I%,J%)=Final#(I%,J%)
          PRINT#1,Huaiwei(I%,J%);",  ";
          NEXT J%
```

```
            Huaiwei(I%,5)=Final#(I%,5)
            PRINT#1,Huaiwei(I%,5)
            NEXT I%
            PRINT#1,"   K=";Xt7
            PRINT#1, "average D/D(H2O)=";Sum
            PRINT#1,"C at x=-∞ is ";Xt1
            PRINT#1,"C at x=∞ is ";Xt2
            PRINT#1,"dx is ";Xt3;"    dt is";Xt8
            PRINT#1, "new time is ";Xt4; "   old time is ";Xt5
            PRINT#1,"D(H2O) or 4Dt=";Xt10;"±";Tem2
            PRINT#1,"X0=";Xt11;"±";Tem3
            PRINT#1,"single r*r≈";R2
            PRINT#1,"std. error for w";Variable$(K2%);" is ";Delta0
            PRINT#1,"step of a is";Xt12
            PRINT#1,"precision of a is";Pre#
            CLOSE #1
            PRINT "Data is stored as: ";File$
6695        ERASE V$,V2$,W1#,W3#,Xp,Nx%,Wp#,water#,water1#,water2#,D.tem#,D1.tem#,D2.tem#
            ERASE Fd#,Fp#,X1#,XA#,X2#,Plot#,Final#,Fdold#,Fpold#,Huaiwei
            GOTO 6000
```

APPENDIX G

QUICKBASIC ROUTINE FOR CONVOLUTING A DIFFUSION PROFILE

Convolution effect can be significant for measuring a short diffusion profile (e.g., less than 200 μm) with FTIR. This routine convolutes a theoretical diffusion profile, and the output profile can be used to fit a measured diffusion profile to find $4D_0t$. It assumes Gaussian distribution $N(x, \sigma^2)$ for convolution effect (x is a certain distance, σ is the standard deviation). For a theoretical total H_2O concentration (in mole fraction) profile X (x), the convoluted H_2O_t concentration $X^\dagger$ at a distance x is

$$X^\dagger(x) = \int_{x-n\sigma}^{x+n\sigma} X(x') \cdot N(x, \sigma^2) dx',$$

where n is an input integer to specify the range for definite integral (such as $n = 8$).

Because the distance in a theoretical profile is dimensionless, the inputted σ is also dimensionless.   The value of σ can be found through trial-and-error until the following relation is satisfied:

$$\sigma_{FTIR} = \sigma\sqrt{4D_0t},$$

where σ_{FTIR} is the standard deviation determined from FTIR measurements across a steep edge.

```
OPTION BASE 1
MAXFIT%=2000
DIM
no%(MAXFIT%),Xs#(MAXFIT%),C#(MAXFIT%),nonew%(MAXFIT%),X(MAXFIT%),Y(MAXFIT%),
Variable$(10)
DEF FNNormal#(eks#,mu#,sig#)=1#/sig#/SQR(2*3.1415926535898#)/EXP((eks#-mu#)^2/2/sig#^2)

     CALL readdata(no%(),Xs#(),C#(),Row%,MAXFIT%,Info$,Variable$())
     CALL convolute(no%(),Xs#(),C#(),nonew%(),X(),Y(),Row%,N%,MAXFIT%,sigma#)
     CALL writedata(nonew%(),X(),Y(),Row%,N%,MAXFIT%,Info$,Variable$(),sigma#)
     ERASE no%,Xs#,C#,nonew%,X,Y,Variable$
     END

SUB readdata(no%(),Xs#(),C#(),Row%,MAXFIT%,Info$,Variable$()) STATIC
     DIM ignor1#(MAXFIT%),ignor2#(MAXFIT%),ignor3#(MAXFIT%)
     PRINT "  input file should be calculated with Zhang's diffusion couple program"
     PRINT "  1st row is info (no comma), 2nd row gives # of rows and # of columns"
     PRINT "  3rd row gives variable names, and then data matrix"
     PRINT
     PRINT "please input the file name (e.g. huaiwei.csv)"
     File$=FILES$(1,"TEXT")
     OPEN "I",#2,File$
     LINE INPUT#2,Info$
     Any%=LEN(Info$) : Any1%=Any%
     WHILE RIGHT$(Info$,1)=","
         Any%=Any%-1 : Info$=LEFT$(Info$,Any%)
     WEND
     INPUT#2,Row%
     LINE INPUT#2,Any$
     Any%=LEN(Any$) : Any1%=Any%
     WHILE RIGHT$(Any$,1)="," OR RIGHT$(Any$,1)=" "
         Any%=Any%-1 : Any$=LEFT$(Any$,Any%)
     WEND
     Column%=VAL(Any$)
     PRINT File$
     PRINT Info$
     PRINT "# of rows=";Row%,"# of columns=";Column%
     FOR J%=1 TO Column%
         INPUT#2,Variable$(J%)
         PRINT Variable$(J%)
     NEXT J%
     FOR J%=1 TO Row%
         INPUT#2,no%(J%),Xs#(J%),C#(J%),ignor1#(J%),ignor2#(J%),ignor3#(J%)
     NEXT J%
     ERASE ignor1#,ignor2#,ignor3#
END SUB

     SUB convolute(no%(),Xs#(),C#(),nonew%(),X(),Y(),Row%,N%,MAXFIT%,sigma#) STATIC
         DIM diff#(MAXFIT%),F#(MAXFIT%),xnew#(MAXFIT%),Cnew#(MAXFIT%)
100      INPUT "please input Gaussian standard deviation",sigma#
         INPUT "How many sigmas for integration range (e.g. 8)?",nsigma%
         range#=sigma#*nsigma%
         Row2%=Row%-1
         PRINT Row%,Row2%
         sumdiff#=0
         FOR J%=1 TO Row2%
```

```
            diff#(J%)=Xs#(J%+1)-Xs#(J%)
            sumdiff#=sumdiff#+diff#(J%)
        NEXT J%
        avediff#=sumdiff#/Row2%
        N%=range#/avediff#
        IF N%<(range#/avediff#) THEN N%=N%+1
        Total%=Row%+4*N%
        IF Total%>MAXFIT% THEN
            PRINT "exceed maximum, please reduce either deviation or range"
            GOTO 100
        END IF

        REM EXTEND array for integration
        FOR J%= 2*N%+1 TO 4*N%
            no%(Row%+J%)=no%(Row%)+(J%-2*N%)
            Xs#(Row%+J%)=Xs#(Row%)+(J%-2*N%)*avediff#
            C#(Row%+J%)=C#(Row%)
        NEXT J%
        FOR J%=Row% TO 1 STEP -1
            no%(J%+2*N%)=no%(J%)
            Xs#(J%+2*N%)=Xs#(J%)
            C#(J%+2*N%)=C#(J%)
        NEXT J%
        FOR J%=1 TO 2*N%
            no%(J%)=no%(2*N%+1)-(2*N%-J%+1)
            Xs#(J%)=Xs#(2*N%+1)-(2*N%-J%+1)*avediff#
            C#(J%)=C#(2*N%+1)
        NEXT J%
        FOR J%=1 TO Row%+4*N%
            PRINT no%(J%),Xs#(J%),C#(J%)
        NEXT J%

        REM CONVOLUTE
        FOR I%=1 TO Row%+2*N%
            nonew%(I%)=no%(N%+I%)
            xnew#(I%)=Xs#(N%+I%)
            Cnew#(I%)=0
            FOR J%=1 TO 2*N%+1
                F#(J%)=C#(I%+J%-1)*FNNormal#(Xs#(I%+J%-1),Xs#(I%+N%),sigma#)
            NEXT J%
            FOR J%=1 TO 2*N%
                Cnew#(I%)=Cnew#(I%)+(F#(J%)+F#(J%+1))*(Xs#(I%+J%)-Xs#(I%+J%-1))/2
            NEXT J%
            X(I%)=xnew#(I%)
            Y(I%)=Cnew#(I%)
        NEXT I%
        ERASE diff#,F#,xnew#,Cnew#
END SUB

SUB writedata(nonew%(),X(),Y(),Row%,N%,MAXFIT%,Info$,Variable$(),sigma#) STATIC
    CLS
    PRINT "File name?"
    A$="convoluted "
    File$=FILES$(0,A$)
    IF File$="" THEN File$="junk.csv"
    OPEN "O",#1,File$
```

```
    PRINT#1,A$;Info$
    PRINT#1,Row%+2*N%; ",  ";3
    PRINT#1,"ID#"; ",  "; Variable$(1); ",  ";Variable$(2)
    FOR I%=1 TO Row%+2*N%
        PRINT#1,nonew%(I%); ",  ";X(I%); ",  ";Y(I%)
    NEXT I%
    sigm=sigma#
    PRINT#1,"Gaussian standard deviation is";sigm
    PRINT#1,"New concentration is the weighted average of ";N%;" points to both left and right"
    CLOSE #1
    PRINT "Data is stored as: ";File$
END SUB
```